UNIVERSITY OF NOTTINGHAM

SCHOOL OF CIVIL ENGINEERING

NUMERICAL STUDY OF IRREGULAR WAVE OVERTOPPING AND OVERFLOW

By

Akram S. M. Soliman, B.Eng (Hons), M.Sc.

Thesis submitted to the University of Nottingham

for the degree of Doctor of Philosophy

November 2003

Supervisor:

Prof. Dominic Reeve

Co-Supervisor:

Prof. Mohamed Raslan

Dr. Nigel Wright

Examiners:

Prof. Andrew Chadwick

Dr. Hervé Morvan.

Abstract

Wave overtopping is one of the most important processes for the design of seawalls. During the past 50 years methods for predicting wave overtopping of coastal structures have continuously been developed.

However, it is evident from the existing literature that additional investigations into overtopping of small positive, zero and negative freeboard are needed. The present thesis describes numerical investigations based in this background.

Wave overtopping is dependent on the processes associated with wave breaking. Therefore, a two dimensional breaking wave numerical model has been developed and used to study the phenomena of wave overtopping. The model is based on the Reynolds averaged Navier-Stokes equations for the mean flow and $(k-\varepsilon)$ equations for turbulent kinetic energy, *k*, and the turbulence dissipation rate, ε.

The model accuracy in simulating propagation of linear and irregular waves has been evaluated. The overall performance of the model is considered satisfactory.

The development of guidelines for calculating overtopping discharge for different seawall slopes is presented. All slopes have been subjected to a wide range of irregular waves. The influence of how the slopes of seawalls, wave type (breaking and non-breaking) and crest freeboard affect the overtopping discharges has been investigated.

Based on the numerical data, a new expression for breaking and non-breaking waves on smooth impermeable slopes is proposed. With the new expression it is possible to predict overtopping discharges of smooth seawalls in small positive, zero and negative freeboard.

Acknowledgements

Thanks to **GOD**, most merciful and most compassionate, without him and his help nothing could be done.

I wish to express my deep appreciation and sincere gratitude to my supervisor, Prof. Dominic Reeve, for his guidance as well as encouragement and valuable suggestions throughout the completion of this dissertation. I thank him for his time spent during our many discussions and for his valuable advice. I believe this will accompany me for the rest of my life.

I would like also to express my deep appreciation and gratitude to my supervisor, Dr. Nigel Wright, for his continuous guidance and useful suggestions.

Furthermore, thanks should also go to Prof. Mohamed Raslan, Arab Academy for Science and Technology, Egypt, for his encouragement, guidance and constructive criticisms.

The thesis has benefit by many other people's works and effort. The numerical model used in the second part is partially based on numerical model of breaking wave, which was developed and kindly provided by Dr. Pengzhi Lin. Dr. Lin offered the author a comprehensive training course in the numerical model at National University of Singapore during June 2002. Especially indebted is given to Dr. Van der Meer for provided the author with his laboratory work of both small and large-scale models which were carried out in Delft Hydraulics laboratory.

I would like to thank my colleagues in Coastal Engineering conference (2003) in Cardiz, Spain and Coastal Structures Conference (2003) in Portland, Oregon. The

feedback and valuable advice especially received from Dr. Peter Trock and Dr. Andreas Kortenhaus were very helpful and give me good guidance.

I am grateful to my sponsor, the Arab Academy for Science and Technology and Maritime transport, AASTMT, for awarding funding to the research. AASTMT has been kind enough to support the research financially.

Finally, I like to express the gratitude from my heart to my parents who have been giving me the invaluable and endless support in my life. A special thank should go to my lovely wife, who supported me throughout my Ph.D. and without whom it would have not been possible. Not only was her patience tested on numerous occasions, but she also sacrificed many evenings, weekends and holidays.

Publications

In addition to the present thesis the research conducted has resulted in a number of other publications. Among these are:

- Soliman, A., M. S. Raslan and D. E. Reeve (2003). Numerical simulation of wave overtopping using two dimensional breaking wave model. Proceedings of Coastal Engineering VI: Computer modelling of seas and coastal regions, Cadiz, Spain, (Ed. C Brebia, D Almorza & F Lopez-Aguayo), pp. 439-447.

- Soliman, A. and D. E. Reeve (2003). Numerical study for small freeboard wave overtopping and overflow of sloping sea wall. To appear in Proceeding of Coastal Structures 2003, Portland, Oregon.

To my parents, my lovely wife and adorable daughters Rawan and Nour.

Table of Contents

List of Figures

List of Tables

List of Symbols

a : Amplitude of regular wave [m]

a,b : Empirical overtopping coefficients [-]

A_c : Armor crest freeboard defined as vertical distance from SWL to armor crest [m]

B : Armor crest width [m]

C_d : Weir equation discharge coefficient.

C_o : Wave phase celerity [m/s]

d : Water depth [m]

E : Total energy density [m^2.sec]

$E(f)$: JONSWAP frequency spectral density function [m^2.sec]

E_p : Potential energy density [m^2.sec]

H : Wave height [m]

H_s : Significant incident wave height [m]

i,j : 1, 2 and 3 for three dimensional flow [-]

L : Wave length [m]

L_{mo} : Deep water wave length based on $\frac{g}{2\pi}T_{mo}^2$ [m]

L_{po} : Deep water wave length based on $\frac{g}{2\pi}T_{po}^2$ [m]

m : Discharge coefficient [-]

g : Acceleration of gravity, where set to 9.81 [m/s^2]

g_i : The i-th component of the gravitational acceleration [m/s^2]

q : Average overtopping discharge per width [$m^3/s/m$]

Q : Dimensionless average overtopping discharge [-]

Or : Ratio of overtopping rate at a given wave attack to that predicted under normal wave attack.

R : Dimensionless freeboard [-]

R_c : Crest freeboard [m]

R^*_c : Crest freeboard dependent on slope angle and crest width [m]

Ru_{max} : Maximum run-up level [m]

$R_{u,2\%}$: Run-up height exceeds by 2% of the incident waves [m]

S_m : Deep water wave steepness defined as $\frac{H_s}{L_{mo}}$ [-]

S_p : Deep water wave steepness defined as $\frac{H_s}{L_{po}}$ [-]

t : Time [s]

T :Wave period [s]

T_m : Mean wave period [s]

T_{mo} : Spectrum deep water mean period [s]

T_{po} : Spectrum deep water peak period [s]

p : Atmospheric pressure [N/m^2]

u : Horizontal velocity vector component [m/s]

v : Vertical velocity vector component [m/s]

x,y, z : Three dimensional coordinates [m]

z_m : Vertical distance between mean sea water surface and wave crest [m]

z_o : Vertical distance between mean sea water surface and seawall crest [m]

α : Slope angle [^{o}]

β : Angle of wave attack [^{o}]

η : Wave elevation [m]

γ : Reduction factor taking the influence of berm, shallow foreshore, roughness and angle of wave attack into account [-]

γ_b : Reduction factor taking the influence of berm into account [-]

γ_h : Reduction factor taking the influence of shallow foreshore into account [-]

γ_r : Reduction factor taking the influence of roughness into account [-]

γ_β : Reduction factor taking the influence of angle of wave attack into account [-]

ρ : Fluid density [kg/m^3]

ξ_m : Surf-similarity parameter defined as $\xi_m = \frac{\tan\alpha}{\sqrt{S_{mo}}}$ [-]

ξ_p : Surf-similarity parameter defined as $\xi_p = \frac{\tan\alpha}{\sqrt{S_{po}}}$ [-]

μ : Molecular (Dynamic) viscosity [kg/m.sec]

σ_{ij} : Rate of the strain tensor defined as $\sigma_{ij} = \frac{1}{2}\left(\frac{\partial u_i}{\partial x_j} + \frac{\partial u_j}{\partial x_i}\right)$ [sec^{-1}]

τ_{ij}^m : Molecular viscosity stress tensor defined as $\tau_{ij}^m = 2\mu\sigma_{ij}$ [N/m^2]

CHAPTER 1

Introduction

Research into wave overtopping of coastal structures has been the subject of numerous investigations over the past 50 years. Since then the overtopping prediction tools for typical sea defense structures have continuously been refined. The term “wave overtopping” is used here to refer to the process where waves hit a sloping structure run up the slope and, if the crest level of the slope is lower than the highest run up level, overtop the structure. The wave overtopping discharge is thus defined as overtopping volume [m^3] per time [s] and structure width [m]. Figure 1.1 shows an example of wave overtopping at Samphire Hoe seawall, UK.

Figure 1.1: Severe wave overtopping at the Samphire Hoe seawall, UK (from CLASH project, www.clash-eu.org (2001)).

Wave overtopping is considered one of the most important processes for the design of seawalls, and also to be responsible for many seawall failures in the past. For example, many seawalls failed due to wave overtopping during the extreme storm surge disasters in 1953 (Netherlands), 1962 and 1976 (Germany and Denmark) (Bleck *et al.*, 2000). In the mean time, the crest levels of seawalls have been increased along the British, German, Dutch and Danish coasts. Nevertheless, wave overtopping cannot be avoided completely due to the random nature of the waves and the uncertainties associated with the determination of the design water levels and the costs of uneconomically high seawall and their damaging effects to the surrounding environment.

The motivation for predicting the overtopping of structures has until now been linked to the design of structures protecting mankind and objects of value against the violent force of the surrounding sea. Typically rubble mound or vertical wall breakwaters have been used for the protection of harbours, and seawalls and offshore breakwaters have been used for the protection of beaches and land. All these structures are designed to avoid overtopping or at least reduce it to a minimum as overtopping can lead either to functional or structural failure of structures.

Here functional failure refers to cases where for example large wave overtopping discharges might damage persons, ships, the structure itself or equipment on it or generate waves behind the structure (in case water is present there), which again is hazardous to the manoeuvring or mooring of ships. An example of such conditions is shown in Figure 1.2. Structural failure refers to cases where the

overtopping discharge is heavy enough to damage the crest or lee side of the breakwater or seawall which ultimately can lead to the collapse of the structure.

Figure 1.2: Wave run-up and overtopping at Zeebrugge breakwater (Belgium), during (mild) storm conditions (from OPTICREST project, awww.rug.ac.be/opticrest (2001)).

Breaking waves in the surf zone play an essential role in nearly all-coastal processes. The breaking waves generate strong turbulence and are in general accompanied by strong energy dissipation. Breaking modifies wave forces on the coastal structures when the wave-structure interaction occurs. This is important when the construction of structures in coastal regions is considered.

The most critical processes for overtopping are the form and severity of wave breaking. Recent studies have showed that current overtopping formulae, which do not take full account of the complexity of wave breaking, can significantly underestimate overtopping discharges (Besley *et al.*, 1998).

Global climate has been changed during the last years and the mean water levels have increased all over the world. Sea level rises will have a number of important impacts on humans. About half of world's population lives within 200 kilometre of the ocean, and many millions live in coastal areas that are less than 5 m above sea level (Hardy, 2003).

Sea level rise impacts include increased beach erosion and flooding of coastal habitats. The existing coastal structures, which were designed for certain water level, are now likely to be attacked by greater amounts of wave overtopping. It is important to be able to predict flood water volumes in this case (small positive freeboard). There is currently no guidance on estimating these volumes.

During storm surges seawalls are exposed to waves. The amount of overtopping water increases when the water level rises. If the water level rises above the crest level of the structure flood water is not only caused by the wave overtopping action, but also by overflow.

Design formulae used to calculate wave overtopping assume that water in front of the structure to be below the crest level of the structure. On the other hand, the existing formulae for overflow (e.g. weir formulae) do not take into account the effect of waves. New formulae for predicting the case of combined wave overtopping and overflow (negative freeboard) are still needed for the planning and engineering response.

1.2 Scope of the study

In light of the outlined state of development of design overtopping formulae, the author has carried out a generic study of wave overtopping of seawalls as a Ph.D.

project. This work aims to provide guidelines for how to calculate overtopping discharges for a range of seawall slopes when subjected to a broad range of irregular breaking and non-breaking waves in small positive, zero and small negative freeboard. Here freeboard is referred to vertical distance between mean water level and seawall crest level.

In this study the influence of how the slopes of seawalls, wave type (breaking and non-breaking) and crest freeboard effect the overtopping discharges have been investigated. This has been achieved through studies of the existing literature, theoretical considerations and numerical model tests.

Numerical models are now playing a very important role in research and design of coastal structures. Some numerical models are under development and have been validated by coastal researchers.

Two numerical models are used in this study. The first numerical model is SOLA-VOF, which is based on the Navier-Stokes equations. SOLA-VOF has been developed by Nichols *et al.* (1980) at Los Alamos National Laboratory, New Mexico, USA. The second model, is a two-dimensional breaking wave numerical model, (2-D BWNM), which is based on the Reynolds Averaged Navier-Stokes equations for mean flow and $(k-\varepsilon)$ equations for turbulent kinetic energy, *k*, and the turbulence dissipation rate, ε. The two-dimensional breaking wave numerical model has been developed by Liu and Lin (1997).

The numerical models have been validated using laboratory data, other numerical models, analytical solutions and empirical design formulae.

By using the numerical model results, the influence of the freeboard on overtopping and combined overflow and overtopping has been investigated. New formulae for cases of small positive, zero and small negative freeboard, which are not covered by existing empirical equations, have been formulated, in the expectation that they will be useful for designers.

The research has three main aims:

- To introduce a new numerical model which is able to simulate random breaking waves in shallow water
- To produce new formulae for the case of small positive and zero freeboard as existing overtopping design formulae do not account for these cases.
- To investigate the case of combined overtopping and overflow and introduce new suggested design formulae that can be used in design purposes.

Summary of the present state of knowledge concerning wave overtopping is presented in next Chapter (Chapter 2). Overtopping discharge levels, an overview of recent overtopping investigations, the effects of wave climate, structure geometry and others topics relevant to the current study are described.

In Chapter 3, the first numerical model (SOLA-VOF) used in this research is illustrated. SOLA-VOF mathematical equations governing fluid motion, volume of fluid (VOF) technique, numerical implementation, boundary conditions and three cases of study are presented.

A literature review concerning the two-dimensional breaking wave numerical model (2-D BWNM), mathematical formulation of 2-D BWNM and initial boundary condition are presented in Chapter 4.

Different cases of study have been investigated to evaluate two-dimensional breaking wave numerical model (2-D BWNM) in Chapter 5.

Cases of small positive, zero and small negative freeboard conditions are studied in Chapters 6 and 7. The results are used in conjunction with existing formulae to propose a unified set of design equations to predict combined overflow and overtopping volumes for different wave conditions as shown in Chapter 8.

Conclusion from the research and recommendations for future work are presented in Chapter 9.

CHAPTER 2

Literature Review

In this chapter a summary of the present state of knowledge concerning wave overtopping is presented. When possible, this review focuses on studies where more canonical/idealised layouts of the structure are investigated (*i.e.*, overtopping of linear smooth slopes rather than site- specific sea defence profiles).

The first section of this chapter described the overtopping discharge levels, then an overview of the recent overtopping investigations. In subsequent sections, the effects of wave climate, structure geometry and others topics relevant to the current study are presented.

2.1 Overtopping discharge levels

Under random wave attack, overtopping discharges vary by up to several orders of magnitude from one wave to another, meaning that wave overtopping is a very non-linear function of wave height and wave period. This time variation is difficult to measure and quantify in the laboratory and hence overtopping discharges are most often given in terms of average discharge. To assess admissible overtopping discharges for different objects, several researchers have studied the impact of overtopping water volumes on different obstacles placed on top of an overtopped structure. Goda (2000) developed overtopping guidelines based on prototype investigations consisting of wave climate measurements and expert impressions of the impact of overtopping volumes on different objects situated on top of breakwaters. These guidelines have been adopted by the

Japanese code of practice, and by Coastal Engineering Manual (Burchartch and Hughes, 2003). Table 2.1.1 present critical values of the average overtopping discharge, q, for typical structure types when considering sea defense structures. The values given in this table must be regarded only as rough guidelines.

	Safety of traffic		Structural safety			
10^0	Vehicles	Pedestrians	Building	Embankment seawalls	Grass sea dikes	Revetments seawalls
	Unsafe at any speed	Very dangerous	Structural damage	Damage even if fully protected	Damage	Damage even for paved promenade
10^{-1}						Damage if promenade not paved
				Damage if back stop not protected		No damage
10^{-2}				Damage if crest not protected		
					Start of damage	
10^{-3}				No damage		
		Dangerous on grass sea dikes			No damage	
10^{-4}	Unsafe parking on horizontal composite break water	Dangerous on Vertical wall B.W				
	Unsafe parking on vertical wall break water					
10^{-5}		Uncomfort-able but not dangerous	Minor damage to fittings, sign posts, etc.			
	Unsafe driving at high speed					
10^{-6}		Wet, but comfortable				
	Safe driving at all speed		No damage			
10^{-7}						

q (m^3/s/ m)

Table 2.1.1: Criteria for critical overtopping discharge (from Burchartch and Hughes (2003)).

2.2 Overview of recent overtopping investigations

When investigating wave overtopping of coastal structures it is evident that the discharge depends not only on environmental conditions such as wave height, wave period and water level, but also on the geometrical layout and material properties of the structure. Thus, there is almost an infinite array of possible combinations. Therefore, although a lot of investigations related to wave overtopping have been conducted, none of these cover all situations. Each of the investigations typically covers one or a few specific cases, which are then conducted by means of physical model tests in the laboratories (typically small-scale models). Such investigations usually lead to an empirical relationship between the environmental conditions, geometrical layout and material properties of the structure and the overtopping discharge.

Methods available to predict overtopping rates include numerical modelling, site-specific model testing and empirical formulae. Most numerical models have been validated using small-scale tests with limited structural and incident wave conditions. In application the dimensionless overtopping discharge, Q, is estimated using interpolation if necessary. Site-specific hydraulic model testing is impractical for preliminary design due to the time and expenses involved. As a result, engineers rely heavily upon empirical overtopping formulae for conceptual and preliminary design. Regular waves are rarely found in the real world, and increasingly less frequently used in the laboratory. The overtopping investigations based on model tests of various coastal structures exposed to irregular waves are summarized briefly in Table 2.2.2, along with the resulting overtopping discharge prediction formulae.

Authors	Structures	Overtopping model	Dimensionless overtopping discharge Q	Dimensionless freeboard R
Owen (1980), Owen (1982)	Impermeable smooth, rough, straight and bermed slopes under offshore random wave. $1.5 \le \left(d/H_s \right) \le 5.5$ $.035 \le \left(H_s/L_{mo} \right) \le .055$ $0.5 \le \left(R_C/H_s \right) \le 4.0$	$Q = ae^{-bR}$	$\frac{q}{gH_sT_{mo}}$ $\left(= \frac{q\sqrt{S_m/2\pi}}{\sqrt{gH_s^3}} \right)$	$\frac{R_c}{H_s}\sqrt{\frac{S_m}{2\pi}}\frac{1}{\gamma_r}$
Bradbury and Allsop (1988)	Rock armoured impermeable slopes with crown walls	$Q = aR^{-b}$	$\frac{q}{gH_sT_{mo}}$	$\left(\frac{R_c}{H_s}\right)^2\sqrt{\frac{S_m}{2\pi}}$
Aminti and Franco (1988)	Rock, cube and Tetrapod double layer armor on rather impermeable slopes crown walls (single sea state)	$Q = aR^{-b}$	$\frac{q}{gH_sT_{mo}}$	$\left(\frac{R_c}{H_s}\right)^2\sqrt{\frac{S_m}{2\pi}}$
Ahrens and Heimbaugh (1988)	7 different sea-wall / revetment designs	$Q = ae^{-bR}$	$\frac{q}{\sqrt{gH_s^3}}$	$\frac{R_c}{\left(H_s^2L_{po}\right)^{\frac{1}{3}}}$
Pedersen and Burchartch (1992)	Rock armoured rather impermeable slopes with crown walls	$Q = aR$	$\frac{qT_{mo}}{L_{mo}^2}$	$\frac{H_s}{R_C}$
Franco *et al.* (1994)	Vertical wall breakwater with and without perforated front. $0.9 \le \left(R_C/H_s \right) \le 2.2$	$Q = ae^{-bR}$	$\frac{q}{\sqrt{gH_s^3}}$	$\frac{Rc}{Hs}\frac{1}{\gamma}$
Van der Meer and Janssen (1995)	Impermeable, smooth, rough, Straight and bermed slopes	$Q = ae^{-bR}$	$\frac{q}{\sqrt{gH_s^3}}\sqrt{\frac{S_p}{\tan\alpha}}$ For $\xi_p < 2$ $\frac{q}{\sqrt{gH_s^3}}$ For $\xi_p \ge 2$	$\frac{R_c}{H_s}\frac{\sqrt{S_p}}{\tan\alpha}\frac{1}{\gamma}$ For $\xi_p < 2$ $\frac{R_c}{H_s}\frac{1}{\gamma}$ For $\xi_p \ge 2$

Table 2.2.2: Models for overtopping discharge formulae, partly based on table VI-5-7 in Burchartch and Hughes (2003).

Authors	Structures	Overtopping model	Dimensionless overtopping discharge (Q)	Dimensionless freeboard (R)
Pedersen (1996)	Rock armoured impermeable slopes with crown walls	$Q = R$	$\frac{qT_{mo}}{L_{mo}^2}$	$3.2 \times 10^{-5} \frac{H_s^5}{R_c^3} \frac{\tan \alpha}{A_c B}$
Hedges and Reis (1998)	Impermeable smooth, rough, straight and bermed slopes [Data from Owen (1982)]	$Q = a(1 - R)^b$ for $0 \le R < 1$ $Q = 0$ for $R \ge 1$	$\frac{q}{\sqrt{gRu_{\max}^3}}$	$\frac{R_c}{Ru_{\max}}$
Hebsgaard *et al.* (1998)	Rubble mound structure with and without super structure, armour layer of rounded stones quarry rocks, and Dolos.	$Q = ae^{-bR}$	$\frac{q}{\ln(S_p)\sqrt{gH_s^3}}$	$\frac{R_c^*}{H_s} \frac{1}{\gamma}$ (R_C^* dependent on slope angle and crest width)
Schuttrumpf *et al.* (2001)	Impermeable smooth 1:6 slope (for no freeboard (R_c=0) and without overtopping ($R_c > R_{max}$)).	$Q = ae^{-bR}$ (a dependent on ξ_m)	$\frac{q}{\sqrt{2gH_s^3}}$	$\frac{Rc}{\xi_m H_s}$

Table 2.2.2 Models for overtopping discharge formulae partly based on table VI-5-7 in Burchartch and Hughes (2003), continued.

Figure 2.2.1 describes the phenomenon of wave overtopping and presents main parameters using in wave overtopping formulae.

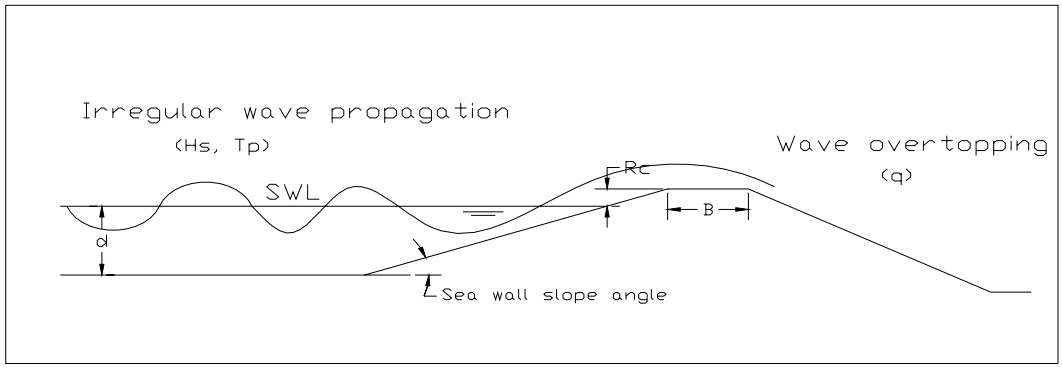

Figure 2.2.1: Diagram of key quantities used to describe wave overtopping at sloping seawalls.

A comprehensive overview of coastal structures in general and also more details of some of the prediction formulae can be found in Burchartch and Hughes (2003). In the following subsections, more focus is given to three empirical formulae [Van der Meer and Janssen (1995), Owen (1980) and Hedges and Reis (1998)] for wave overtopping of a simple sloped seawall subjected to random waves approaching normal to the slope. These formulae are chosen for comparison and validation the numerical model performance in Chapter 5 (Section 5.5.2.4). Reasons of why choosing these three formulae are illustrated in following three subsections.

2.2.1 Van der Meer and Janssen overtopping formulae

Van der Meer and Janssen (1995) made a distinction between breaking (plunging) and non-breaking (surging) waves on the slope. Their set of formulae is related to breaking waves and is also valid up to a maximum of non-breaking region.

Van der Meer's formulae for straight impermeable sloped seawalls are:

For breaking waves: $\xi_p < 2$

$$Q = \frac{q}{\sqrt{gH_s^3}} \frac{\sqrt{\tan\alpha}}{\xi_p} = 0.06 \exp\left(-5.2R \frac{1}{\gamma_r \gamma_b \gamma_h \gamma_\beta} \right) \tag{2.2.1}$$

$$R = \frac{R_c}{H_s \xi_p}, \quad \xi_p = \frac{\tan\alpha}{\sqrt{S_p}} \quad \text{and} \quad S_p = \frac{2\pi H_s}{g T_{po}^2} \tag{2.2.2}$$

For non-breaking waves: $\xi_p > 2$

$$Q = \frac{q}{\sqrt{gH_s^3}} = 0.2 \exp\left(-2.6 \frac{R_c}{H_s} \frac{1}{\gamma_r \gamma_b \gamma_h \gamma_\beta} \right) \tag{2.2.3}$$

The coefficients $\gamma_b, \gamma_h, \gamma_r$ and γ_β are introduced to take into account the influence of a berm, shallow foreshore, roughness and angle of wave attack, respectively.

All these coefficients are in the range 0.5 to 1.0, meaning that when maximizing overtopping, the coefficients should be 1.0, which is the case for no berm, no shallow foreshore, smooth slope (no roughness and impermeable) and head-on waves. Van der Meer and Janssen (1995) study based on both small and large-scale model tests and includes tests with geometries usable in the current study (straight and impermeable slopes).

Van der Meer's formulae are the most commonly used method for calculation of the average overtopping rate. Schüttrumpf and Oumeraci (2000) recommended Van der Meer's formulae for the design of sea dikes in Germany.

Results from small wave flume of the Leichtweiss Institute (LWI) for Hydraulics of the Technical University of Braunschweig, Oumeraci *et al.* (1999), with nature sea spectra, have shown that the overtopping model by Van der Meer fits well for single peak wave spectra.

2.2.2 Owen overtopping formulae

Owen (1980) proposed an exponential relationship between dimensionless mean overtopping discharge (Q) and dimensionless freeboard (R). He carried out an extensive series of model tests for a range of seawall designs subject to different random wave climates. The modelled seawalls were all of the same general type: a flat-topped embankment fronted in some cases by a flat berm.

In Owen's method, the wave height is represented by an equivalent post-breaking wave height. The post-breaking wave height is an equivalent wave height designed to give the correct overtopping discharge as confirmed from physical model tests where significant wave breaking take place (Besley, 1999).

Owen's formula for an impermeable smooth straight seawall is:

$$Q = \frac{q}{gH_S T_{mo}} = a \exp(-bR) \tag{2.2.4}$$

$$R = \frac{R_c}{T_{mo}\sqrt{gH_s}} \tag{2.2.5}$$

Table 2.2.3 contains the values of a and b which are empirically derived coefficients depend on the profile of the seawall.

Seawall slope	a	b
1:1	0.00794	20.1
1:1.5	0.00884	19.9
1:2	0.00939	21.6
1:2.5	0.01030	24.5
1:3	0.01090	28.7
1:3.5	0.01120	34.1
1:4	0.01160	41.0
1:4.5	0.01200	47.7
1:5	0.01310	55.6

Table 2.2.3: Values of empirical coefficients a and b in equation 2.1.4 from Besley (1999)

Owen measured data for a number of different types of simply sloping seawalls. The data is therefore is more structure-specific than the Van der Meer method, which combines all data together. Besley (1999) recommended that the method proposed by Owen (1980) is used for estimating overtopping discharge at smooth, simply sloping and bermed seawalls around UK coastline.

When the seawall has zero freeboard, equations (2.1.1, 2.1.3 and 2.1.4) correctly predict that the overtopping discharge is finite. However, these equations predict that Q is finite even when seawall has a very large freeboard well in excess of any possible run-up.

2.2.3 Hedges & Reis overtopping formulae

Hedges and Reis (1998) constructed a model based on a regression against Owen's data subject to the constraint that there is no overtopping if the sea-wall freeboard exceeds the maximum run-up on the face of the seawall.

The physical boundary conditions Hedges and Reis (1998) studied are:

- When the seawall has a large freeboard, the predicted overtopping discharge should be zero.
- When the seawall has zero freeboard then the predicted overtopping discharge may be large but should still remain finite.

Hedges & Reis's formula is:

$$Q = \frac{q}{\sqrt{g\,(CH_s)^3}} = a\left(1 - \frac{R_c}{CH_s}\right)^b \qquad (2.2.6)$$

where C is the ratio of the maximum run-up (Ru_{max}) to the significant height of the incident wave [$C = 1.52 \times \left(1.35 \times \xi_p\right)$ for $\xi_p < 2$].

The important features of the model are as follows (Hedges and Reis, 1998):

- It satisfies the relevant physical boundary conditions, a feature which is especially important when the model is used near these boundaries.
- It explicitly recognizes that regression coefficient (a) depends on the shape of the structure since the shape, partially at its crest, affects the discharge coefficient; coefficient (a) represents the dimensionless discharge when the dimensionless freeboard is zero.
- Coefficient (b) depends on the detailed behaviour of the water surface on the seaward face of the structure; it increases as front slopes become flatter.

- Coefficient (C) relates the maximum run-up (Ru_{max}) to the significant height of the incident waves and may be chosen to allow for the influences of the sea-wall slope, the surface roughness and porosity, and the incident wave steepness. Coefficient (C) can also account for storm duration in influencing Ru_{max}.

Hedges and Reis (1999) show that, for small allowable overtopping discharges associated with normal design conditions, there are considerable differences between predictions based on Owen's model.

2.3 Effect of wave climate

The overtopping discharge is, as can be seen from Tables 2.1.1 and 2.2.2, dependent on the wave climate as given by the significant wave height, the water level (through the crest freeboard), and also in many cases the wave peak or mean period. However, various studies have also shown some dependency on other parameters related to the wave climate. These dependencies are considered in the following.

2.3.1 Oblique waves

Several authors have investigated the effect of oblique angles of wave attack. Banyard and Herbert (1995) have developed an equation that enables an overtopping ratio, O_r, to be calculated.

O_r is defined as the ratio of overtopping at a given angle of wave attack, β, to that predicted under normal wave attack.

Banyard and Herbert's (1995) equation for simply sloping seawalls is:

$$O_r = 1 - 0.000152\beta^2 \qquad (2.3.7)$$

It is inferred from this equation that the predicted overtopping discharge is lower for all oblique angles of attack than for normal attack. It is also found that the slope of the seawall have a little effect in the predicted overtopping discharge (Besley, 1999).

The effect of oblique wave attack is also included in the overtopping expressions by Van der Meer and Janssen (1995) through the reduction factor γ_β for sloping structures.

Napp *et al.* (2002) suggested that mean overtopping discharges of vertical seawalls reduce significantly with increasing angle of wave attack and that the occurrence of impulsive overtopping diminishes rapidly with obliquity of wave attack $> 30^o$.

2.3.2 Directional spreading

Franco *et al.* (1995) comment on the effect of directional spreading on overtopping discharge on both slopes and vertical walls. For slopes the effect of directional spreading is minimal for head on waves but results in faster decay for increasing angle of attack compared with long crested waves. For vertical wall structures the directional spreading reduces the overtopping discharge significantly even for head on waves. The reduction in overtopping discharge for multi directional and oblique waves is also reported by Sakakiyama and Kajima (1997).

2.3.3 Spectral shape

Typically, the model tests performed in overtopping investigations utilize standard wave spectra such as TMA (Bouws *et al.,* 1985) or JONSWAP (Carter,

1982). These spectra apply to offshore conditions or conditions with simple foreshores. TMA spectrum was derived specifically for shallow water conditions. In order to take more complicated situations into account, Van der Meer and Janssen (1995) incorporated double peaked spectra in their overtopping formulae by splitting the spectra into two, identifying the peak periods for each of the two parts and combining these into an equivalent peak period.

Hawkes (1999) comments on swell and bimodal seas and states that they possibly represent the worst case (here worst case refers to most overtopping) sea states with regard to mean overtopping discharge.

Hedges and Reis (1998) and Van der Meer and Janssen (1995) methods incorporate separate formulae for plunging waves, where overtopping is strongly dependent on wave period, and for surging waves, where it is much less dependent. According to Hawkes (1999), Hedges and Reis (1998) method seems the most promising.

Schuttrumpf *et al.* (2001) performed large-scale model tests with natural spectra from field measurements which are multi peaked due to the influence of the foreshore. Schuttrumpf *et al.* (2001) concluded that the peak period (T_{po}) is of limited use for describing run up and overtopping and have proposed the mean period (T_{mo}) instead, as it appears in Table 2.2.2.

2.4 Effect of structure geometry

The overtopping discharge, as seen from Tables 2.1.1 and 2.2.2, is also dependent on the structure geometry. The most important parameter is the crest freeboard (Koford, 2002). However a number of other parameters describing the structure

geometry also influence the overtopping discharge. These parameters are considered in the following.

2.4.1 Surface roughness and permeability

Obviously, introducing surface roughness and permeability of the slope will reduce the overtopping discharges compared with an impermeable and smooth slope. Both Van der Meer and Janssen (1995) and Owen (1980) have given reduction factors to take this into account.

2.4.2 Crest width

Both Juhl and Sloth (1995) and Hebsgaard *et al.* (1998) have incorporated the effect of the width of the crest on the overtopping discharge by modifying the crest level in the expression for the overtopping discharge, depending on the crest width. As would be expected an increasing crest width results in decreasing overtopping discharges in the same roughness and permeability conditions (Koford, 2002).

2.4.3 Slope angle and shape

The dependency of the slope angle is typically included in the prediction formulae via ξ_p, i.e., in Van der Meer and Janssen (1995). However according to Van der Meer and Janssen (1995) the dependency of ξ_p disappears for surging waves. Other authors have made various statements regarding the influence of slope angle and shape that are reverent to the present study.

Le Méhauté *et al.* (1968) also quote Grantham (1953) who stated that maximum run-up occurs for a given incident wave for slope angle $\alpha=30^o$.

In TACPAI (1974), it is mentioned that convex slopes increase run-up. According to CIRIA / CUR (1991) the slope angle becomes less important as crest heights are lower and larger overtopping occurs.

2.4.4 Crest level

Oumeraci *et al.* (1999) investigated overtopping of seawalls with very low crest freeboards (R_c down to zero) caused by high water levels. Their results agreed well with those of Van der Meer and Janssen (1995) for relative crest freeboards in the range tested by Van der Meer and Janssen (1995). However, for relative crest freeboards R $\left(R = {R_c}/{H_s} \right)$ close to zero the tests by Oumeraci *et al.* (1999) show that the expression given by Van der Meer and Janssen (1995) overpredicts the average overtopping discharge. These data are also used by Schuttrumpf *et al.* (2001) to establish the overtopping expressions for no freeboard condition, as referred to in Table 2.2.2.

2.5 Accuracy of overtopping discharge predictions

Douglass (1986) reviewed and compared a number of methods for estimating irregular wave overtopping discharges. He concluded that calculated overtopping discharges using empirically derived equations should only be considered within a factor of 3 of the actual overtopping discharge. The methods considered deal with overtopping of coastal defense structures, and so the typical crest freeboards are relatively high and the overtopping discharges low. Under such conditions the overtopping discharge depends on relatively few and relatively large overtopping events, which again means that the overtopping discharge becomes very sensitive to the stochastic nature of irregular waves. It is expected that the uncertainty of

the overtopping discharge estimation will be reduced as the crest freeboard is reduced, since more and more of the waves overtop the structure (Koford, 2002).

2.6 Theoretical and numerical calculations

Hiroyoshi and Kono (1970) presented an overtopping expression based on a weir analogy. The expression was verified by model tests with regular waves. The dimensionless overtopping formula is:

$$\frac{q}{TH\sqrt{2gH}} = \frac{2}{15} mk^{3/2} \left(1 - \frac{z_o}{kH}\right)^{5/2} \qquad (2.6.8)$$

where, $k = z_m / H$ and z_m is the vertical distance between mean sea water surface and wave crest.

Based on this model Oezhan and Yalciner (1991) introduced an analytical model for solitary wave overtopping of a seawall.

Another method based on wave energy considerations is used by Umeyama (1993) to formulate the wave overtopping discharge on a vertical barrier, and the model is compared with physical model tests.

The recent years many attempts have been made to numerically model wave overtopping. Kobayashi and Wurjanto (1989) performed numerical modelling of regular wave overtopping of impermeable coastal structure on sloping beach. Their numerical model is used to predict the fairly detailed hydrodynamics associated with wave overtopping over the crest of a smooth impermeable seawall located on a sloping beach.

Hiraishi and Maruyama (1998) presented a numerical model for calculation of overtopping discharges for a vertical breakwater in multi directional waves. The

basic assumption is that the overtopping discharge can be described by a weir expression as suggested by Hiroyoshi and Kono (1970).

Hu *et al.* (2000) presented a 2-D numerical model for calculation of overtopping using non-linear shallow water equations. However, even this very recent study was primarily validated using regular waves.

It seems that even with the computing power available today the task of numerical modelling of wave overtopping processes is still very demanding. However, once the computational power is sufficient, methods like the ones mentioned above, as well as other methods based on, e.g. volume of fluid (VOF), probably will be able to predict overtopping discharges also in irregular and 3-D waves. This will make it possible to study the overtopping process in greater detail than is possible in physical model tests. Again this will make it easier to design structures that better fulfil their purpose than do the structures of today (Koford, 2002).

2.7 Numerical simulation of wave overtopping in breaking zone

Breaking waves in surf zone play an essential role in nearly all-coastal processes. Breaking waves generate strong turbulence and are in general accompanied by strong energy dissipation. Breaking wave also modify wave forces on the coastal structures when the wave-structure interaction occurs. On the other hand, wave overtopping is a complex process to model which involves shoaling, wave reflection, wave breaking and turbulence and in which the random nature of the waves must be taken into account.

The total volume of sea water overtopping in a particular storm is generally well predicted by current methods [Owen (1980), Van der Meer and Janssen (1995)

and Hedges and Reis (1998)]. However, Goda (2000) has showed that current formulae, which do not take full account of the complexity of wave breaking in shallow water, can significantly underestimate overtopping discharges. Analysis by Besley *et al.* (1998) shows that methods that exclude these effects can severely underestimate overtopping under breaking wave conditions, a finding supported by the numerical study of Hu *et al.* (2000).

The simulation of breaking wave has been a challenging problem to many coastal researchers due to the complicated flow and turbulence structures. Recently, Lin and Liu (1998) presented a two-dimensional numerical model which solves the Reynolds Averaged Navier-Stokes (RANS) equations for mean flow field and the ($k-\varepsilon$) equations for turbulent kinetic energy, *k*, and the turbulence dissipation rate, ε. In this model the volume of fluid (VOF) algorithm (Hirt and Nichols, 1981) method is employed to track the free surface movements. Liu *et al.,* (1999) extended the model by adding the capability of simulating flows in porous media and an improved $k-\varepsilon$ turbulence model with a non-linear algebraic Reynolds stress closure model is applied to describe the corresponding turbulence field. Lin and Liu, (1999) added an internal designed mass source functions for the equation of mass conservation in the internal flow region source to generate specific wave trains. The model is extended to simulate any kind of spectrum sea waves which is represented by a superposition of a finite number of linear wave modes with different wave height and wave period. Soliman *et al.,* (2003) simulated and used the JONSWAP spectrum for studying random wave overtopping. More details about the numerical breaking wave model are presented in Chapter 4.

2.8 Wave overtopping at zero freeboard

The existing formulae for wave overtopping do not account for the case of zero freeboard (R_c=0). Schuttrumpf *et al.* (2001) reported that the existing overtopping models for average overtopping rates by Van der Meer and Janssen (1995) and Van Gent (1999) are not valid for the boundary conditions R_c=0.

Within the project "Loading of the inner slope of sea dikes by wave overtopping" (BMBF KIS 009) small and large scale model tests were performed to investigate the overtopping flow field and the interaction of wave overtopping with the soil properties. The small-scale model tests were performed in the small flume of the Leichtweiss Institute (LWI) for Hydraulics of the Technical University of Braunschweig. A more detailed description of the small-scale model tests is given by Oumeraci *et al.* (1999). The large-scale tests were performed in the large wave channel (GWK) of the Coastal Research Centre FZK, Hannover. More details of the large-scale model tests can be found in Oumeraci *et al.* (2001).

Both models tests have been carried out with theoretical wave spectra like TMA or JONSWAP-spectra and with actually measured wave spectra in the field. Wave spectra have been collected from the German North Sea coast and Baltic coast and from the Dutch coast.

Schüttrumpf (2001) conducted model tests with zero freeboard (R_c=0) and without overtopping (R_c>R_{max}) and derived the following formulae:

$$Q = \frac{q}{\sqrt{2gH_s^3}} = 0.038.\xi_m \exp\left(-b\frac{R_c}{R_{u,2\%}}\right) \qquad \xi_m < 2 \qquad (2.8.9)$$

$$Q = \frac{q}{\sqrt{2gH_s^3}} = (0.096 - \frac{0.160}{\xi_m^3})\exp\left(-b\frac{R_c}{R_{u,2\%}}\right) \qquad \xi_m \geq 2 \qquad (2.8.10)$$

with: $R_{u,2\%}$ = run-up height exceeded by 2% of the incident waves $\left(=\xi_m \times H_s\right)$.

The results of Schüttrumpf (2001) are validated and extended for statistical overtopping parameters based on both the small scale (Oumeraci *et al.*, 1999) and the large scale model (Oumeraci *et al.*, 2001).

Analysing the small-scale model tests for natural sea spectra and also for theoretical wave spectra (TMA) it was found, that the model by Schüttrumpf (2001) fits the laboratory data well. The dimensionless overtopping parameters show scattering for natural wave spectra. The reliability of the overtopping function is given by taking the b-coefficient as a normally distributed stochastic variable with an average of -3.67 and a standard deviation of 0.55 (Oumeraci *et al.*, 2001).

As mentioned before, the natural wave spectra collected at the German and Dutch coasts are generally multi peak spectra with a complex shape. The wave spectra will be divided into spectra that are measured in Wadden seas and estuaries and in spectra from open coasts.

The more generic overtopping function developed by Schüttrumpf (2001) lies between that one for open coasts and that one for Wadden seas and estuaries. The generic formula by Schüttrumpf (2001) can be used for all natural wave spectra because it fits for all data as well as the special functions. The standard deviation σ is similar for all formulas (Oumeraci *et al.*, 2001).

2.9 Wave overtopping and overflow

Existing defences, particularly those of more mature design, are likely to have been designed and constructed without the benefit of recent research on the

impacts of climate change on water levels and wave conditions. In many places, still water levels are predicted to rise. Furthermore, changes in atmospheric climate patterns may lead to potentially adverse changes in near shore wave conditions. The net result being that, without remedial works, existing structures will provide a diminishing level of service in relation to their original design. In turn this is likely to be accompanied by increased overtopping and incidence of flooding. Under extreme storm conditions, where high tide levels may be accompanied by meteorological surge, wave and wind set-up, the sea defences may operate under situations of small or even negative freeboard. For strategic and emergency response planning it is helpful to have some means of providing reliable estimates of flood volumes under these conditions. Existing design formulae exist for both overflow and overtopping, but not in combination. Furthermore, most empirical overtopping formulae have been derived on the basis of sets of laboratory experiments in which the freeboard is relatively large. Overflow and overtopping are often treated as separate mechanisms, whereas they are part of a continuum of hydrodynamic processes that can lead to severe flooding and damage to flood defences. In part this separation of processes is due to very distinct structural design criteria for each case; seawalls are designed to limit overtopping and weirs are designed for particular overflow characteristics.

However, this means that for the situations described above there is a gap in the guidance that current design formulae can provide. Namely, for negative freeboard when combined overtopping and overflow occurs.

CHAPTER 3

SOLA-VOF

The numerical model (SOLA-VOF) is based on the Navier-Stokes Equations (NSE) which describe the motions of essentially any fluid. The SOLA-VOF code calculates the solution of two-dimensional transient fluid flow with free boundaries and is based on the fractional volume of fluid (VOF) concept. In this chapter the mathematical equations governing fluid motion will be presented in Section 3.2. The volume of fluid (VOF) technique is given in section 3.3 and then is followed by the numerical implementation of the model. The boundary conditions of the model are illustrated in section 3.5. The behaviour of the open boundary condition in three cases of study will be presented in section 3.6.

3.1 Introduction

In structural dynamics, it is customary to employ Lagrangian coordinates as the basis for numerical solution algorithms. In fluid dynamics both Lagrangian and Eulerian coordinates have been used with considerable success. Because each coordinate representation has unique advantages and disadvantages, the choice of which representation to use depends on the characteristics of the problem to be solved. Lagrangian methods are characterized by a coordinate system that moves with the fluid. Accordingly, each computational cell always contains the same fluid elements. Body and surface forces on these elements are easy to define, so it is relatively straightforward to compute the dynamic response of the elements. In an Eulerian representation the grid remains fixed and the identity of individual

fluid elements is not maintained. The two methods differ, however, in the manner which the fluid elements are moved to next positions after their new velocities have been computed. In the Lagrangian case the grid simply moves with computed element velocities while in an Eulerian calculation it is necessary to compute the flow of fluid through the mesh. The main advantage of the Eulerian approach is that the fluid can undergo arbitrarily large distortions without loss of accuracy, in contrast to Lagrangian methods. In particular, for problems where free boundaries undergo large deformations it is difficult to use Lagrangian methods (Nichols *et al.*. 1980); SOLA-VOF, solves the Eulerian equations of water for fluid dynamics problems involving free boundaries.

Eulerian finite-difference methods for computing the dynamics of incompressible fluids are well established. The first method to successfully treat problems involving complicated free surface motions was the Marker and cell (MAC) method (Harlow and Welch, 1965). This method was also the first technique to use pressure and velocity as the primary variables. The MAC method employed a distribution of marker particles to define fluid regions, and simply set free surface pressure at the centres of cells defined to contain the surface. No attempt was made to apply the pressure boundary condition at the actual location of the boundary with / in the surface-containing cell. This crude approximation was improved (Chan and Street, 1970) and marker particles were eliminated in favour of particle chains on the free surfaces (Nichols and Hirt, 1971). A simplified version of the basic solution algorithm (SOLA) used in the MAC method is available in a user-oriented code called SOLA. Although SOLA does not treat

free surfaces, an extended version, SOLA-SURF uses a surface height function method (Hirt *et al.*, 1975). The basic simplicity and flexibility of the SOLA codes makes them excellent foundations for the development of more sophisticated codes. For this reason, a variable mesh version of the SOLA code, SOLA-VM, was chosen as a basis for the VOF technique. An experimental version of this new code, SOLA-VOF, was first reported in Nichols and Hirt (1975). The SOLA-VOF code, which considers the basic for most of the VOF type numerical models as shown in Table 3.1.1, is used in the first part of this study (Chapter 3). Since that time, many improvements have been made and the basic technique has matured through applications to a wide class of problem. For example McMaster and Gong (1979) and McMaster *et al.* (1980) have combined the SOLA-SURF code with a different interface tracking technique based on a VOF-like concept. Nichols *et al.* (1980) presented the updated version of SOLA-VOF code which has been used during the first part of this study. This general purpose code was selected because it has very promising features and is generally acknowledged as the basis for all subsequent developments. Figure 3.1.1 shows the family tree of VOF numerical models. The NASA-VOF2D code (Torrey *et al.*. 1985) contains many improvements. A partial-cell treatment FAVOR allows for curved or sloping boundaries without the need for curvi-linear coordinates.

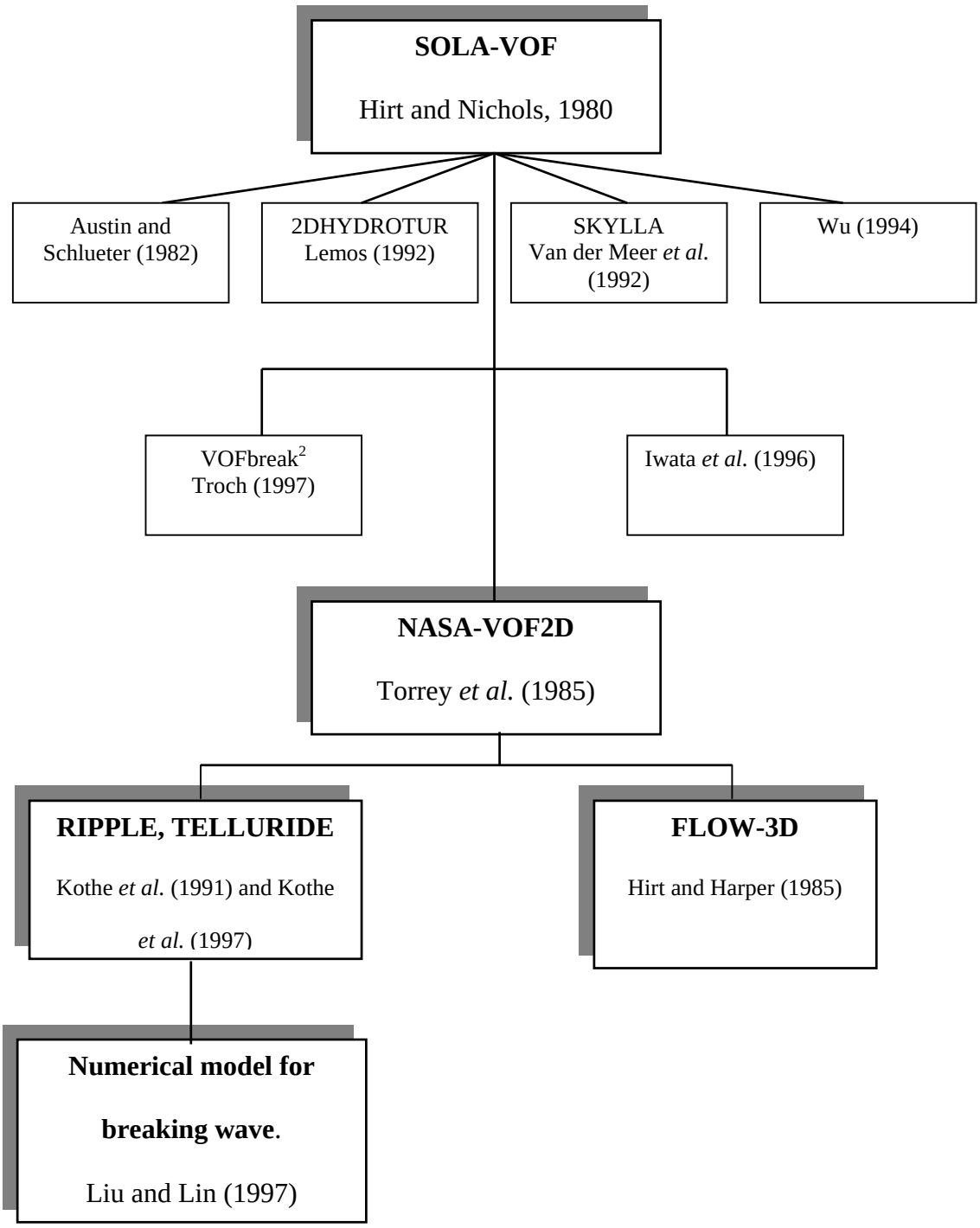

Figure 3.1.1: Overview of key developments of VOF type numerical models.

SOLA-VOF and NASA-VOF2D codes have been developed at Los Alamos National Laboratory, (LANL), New Mexico, USA. After that, Hirt continued developments on the VOF model in the commercial CFD code FLOW-3D. It is regarded as a state-of-the-art CFD code with general applicability. At LANL, other successor codes have been developed since then: RIPPLE (Kothe *et al.,* 1991) for 2D and TELLURIDE (Kothe *et al.,* 1997) for 3D simulations were developed at Los Alamos National Laboratory. In RIPPLE and TELLURIDE, a projection method is used to solve the incompressible flow. The pressure Poisson equation is solved with an incomplete Cholesky conjugate gradient technique. Particularly, the modelling of problems in which the surface tension is important, such as the filling, cooling and solidification processes of castings have been enhanced.

Austin and Schlueter (1982) presented the first application of the SOLA-VOF model in the field of coastal engineering. The model predicted the flow field in a porous armour layer of a breakwater schematised as a rectangular block system. Although in a relatively crude form, these calculations were the start of the simulation of wave propagation and interaction with structures in coastal engineering. Lemos (1992) incorporated a $k-\varepsilon$ turbulence model in a SOLA-VOF based code 2DHYDROTUR that allowed a limited description of the turbulence field. Lemos (1992) also implemented higher order finite difference schemes in a VOF-based code for improving stability and accuracy of the numerical solutions. These improved schemes were applied to simulations of wave impact on structures, and included the computation of the wave impact

forces. No wave absorption boundaries or open sea boundaries have been implemented. The SKYLLA model (Van der Meer *et al.,* 1992) was developed at Delft Hydraulics. The first computations showed that it is possible to simulate breaking waves on a slope. Several extensions have been added since then. The most important is the inclusion of a conjugate gradient solver for the pressure Poisson equation (Van der Meer *et al.,* 1992). Wu (1994) applied a VOF model based on the SOLA-VOF model for the simulation of breaking and non-breaking wave kinematics at and on vertical structures with various impermeable foreshore geometries. Wu (1994) simulated the complete impact pressure and the resulting loading while neglecting entrapped air. A weakly reflecting boundary condition similar to the SKYLLA model has been implemented in Wu's model. Iwata *et al.* (1996) used a modified SOLA-VOF model for numerical comparison with experimental data from breaking and post-breaking wave deformation due to submerged impermeable structures. Waves were generated internally in the computational domain using the source generation technique (Brorsen and Larsen, 1987). Absorption of the waves was done using the Sommerfeld radiation boundary condition. Troch (1997) presented the numerical model VOFbreak^2 based on the SOLA-VOF code. Several modifications are implemented to refine the numerical model for wave motion on and in coastal structures. Special attention is paid to applications involving rubble mound breakwaters. Wave boundary conditions are added, where any wave theory can be applied to provide the surface elevation and the velocity components in horizontal and vertical direction. The governing equations have been extended, to include the simulation

of porous flow inside the permeable coastal structure. The numerical model has been verified with both physical model data and prototype data. Some selected improvements from NASA-VOF2D have been implemented into VOFbreak^2, such as a numerical deformer technique, and fixes on the donor–acceptor algorithm. Liu and Lin (1997) presented a numerical model for calculating the evolution of a breaking wave. The model is a combination of a modified version of RIPPLE (Kothe *et al.,* 1991) and $k-\varepsilon$ turbulence model. The breaking wave numerical model is used in the second part of this study. More details of the breaking wave numerical model and its developments are presented in Chapter 4. Isobe *et al.* (1999) and Isobe (2001) developed a numerical wave flume for practical use in designing maritime structures which based on NASA-VOF2D. The computer code was named "CADMAS-SURF" which was open for general uses.

3.2 Mathematical formulation of SOLA-VOF

3.2.1 Navier-Stokes equations (NSE)

Any flow of an incompressible Newtonian fluid subject to gravity can be described in the three dimensional flow by the Navier Stokes equations in a bounded domain Ω:

$$\frac{\partial u_i}{\partial t}+u_j\frac{\partial u_i}{\partial x_j}=-\frac{1}{\rho}\frac{\partial p}{\partial x_i}+g_i+\frac{1}{\rho}\frac{\partial \tau_{ij}^m}{\partial x_j} \tag{3.2.1}$$

$$\frac{\partial u_i}{\partial x_i}=0 \tag{3.2.2}$$

The above equations represent the conservation of momentum and mass per unit mass in which u_i is the i-th velocity vector component (m/sec.), ρ the fluid

density (kg/m^3), p the pressure (N/m^2), g_i the i-th component of the gravitational acceleration (m/s^2), and τ_{ij}^m the molecular viscosity stress tensor (N/m^2).

The momentum equation is derived from Newton's second law which state that the rate of increase of momentum of a fluid particle is equal to sum of the forces on the fluid particle. The conservation equation is based on the concept of mass balance for a fluid element, *i.e.* the rate of increase of mass in a fluid element is equal to net rate of flow of mass into the fluid element. Details for the derivation of the Navier Stokes equations can be found in Versteeg and Malalasekera (1995). For a Newtonian fluid, $\tau_{ij}^m = 2\mu\sigma_{ij}$ with μ being the molecular viscosity (kg/m.sec.) and $\sigma_{ij} = \frac{1}{2}\left(\frac{\partial u_i}{\partial x_j} + \frac{\partial u_j}{\partial x_i}\right)$, the rate of the strain tensor.

The kinematic boundary which describes the free surface motion is expressed as,

$$\frac{\partial p}{\partial t} + u_i \frac{\partial p}{\partial x_i} = 0 \qquad (3.2.3)$$

3.3 Free surface fluid flow

3.3.1 Introduction

The accurate tracking of the free surface is very important for wave simulations. As mentioned earlier in Section 3.1, there are two types of approaches, Eulerian and Lagrangian. The Eulerian approach, which is more consistent with most of solvers of the NSE, tracks changes at fixed locations. This approach is the basis of the so-called volume of fluid (VOF) method originally developed by Nichols *et al.* (1980) and Hirt and Nichols (1981). The Lagrangian approach follows each particle on the free surface and/or in the interior domain based on the ambient

flow velocities. A brief review of these numerical algorithms for the analysis of viscous flows with moving interface is presented in the following sections.

3.3.2 Eulerian methods

Eulerian methods are characterized by a coordinate system that is either stationary in the laboratory reference frame or moving in a certain prescribed manner in order to accommodate the continually changing shape of the solution domain (Floryan and Rasmussen, 1989). The Eulerian algorithms can be divided into three main types: fixed grid methods, adaptive grid methods, and mapping methods.

3.3.2.1 Fixed grid methods

In this method the grid is fixed in the domain. There are two basic ways of tracking the interface, i.e., surface tracking and volume tracking. The surface tracking methods represent an interface as a series of interpolated curves through a discrete set of points on the interface. At each time step, the information about the location of the points and sequence in which they are connected is saved. The points are then moved according to an interface evolution equation. The information regarding location as well as orientation and curvature of the interface is explicitly available during the whole calculation process.

The volume tracking methods do not store a representation of the interface but reconstruct it whenever necessary. The reconstruction is done cell by cell and is based on the presence of a marker quantity within the cell.

MAC method

The simplest reconstruction algorithm for the volume tracking method has been proposed by Welch *et al.* (1966) as part of the MAC method. The MAC method marks different fluids with massless marker particles. The interface is defined as being somewhere inside the cells that contain marker particles of both fluids. The MAC method does not give any details of the exact location, orientation, and the curvature of the interface.

Volume of Fluid Method (VOF)

Many reconstruction algorithms use the fraction of cell volume occupied by one of the fluids as the marker quantity. If this fraction is 0 for a given cell, the fluid does not occupy the cell and there is no interface in that cell. Conversely, if the fraction is 1, the cell is completely occupied by the fluid and again there is no interface present. An interface is to be constructed only if the fraction is between 0 and 1. Since there is only one piece of information regarding the interface per cell available, certain arbitrariness is reconstructing the shape of the interface has to be allowed. The accuracy with which the reconstructed interfaces approximate the real interface is difficult to judge and different types of distortions are possible (Barr and Ashurst, 1984). The VOF (volume of fluid) method of Hirt and Nichols (1981) defined a function F (x,y,t) that is equal to unity at any point occupied by fluid and zero elsewhere. When averaged over the cells of a computational mesh, the average value of F in a cell is equal to the fractional volume of the cell occupied by fluid. In particular, a unit value of F corresponds to a cell full of fluid, whereas a zero value indicates that the cell contains no fluid. Cells with F

values between zero and one contain a free surface. The VOF method requires only one storage for each mesh cell, which is consistent with the storage requirements for all other dependent variables.

In addition to defining which cells contain a boundary, the F function can be used to define where fluid is located in a boundary cell. The normal direction to the boundary lies in the direction in which the value of F changes most rapidly. Because F is a step function, however, its derivatives must be computed in a special way, as described below. When properly computed, the derivatives can then be used to determine the boundary normal. Finally, when the normal direction and the value of F in a boundary cell are known, a line cutting the cell can be constructed that approximates the interface there. In addition, surface curvatures can be computed for the definition of surface tension forces.

The time dependence of F is governed by the equation,

$$\frac{\partial F}{\partial t} + u\frac{\partial F}{\partial x} + v\frac{\partial F}{\partial y} = 0 \tag{3.3.4}$$

For a computational cell centred at (i,j) the above equation can be rewritten in the following finite difference form,

$$F_{i,j}^{n+1} = F_{i,j}^{n} - \frac{\Delta t}{\Delta x_i}\left(u_{i+\frac{1}{2},j}^{n+1} F_R^n - u_{i-\frac{1}{2},j}^{n+1} F_L^n \right) - \frac{\Delta t}{\Delta y_i}\left(\upsilon_{i,j+\frac{1}{2}}^{n+1} F_T^n - \upsilon_{i,j-\frac{1}{2}}^{n+1} F_B^n \right) \tag{3.3.5}$$

in which F_R^n, F_L^n, F_T^n and F_B^n denote the F values on the right, left, top and bottom faces of the computational cell, respectively.

In an Eulerian mesh, the flux of F moving with the fluid through a cell must be computed, the standard finite difference form would lead to a smearing of the F function and interfaces would lose their definition. Fortunately, the fact that F is a

step function with values of zero or one, permits the use of a Donor-Acceptor method which was originally developed by Johnson (1970). Thus, the VOF technique provides a means of following fluid regions through an Eulerian mesh of stationary cells. The VOF method uses a minimum of stored information, and because it follows regions rather than boundaries, it avoids problems associated with intersecting surfaces. The VOF method was also be extended to three-dimensional computations, where its conservative use of stored information is advantageous.

3.3.2.2 Adaptive grid methods

Adaptive grid methods alter the computational grid so that the interface always coincides with one of the grid lines. The interface is then a well-defined, continuous curve and information regarding its location, orientation, and curvature is readily available. The main advantage of this approach is that it is possible to maintain sharp resolution of the interface, while the disadvantage is the difficulty in adjusting the grids to follow the highly deformed interfaces (Floryan and Rasmussen, 1989).

3.3.2.3 Mapping methods

In the mapping method the unknown irregularly shaped flow domain is transformed onto a fixed regularly shaped computational domain. The mapping appears explicitly as one of the unknown functions and has to be determined together with the field variables (Floryan and Rasmussen, 1989).

3.3.3 Lagrangian methods

Lagrangian methods are characterized by a coordinate system that moves with the fluid. Accordingly, each computational cell always contains the same fluid elements. These methods are suited for moving boundary problems as they permit material interfaces to be specifically delineated and precisely followed. The main two problems with the Lagrangian methods are mesh tangling and numerical inaccuracy due to highly irregular meshes (Floryan and Rasmussen, 1989). The mesh-tangling problem arises because a mesh fixed topology quickly becomes singular in flows undergoing large distortions as shown in Figure 3.3.2.

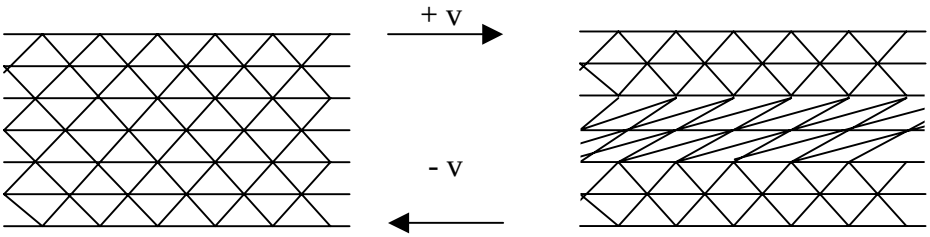

Figure 3.3.2: Grid deformation for a shear flow calculation using a Lagrangian triangular grid (Floryan and Rasmussen, 1989).

3.3.4 Discussion

The methods developed for the analysis of moving boundary problems for the Navier-Stokes equations have been described very briefly. Among these, the volume of fluid (VOF) methods allows practical treatment of the complex free surface condition. In principle, the VOF method could be used to track any surface of discontinuity in material properties, in tangential velocity, or any other property. The particular case being represented determines the specific boundary

conditions that must be applied at the location of the boundary. The VOF method in conjunction with the marker and cell method (MAC) is employed in SOLA-VOF code and in the Two-dimensional breaking wave numerical model, (2-D BWNM), which is used in the second part of this study (Chapter 4).

3.4 Model implementation

The success of modelling wave propagation using the Navier-Stokes equations relies on the accuracy of the numerical solver to the mathematical equations which include the scheme to track the free surface. As mentioned before, the finite difference method is used throughout the computation. A rectangular computational domain is first discretized by $m \times n$ rectangular cells as sketched in Figure 3.4.3. Cells have variable sizes, Δx_i for the i^{th} column and Δy_j for the j^{th} row. All scalar quantities, i.e., p, are defined in the centre of the cells. The vector, i.e., the x-component and y-component of the mean velocities, u and υ, are defined in the cell faces as shown in Figure 3.4.3. The volume of fluid function F is used to identify mesh cell that contains fluid of density ρ_F. A free surface or interface cell (i,j) is defined as a cell containing a non-zero value of F and having at least one neighbouring cell (i ±1, j) or (i, j±1) that contains a zero value of F. Cells with zero F values are empty. Cells with non-zero F values and no empty neighbours are treated as cells full of ρ_F fluid (Nichols *et al.*, 1980).

Finite difference solutions of the four unknowns u, υ, p and F, are obtained as following:

1- Explicit approximations of the Navier–Stokes, (Equation 3.2.1), are used to compute the first guess for new-time-level velocities.

2- To satisfy continuity, Equation 3.2.2, the pressure–velocity iteration is used, pressures are iteratively adjusted in each cell and the velocity changes induced by each pressure change are added to the velocities computed in step 1.

3- The F function defining fluid regions must be updated to give the new fluid configuration. Repetition of these steps will advance a solution through any desired time interval. At each step, of course, suitable boundary conditions must be imposed at all mesh and free surface boundaries.

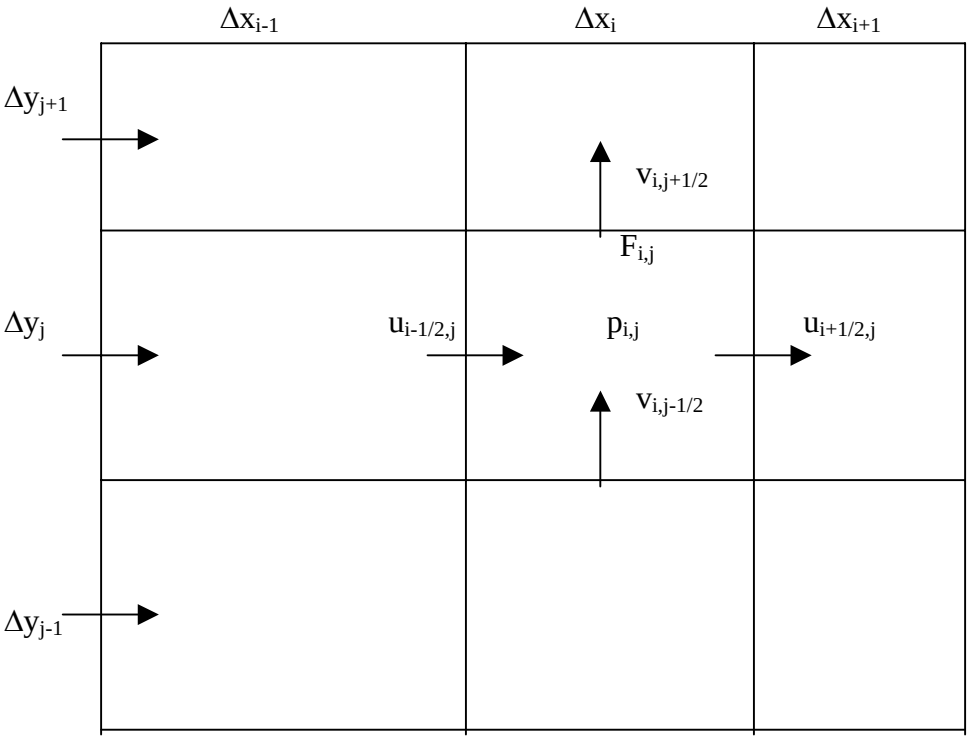

Figure 3.4.3: Finite difference meshes and cell classifications in SOLA-VOF model.

3.5 Boundary conditions

It is important to set boundary conditions at all mesh boundaries and at surface of all internal structures. In the following two sections the details of these boundary conditions is presented.

3.5.1 Mesh boundaries

Two conditions may be set using the layer of cells surrounding the mesh, the free slip condition and no-slip condition.

Consider for example the left boundary:

1- No-slip Condition: The normal velocity and the tangential velocity component are set to be zero for all j cells.

$u_{1,j} = 0$, $\upsilon_{1,j} = -\upsilon_{2,j}$, $p_{1,j} = p_{2,j}$ and $F_{1,j}=F_{2,j}$.

According to this condition, all components of the velocity on the bottom are zero, however, this boundary condition is applicable only when the resolution is fine enough to resolve the viscous boundary layer. If a coarse grid is used, the application of the no-slip condition can result in an underestimation of the velocity immediately above the bottom (Lin, 1998).

2- Free slip condition: The normal velocity must be zero and the tangential velocity should have no normal gradient for all j cells.

$u_{1,j} = 0$, $\upsilon_{1,j} = \upsilon_{2,j}$, $p_{1,j} = p_{2,j}$ and $F_{1,j}=F_{2,j}$.

This condition provides more accurate velocity information near a solid boundary (Lin, 1998). For that reason, the free slip condition is used in this study instead of the no-slip condition on the solid boundary.

3.5.2 Free surface boundary conditions

This boundary condition is satisfied by setting the surface cell pressure ($p_{i,j}$) equal to the value obtained by a linear interpolation between the pressure specified at the surface (p_s) and the pressure inside the fluid (p_n). For this scheme to work, the adjacent cell chosen for the interpolation should be such that the line connecting its centre to the centre of the surface cell is closest to the normal to the free surface (Nichols *et al.*, 1980). An equation for the surface, S, giving this result is

$$S = (1-\eta)\,p_n + \eta\,p_s - p_{i,j} \qquad (3.5.6)$$

where, ($\eta = d_c / d$) is the ratio of the distance between the cell centres and the distance between the free surface and the centre of the interpolation cell as shown in Figure 3.5.4 (Nichols *et al.*, 1980).

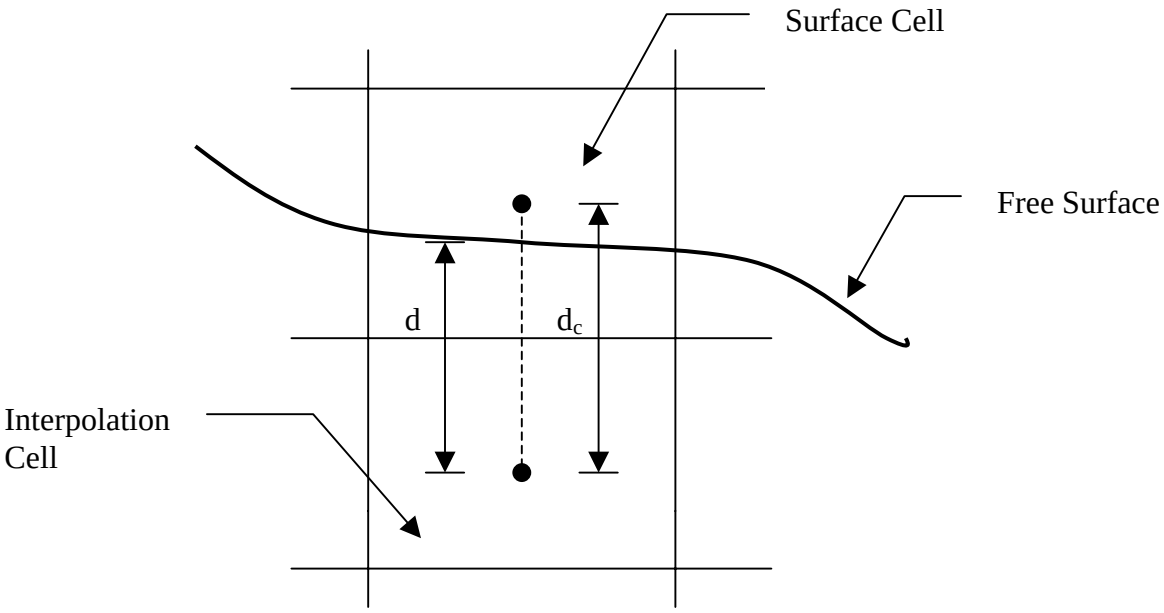

Figure 3.5.4 Definition of quantities used in defining free surface pressure boundary condition.

3.5.3 Open (Radiation) outflow boundary condition

A radiation boundary condition is used at the open sea boundary to minimise non-physical wave reflections. The open boundary condition, which is also referred to as the radiation boundary condition, is then needed to allow the wave going out of the computational domain without significant reflection.

The mathematical formulation of the open boundary condition on the right side of the computational domain is described as follows:

$$\frac{\partial \phi}{\partial t} + C_o \frac{\partial \phi}{\partial x} = 0 \tag{3.5.7}$$

where, C_o is the phase celerity of wave at the open boundary and ϕ represents the wave property such as the mean velocities or mean free surface displacement (Lin, 1998).

The phase velocity is calculated as follows, with neglecting variations in the atmospheric pressure:

$$C_o = \sqrt{\frac{gL}{2\pi} \tanh\left[\frac{2\pi}{L}(d+a)\right]} \qquad \text{for short wave} \tag{3.5.8}$$

$$C_o = \sqrt{g(d+a)} \qquad \text{for long wave} \tag{3.5.9}$$

Other numerical test shows that this boundary condition works fairly well up to the intermediate non-linear waves, i.e., H/d < 0.3 (Lin, 1998).

3.5.4 Sponge boundary condition

Another alternative for the open boundary condition is absorbing (sponge) boundary condition. The absorbing boundary condition is allowing the generated and reflected waves to leave the computational domain. Larsen and Dancy (1983) presented an efficient numerical passive absorber for use in short wave models.

An absorption function a(x) is applied on velocities in a numerical sponge layer with length x_s after each time step calculation. As shown in Figure 3.5.5, the absorption function at the start of the sponge layer equals 1 and gradually decreases to 0 near the end. The sponge layer is located at the closed end of the wave flume. The width of the sponge layer can vary between (0.60 - 1.0) wavelength and the absorption function tubes an elliptic form (see e.g. Troch and De Rouck (1998)):

$$a(x) = \sqrt{1 - \left(\frac{x - x_1}{x_s} \right)^2} \tag{3.5.10}$$

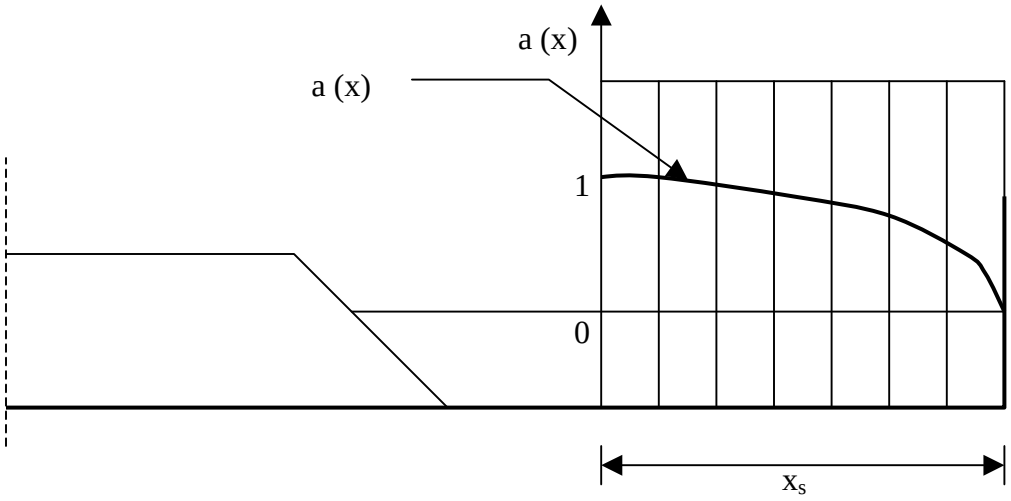

Figure 3.5.5: Numerical sponge layer with width x_s placed at the end of the numerical wave model (Troch and De Rouck, 1998).

The disadvantage of this latter method is that the length of the computational domain is considerably increased because a relatively long absorption layer is required for absorption of the generated and reflected waves at the boundaries.

3.5.5 Internal obstacle boundaries

An internal obstacle can be simulated by flagging those cells of a mesh that are to be blocked out. Because the relaxation factor $BETA_{i,j}$ used in the pressure iteration must be positive, using negative values of this variable is a suitable flag for obstacle cells. A convenient, but arbitrary choice, is to assign a value of BETA= -1.0 to obstacle cells. No velocities or pressures are calculated in obstacle cells, and all the velocity components on faces of obstacle cells are automatically set to zero. In the boundary conditions subroutine, values for volume fractions and pressure are set in all obstacle cells bordering fluid cells. These values are computed to be equal to the averages of these quantities in the adjacent fluid cells. All other obstacle cells have zero values for F and p. With this prescription, the fluid obstacle boundaries are prevented from being interpreted as free surfaces, as they would be without some sort of additional testing. In addition, it should be noted that because all velocity components within obstacle cells are set to zero, no-slip tangential velocity conditions at obstacle boundaries are only first order accurate. That is, tangential velocities are zero at locations shifted into the obstacles one-half of a cell width from the actual boundary location.

3.6 Model testing

Three cases of study are presented using the numerical model, SOLA-VOF (non-breaking numerical model). The first case is linear wave propagation on a

constant depth. Then a standing wave is generated in rectangular channel with a flat bed. Finally, the model is employed to study the non-breaking solitary wave run-up on a steep slope.

3.6.1 Linear wave theory

Linear wave theory was derived using the concepts of two-dimensional ideal fluid flow. This is a reasonable starting point for deep-water waves, which are not greatly influenced by viscosity, surface tension and turbulence. Figure 3.6.6 depicts a sinusoidal wave of wave length (L), height (H) and period (T).

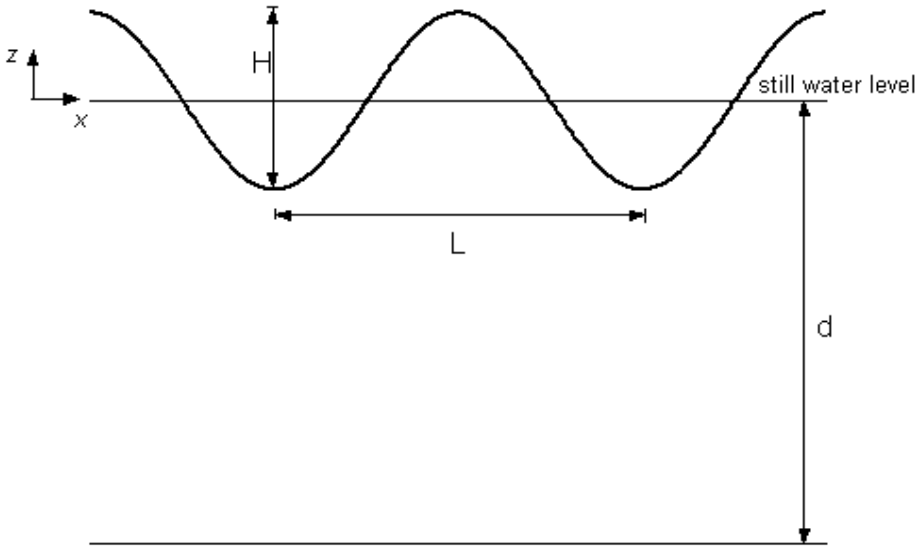

Figure 3.6.6: Definition sketch for the linear wave theory.

The variation of surface elevation with time, from the still water level, is denoted by η and given by:

$$\eta=\frac{H}{2}\cos 2\pi\left(\frac{x}{L}-\frac{t}{T}\right) \tag{3.6.11}$$

The corresponding equations for the horizontal (ζ, *u*) and vertical (ξ, υ) displacements and velocities of a particle at a mean depth (d) below the still water level are:

$$\zeta=-\frac{H}{2}\left[\frac{\cosh k(z+d)}{\sinh kd}\right]\sin 2\pi\left(\frac{x}{L}-\frac{t}{T}\right) \tag{3.6.12}$$

$$u=-\frac{\pi H}{T}\left[\frac{\cosh k(z+d)}{\sinh kd}\right]\cos 2\pi\left(\frac{x}{L}-\frac{t}{T}\right) \tag{3.6.13}$$

$$\xi=\frac{H}{2}\left[\frac{\sinh k(z+d)}{\sinh kd}\right]\cos 2\pi\left(\frac{x}{L}-\frac{t}{T}\right) \tag{3.6.14}$$

$$\upsilon=\frac{\pi H}{T}\left[\frac{\sinh k(z+d)}{\sinh kd}\right]\sin 2\pi\left(\frac{x}{L}-\frac{t}{T}\right) \tag{3.6.15}$$

3.6.2 Linear wave inflow boundary condition

The linear wave inflow boundary condition is programmed into the boundary condition subroutine of the SOLA-VOF code. In order to test the seaward linear wave boundary condition and the outflow radiation boundary condition, a simulation of regular wave propagation has been conducted as presented in the following subsection.

3.6.3 Linear wave propagation in constant water depth

In this simulation a sequence of regular waves with 1.0 m wave height, 3.0s wave period and 14.0 m wave length are introduced into 6.0 m deep still water. Comparison with the theoretical water level is presented in the Figure 3.6.7. Near the beginning of the domain, the regular wave level is observed with wave heights and lengths consistent with the theoretical calculation. After one wave length significant difference between the SOLA-VOF results and the theoretical one could be observed.

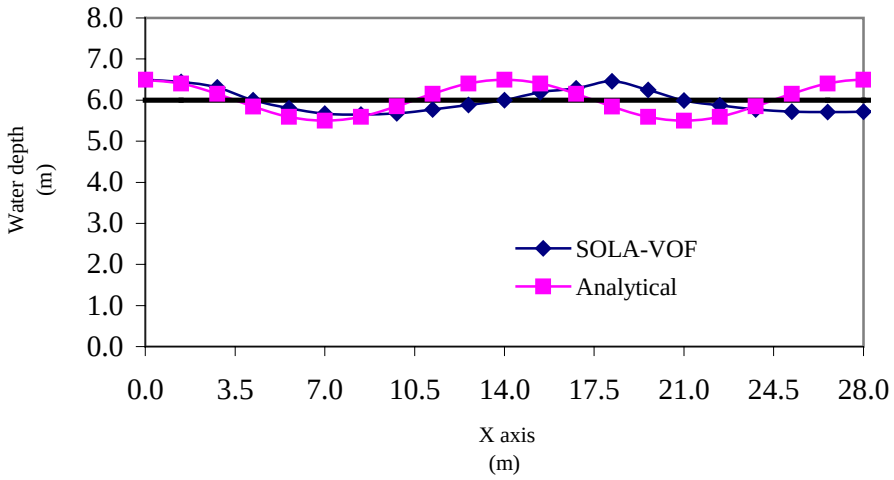

Figure 3.6.7: Comparison between the SOLA-VOF and the analytical free wave surface after t =21.0 sec. (T = 3.0 sec., L =14.0 m, H = 1.0 m and d =6.0 m).

This difference is due to insufficient efficiency of the open boundary condition at the end of the domain. The open boundary condition in SOLA-VOF still needs more improvement allowing all the amount of wave transfer to go out of the domain. Another reason may be the non-linearity of the input wave since $d/L < 0.5$.

3.6.4 Standing wave reflection at a vertical wall

A standing wave is generated in rectangular channel with a flat bed. The right boundary is considered to be an impermeable vertical wall with 100% reflection. The other end of the channel is an inlet boundary where sinusoidal waves are imposed. The incident sinusoidal generated wave height is 0.01 m with a wave period = 2.0 sec. and the mean water depth is 0.20 m. The length of the incident wave calculated by linear wave theory is 2.7 m. The channel is 5.4 m long which is equal to two wave lengths.

In total, 270 cells are used in the *x*-direction with a cell size of 0.02 m. In the *y*-direction 64 cells are used with a cell size of 0.005 m. The basic time step is 0.04 second and the simulation time is t=8.0 seconds. After approximately 6.0 seconds, theoretically, the above arrangement creates standing waves with a height of 0.04 m as shown in Figure 3.6.8. Computationally, this provides an opportunity to test the obstacle boundary condition at the end of the domain which is considered to be an impermeable vertical wall with 100% reflection. Figure 3.6.9 illustrates the simulated standing wave pattern by showing snapshots of the free surface configuration and velocity field at five time instants within a time interval of 0.5 sec. Troch and De Rouck (1999) studied same example with the same wave characteristics and water depth using VOFbreak^2 numerical model. Troch and De Rouck (1999) applied an active wave generating-absorbing boundary condition in start of the domain of study. Analytical comparison of the calculated free surface configuration and velocity field between SOLA-VOF and VOFbreak^2 numerical models gives approximately 90% agreement.

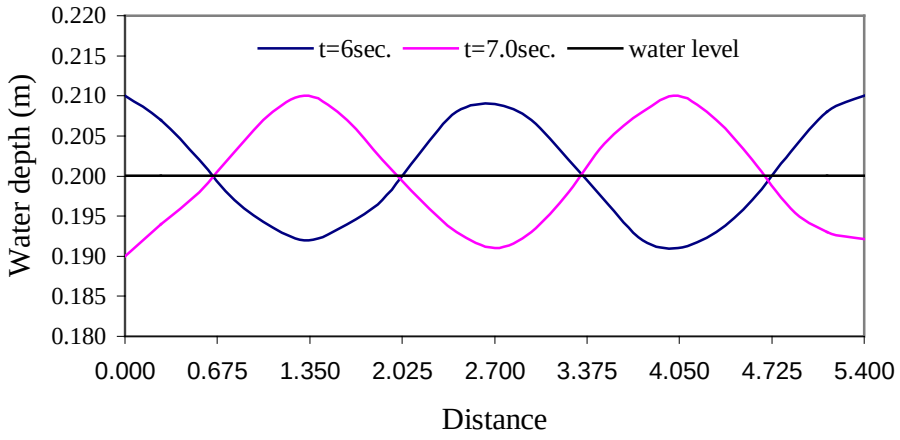

Figure 3.6.8: Computed standing waves due to reflection from a vertical wall (Incident wave characteristics Hi = 0.01 m, T = 2.0 s, d = 0.20 m).

The main difference between the previous two examples is the right boundary condition at the end of the domain. In the first example when the radiation boundary condition was used, significant difference between the numerical and theoretical free surface and wave velocity are observed (Figure 3.6.7). While in the second example when the impermeable vertical wall with 100% reflection used, good agreement was found (Figures 3.6.8 and 3.6.9). If the time of calculation exceeds than 8.0 seconds the free surface profile gives significant difference in comparison with the theoretical solution due to the inefficiency in the radiation boundary condition in the start of the domain.

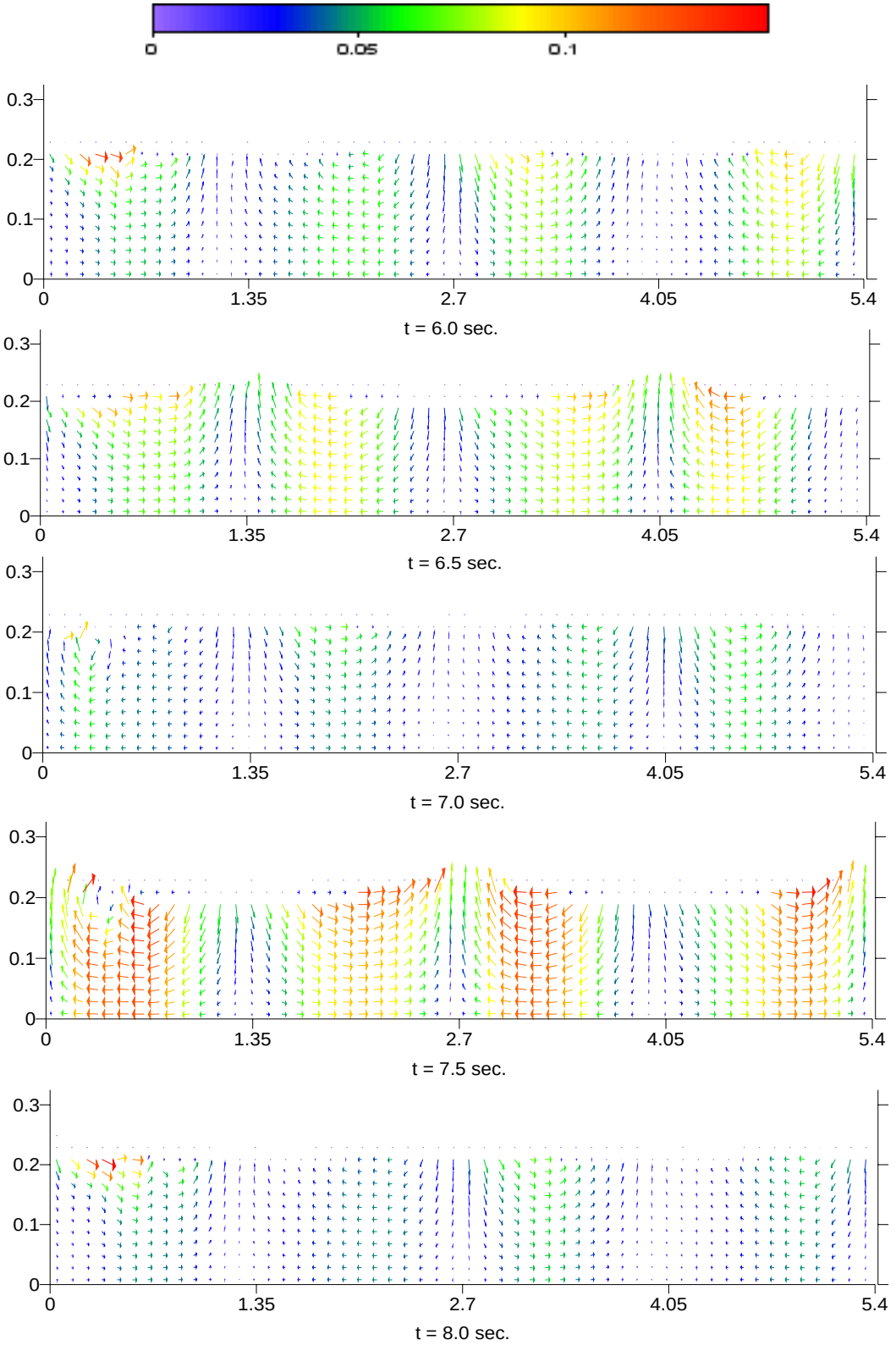

Figure 3.6.9: Snapshots of free surface configuration and velocity field for standing wave period. (Incident wave characteristics Hi = 0.01 m, T = 2.0 s, d = 0.20 m.)

3.6.5 Solitary wave inflow boundary condition

The solitary wave is a finite amplitude wave with permanent shape; the non-linearity and frequency dispersion are perfectly balanced during the wave propagation. The solitary wave form lies entirely above the still water level. It is a wave translation because the water particles are displaced a distance in the direction of wave propagation as the wave passes. Based on the potential flow approximation, a Boussinesq equation can be derived. The solitary wave is a special solution of the Boussinesq equation. The free surface of the solitary wave is given by (Liu and Lin, 1997):

$$\eta(x,t) = H \sec h^2 \left[\sqrt{\frac{3}{4}\frac{H}{d^3}} (x - ct) \right] \tag{3.6.16}$$

The solitary wave celerity is:

$$c = \sqrt{g(H + d)} \tag{3.6.17}$$

3.6.6 Non-breaking solitary wave run-up on beach

In this case of study, non-breaking solitary wave run-up on a steep beach with a slope of 30^o is investigated. The toe of the beach is 6.49 m away from the solitary wave boundary condition. The still water level is 0.18 m and the wave height is 0.03 m. The computational domain is discretized with a 140×20 cell uniform grid with Δx= 0.05m and Δy=0.015m. The wave celerity (c) and the free surface displacement η are specified at the left boundary conditions similarly to that in section 3-6-4. The results of the non-breaking solitary wave at time t = 4.0 and 4.2 sec. are shown in Figures 3.6.10 and 3.6.11. These time series are chosen to be consistent with results of Liu and Lin (1997). Comparison between the numerical

model results (SOLA-VOF) and experimental results of Liu and Lin (1997) gives good agreement in the velocity magnitude and direction.

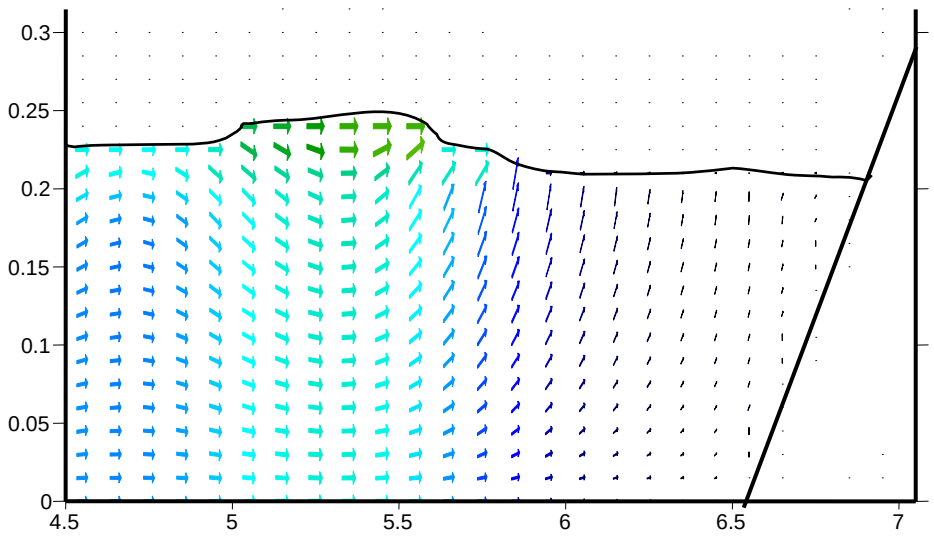

Figure 3.6.10: The velocities component according to the solitary wave theory at t=4.0 sec.

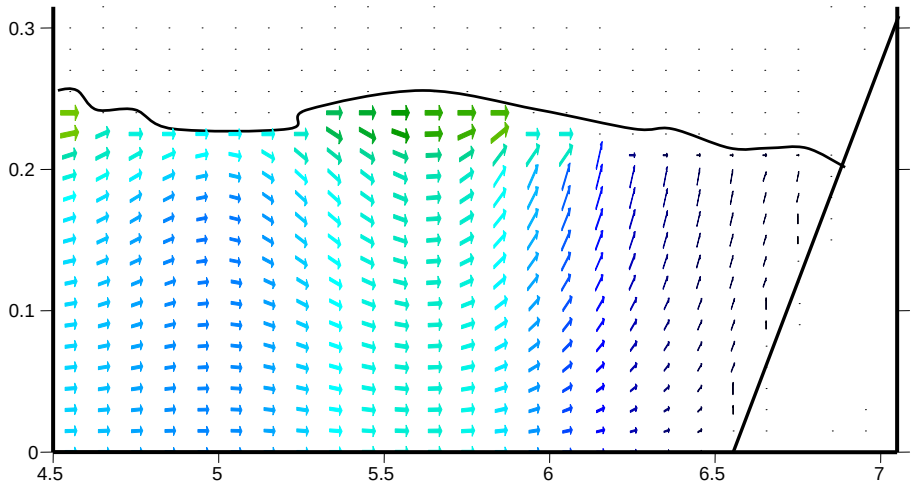

Figure 3.6.11: The velocities component according to the solitary wave theory at t=4.2 sec.

Figures 3.6.12 and 3.6.13 present comparison of free surface profile between modified SOLA-VOF and Liu and Lin (1997) numerical model. The comparison of the free surface profiles goes towards the same trend raised in the previous two examples (Sections 3.6.3 and 3.6.4).

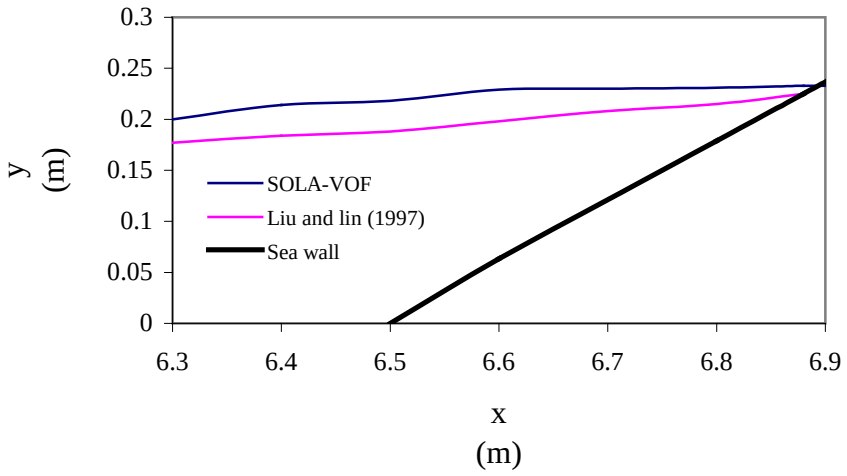

Figure 3.6.12: Comparison of the free surface elevation between SOLA-VOF and Liu and Lin's numerical models at t=4.0 sec.

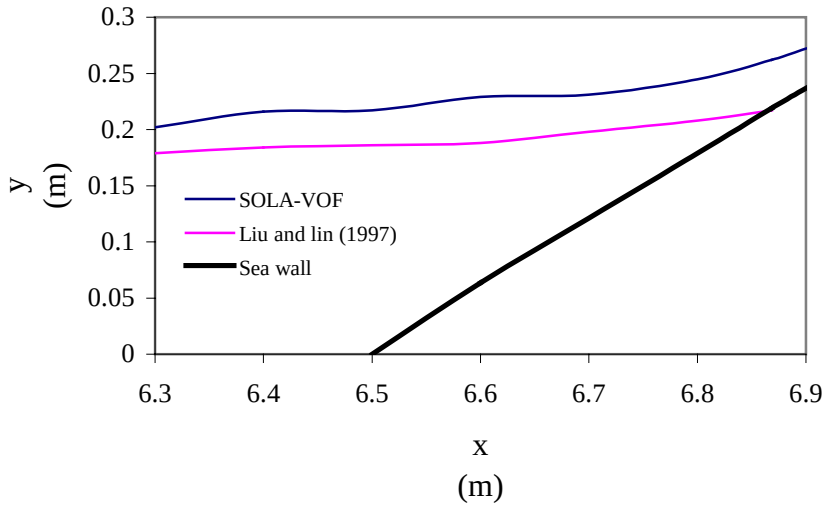

Figure 3.6.13: Comparison of the free surface elevation between SOLA-VOF and Liu and Lin's numerical models at t=4.2 sec.

It is clear from Figures 3.6.12 and 3.6.13 that at the boundaries, more efficient "open boundary" or "absorbing boundary" condition is required, allowing the transmitted and reflected waves to leave the computational domain without disturbing the interaction of the incident waves with the seawall.

3.7 Conclusions

Three cases of study using the new development non-breaking numerical model SOLA-VOF are presented. The linear wave inflow boundary condition was tested first, it is clear from this case of study that after one wave length there are significant difference between the SOLA-VOF results and the theoretical one. The open boundary condition needs more improvement allowing all the amount of wave transfer to leave the domain without any effect towards the new generating waves.

In the second case of study, the reflected wave boundary condition has been validated. The reflected wave boundary condition has been successfully tested against known exact solutions.

In some of the wave hydrodynamics studies, the reflected wave needs to propagate out of the computational domain or be absorbed by the inflow boundary. That is very clear in the third case of study which the non-breaking solitary wave run-up on beach has been studied. The results show that there is a requirement for an open boundary condition at the seaward end of the domain. Recently, new researchers introduce new absorbing boundary condition i.e. Liu and Lin (1997); Troch and De Rouck (1999); Isobe (2001) which solve the difficulties in the modified version of the SOLA-VOF numerical model.

The two-dimension breaking wave numerical model (2-D BWNM) which is used in the second part of this study (Chapters 4, 5, 6 and 7) covers the shortcoming in the SOLA-VOF moded. The 2-D BWNM solves very efficiently the problem of wave generation and radiation at the seaward boundary, and is discussed in detail in Chapter 4. The model of Troch and De Rouck (1999) and Isobe (2001) uses adaptive wave absorption at the seaward boundary and required detailed calculation to modify the wave generating conditions at the seaward boundary. Isobe (2001) model is just tested against regular waves. The model can be also applied to irregular waves but the calculation time is substantially increased by about 10 times compared to that with regular waves (Takahashi *et al.* (2002)). The 2-D BWNM model has the capability to simulate any kind of regular and irregular wave boundary condition as shown in Chapter 5.

The SOLA-VOF does not account for the case of breaking waves which are included and successfully tested in the 2-D BWNM as described in details in Liu and Lin (1997). More details of the two-dimensional breaking wave numerical model are given in the following chapters.

CHAPTER 4

Two-Dimensional Breaking Wave Numerical Model (2-D BWNM)

A two - Dimensional Breaking Wave Numerical Model (2-D BWNM) which is capable of simulating regular and irregular wave overtopping over coastal structures is presented in this chapter. The 2-D BWNM is based on the model developed by Lin (1998) which solves the Reynolds Averaged Navier-Stokes (RANS) equations for mean flow field and the second order $(k-\varepsilon)$ equations for turbulent kinetic energy, *k*, and the turbulence dissipation rate, ε. A literature review concerning the breaking wave numerical models is presented in Section 1. The mathematical formulation of the 2-D BWNM is illustrated in Section 2. Section 3 contains the initial boundary condition which is used in the numerical simulation.

4.1 Introduction

Breaking waves in the surf zone play an essential role in nearly all-coastal processes. For example, breaking waves generate strong turbulence which increases the mixing rate and therefore has an important impact on sediment transport in the surf zone. As a result, the beach profile is changed under the continuous action of breaking waves. Breaking waves also modify wave forces on the coastal structures when wave-structure interaction occurs. This is important when the construction of structures in coastal regions is considered. Wave breaking processes are in general accompanied by strong energy dissipation

which transfers the organized wave energy to heat. Therefore, to protect coastal structures along the shoreline, wave breaking could be artificially induced to damp out the wave energy by constructing a certain shape of submerged structure in surf zone.

The simulation of breaking wave has been a challenging problem to many coastal researchers due to the complicated flow and turbulence structures. The progress in creating numerical models for wave breaking processes has been relatively slow. Because of the limitation of computer speed, the early numerical simulation of breaking wave was mainly based on the depth-averaged equations, which include both shallow water equations and Boussinesq equations (Peregrine, 1967). The energy dissipation due to the breaking processes was incorporated into these equations through simple dissipative terms. For example, the momentum correction method was used by Schaffer *et al.* (1993) and Johnson *et al.* (1996) to represent the dissipation induced by the breaking wave. The eddy viscosity model was used by Zelt (1991), and Karambas and Koutitas (1992) in their breaking wave simulations. Dodd (1998), presented an upwind finite volume numerical model based on the one-dimensional non-linear shallow water equations on a sloping bed, including the effects of bed shear stress. Hu *et al.* (2000), presented one-dimensional high resolution finite volume model (AMAZON). The AMAZON model is based on solving the non linear shallow water equations. A modern upwind scheme of the Godunov-type using an HLL approximate Riemann solver is used which captures bore waves in both transcritical and supercritical flows. The robust HLL-type approximate Riemann solver has been

used instead of the more computationally expensive exact Riemann solver. Though computationally efficient, this approach cannot predict the details of the characteristics of turbulence transport during the wave breaking. The vertical variations of velocities are also lost due to the depth averaging process. To obtain the turbulence and vorticity transport information as well as the vertical variations of velocity information, a more sophisticated hydrodynamic model is needed.

Like any turbulent flow of incompressible fluid, the breaking wave can also be described by the basic incompressible Navier-Stokes equations (NSE). In principle, the direct numerical simulation for the NSE, which was pioneered by, Orszag and Patterson (1972) and Rogallo (1981) using pseudo-spectral methods, can also be used to study wave breaking. However, due to the large demand of computational time required by direct numerical simulation, most of its applications are for low Reynolds number (R_e) flows (Kim *et al.,* 1987). For breaking waves with high R_e and the added complication of strong free surface deformation, the direct numerical simulation is not feasible with the current computer power.

Another alternative is based on the Reynolds Averaged Navier-Stokes (RANS) equations. In the RANS equations, only the mean flow motion is described and the effects of turbulence on the mean flow are represented by Reynolds stresses which are proportional to the correlation of turbulence velocities. Lin (1998) and Lin and Liu (1998) proposed a new model to investigate the breaking waves by solving the RANS equations for the mean flow. Their model is a combination of the modified version of RIPPLE which was originally developed at Los Alamos

National Laboratory (Kothe *et al.*, 1991) and the $k-\varepsilon$ turbulence model (Liu and Lin, 1997). Finite difference solutions to the incompressible Reynolds equations for the mean flow field and the $k-\varepsilon$ equations for the turbulent field are obtained on a non-uniform mesh. The volume of fluid (VOF) algorithm (Nichols *et al.*, 1980 and Hirt and Nichols, 1981) method is employed to track the free surface movements. Lin (1998) compared numerical solutions with the experimental data for both spilling breaking waves (Ting and Kirby, 1996) and plunging breaking waves (Ting and Kirby, 1995) in terms of free surface elevation, mean velocity components and turbulence intensity. The overall agreement was satisfactory. More details of the comparison can be found in Lin (1998).

Following this, many developments were added to the original code. Liu *et al.*, (1999) extended the model by adding the capability of simulating flows in porous media and an improved $k-\varepsilon$ turbulence model with the non-linear algebraic Reynolds stress closure model was applied to describe the corresponding turbulence field. Then, Lin and Liu, (1999) added an internal designed mass source functions for the equation of mass conservation in the internal flow region source to generate specific wave trains. Also, they extended the model to simulate any kind of spectrum sea waves which is represented by a superposition of a finite number of linear wave modes with different wave height and wave period. The author used the JONSWAP spectrum to study the phenomena of wave overtopping (Soliman *et al.*, 2003). These required modifications of the source term to model JONSWAP characteristics (See Section 4.3.3.3).

4.2 Mathematical formulation of 2-D BWNM

4.2.1 Reynolds Averaged Navier-Stokes equations (RANS)

Navier Stokes equations describe the governing equation for a wide range of flow motions, including potential flow and turbulent flow. However, in the case of turbulent flows with high Reynolds number (R_e), small-scale turbulent fluctuations with high resolution are required. The direct numerical simulation for Navier Stokes equations in these cases is extremely difficult.

The Reynolds number is defined by, $R_e = \frac{U_c D_c}{\nu}$

Where, U_c is the characteristic velocity scale, D_c is the characteristic length scale and $\nu = \mu / \rho$ is the kinematic viscosity.

As an alternative to the direct solution of the NSE, another method has been derived to describe the mean motions of turbulence flows. Both the velocity field and the pressure field are split into mean component and turbulent fluctuations as follows:

$$u = \langle u_i \rangle + u_i' \tag{4.2.1}$$

$$p = \langle p \rangle + p' \tag{4.2.2}$$

$$\rho = \langle \rho \rangle + \rho' \tag{4.2.3}$$

in which $\langle\ \rangle$ denotes the mean quantities, the prime $'$ represents the turbulent fluctuations. By assuming that the turbulent fluctuations are random, we have $\langle u_i' \rangle = \langle p' \rangle = \langle \rho' \rangle = 0$. Substituting (4.2.1), (4.2.2), and (4.2.3) into (3.1.1) and (3.2.1) and taking the ensemble average of the resulting equations, we obtain the

governing equations for the mean flow field, which is called the Reynolds Averaged Navier Stokes (RANS) equations,

$$\frac{\partial\langle u_i\rangle}{\partial t}+\langle u_j\rangle\frac{\partial\langle u_i\rangle}{\partial x_j}=-\frac{1}{\langle\rho\rangle}\frac{\partial\langle p\rangle}{\partial x_i}+g_i+\frac{1}{\langle\rho\rangle}\frac{\partial\langle\tau_{ij}^m\rangle}{\partial x_j}-\frac{\partial\langle u_i'u_j'\rangle}{\partial x_j} \tag{4.2.4}$$

$$\frac{\partial\langle u_i\rangle}{\partial x_i}=0 \tag{4.2.5}$$

where $\langle\tau_{ij}^m\rangle$ is the mean viscous stress, $\langle\tau_{ij}^m\rangle=2\mu\langle\sigma_{ij}\rangle$ with $\langle\sigma_{ij}\rangle=\frac{1}{2}\left(\frac{\partial\langle u_i\rangle}{\partial x_j}+\frac{\partial\langle u_j\rangle}{\partial x_i}\right)$.

By merging the viscous stress and the Reynolds stress together, i.e., $\langle\tau_{ij}\rangle=\langle\tau_{ij}^m\rangle-\rho\langle u_i'u_j'\rangle$, and neglecting density fluctuations near the free surface, Equation 4.2.4 can be rewritten as follows:

$$\frac{\partial\langle u_i\rangle}{\partial t}+\langle u_j\rangle\frac{\partial\langle u_i\rangle}{\partial x_j}=-\frac{1}{\langle\rho\rangle}\frac{\partial\langle p\rangle}{\partial x_i}+g_i+\frac{1}{\langle\rho\rangle}\frac{\partial\langle\tau_{ij}\rangle}{\partial x_j} \tag{4.2.6}$$

The main factor that is taken into account by Lin (1998) in the mean flow computation are the Reynolds stresses, $R_{ij}=-\langle\rho\rangle\langle u_i'u_j'\rangle$. This correlation had been modelled by a non-linear eddy viscosity model (improved $k-\varepsilon$ equations) as described in detail in the following section.

4.2.2 Turbulence closure model

To solve the Reynolds equations for the mean flow, one must relate Reynolds stresses to the mean velocity. Extensive research work has been done to seek the proper closure model for the Reynolds stresses (e.g. Launder *et al.* (1975) and

Launder *et al.* (1972)). Liu *et al.*, (1999) recommended the $k-\varepsilon$ model approaches and defined k and ε as follows:

$$k=\frac{1}{2}\left\langle u_i'u_i'\right\rangle \qquad , \ \varepsilon=\nu\left\langle\left(\frac{\partial u_i'}{\partial x_j}\right)^2\right\rangle \tag{4.2.7}$$

4.2.3 Reynolds stress transport model

Launder *et al.*, (1975) presented the general transport equations for the Reynolds stresses which is considered the basic equation for the $k-\varepsilon$ as follows:

$$\begin{aligned}&\frac{\partial\left\langle u_i'u_j'\right\rangle}{\partial t}+\left\langle u_k\right\rangle\frac{\partial\left\langle u_i'u'\right\rangle}{\partial x_k}=-\frac{1}{\rho}\frac{\partial}{\partial x_k}\left(\left\langle u_i'p'\right\rangle\delta_{jk}+\left\langle u_j'p'\right\rangle\delta_{ik}\right)\\&-\frac{\partial}{\partial x_k}\left(\left\langle u_i'u_j'u_k'\right\rangle-\nu\frac{\partial\left\langle u_i'u_j'\right\rangle}{\partial x_k}\right)-\left\langle u_i'u_k'\right\rangle\frac{\partial\left\langle u_j\right\rangle}{\partial x_k}-\left\langle u_j'u_k'\right\rangle\frac{\partial\left\langle u_i\right\rangle}{\partial x_k}\\&+\left\langle\frac{p'}{\rho}\left(\frac{\partial u_i'}{\partial x_j}+\frac{\partial u_j'}{\partial x_i}\right)\right\rangle-2\nu\left\langle\left(\frac{\partial u_i'}{\partial x_k}\frac{\partial u_j'}{\partial x_k}\right)\right\rangle\end{aligned} \tag{4.2.8}$$

The left hand side of the equation calculates the rate of the change of turbulence kinetic energy following the mean flow field. The first two terms on the right hand side represent the total diffusion of Reynolds stress through the turbulent pressure work, turbulent fluxes, and molecular viscous force. The third row term denotes the production of Reynolds stress due to the working of Reynolds stresses against the mean flow gradients. The fourth term represents the interaction between the pressure fluctuation and the rate of strain of turbulence which does not contribute to the total change of turbulence energy but redistribute the turbulence energy in different directions. The last term is the tensor of viscous energy dissipation rate ε_{ij}. The transport equation, (Equation 4.2.8), contains a few higher order correlation terms, i.e., diffusion terms, pressure strain rate

correlation term, and dissipation term. The numerical solution to the Reynolds stress transport model is computationally expensive, the applications of such model are usually for small scale problems. Moreover, the difference among many proposed closure models for the diffusion and pressure strain rate correlations terms also increases the uncertainties of the model (Lin, 1998).

For these reasons, Liu *et al.*, (1999) recommended the $k-\varepsilon$ model which considers a simple model with the similar accuracy of the Reynolds stress transport model and less uncertainty of closure models. Details of the model and the applied improvements are explained in the following section.

4.2.4 $k-\varepsilon$ model

In $k-\varepsilon$ model, instead of tracking Reynolds stress components through the transport equations, the model solves only two transport equations for the turbulence energy which characterizes the velocity scale of turbulence. The transport equation for *k* can be easily derived from Equation 4.2.8 by letting *i*=*j*,

$$\frac{\partial k}{\partial t}+\langle u_j\rangle\frac{\partial k}{\partial x_j}=-\frac{1}{\rho}\frac{\partial}{\partial x_j}\left(\langle u_j' p'\rangle+\rho\langle u_j' k\rangle-\mu\frac{\partial\langle k\rangle}{\partial x_j}\right)-\langle u_i' u_j'\rangle\frac{\partial\langle u_i\rangle}{\partial x_j}-\varepsilon \qquad (4.2.9)$$

The above equation is much simpler than Equation 4.2.8 since the pressure strain rate correlation term disappeared due to the indices summation and the dissipation term become a scalar. The diffusion and dissipation terms in Equation 4.2.9 can be modelled by the gradient diffusion given the following equations (Lin, 1998),

$$\frac{\partial k}{\partial t}+\langle u_j\rangle\frac{\partial k}{\partial x_j}=\frac{\partial}{\partial x_j}\left(\left(\frac{\nu_t}{\sigma_k}+\nu\right)\frac{\partial k}{\partial x_j}\right)-\langle u_i' u_j'\rangle\frac{\partial\langle u_i\rangle}{\partial x_j}-\varepsilon \qquad (4.2.10)$$

$$\frac{\partial \varepsilon}{\partial t}+\langle u_j\rangle\frac{\partial \varepsilon}{\partial x_j}=\frac{\partial}{\partial x_j}\left(\left(\frac{\nu_t}{\sigma_\varepsilon}+\nu\right)\frac{\partial \varepsilon}{\partial x_j}\right)+C_{1\varepsilon}\frac{\varepsilon}{k}2\nu_t\langle\sigma_{ij}\rangle\frac{\partial\langle u_i\rangle}{\partial x_j}-C_{2\varepsilon}\frac{\varepsilon^2}{k} \qquad (4.2.11)$$

where, σ_k, σ_ε, $C_{1\varepsilon}$ and $C_{2\varepsilon}$ are empirical coefficients. These empirical coefficients have been determined by performing many simple experiments; The recommended values are (Rodi, 1980):

$$\sigma_k = 1.0,\ \sigma_\varepsilon = 1.3,\ C_{1\varepsilon} = 1.44,\ C_{2\varepsilon} = 1.92 \qquad (4.2.12)$$

Since the Reynolds stresses are not calculated directly from the transport equations, a closure model that relates the Reynolds stresses to $k, \varepsilon,$ and the strain rates of the mean flow is needed.

Conventionally, the linear isotropic eddy viscosity model is used for this purpose (Rodi, 1980). However, this model has the weakness from both the theoretical point of view and the actual computations. Because of the use of isotropic eddy viscosity concept, the anisotropy of both viscosity and turbulence cannot be realistically represented. In addition, because a linear relation is used, some higher-order physical mechanisms between the Reynolds stresses and mean strain rates are omitted. In the actual numerical computation, the conventional eddy viscosity model may fail under some extreme cases such as the strong vorticial motion. One possible cure for this problem is to employ a non-linear algebraic Reynolds stress model with the enforcement of realizability as proposed by Pope (1975) and Shih *et al.* (1996). With the use of such a model, the simplicity of the $k-\varepsilon$ model is retained and the accuracy of the modelling result is improved. This turbulence closure model is used in this study.

Other even simpler turbulence models are also available. For example, the so-called one-equation model, *k* model (Rodi, 1980), or the Prandtl's mixing length model can also be used to estimate Reynolds stresses. These models are easy to

apply, but the accuracy of the modelling results is questionable for complex flows. Furthermore, the coefficients used in these models vary case by case that increases the uncertainties when the model is applied to a new case.

4.2.4.1 Linear eddy viscosity model

The linear isotropic eddy viscosity model is applied to approximate the Reynolds stresses using the information of k and ε as well as the strain rate of the mean flow. The model specify the relation between Reynolds stresses and the rates of strain of the mean flow as follows

$$\left\langle u_i' u_j' \right\rangle = -2\nu_t \left\langle \sigma_{ij} \right\rangle + \frac{2}{3} k \delta_{ij} \tag{4.2.13}$$

in which ν_t is the turbulent eddy viscosity, depending on the local state of turbulence and can be approximated by,

$$\nu_t = C_d \frac{k^2}{\varepsilon} \tag{4.2.14}$$

where C_μ is empirical coefficient (C_μ = 0.09 , (Rodi, 1980)) and δ_{ij} is the Kronecker delta.

4.2.5 Improved $k-\varepsilon$ model

Because of the use of isotropic eddy viscosity assumption, Equation 4.2.13 will not represent the correct physics for anisotropic turbulence in complex turbulent flows (Lin, 1998). To solve this problem, Pope (1975), proposed a general closure model, a non-linear algebraic stress model, which called the non-linear eddy viscosity model. The function of the linear terms of the strain rate of the mean flow has been implemented as well as the higher order terms. Shih *et al.* (1996) proposed set coefficients for all quadratic terms for this type of model and

calibrated the coefficients using turbulent flow over a step. Lin and Liu (1999), adapted Shih *et al.* (1996)'s approach to give:

$$\begin{aligned}\left\langle u_i'u_j'\right\rangle &= \frac{2}{3}k\delta_{ij} - C_\mu \frac{k^2}{\varepsilon}\left(\frac{\partial\langle u_i\rangle}{\partial x_j}+\frac{\partial\langle u_j\rangle}{\partial x_i}\right)\\ &-\frac{k^2}{\varepsilon^2}\left[\begin{array}{l} C_1\left(\frac{\partial\langle u_i\rangle}{\partial x_l}\frac{\partial\langle u_l\rangle}{\partial x_j}+\frac{\partial\langle u_j\rangle}{\partial x_l}\frac{\partial\langle u_l\rangle}{\partial x_i}-\frac{2}{3}\frac{\partial\langle u_l\rangle}{\partial x_k}\frac{\partial\langle u_k\rangle}{\partial x_l}\delta_{ij}\right)\\ +C_2\left(\frac{\partial\langle u_i\rangle}{\partial x_k}\frac{\partial\langle u_j\rangle}{\partial x_k}-\frac{1}{3}\frac{\partial\langle u_l\rangle}{\partial x_k}\frac{\partial\langle u_l\rangle}{\partial x_k}\delta_{ij}\right)\\ +C_3\left(\frac{\partial\langle u_k\rangle}{\partial x_i}\frac{\partial\langle u_k\rangle}{\partial x_j}-\frac{1}{3}\frac{\partial\langle u_l\rangle}{\partial x_k}\frac{\partial\langle u_l\rangle}{\partial x_k}\delta_{ij}\right)\end{array}\right]\end{aligned} \tag{4.2.15}$$

The values of the empirical coefficients C_1, C_2 and C_3 are as follows:

C_1=0.0054, C_2= -0.0171, C_3=0.0027.

The details of the procedures to get all the previous empirical coefficients can be found in Lin (1998).

Lin (1998) modified the empirical coefficients in the following ways to satisfy the realisable requirements, i.e.,

$$\begin{aligned} C_\mu &= \frac{2}{3}\left(\frac{1}{7.4+S_{\max}}\right), C_1 = \frac{1}{185.2+D_{\max}^2}\\ C_2 &= -\frac{1}{58.5+D_{\max}^2}, C_3 = -\frac{1}{370.4+D_{\max}^2}\end{aligned} \tag{4.2.16}$$

$$\text{where, } S_{\max} = \frac{k}{\varepsilon}\max\left[\frac{\partial\langle u_i\rangle}{\partial x_i}\right], D_{\max} = \frac{k}{\varepsilon}\max\left[\frac{\partial\langle u_i\rangle}{\partial x_j}\right] \tag{4.2.17}$$

The adaption of above modification will ensure the non-negativity of turbulence velocity and bounded Reynolds stress. The employment of the non-linear algebraic stress model can greatly improve the accuracy of numerical results

because of the fulfilment of more physical constraints. The non-linear algebraic stress model captures most of physics described by the Reynolds stress transport model but also retains the simple form of $k-\varepsilon$ model. For simplicity, the Lin and Liu (1998) model included only the quadratic terms which represent most of the non-linear anisotropy characteristics of turbulence.

4.3 Initial conditions

The initial conditions for the mean flow can be based on the laboratory measurements or analytical solutions. In most cases, the initially quiet flow is specified with the zero mean velocities and hydrostatic pressure. For the turbulence field, the specification of initial condition requires more careful treatment. Lin (1998) conducted numerical experiments to specify the initial condition for the turbulence flow. According to these experiments, the initial values of k and ε suggested by Lin are as follows:

$$k=\frac{1}{2}u_t^2 \text{ with, } u_t=\delta c_i \tag{4.3.18}$$

$$\varepsilon=C_d\frac{k^2}{\nu_t} \text{ with, } \nu_t=\xi\nu \tag{4.3.19}$$

where, c_i is the wave celerity on the inflow boundary, δ=0.0025 and ξ = 0.1.

4.3.1 Boundary condition on solid boundary and free surface for mean flow

In the wave hydrodynamics study, the most common solid boundary is the impermeable bottom which is generally static. At the solid boundary, the fluid velocity must be the same as that of the boundary itself (*Ui*), u_i = *Ui*.

In the 2-D BWNM, the free slip boundary condition is defined, $\langle u_n \rangle = 0$ and $\frac{\partial \langle u_{\tau_k} \rangle}{\partial n} = 0$, where the subscripts n and τ_k denote the outward normal direction and two orthogonal tangential directions $(k = 1, 2)$, respectively. The free slip boundary condition which imposes less impact of boundary on the tangential velocity component provides some accurate velocity information near the solid boundary (Lin, 1998).

On the other hand, along the free surface the continuity of both normal and tangential stress components are required. By neglecting the surface tension, the dynamic boundary conditions are expressed as (Lin, 1998):

$$-p + 2\mu \frac{\partial u_n}{\partial n} = S_n \qquad , \ \mu \left(\frac{\partial u_{\tau_k}}{\partial n} + \frac{\partial u_n}{\partial \tau_k} \right) = S_{\tau_k} \tag{4.3.20}$$

where, S_n and S_{τ_k} are the specific stress components induced by air on the free surface. The kinematic boundary condition which describe the free surface motion is expressed as,

$$\frac{\partial \rho}{\partial t} + u_i \frac{\partial \rho}{\partial x_i} = 0 \tag{4.3.21}$$

Using equation (4.3.20) may lead to the spurious oscillations of free surface as observed and discussed by Nichols and Hirt (1971). In the 2-D BWNM, the simpler boundary conditions on the free surface are used, *i.e.*, $p = 0$ and $\frac{\partial \langle u_{\tau_k} \rangle}{\partial n} = 0$, these conditions neglect the air effect and normal stress of fluid. The numerical tests show that such boundary conditions produce rather accurate free

surface information when a grid larger than the thickness of the free surface boundary layer is used (Lin, 1998).

4.3.2 Boundary condition on solid boundary and free surface for $k-\varepsilon$ model

In principle, k becomes zero on the solid surface. However, in practical computations, the grid size normally cannot adequately resolve the turbulent boundary layer. Thus, the boundary conditions for k and ε are generally specified in the turbulent boundary layer instead of right on the wall. In the turbulent boundary layer the cross-stream shear stress dominates and remains a constant. Invoking the boundary layer approximation, Liu and Lin (1997) derived the following equation:

$$-\frac{\partial\langle u'v'\rangle}{\partial y}+\nu\frac{\partial^2\langle u\rangle}{\partial y^2}=0 \tag{4.3.22}$$

with y being the coordinate normal to the mean flow direction. By taking the integration from the wall to the place out of the viscous sub layer, where the viscous effect can be neglected, produce the following equation:

$$-\langle u'v'\rangle\Big|_{y=y}=-\nu\frac{\partial\langle u\rangle}{\partial y}\Big|_{y=0}=\frac{1}{\rho}\tau_w=u_*^2 \tag{4.3.23}$$

Based on dimensional analysis the mean velocity gradient in this region can be expressed as:

$$\frac{d\langle u\rangle}{dy}=\frac{u_*}{ky} \tag{4.3.24}$$

with $u_*=\sqrt{\tau_w/\rho}$ being the fractional velocity where τ_w is the cross stream shear stress on the wall and k=0.41 being the von Karman constant (Lin, 1998).

Integration equation 4.3.24 lead to the so-called logarithmic-law profile for the streamwise velocity:

$$\frac{\langle u \rangle}{u_*} = \frac{1}{k} \ln\left(E \frac{u_* y}{\nu} \right) \tag{4.3.25}$$

where, E=9.0 for smooth wall (Lin, 1998). Because the dissipation rate is approximately the same as the production rate, *i.e.,* $P = \varepsilon$, from equations 4.3.23 and 4.3.24 we have:

$$P = \varepsilon = -\langle u'v' \rangle \frac{d\langle u \rangle}{dy} = \frac{u_*^3}{ky} \tag{4.3.26}$$

From equation 4.2.13 the eddy viscosity ν_t can be obtained

$$\nu_t = -\frac{\langle u'v' \rangle}{\frac{d\langle u \rangle}{dy}} = k u_* y \tag{4.3.27}$$

The eddy viscosity is proportional to the distance from the wall in the turbulent layer. Substituting equations 4.3.26 and 4.3.27 into equation 4.2.14 yields

$$k = \frac{u_*^2}{\sqrt{C_\mu}} \tag{4.3.28}$$

Equations 4.3.26 and 4.3.28 constitute the boundary conditions for k and ε at the computational point immediately adjacent to the solid boundary. The fractional velocity can be found from equation 4.3.25 once the mean velocity $\langle u \rangle$ has been calculated.

On the free surface, Lin (1998) assumed that turbulence does not diffuse across the free surface. Consequently, the normal flux of k and ε should vanish on the free surface,

$$\frac{\partial k}{\partial n} = 0 \quad , \frac{\partial \varepsilon}{\partial n} = 0 \tag{4.3.29}$$

4.3.3 Internal inflow boundary condition

The 2-D BWNM uses a new scheme to specify the inflow boundary condition which was originally developed by Lin and Liu (1999). The scheme is based on the concept that any specific wave trains can be generated by using a designed mass source function for the equation of mass conservation in the internal flow region.

The new scheme removes the difficulty in specifying incident waves through an inflow boundary with the presence of strong wave reflection as shown in the Chapter 3 model tests (Section 3.6).

This method is very useful for a long duration simulation of coastal wave dynamics where the wave reflection is significant. A wide range of waves commonly met in field and used in the laboratory, i.e., linear wave, random wave, Stokes wave, cnoidal wave and solitary wave can be generated. The new scheme was compared with theories, Lin and Liu (1999), and the accuracy is very good. It is also demonstrated, from both theoretical argument and numerical tests that the reflected wave will not interfere with the wave generation process using the source function, which is an important consideration when doing lengthy computations when reflected waves are present. Thus, this scheme is very suitable to the case of wave overtopping over seawall structures.

4.3.3.1 Mathematical formulation

To generate a wave using a mass source, the conservation of mass equation (Equation 3.2.2) is modified as follows:

$$\frac{\partial \langle u \rangle}{\partial x} + \frac{\partial \langle \upsilon \rangle}{\partial y} = s(x, y, t) \tag{4.3.30}$$

where $s(x, y, t)$ = nonzero mass source function within the source region.

In actual computations using the finite difference scheme, a rectangular source region composed of $m \times n$ cells is applied. The relation between the source function $s(x, y, t)$ and the expected time history of free surface displacement $\eta(t)$ above the source region is as follows (Lin and Liu, 1999):

$$\int_0^t \int_\Omega s(x, y, t) d\Omega dt = 2 \int_0^t C_o \eta(t) dt \tag{4.3.31}$$

where, C_o = phase velocity of the target wave and Ω is the source region. The factor 2 is used in the right side of Equation 4.3.31 because the waves are generated on both sides of the source region.

4.3.3.2 Linear wave

The linear wave theory was derived using the concepts of two-dimensional ideal fluid which consider a reasonable starting point for ocean waves which are not greatly influenced by viscosity, surface tension and turbulence. Details of linear wave theory were explained earlier in Section (3.6.1).

Substituting Equation 3.6.11 into Equation 4.3.31, the corresponding source function can be derived

$$s(t) = \frac{C_o H}{A} \cos(\omega t) \tag{4.3.33}$$

where ω is the wave frequency and A is the source region area.

4.3.3.3 Irregular wave

An irregular wave train is represented in the model by a superposition of a finite number of linear wave modes with different wave height and wave frequency. For a known energy spectrum of an irregular wave train, the inverse Fourier transformation can be used to reconstruct the wave train with a finite number of wave modes. So, the random wave train can be generated by superposing different wave modes from i=1 to n as follows:

$$s(t) = \sum_{i=1}^{n} \frac{C_{o_i} H_i}{A} \sin\left(\omega_i t + \theta_i\right) \tag{4.3.34}$$

where θ_i is the phase angle of the i^{th} wave modes.

4.3.3.4 Internal mass source location and size

Several numerical experiments were conducted by Lin and Liu (1999) using the same source function at a different source region. It is found that a source region located about one third of the water depth from the still water surface level, generates waves that best match the theory. The placement of the source region very close to the free surface generates a steeper wave, while the source region very close to the bottom generates smaller wave. More details of the numerical experiments can found in Lin and Liu (1999).

Additional numerical tests show that the generated wave is insensitive to the size of the source region, as long as the height of the source region is greater than one to tenth of water depth.

Further extensive numerical experiments indicate that the optimal design of the source region should satisfy the following rules of thumb (Lin and Liu, 1999):

- The width of the source region should be less 5% of the wave length.

- The height of the source region should be in the range of 1/4 – 1/2 of the water depth (Lin and Liu, 2000).
- The distance between the centre of the source region and the still water level should be in the range of 1/3 – 1/2 of the water depth.
- The source region should be at least 1/2 wave length away from the open boundary to avoid unwanted artificial reflection (Lin and Liu, 2000).

These rules have been followed in all numerical simulations produced by 2-D BWNM.

4.3.4 Open (Radiation) outflow boundary condition

The new scheme to specify the inflow boundary condition, which was described in Section 4.3.3, removes the difficulty in specifying incident waves through an inflow boundary condition with the presence of strong reflection. Only the open (radiation) boundary condition is needed at the boundaries in the simulation to allow the wave going out of the computational domain. The open boundary condition was described in Section 3.5.3.

4.4 Summary of the governing and boundary conditions equations:

It is useful here to have a brief summary of the 2-D BWNM governing equations as follows:

- The equations governing the mass and momentum conservation of the mean flow are:

$$\frac{\partial \langle u_i \rangle}{\partial x_i} = 0 \qquad (4.4.35)$$

$$\frac{\partial \langle u_i \rangle}{\partial t} + \langle u_j \rangle \frac{\partial \langle u_i \rangle}{\partial x_j} = -\frac{1}{\langle \rho \rangle} \frac{\partial \langle p \rangle}{\partial x_i} + g_i + \frac{\partial \langle \tau_{ij} \rangle}{\partial x_j} \tag{4.4.36}$$

- The $k-\varepsilon$ model reads (Lin and Liu, 1998):

$$\frac{\partial k}{\partial t} + \langle u_j \rangle \frac{\partial k}{\partial x_j} = \frac{\partial}{\partial x_j}\left(\left(\frac{\nu_t}{\sigma_k} + \nu \right) \frac{\partial k}{\partial x_j} \right) - \langle u_i' u_j' \rangle \frac{\partial \langle u_i \rangle}{\partial x_j} - \varepsilon \tag{4.4.37}$$

$$\frac{\partial \varepsilon}{\partial t} + \langle u_j \rangle \frac{\partial \varepsilon}{\partial x_j} = \frac{\partial}{\partial x_j}\left(\left(\frac{\nu_t}{\sigma_\varepsilon} + \nu \right) \frac{\partial \varepsilon}{\partial x_j} \right) + C_{1\varepsilon} \frac{\varepsilon}{k} 2\nu_t \langle \sigma_{ij} \rangle \frac{\partial \langle u_i \rangle}{\partial x_j} - C_{2\varepsilon} \frac{\varepsilon^2}{k} \tag{4.4.38}$$

- The initial turbulence model conditions are:

$$k = \frac{1}{2} u_t^2 \text{ with, } u_t = \delta c_i \tag{4.3.39}$$

$$\varepsilon = C_d \frac{k^2}{\nu_t} \text{ with, } \nu_t = \xi \nu \tag{4.3.40}$$

- The boundary conditions for mean flow are:

At solid boundary:

$$\langle u_n \rangle = 0 \text{ and } \frac{\partial \langle u_{\tau_k} \rangle}{\partial n} = 0 \tag{4.4.41}$$

At free surface:

$$p = 0 \text{ and } \frac{\partial \langle u_{\tau_k} \rangle}{\partial n} = 0 \tag{4.4.42}$$

- The boundary conditions for turbulence flow are:

At solid boundary:

$$k = \frac{u_*^2}{\sqrt{C_d}} \text{ and } \varepsilon = -\langle u' v' \rangle \frac{d \langle u \rangle}{dy} = \frac{u_*^3}{ky} \tag{4.4.43}$$

At free surface:

$$\frac{\partial k}{\partial n} = 0 \text{ and } \frac{\partial \varepsilon}{\partial n} = 0 \tag{4.4.44}$$

4.5 Numerical implementation

In the numerical model, the RANS equations are solved using the finite difference two-step projection method (Chorin, 1968). The forward time difference method is used to discretize the time derivative. The convection terms are discretized by the combination of central difference method and upwind method (Hybrid scheme). The central difference method is employed to discretize the pressure gradient terms and stress gradient terms. The transport equations for k and ε are solved with similar methods. For further details on the numerical implementation, readers are referred to Lin and Liu (1997, 1998).

In the following chapter, different cases of study have been investigated to evaluate the performance of the 2-D BWNM.

CHAPTER 5

Model Testing

5.1 Introduction

The purpose of this chapter is to describe the evaluation of the performance of the 2-D BWNM. After the presentation of the mathematical formulation and the initial boundary condition of the 2-D BWNM in the previous chapter, the performance of the numerical model needs to be tested. Three main cases of study have been studied to check the accuracy of the numerical model. The first case shows the overflow without waves over vertical structures. Results of the average discharge are compared with the well-known weir equation. Secondly, the case of linear wave overtopping over a sloping seawall is presented and the results are compared with other analytical and laboratory data. The third case studies irregular wave overtopping of seawalls with slopes in the range from 1:1 to 1:6. The computed average discharge is compared with the laboratory data collected by Van der Meer and Janssen (1995) and with the well-known overtopping design formulae used for design. New formulae are proposed for the case of irregular wave overtopping over smooth sloped seawall on the basis of a series of numerical simulations. The chapter concludes with a detailed discussion of these cases and the performance of the 2-D BWNM.

5.2 Mesh setup

The aspect ratio of Δx and Δy is important issue closely related to the VOF free surface tracking method. Normally, the aspect ratio of $\Delta x/\Delta y = 1$ is preferred (Lin and Liu, 2000). However, for certain cases, say, a small amplitude long wave with

its horizontal length scale (characterized by wave length) being much larger than the vertical scale (characterized by water depth or wave height), to maintain an aspect ratio of one is too expensive to be feasible. In such case, Δx normally needs to be order of magnitude greater than Δy to make the computation economical.

When a wave breaking problem is investigated, the requirement of the certain aspect ratio is more stringent. Normally, a wave breaks when the wave front slope reaches tan (22^o) = $\Delta y/\Delta x$ (0.4) (Lin and Liu, 2000). If the aspect ratio of Δx and Δy is much larger than 1/0.4 = 2.5, a wave may experience false breaking before it actually breaks, following the same argument above. Therefore, for breaking wave simulation, the aspect ratio should be smaller than or equal 2.5 to avoid numerical inaccuracies due to false breaking (Lin and Liu, 2000).

For the mesh cells dimensions (Δx and Δy), the rules applied for the source region that was explained in details in Chapter 4 (Section 4.3.3.4) are applied here also.

5.3 Overflow without waves at vertical seawall

If the water level rises above the crest level of the structure, for example during extreme storm surges, overflow occurs. That is, sea water flows over the top of the crest of the seawall. Design formulae used to calculate wave overtopping assume that water in front of the structure to be below the crest level of the structure. One can extrapolate for water levels at the crest of the structure, but scale model tests for seawalls show, that the amount of overtopping is overestimated by the existing formulae for zero freeboard (R_c=0), (Bleck *et al.*, 2000). On the other hand, the existing formulae for overflow (e.g. weir formulae) do not take into account the effect of waves.

The case of overflow without waves at a broad crested weir is studied first using the 2-D BWNM. In this case the water level is above the crest level of the structure and the freeboard (R_c) is negative. This is an introductory situation for the case of combined wave overtopping and overflow which is presented and discussed in the next chapter. Chadwick and Morfett (1998) expressed the discharge formula over a broad crested weir as follows:

$$q_{weir} = 1.705 \times C_d \left| R_c \right|^{\frac{3}{2}} \tag{5.3.1}$$

where, R_c is the overflow depth and C_d is the discharge coefficient.

A number of empirical discharge formulae have been developed which incorporate the value of C_d. It can be shown by dimensional analysis that $C_d = f\left(R_e, R_c / d_s \right)$, where, R_e is Reynolds number and d_s is the weir height.

The problems of calibration (*i.e*. adjusting C_d experimentally) become far greater when the discharge is small. Under these conditions, the effect of viscosity and surface tension combine to bring about unstable, fluctuating flow conditions.

A number of empirical discharge formulae have been developed which incorporate C_d. In Chadwick and Morfett (1998) an equations for C_d are in the form:

$$C_d = 0.848 C_F \tag{5.3.2}$$

$$C_F \simeq 0.91 + 0.21 \frac{R_c}{B_L} + 0.24 \left(\frac{R_c}{R_c + d_s} - 0.35 \right) \tag{5.3.3}$$

where, B_L is the weir width.

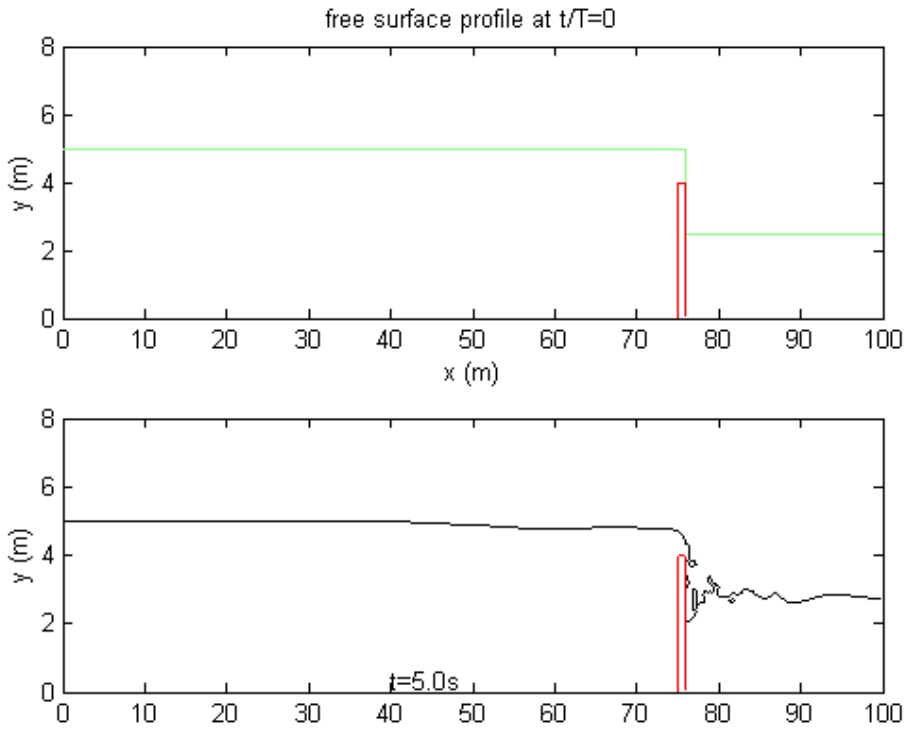

Figure 5.3.1: The free surface profile for the overflow without wave ($R_c \leq 0$).

Figure 5.3.1 gives the cross section of the structure and the water surface profile. The water depth is 4.0m, weir width is 1.0m and the freeboard (R_c) ranges from 0.0 to –0.8m. In total 400 cells are used in the *x*-direction with a cell size of 0.25m and 80 cells in the *y*-direction with a cell size of 0.1m. The basic time step is 0.04s and the total simulation time is 30s.

The comparison between discharge rate of weir equation and the 2-D BWNM is presented in Table 5.3.1 and Figure 5.3.2. It can be seen from the Figure 5.3.2 that the results produced from the 2-D BWNM compare very well with the weir equation for small negative freeboard. For freeboard less than -0.5m the 2-D BWNM underpredicts the overflow discharge as much as 1% to 12% compared to the weir equation. This may be related to the uncertainty in discharge coefficient

(C_d) value. Another reason for the difference between the weir equation and 2-D BWNM discharge rates is that the weir equation is based on the Bernoulli equation as a starting point. The actual flow over a weir is complex, usually being unsteady and involving viscous effects. These effects are not covered in the Bernoulli equation. Another reason is related to the numerical model accuracy in calculating discharge volume due to mesh size. Using smaller mesh size will lead to more accurate results.

Run No.	R_c [m]	q_{weir} [$m^3/m`/s$]	$q_{2\text{-D BWNM}}$ [$m^3/m`/s$]
W-1	0.0	0.000	0.000
W-2	-0.1	0.039	0.024
W-3	-0.2	0.114	0.127
W-4	-0.3	0.215	0.233
W-5	-0.4	0.341	0.340
W-6	-0.5	0.490	0.483
W-7	-0.6	0.662	0.626
W-8	-0.7	0.857	0.782
W-9	-0.8	1.075	0.938

Table 5.3.1: Comparison between 2-D BWNM and modified weir equation.

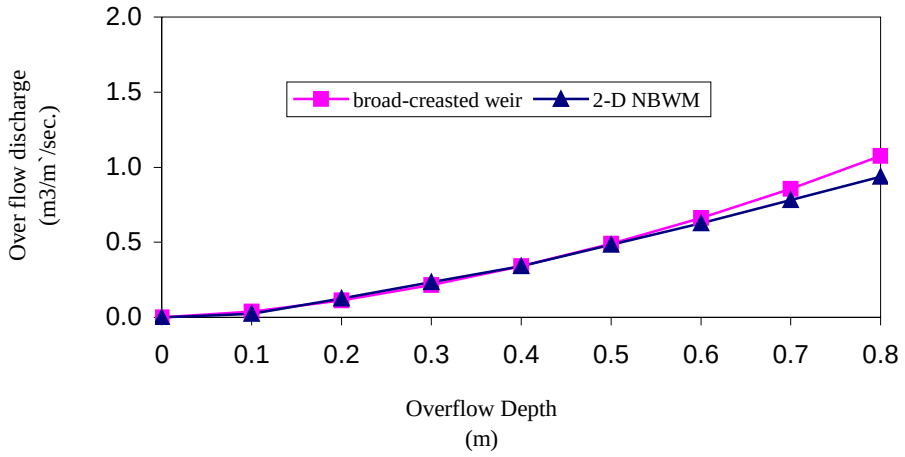

Figure 5.3.2: Comparison between the 2-D BWNM and the weir equation for the case of overflow without waves.

5.4 Linear wave overtopping at sloping seawalls

Saville (1955) collected extensive small-scale laboratory test data for wave overtopping at sloping seawalls. The experiments were based on regular waves overtopping a sloping seawall with slopes of 1:3. Hu *et al.* (2000) summarised this data and used it to test a numerical model (AMAZON) which is based on the non-linear shallow water (NLSW) equations. The profile of tested seawalls is illustrated in Figure 5.4.3, where d_t, d_s, and R_c represent water depth below SWL at the seaward boundary, water depth below SWL at the toe of the structure and the crest level of the structure above SWL (freeboard).

Twenty cases of study cover a wide range of wave characteristics, positive freeboard and water depths with 1:10 smooth beach slope. The configuration and the results for these runs are presented in Table 5.4.2 and also illustrated in Figure 5.4.4. The dimensionless discharge Q was defined by Hu *et al.* (2000) as:

$$Q = \frac{q}{H\sqrt{gH_s}} \tag{5.4.4}$$

where, q is the dimensional average overtopping discharge, g is the gravitational acceleration and H_s is the significant wave height.

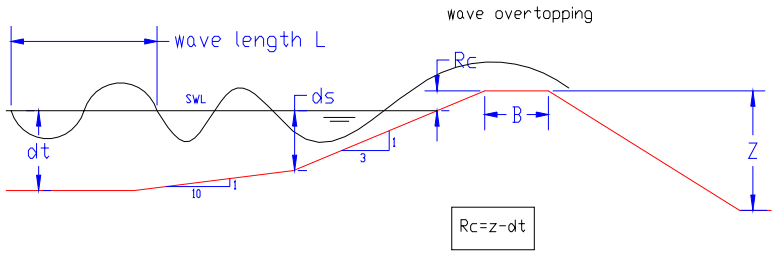

Figure 5.4.3: Sketch explains the case study of regular waves overtopping at sloping seawalls.

To be consistent with the results produced Hu *et al.* (2000), the boundary wave conditions were the same as specified by Hu *et al.* (2000) and an average value of Q was calculated during the fourth and fifth wave period $(4 \le T \le 5)$.

The results produced with 2-D BWNM compared well with the measured data as shown in Figure 5.4.4. Table 5.4.2 shows details of each run and the output from 2-D BWNM model together with the laboratory experiments and the AMAZON results.

As measured by the sum of the modulus of the differences between the laboratory and model results over the 20 cases, 2-D BWNM provides 12% improvement in the performance of AMAZON. On purely theoretical grounds one would expect the Navier-Stokes equations to provide a more robust means for the simulation of wave overtopping than the non-linear shallow water equations; the latter are

derived on the assumption that the vertical velocity is much less that the horizontal velocity, i.e. hydrostatic pressure is assumed. This assumption is not strictly applicable in the surf zone.

Run No.	S.W Slope	d_t (m)	d_s (m)	R_c (m)	H_s (m)	T (s)	$Q(10^{-3})$ Amazon	$Q(10^{-3})$ Saville	$Q(10^{-3})$ [-] 2-D BWNM
1	1:3	3.0	0.75	0.50	0.95	4.73	39	66	46
2	1:3	3.0	0.75	1.00	0.95	4.73	15	41	3
3	1:3	3.0	1.50	0.50	0.95	4.73	81	64	72
4	1:3	3.0	1.50	1.00	0.95	4.73	24	36	25
5	1:3	4.0	2.00	0.67	0.99	6.55	86	90	86
6	1:3	4.0	0.75	0.50	1.08	7.98	64	60	66
7	1:3	4.5	0.75	1.00	1.06	7.98	27	17	40
8	1:3	4.0	0.75	1.50	1.08	7.98	11	4	4
9	1:3	4.0	1.50	0.50	1.08	7.98	101	94	103
10	1:3	4.0	1.50	1.00	1.08	7.98	53	40	48
11	1:3	4.0	1.50	1.50	1.08	7.98	24	8	33
12	1:3	6.0	1.00	0.67	1.20	12.8	90	91	115
13	1:3	6.0	2.00	0.67	1.20	12.8	108	130	138
14	1:3	6.0	2.00	1.33	1.20	12.8	41	77	61
15	1:3	6.0	2.00	2.00	1.20	12.8	7.5	25	30
16	1:3	6.0	2.00	2.67	1.20	12.8	0	11	11
17	1:1.5	4.92	0.75	0.50	1.04	7.98	50	49	63
18	1:1.5	4.92	0.75	1.50	1.04	7.98	5.6	13	19
19	1:1.5	4.17	0.0	0.50	1.07	7.98	34	39	39.7
20	1:1.5	4.17	0.0	1.00	1.07	7.98	8.9	20	13

Table 5.4.2: Comparison between 2-D BWNM and AMAZON numerical models with the laboratory measured dimensionless overtopping discharges.

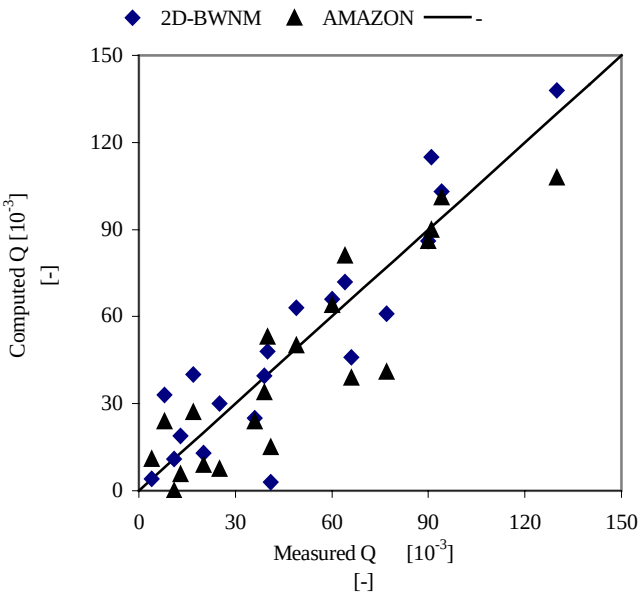

Figure 5.4.4: Comparison between 2-D BWNM and AMAZON models with the laboratory measured dimensionless overtopping discharges.

5.5 Irregular wave overtopping at sloping seawalls

5.5.1 Sea states used in the 2-D BWNM tests

The irregular waves which are used in the following model tests are generated using the parameterised JONSWAP-spectrum (Carter, 1982):

$$E(f) = 0.205 H_s^2 T_p^{-4} f^{-5} \exp\left(-1.25 T_p^{-4} f^{-4}\right) \gamma^{\delta} \tag{5.5.5}$$

$$\delta = \exp\left[\frac{(-T_p f - 1)^2}{2\sigma^2}\right] \tag{5.5.6}$$

where:

$E(f)$ is frequency spectral density function.

$\sigma = 0.07$ for $T_p f \le 1$ and $\sigma = 0.09$ for $T_p f > 1$.

f is the wave frequency.

γ is spectral enhancement factor.

The JONSWAP spectrum is characterized by a parameter γ which is called the peak enhancement parameter; this controls the sharpness of the spectral peak. The value of the peak enhancement parameter (γ) of 3.3 is an average figure derived by Hasselmann (1973). They found individual values within the range of 1-6. Detailed analysis of these γ values by Ochi (1979) showed that they have a normal distribution with a mean 3.3 and a standard deviation of 0.79, i.e. 95% between 1.75 and 4.85.

For linear waves the total energy density, E, is twice the potential energy density (E_p) of a wave,

$$E = 2E_p = \frac{\rho g H^2}{8} \tag{5.5.7}$$

Using Equations (4.3.34, 5.5.6 and 5.5.7) heights of representative waves can be estimated. Figure 5.5.5 shows an example of JONSWAP frequency spectral density function with peak enhancement parameter γ = 1, 3.3 and 6.

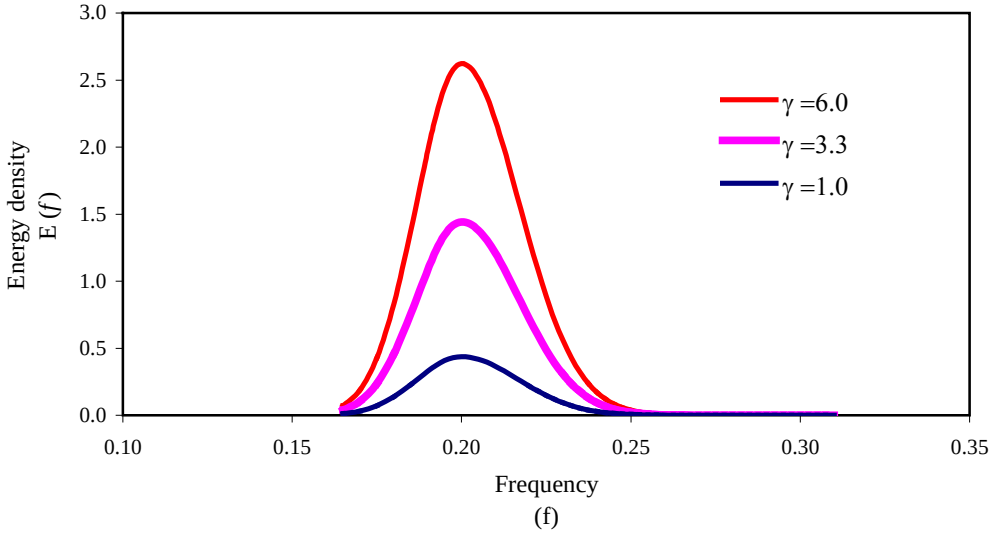

Figure 5.5.5: Relation between JONSWAP spectrum and wave frequency (H_s = 1.22m, T_m = 3.80s and T_p = 5.0s).

Many cases of study with different significant wave heights, peak and mean wave periods are made to identify the number of components frequencies should be used to well adequately represent the JONSWAP spectrum. It is found from reanalysis of the generated waves that between 35 to 45 frequencies are required to present the JONSWAP spectrum well. The statistical analysis of the generated irregular wave gives the same input wave characteristics *i.e.* significant wave height, peak wave period and mean wave period. The error between input and generated significant wave heights, mean and peak wave periods range from 5 to 10% in all cases. Examples of the generated irregular waves which used in the following cases of study are shown in Figures 5.5.6 to 5.5.9.

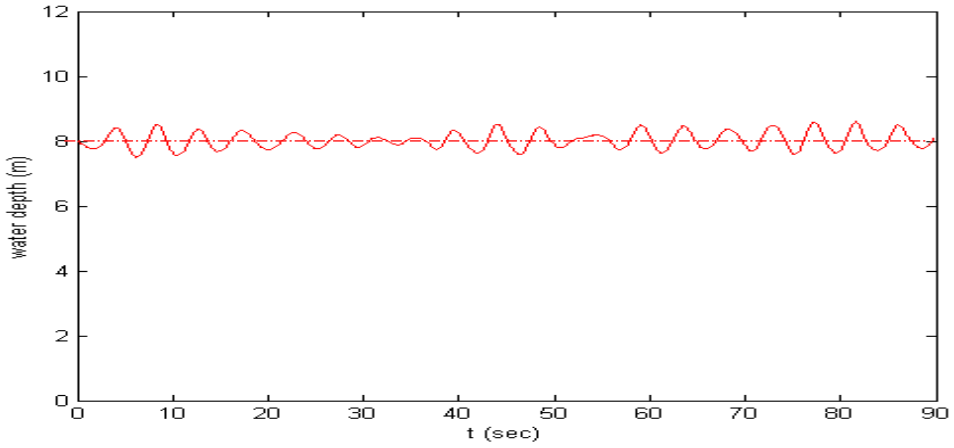

Figure 5.5.6: Input irregular wave (JONSWAP spectrum H_s = 1.24m, T_p = 4.43s, T_m = 3.85s and d_s=8.0m).

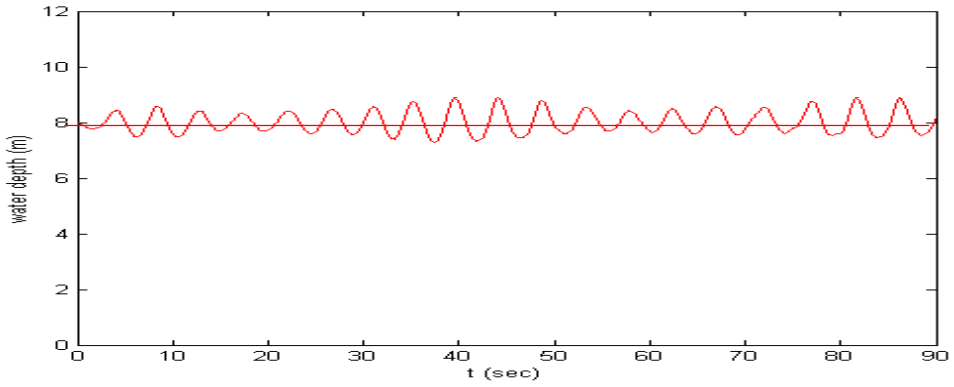

Figure 5.5.7: Input irregular wave (JONSWAP spectrum H_s = 1.40m, T_p = 4.55s, T_m = 3.96s and d_s=8.0m).

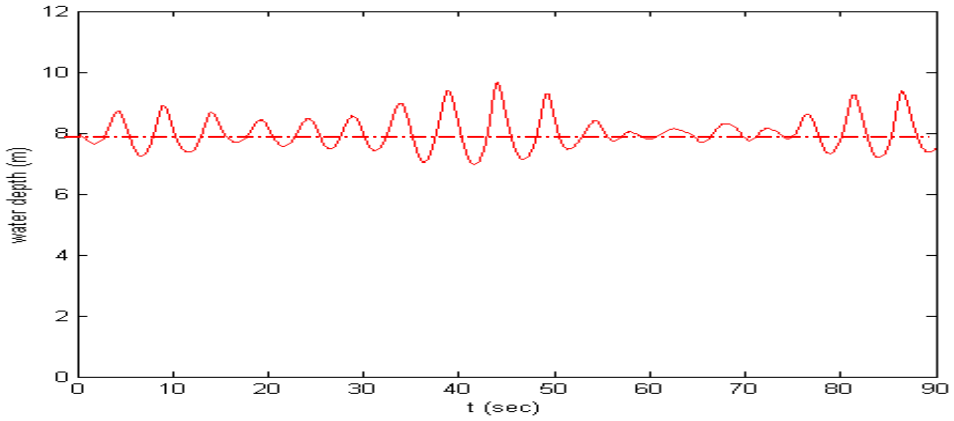

Figure 5.5.8: Input irregular wave (JONSWAP spectrum, H_s = 1.75m, T_p = 5.13s, T_m = 4.46s and d_s=8.0m).

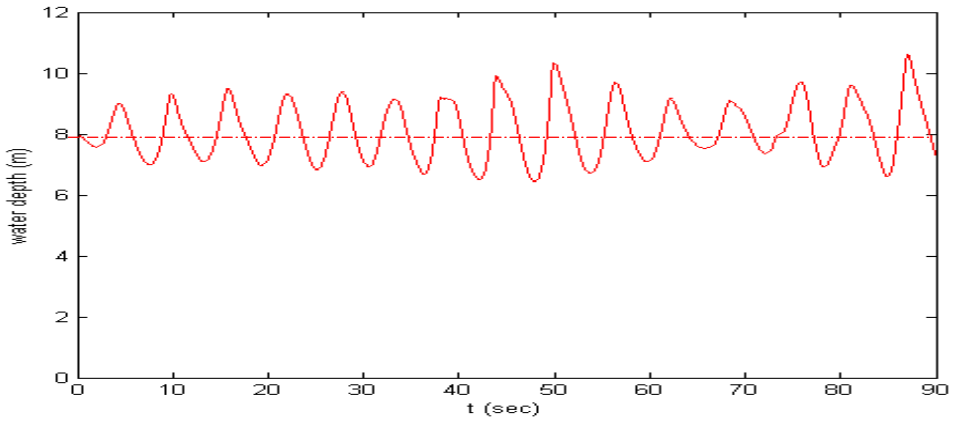

Figure 5.5.9: Input irregular wave (JONSWAP spectrum H_s = 2.34m, T_p = 6.04s, T_m = 5.52s and d_s=8.0m).

5.5.2 Irregular wave overtopping over smooth sloped seawalls

Van der Meer and Janssen (1995) proposed set of wave overtopping formulae for irregular waves. They based their formula on an extensive series of both small and large scale model tests on the overtopping response of various seawalls. The experiments were carried out in Delta flume of Delft Hydraulics laboratory. The laboratory results of the irregular wave overtopping (JONSWAP spectrum) have been used to evaluate the 2-D BWNM. Three different slopes of smooth seawall are studied 1:1, 1:2 and 1:4. Details of these different cases are described in the following sections.

5.5.2.1 Comparison with laboratory data for seawalls with slope 1:1

In this case, a total of 16 tests have been run using 2-D BWNM. Figure 5.5.10 gives the cross section of the 1:1 sloped seawall with the wave surface profile. The water depth is 8.00m and the generated irregular wave accordance with JONSWAP spectrum.

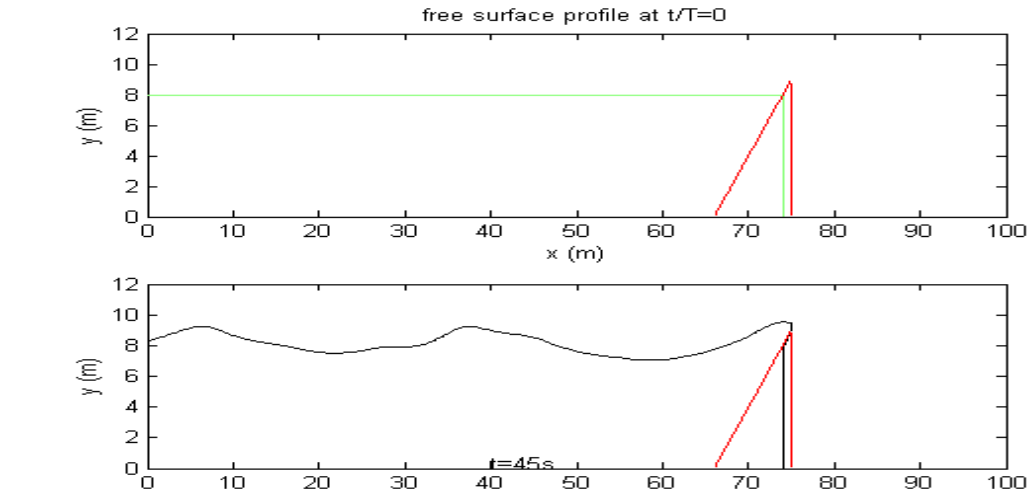

Figure 5.5.10: Cross section for seawall with slope 1:1 with the non-breaking wave surface profile after 45 sec.

Run No.	R_c (m)	H_s (m)	T_p (s)	T_m (s)
L-1	1.00	0.79	3.50	3.04
L-2	1.00	1.23	4.35	3.78
L-3	1.00	1.73	5.18	4.50
L-4	1.50	0.86	3.50	3.04
L-5	1.50	1.29	4.39	3.82
L-6	1.50	1.75	5.22	4.54
L-7	2.00	0.86	3.50	3.04
L-8	2.00	1.29	4.39	3.82
L-9	2.00	1.75	5.22	4.54
L-10	2.00	2.34	6.04	5.25
L-11	2.50	1.40	4.55	3.96
L-12	2.50	1.85	5.30	4.61
L-13	2.50	2.42	6.08	5.29
L-14	3.00	1.25	4.38	3.81
L-15	3.00	1.69	5.16	4.49
L-16	3.00	2.26	6.01	5.23

Table 5.5.3: Configuration of the small-scale tests of seawall with slope 1:1.

Details of the configuration for 16 runs are presented in Table 5.5.3. In total 400 cells are used in the *x*-direction with a cell size of 0.25m. In the *y*-direction 120 cells are used with a cell size of 0.1m.

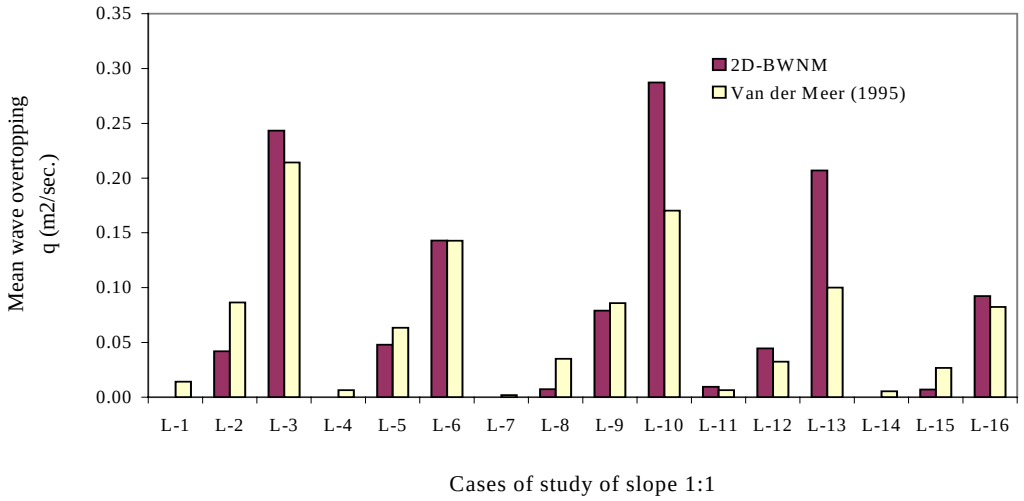

Figure 5.5.11: Comparison between 2-D BWNM and Laboratory measured dimensional overtopping discharges.

In Figure 5.5.11 the results from the tests with linear slopes are plotted together with results given by Van der Meer and Janssen (1995). The comparison between the laboratory and 2-D BWNM overtopping discharge shows that there is good agreement between the laboratory data and the numerical results. Analytically, the average error between the laboratory work and the numerical model is 17.5 %. However, scale effects are an important parameter in the laboratory work. Grune (1982) studied examples of the scale effects on run up and overtopping. Here it emerges that the run-up is generally larger than predicted by commonly used formulae such as Van der Meer *et al.* (1992) and Owen (1980).

The same tendency is found by Van de Walle *et al.* (2002) from full-scale measurements on the Zeebrugge breakwater in Belgium. Van de Walle *et al.* (2002) compare full-scale run-up measurements with the measurements from small-scale model tests performed with wave conditions reproducing the full-scale conditions. They concluded that the differences between the field and the laboratory results are due to scale effects. In the 2D-BWNM simulations real scale has been taken (scale 1:1) while large-scale tests have been used in the laboratory work. It is clear from figure 5.5.11, that the significant difference between the numerical and laboratory results occurs in L-3, L-10 and L-13. These cases have the largest wave characteristics *i.e.* significant wave height and mean wave period. Scale has a strongest impact in these cases. The average error decreases to 10% with the exclusion of these three cases. Other reasons are referred to the uncertainty in laboratory work, as well as numerical and modelling errors in the computational model.

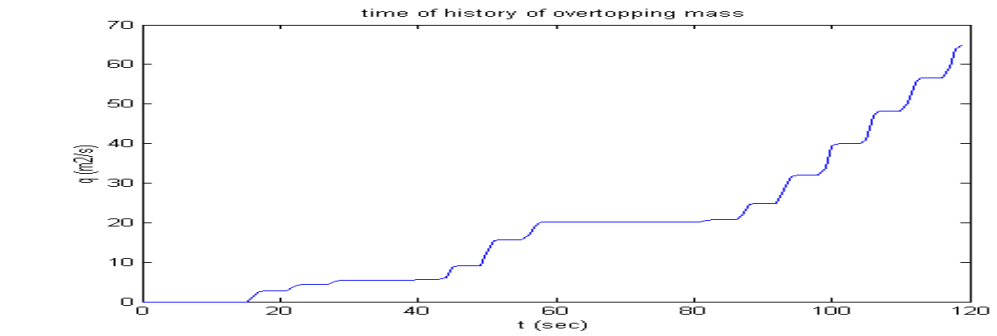

Figure 5.5.12: Time history of the cumulative overtopping volume for case L-10, (H_s = 2.34m, T_p = 6.04s, T_m = 5.25s and d_s=8.0m).

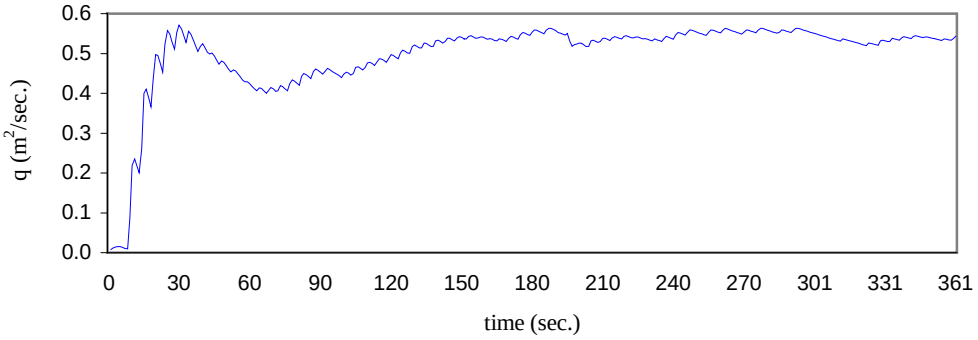

Figure 5.5.13: Time history of the instantaneous overtopping volume, (H_s = 0.83m, T_p = 5.00s, T_m =3.60).

The overtopping rate is an important parameter to measure the effectiveness of the sloped seawall. Figures 5.5.12 and 5.5.13 show the cumulative and instantaneous overtopping volume calculated by the numerical model. The non-linearity in the overtopping mass is clear from the figures and this is due to the irregular nature of the waves as shown in Figures 5.5.5 to 5.5.8. Figure 5.5.13 shows that the instantaneous overtopping volume is almost constant after the first 30 seconds. In order to reduce the calculation time and have the opportunity to investigate a large range of cases the simulation time has been defined as 180s, with a basic time step of 0.04s. Unfortunately, Van der Meer and Janssen (1995) did not give details about the way their determined the computational time.

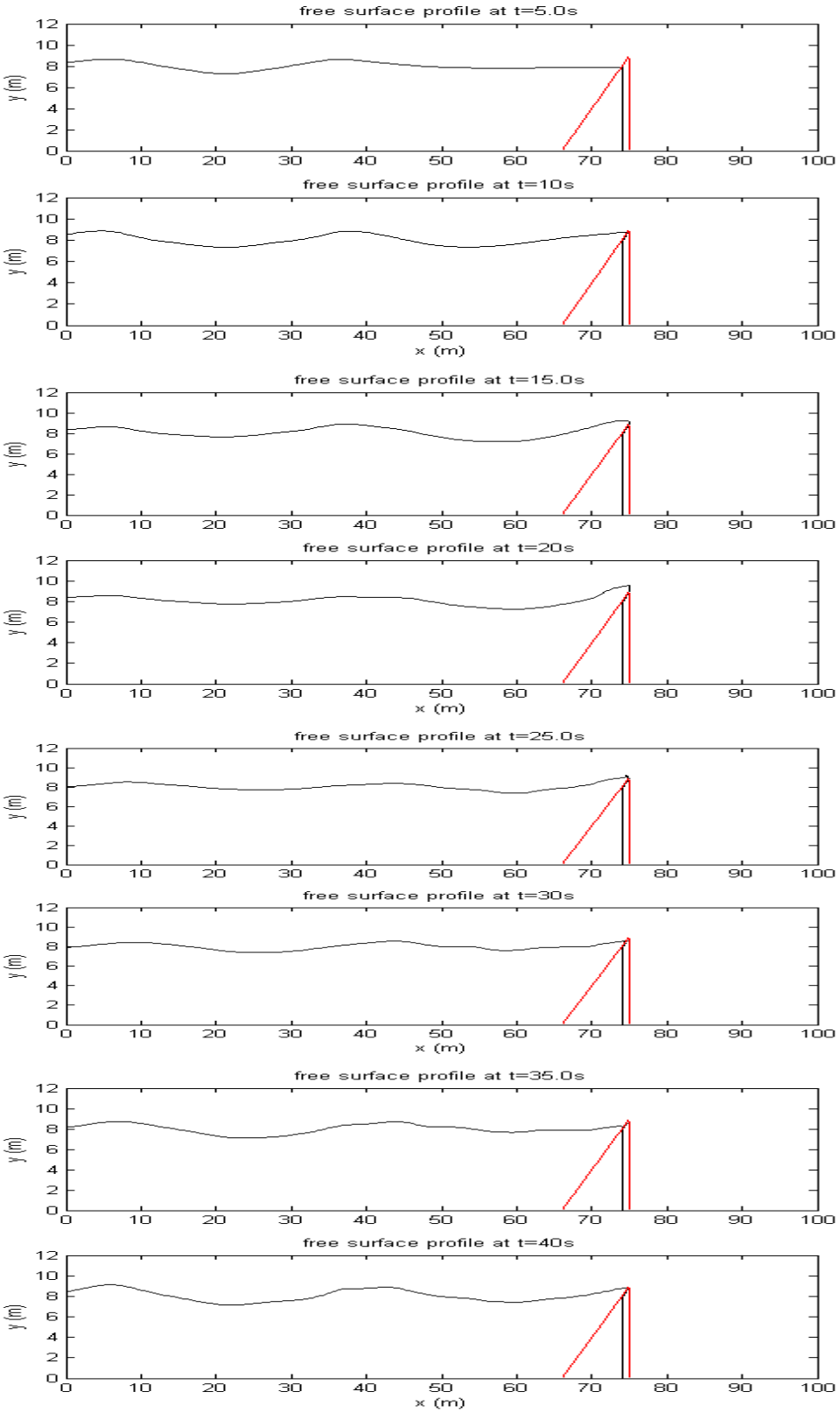

Figure 5.5.14: Irregular wave overtopping on a 1:1 sloping seawall from time 5 to 40s. (H_s = 1.73m, T_p = 5.18s, T_m = 4.5s and d_s=8.0m).

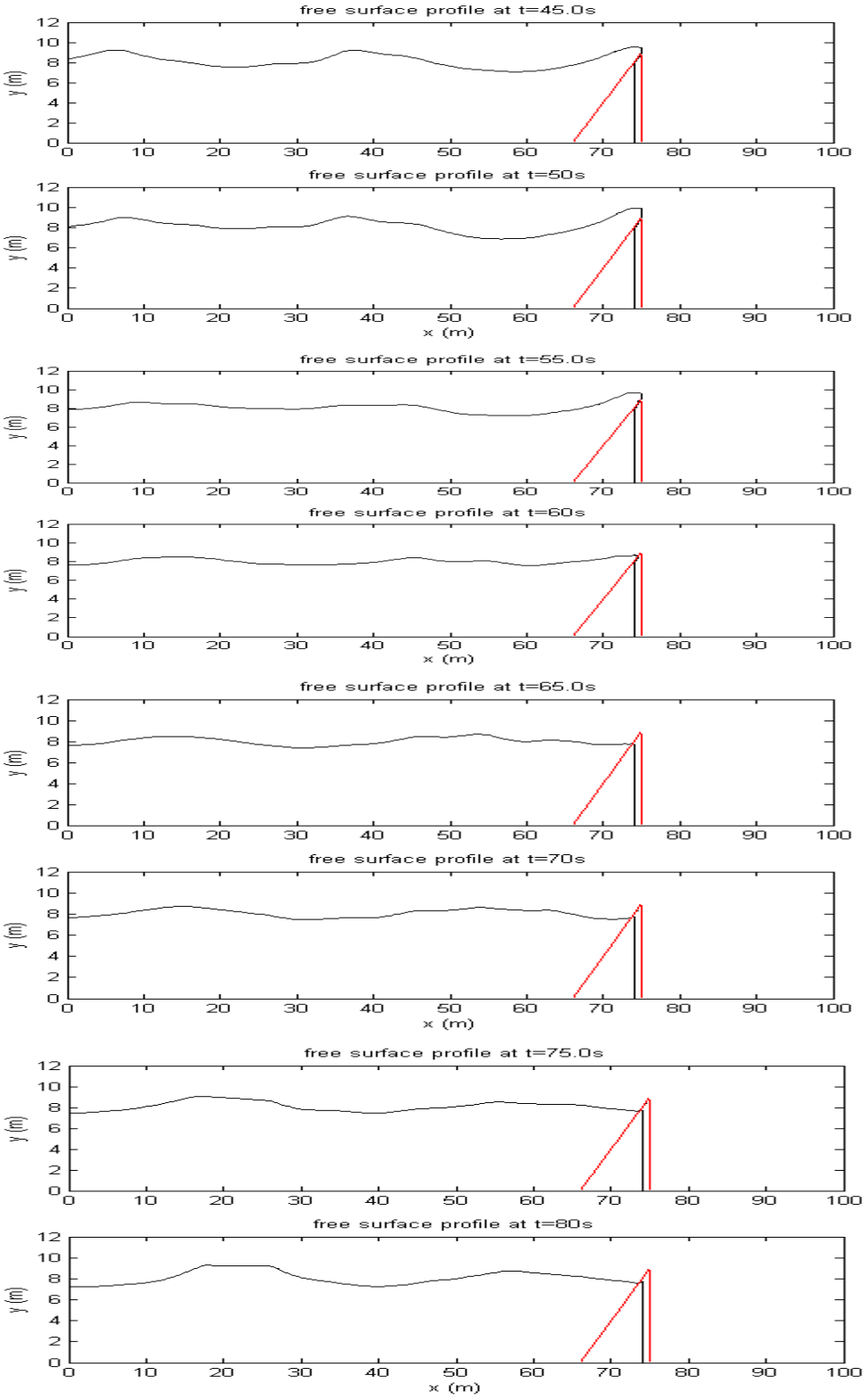

Figure 5.5.15: Irregular wave overtopping on a 1:1 sloping seawall from time 45 to 80s. (H_s = 1.73m, T_p = 5.18s, T_m = 4.5s and d_s=8.0m).

One example of the propagation of the irregular wave over the sloped seawall is shown in Figures 5.5.14 and 5.5.15. The input irregular wave characteristics (JONSWAP spectrum) are H_s = 1.73m, T_p = 5.18s, T_m = 4.5s and d_s=8.0m. These Figures demonstrate clearly the shape of wave over the calculation period and illustrate how the overtopping volume increases over time.

5.5.2.2 Comparison with laboratory data for seawalls with slope 1:2

In this case, a total of 16 tests have been run using 2-D BWNM. Figure 5.5.16 gives the cross section of the 1:2 sloped seawall and the free surface profile. Details of the configurations for 16 runs are presented in Table 5.5.4. The model has the same mesh set-up, time step and the simulation time as the previous case.

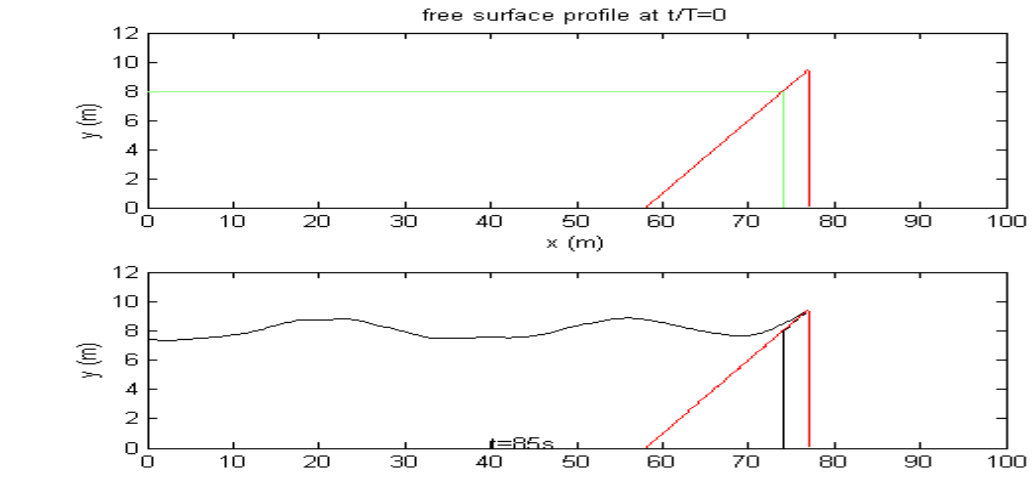

Figure 5.5.16: Cross section for seawall with slope 1:2 with the non-breaking wave surface profile after 85 sec.

Figure 5.5.17 suggests a similar conclusion to that of Figure 5.5.11. That is, the 2-D BWNM gives results in close agreement with the laboratory work by Van der Meer and Janssen (1995). An average error between the laboratory work and the numerical model is 25%. It can be noticed from figure 5.5.16 that the most

significant errors happened for cases with very small wave overtopping volumes (K-5 and K-8). One reason could be numerical errors due to an inappropriate mesh size. Using smaller mesh size could have improved the accuracy of the numerical model results.

Run No.	R_c (m)	H_s (m)	T_p (s)	T_m (s)
K-1	1.00	0.79	3.51	3.05
K-2	1.00	1.23	4.43	3.85
K-3	1.00	1.73	5.13	4.46
K-4	1.50	0.86	3.54	3.08
K-5	1.50	1.29	4.31	3.75
K-6	1.50	1.75	5.14	4.47
K-7	2.00	0.86	3.51	3.05
K-8	2.00	1.29	4.37	3.80
K-9	2.00	1.75	5.20	4.52
K-10	2.00	2.34	6.04	5.25
K-11	2.50	1.40	4.60	4.00
K-12	2.50	1.85	5.37	4.67
K-13	2.50	2.42	6.08	5.29
K-14	3.00	1.25	4.39	3.82
K-15	3.00	1.69	5.19	4.51
K-16	3.00	2.26	6.01	5.23

Table 5.5.4: Configuration of the small-scale tests of seawall with slope 1:2.

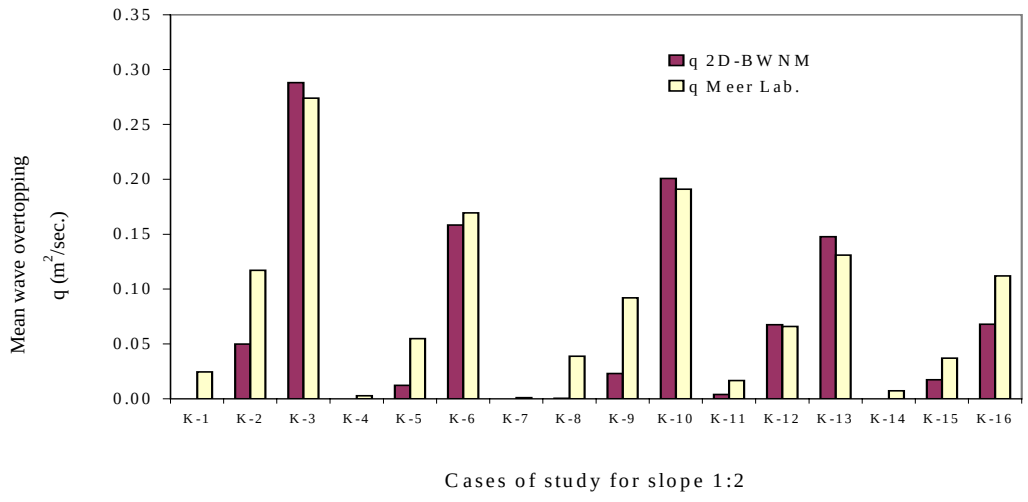

Figure 5.5.17: Comparison between 2-D BWNM and Laboratory measured dimensional overtopping discharges.

Figure 5.5.18 shows relationship between dimensionless freeboard and dimensionless non-breaking wave overtopping of the 2-D BWNM, Van der Meer and Janssen (1995)'s design formula (Equation 2.2.3) and Van der Meer and Janssen (1995)'s laboratory data for 1:1 and 1:2 sloped seawalls.

As measured by the sum of the modulus of the differences between the Van der Meer and Janssen (1995)'s formula and 2-D BWNM results, the 2-D BWNM provides 15% improvement in the performance of laboratory data.

Significant differences between the numerical and laboratory data could be noticed in some cases especially in very small volume of wave overtopping $(Q < 0.001)$. This average error could be due to the scale effects, the finite duration of both the numerical simulation time and laboratory test time in dealing with random wave, and the uncertainty in laboratory work, as well as numerical rounding errors in the computational model.

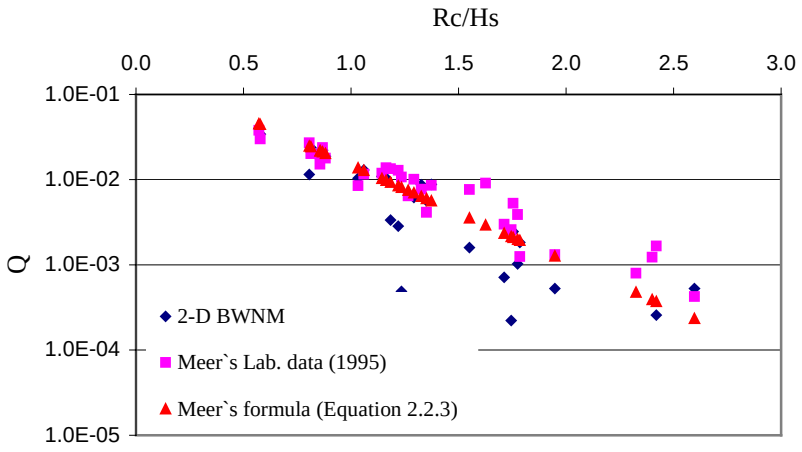

Figure 5.5.18: Comparison between 2-D BWNM results, Van der Meer's formula and Van der Meer's laboratory data as basis for equation 2.1.3 (non-breaking wave, $\xi_p > 2$).

5.5.2.3 Comparison with laboratory data for seawalls with slope 1:4

A total of 11 tests have been run using 2-D BWNM. Figure 5.5.19 gives the cross section of the 1:4 sloped seawall and the free surface profile. Details of the configurations for 16 runs are presented in Table 5.5.5. The model has the same mesh set-up, time step and the simulation time as the previous two cases of study.

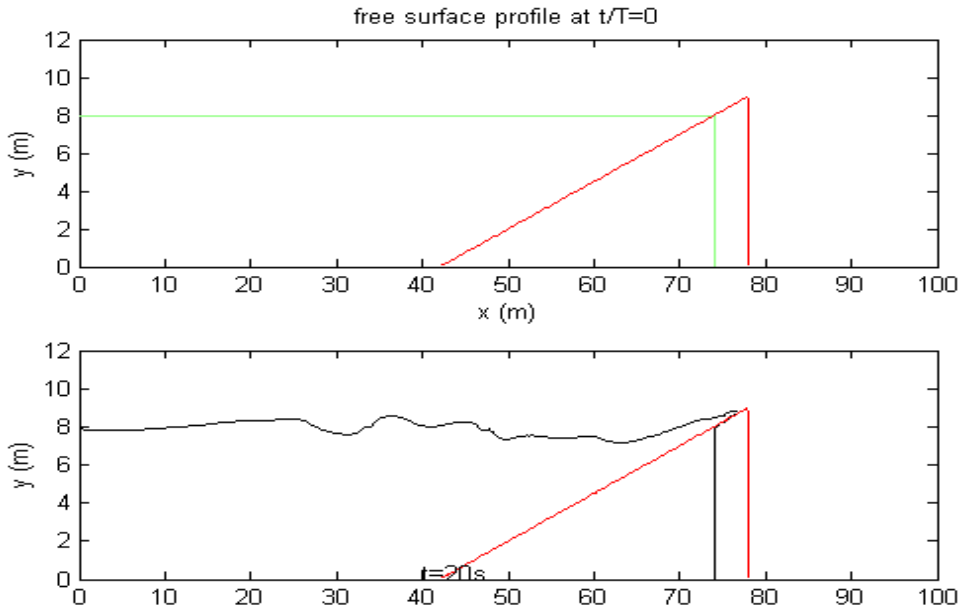

Figure 5.5.19: Cross section for seawall with slope 1:4 with the breaking wave surface profile after 20 sec.

Run No.	R_c (m)	H_s (m)	T_p (s)	T_m (s)
J-1	1.00	0.78	3.53	3.07
J-2	1.00	1.22	4.38	3.81
J-3	1.00	1.7	5.19	4.51
J-4	1.50	1.26	4.38	3.81
J-5	1.50	1.75	5.16	4.49
J-6	1.50	2.35	6.03	5.24
J-7	2.00	1.26	4.38	3.81
J-8	2.00	1.71	5.16	4.49
J-9	2.00	2.29	4.88	4.24
J-10	3.00	1.72	5.19	4.51
J-11	3.00	2.32	6.07	5.28

Table 5.5.5: Configuration of the small-scale tests of seawall with slope 1:4

The same tendency of slope 1:1 and slope 1:2 has been found in slope 1:4 as can seen in Figure 5.5.20. The results of the numerical model match well with the laboratory work by Van der Meer and Janssen (1995). The average difference between the laboratory work and the numerical model is 23%.

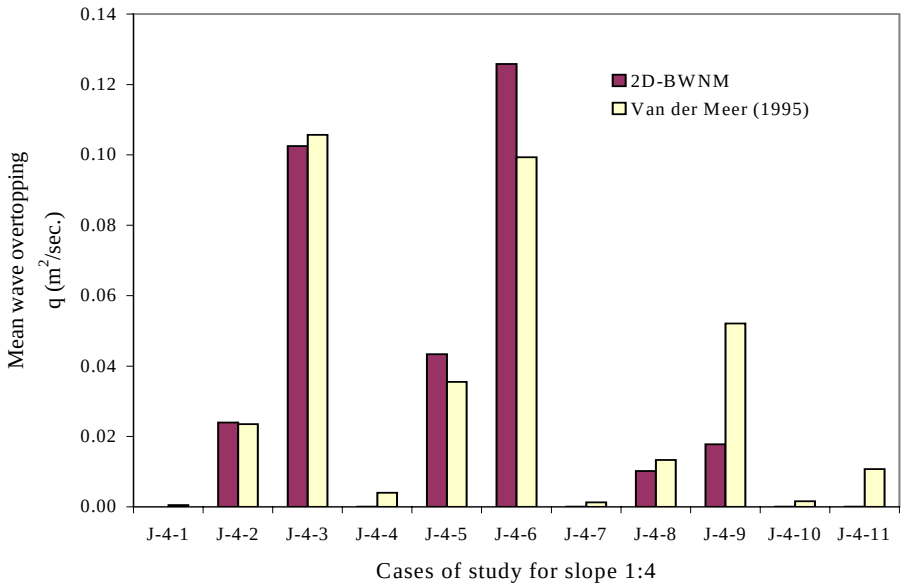

Figure 5.5.20: Comparison between 2-D BWNM and Laboratory measured dimensional overtopping discharges.

Figure 5.5.21 presents the comparison between dimensionless wave overtopping of 2-D BWNM, Van der Meer's formula and the laboratory data used as the basis for the Van der Meer and Janssen's (1995) design formula for breaking wave.

As measured by the sum of the modulus of the differences between the Van der Meer and Janssen (1995)'s formula and 2-D BWNM results, the 2-D BWNM provides 29% improvement in the performance of laboratory data.

Figure 5.5.21 has the same tendency of Figure 5.5.18 that there are significant differences between the numerical and laboratory data in some cases. These differences concentrate in very small volume of wave overtopping $(Q \le 0.0001)$.

It can be referred here also to the same reasons explained before in Section 5.5.2.2, that scale effects, laboratory measurements accuracy, finite duration of both the numerical simulation time and laboratory test time in dealing with the random waves and the numerical rounding errors in the computational model could be reasons of the significant differences.

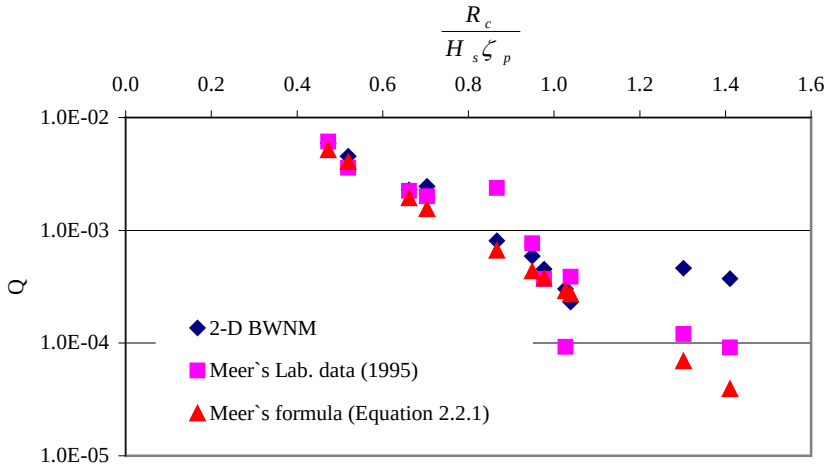

Figure 5.5.21: Comparison between 2-D BWNM results, Van der Meer's formula and Van der Meer's laboratory data as basis for equation 2.1.3 (breaking wave, $\xi_p < 2$).

5.5.2.4 Comparison with the existing design formula for seawalls with slope 1:3 and 1:4

As mentioned earlier in Chapter two (section 2.2), three empirical design formulae for wave overtopping of a simple sloped seawall subjected to irregular waves approaching normal to the slope are chosen here to validate the 2-D BWNM:

- Owen (1980).
- Van der Meer and Janssen (1995).
- Hedges and Reis (1998).

A total of 18 tests were run with a water depth of 4.5m, dimensionless freeboard (R) ranging from 0.3 to 1.0 and irregular breaking waves with a JONSWAP spectrum with significant wave height (H_s) from 0.83 - 1.48m, mean wave period (T_m) from 3.8-4.6s and peak wave period (T_p) from 5.0 – 6.02s. In total 320 cells are used in the *x*-direction with a cell size of 0.25m. In the *y*-direction 120 cells are used with a cell size of 0.1m. The basic time step is 0.04s and the simulation time is 90s. The value of γ in the JONSWAP spectrum is set to 3.3 and the spectrum is represented by 40 component frequencies between 0.15 and 0.265 Hz. Figure 5.5.22 gives the cross section of the seawall with slope 1:3 and shows the breaking wave surface.

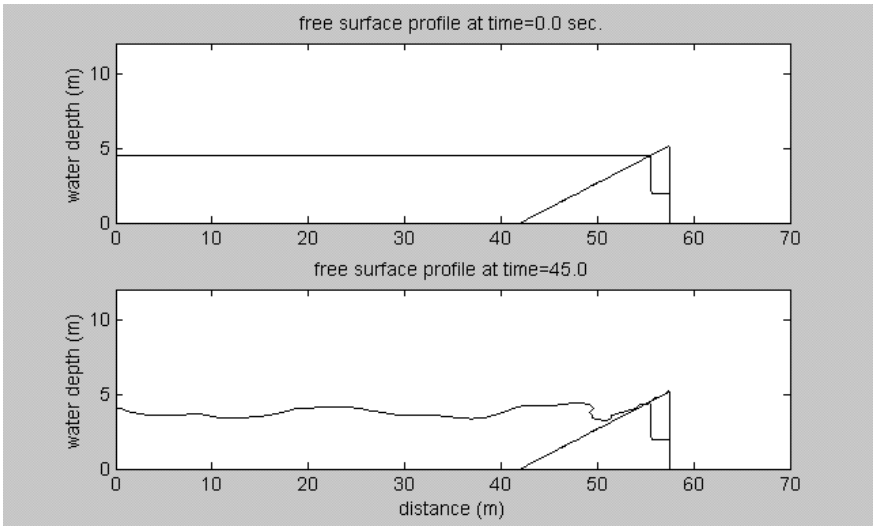

Figure 5.5.22: Cross section for seawall with slope 1:3 with the breaking wave surface profile after 45 sec.

Figures 5.5.23 and 5.5.24 show the comparison between the results produced by 2-D BWNM and the empirical formulae for dimensionless freeboard (R) range from 0.3 to 1.0. It can be seen from the figures that the empirical formulae

underestimate the amount of breaking wave overtopping under irregular wave attack in comparison with the numerical results. The new numerical approach goes some way towards addressing the issues raised by Besley *et al.* (1998) and Goda (2000), which were that if wave breaking in shallow water is not taken into account, prediction methods developed for deep water will significantly underestimate overtopping discharge. The difference between the numerical results and empirical formulae increases when dimensionless freeboard decreases. Schuttrumpf *et al.* (1998) reported that the amount of overtopping is underestimated by the existing empirical formulae for small and zero freeboard which supports the results of the 2-D BWNM (Figures 5.5.19 and 5.5.20).

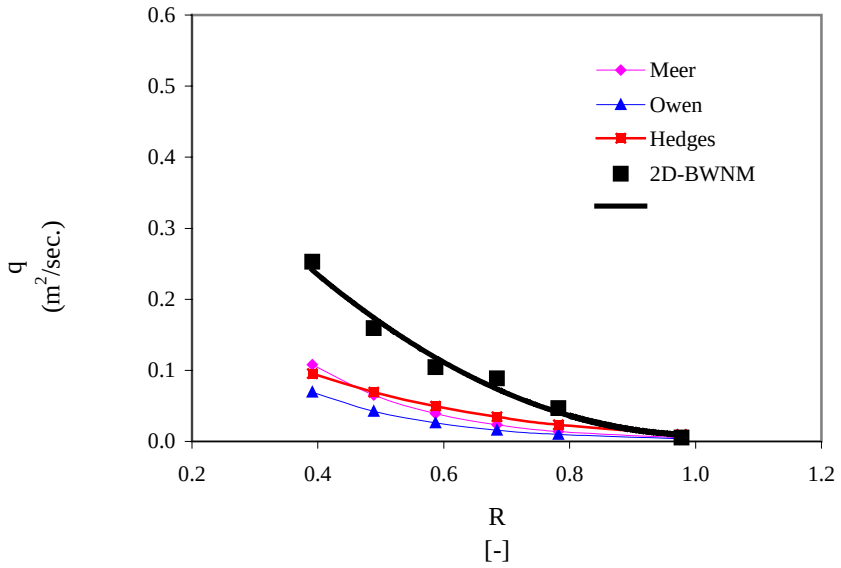

Figure 5.5.23: Comparison between 2-D BWNM and empirical design formulae for irregular breaking wave overtopping over 1:3 sloped seawall.

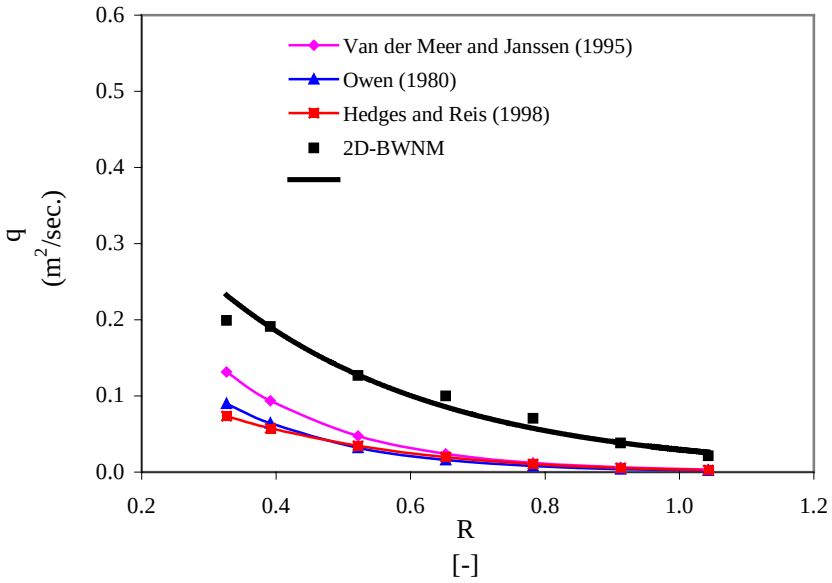

Figure 5.5.24: Comparison between 2-D BWNM and empirical design formulae for irregular breaking wave overtopping over 1:4 sloped seawall.

The analysis of the results from these series of cases for two different slopes (1:3 and 1:4) under irregular breaking wave attack ($\zeta_p < 2$) are used to define the following new suggested design formula:

$$Q = \frac{q}{\sqrt{gH_s^3}} \frac{\sqrt{\tan\alpha}}{\zeta_p} = 0.09 \exp\left(-4.12R\right) \qquad \left(0.3 \le R < 1\right) \qquad (5.5.8)$$

An exponential form has used here formulae to be consistent with Van der Meer's formulae. More details about Van der Meer's formulae and its advantage could be found in Chapter 2 (Section 2.2.1 and Section 2.2.2).

The comparison between the Equation 5.5.8 and Van der Meer's equation is shown in Figure 5.5.25. The Figure supports the acknowledgement that widely current overtopping design formulae are significantly underestimating the overtopping discharge.

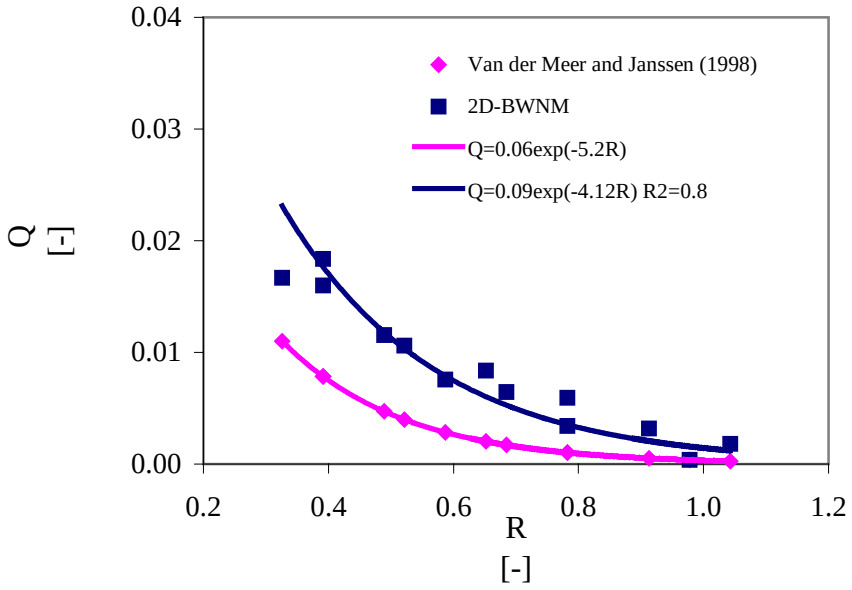

Figure 5.5.25: Comparison of 2-D BWNM suggested design formula and Van der Meer and Janssen's (1995) design formula for 1:3 and 1:4 sloped seawall $(0.3 \le R < 1)$.

5.6 Discussion

This chapter introduces the results for three cases. These results are used to evaluate the performance of the 2-D BWNM by making a comparison between the numerical results and laboratory data, other numerical models and empirical design formulae used in the design purposes.

The first case of study did not include the effect of waves. It tested the performance of the 2-D BWNM for the case of negative freeboard without waves over a vertical structure. The results for different negative freeboard for the range $(0 \le \frac{R_c}{d_s} \le -0.20)$ were presented and compared very well with the weir equation.

Comparison of results between the numerical model and the weir equation

indicates that 2-D BWNM gives between 1% to 12% less overflow volume than weir equation. Reasons for that difference were discussed in Section 5.3.

This case considers the basic for studying the case of wave overtopping and overflow. The case of overtopping and overflow will be presented in Chapter 7.

Secondly, the case of wave overtopping over 1:3 and 1:1.5 smooth slope seawalls was considered. In this case the linear wave boundary condition is chosen as an inflow boundary condition. The average dimensionless wave overtopping rates were compared with other numerical model results based on the non-linear shallow wave equation (AMAZON) and with laboratory data. The performance of the new model is good and the analysis of the result has shown that the 2-D BWNM can give a 12% improvement over the AMAZON numerical model as a general guide.

Finally, the third case considered wave overtopping with irregular wave boundary condition. This case is divided into two cases, the first one studied three different seawall slopes 1:1, 1:2 and 1:4. The numerical results are compared with the laboratory data collected by Van der Meer and Janssen (1995) which they used to investigate their design formulae for breaking and non-breaking wave overtopping. The comparison for the non-breaking wave (slope 1:1 and 1:2) and breaking wave (slope 1:4) gives good agreement between the numerical results and the laboratory results. Analysis of the results for the three slopes gives 22% difference between the numerical and laboratory work. This average error could be due to the scale effects and the uncertainty in laboratory work.

The second case studied seawall slopes of 1:3 and 1:4, for which the numerical results were compared with the empirical design formulae of Owen (1980); Van der Meer and Janssen (1995) and Hedges and Reis (1998). The comparison highlights the same issue raised by Besley *et al.* (1998) and Goda (2000), that the existing design formulae underestimate the amount of wave overtopping for small freeboard.

The analysis of the 2-D BWNM results leads to a new proposed design formula for overtopping by breaking waves. The new design formula is as follows:

$$Q = \frac{q}{\sqrt{gH_s^3}} \frac{\sqrt{\tan\alpha}}{\zeta_p} = 0.09 \exp\left(-4.12R\right) \qquad \left(0.3 \le R < 1\right) \tag{5.5.9}$$

More validation with filed data is recommended in the future work before the new overtopping formula used for design purposes.

All the previous examples and the comparison with other tested numerical models, laboratory data and empirical formulae indicate that the numerical model performs well. The next two chapters concentrate on the cases which are not covered completely by the current design formulae. The 2-D BWNM is used as a numerical flume to perform a series of experiments for small, zero and negative freeboard conditions. Curves describing a functional relationship between overtopping volume, freeboard and wave conditions are derived. The results are used in conjunction with existing formulae to propose a unified set of design equations to predict combined overflow and overtopping volumes for different wave conditions.

CHAPTER 6
Small Positive and Zero Freeboards

6.1 Introduction

The design crest height of a coastal structure is strongly dependent on the design water level. If the structure crest level is less than the maximum run up the wave overtopping occurs. Structures are normally designed to limit overtopping to a predefined level (not necessary zero), under specified design conditions. Under extreme storm conditions some wave overtopping may be expected due to the uncertainties in the estimation of incoming wave parameters and the design water level. As a result wave overtopping is an important parameter for the design of many coastal structures.

In the last years, the climate has been changed and the global sea level rises. Tide-gauge records, in some cases covering the last 100 years, show a general increase in sea level of 2.4±0.9 mm per year (Hardy, 2003). The existing coastal structures which were designed for certain water levels may now experience higher water levels, wave frequently, and experience a greater amounts of wave overtopping, due to reduced freeboard.

Existing overtopping design formulae do not account for the case of small freeboard. Schuttrumpf *et al.* (2001) reported that the existing overtopping models for average overtopping rates by Van der Meer and Janssen (1995) and Van Gent (1999) are not valid for the condition of small and / or zero freeboard. For example, the Van der Meer formula for breaking waves (Equation 2.2.1) is applicable in the range $2.0 > R > 0.3$ (Burchartch and Hughes, 2003). It will be

helpful for engineers to have new design formulae cover the case of small positive until zero freeboard.

The performance of 2-D BWNM had been evaluated in the previous chapter. In this chapter, the cases of small and zero freeboard are presented. New design formulae for these two cases is shown with their comparison with the recent design formulae of Schuttrumpf *et al.* (2001).

Generally, The main purpose of this chapter is to study wave overtopping using 2-D BWNM and to introduce new proposed formulae for designers that cover two main cases:

- Small positive freeboard $\left(0.3 \geq R > 0.0\right)$.
- Zero freeboard $\left(R = 0.0\right)$.

6.2 Wave overtopping at small positive freeboard under irregular wave conditions

The case of irregular wave overtopping over sloped seawalls had been presented in Chapter 5. Comparison between calculated wave overtopping volume with laboratory work of Van der Meer and Janssen (1995) and with the well known empirical design formulae of Owen (1980), Van der Meer and Janssen (1995) and Hedges and Reis (1998) have been shown in Section 5.5.2 and good agreement has been found. In this part of this chapter, further investigation is presented for the case of small freeboard, $\left(0.3 \geq R > 0.0\right)$, which is outside the range of applicability of engineering design formulae.

Run No.	H_s (m)	T_m (s)	T_p (s)	R_c (m)	ξ_p [-]	R [-]
1	1.22	3.8	5.00	0.1125	1.89	0.05
2	1.22	3.8	5.00	0.2250	1.89	0.10
3	1.22	3.8	5.00	0.3375	1.89	0.15
4	1.22	3.8	5.00	0.4500	1.89	0.20
5	1.22	3.8	5.00	0.5625	1.89	0.24
6	1.22	3.8	5.00	0.6750	1.89	0.29
7	1.39	4.0	5.00	0.1125	1.77	0.05
8	1.39	4.0	5.00	0.2250	1.77	0.09
9	1.39	4.0	5.00	0.3375	1.77	0.14
10	1.39	4.0	5.00	0.4500	1.77	0.18
11	1.39	4.0	5.00	0.5625	1.77	0.23
12	1.39	4.0	5.00	0.6750	1.77	0.27
13	1.39	4.0	5.00	0.7875	1.77	0.32
14	1.24	3.9	5.00	0.1125	1.87	0.05
15	1.24	3.9	5.00	0.2250	1.87	0.10
16	1.24	3.9	5.00	0.3375	1.87	0.15
17	1.24	3.9	5.00	0.4500	1.87	0.19
18	1.24	3.9	5.00	0.5625	1.87	0.24
19	1.24	3.9	5.00	0.6750	1.87	0.29
20	0.83	3.6	5.00	0.1125	2.29	0.14
21	0.83	3.6	5.00	0.2250	2.29	0.27
22	1.48	4.6	6.02	0.1125	2.06	0.08
23	1.48	4.6	6.02	0.2250	2.06	0.15
24	1.48	4.6	6.02	0.3375	2.06	0.23
25	1.48	4.6	6.02	0.4500	2.06	0.30
26	0.72	4.7	7.30	0.0563	3.58	0.08
27	0.72	4.7	7.30	0.1125	3.58	0.16
28	0.72	4.7	7.30	0.1688	3.58	0.23

Table 6.2.1: Irregular wave characteristics used in the case of small freeboard wave overtopping at 1:3 sloped seawall $\left(0.3 \geq R > 0.0\right)$

6.2.1 Wave overtopping at small positive freeboard under irregular wave attack for 1:3 sloped seawall

A total of 28 tests were run using the 2-D BWNM for 1:3 sloped seawall. The setup of these tests is shown in Figure 6.2.1 and in Table 6.2.1. As is clear from Table 6.2.1, the wave characteristics are chosen to cover wide range of significant wave heights, mean and peak wave periods and freeboard height. The runs cover the breaking and non-breaking waves and are concentrated within the range of small dimensionless freeboard, $(0.3 \geq R > 0.0)$. In total 320 cells are used in *x*-direction and 120 in *y*-direction. The cell size is 0.25m and 0.1m in x and y directions. The JONSWAP spectrum is chosen to simulate the nature of irregular waves as described in details in Chapter 5 (Section 5.5.1).

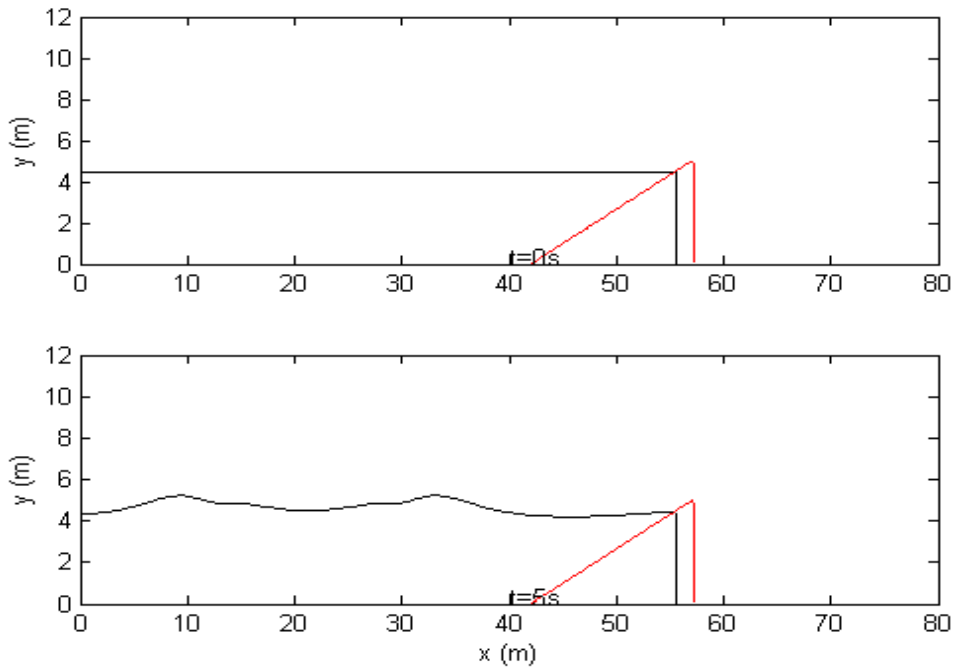

Figure 6.2.1: Definition sketch of the computational domain and free water surface used for the numerical simulation of wave overtopping at small freeboard $(0.3 \geq R > 0.0)$ [Run no. 5 (Table 6.2.1): H_s = 1.22m, T_m = 3.80s and T_p = 5.0s].

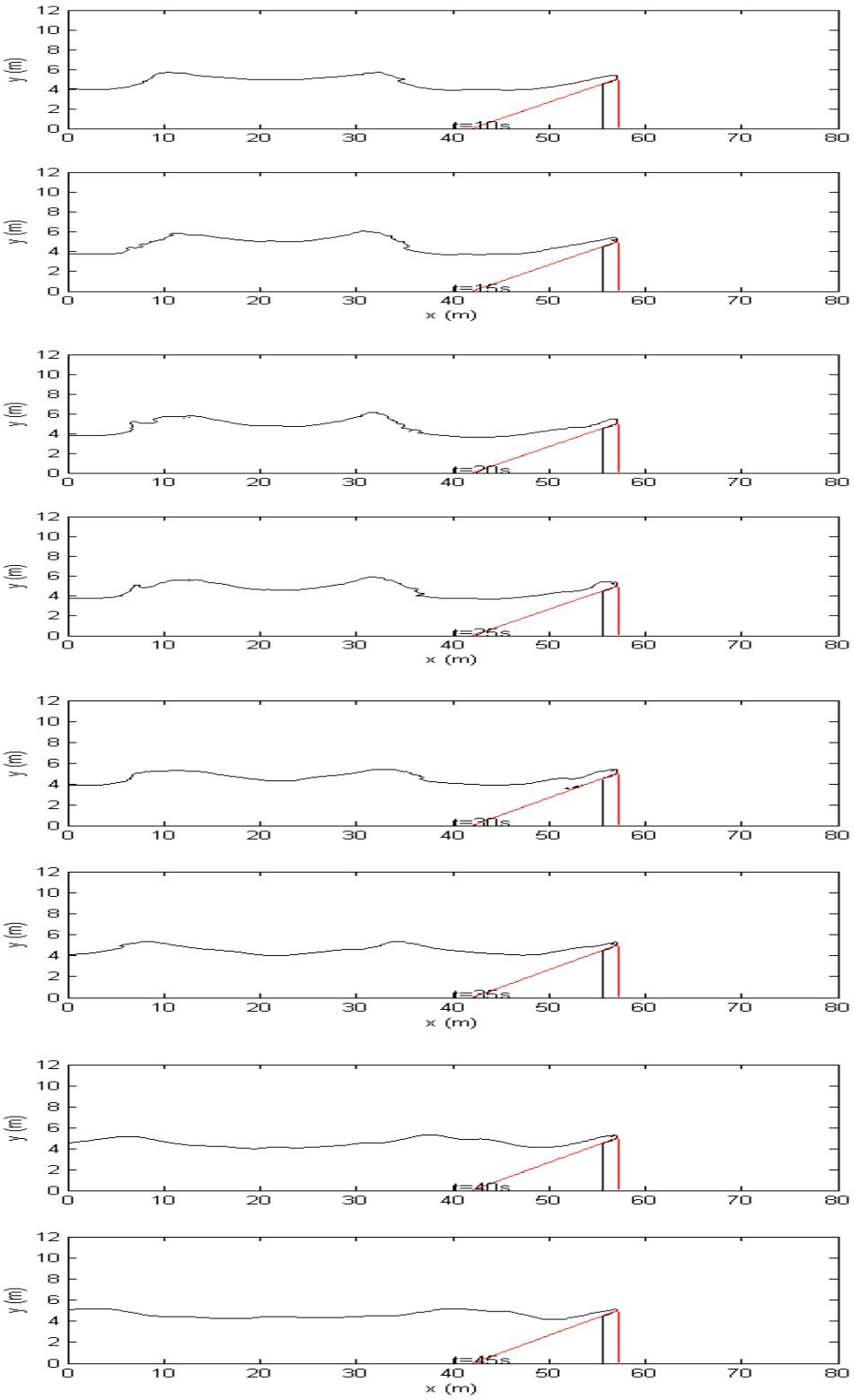

Figure 6.2.2: Irregular wave overtopping on a 1:3 sloping seawall from time 10 to 45s. [Run no. 5 (Table 6.2.1): H_s = 1.22m, T_m = 3.80s and T_p = 5.0s].

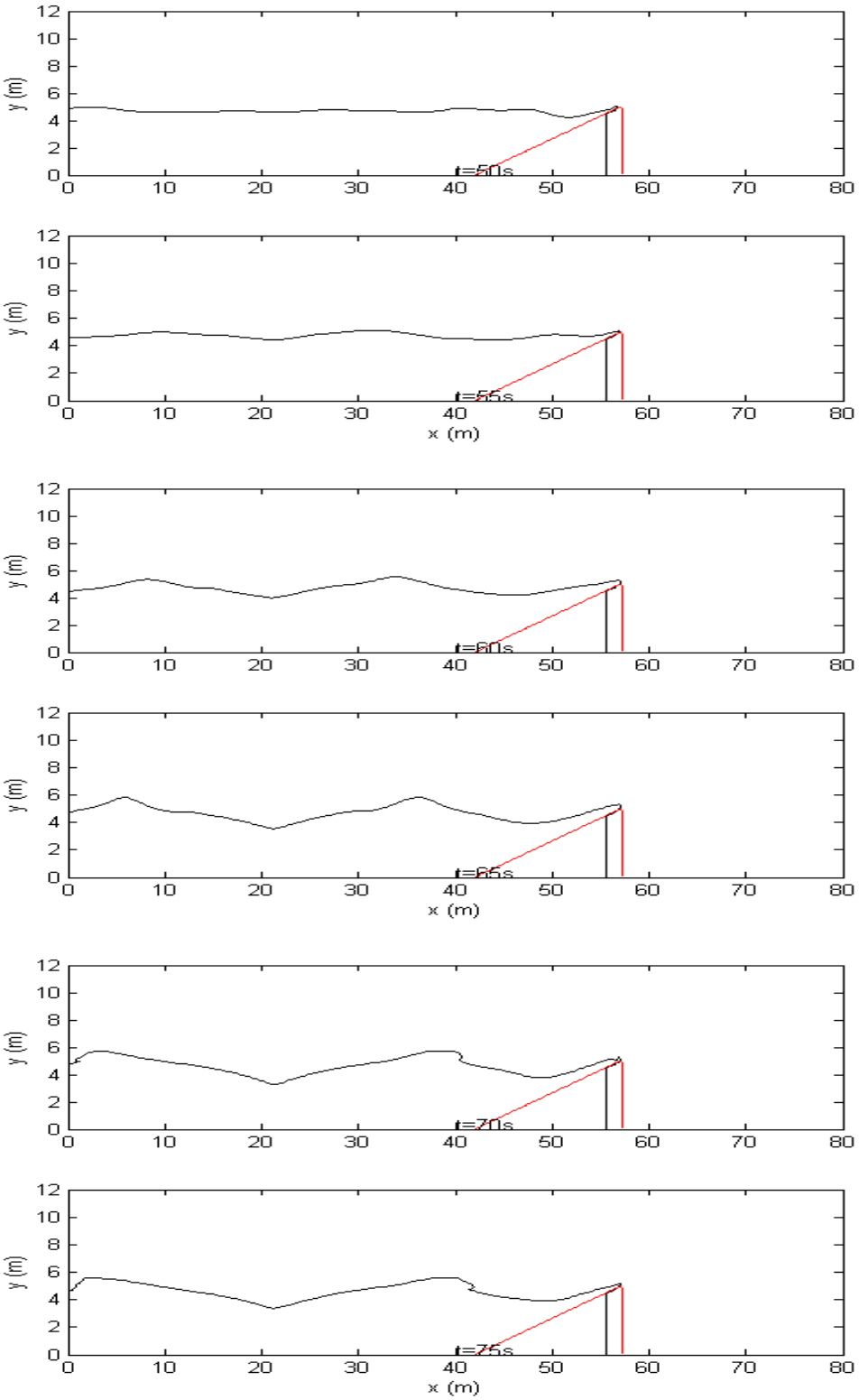

Figure 6.2.3: Irregular wave overtopping on a 1:3 sloping seawall from time 50 to 75s. [Run no. 5 (Table 6.2.1): H_s = 1.22m, T_m = 3.80s and T_p = 5.0s].

The duration of the calculation is 90 seconds with an initial time step of 0.04s. Reasons for choosing this time interval were explained in Figures 5.5.12 and 5.5.13 for calculated cumulative and instantaneous overtopping volume. Figure 5.5.13 showed that the instantaneous overtopping volume is almost constant after the first 30 seconds. It was possible to reduce the simulation time down to 90 seconds here for small positive, zero and negative freeboards due to the continuity of wave overtopping action during the calculation time.

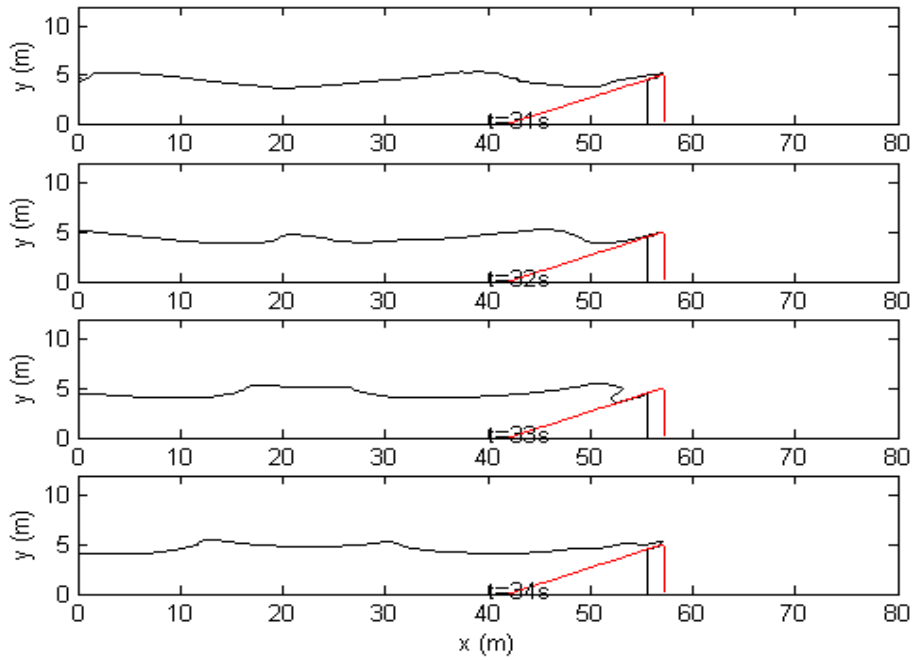

Figure 6.2.4: Plunging breaking wave produces by 2-D BWNM on a 1:3 sloping seawall [Run no. 5 (Table 6.2.1): H_s =1.22m, T_m = 3.80s, T_p = 5.0s and ξ_p =1.89].

Propagation of irregular waves is shown in Figures 6.2.2 and 6.2.3 for case study No. (5), with H_s = 1.22m, T_m = 3.80s, T_p = 5.00s and d_s =4.5m. The surf similarity parameter (ξ_p) in this case is equal to 1.89. The plunging breaking is expected for this value. The plunging breaker normally occurs on a relatively steep slope.

Right before the wave plunges, the wave shape become asymmetric and the wave front steepness and curls downward, forming a large plunging jet. As this stage of wave overturning, the flow motion remains essentially irrotational. The numerical model produces the plunging wave well as presented in Figure 6.2.4

Details of the irregular waves propagation over sloped seawall at small positive freeboard can be found in Appendix A.

More details about comparison of the numerical solutions with experimental data for both plunging and spilling breaking waves can be found in Lin (1998) and Lin and Liu (1998) in terms of free surface elevation, mean velocity components and turbulence intensity.

Figure 6.2.5 shows the calculated overtopping volume along with the time of calculation. The non-linearity in the overtopping mass is clear in Figure 6.2.5 and this due to the irregular nature of the waves.

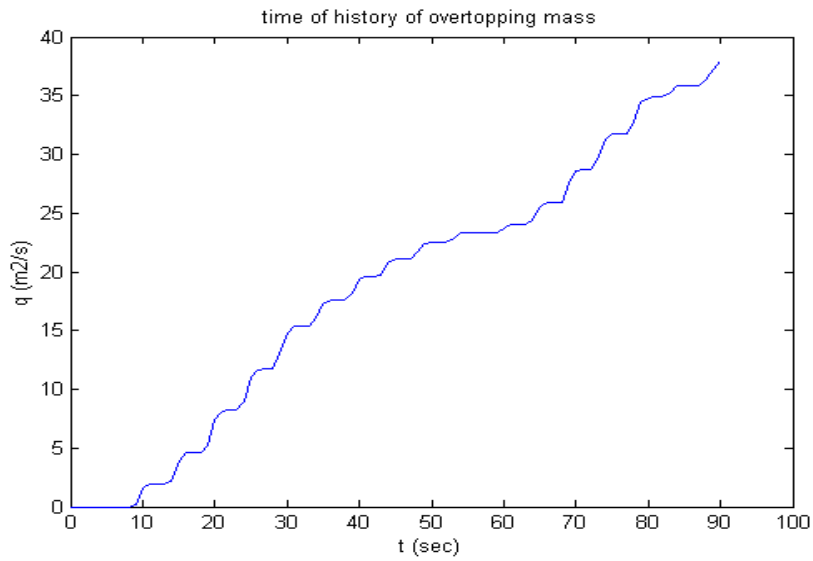

Figure 6.2.5: Time history of the cumulative wave overtopping volume for 1:3 sloped seawall for small positive freeboard $(0.3 \geq R > 0.0)$. [Run no. 5 (Table 6.2.1): H_s = 1.22m, T_m = 3.80s and T_p = 5.0s].

Comprehensive analysis has been done to the overtopping volume calculated from the 2-D BWNM. The cases of study have been divided into breaking and non-breaking waves according to the value of surf similarity parameter ξ_p of Van der Meer and Janssen (1995).

Figure 6.2.6 explains the relation between the dimensionless freeboard and the dimensionless wave overtopping for breaking and non-breaking waves. The exponential function is used here to define the relation between dimensionless overtopping discharge and dimensionless freeboard. Owen (1980) was the first who gave explicitly the exponential relationship. Most of other researches have used this kind of relationship to describe their overtopping data as can be found in details in Chapter 2 (Section 2.1).

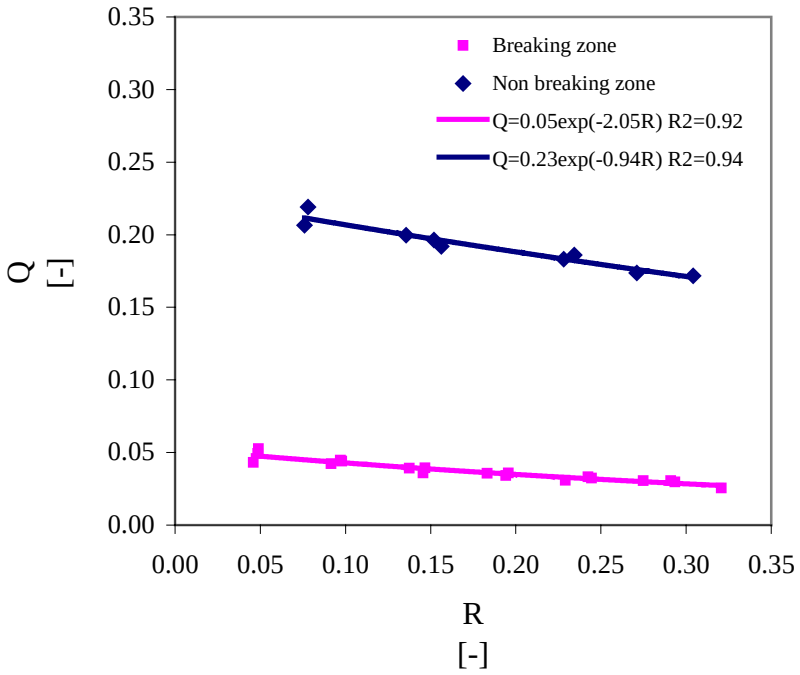

Figure 6.2.6: New design formulae for irregular wave overtopping over 1:3 sloped seawall for breaking and non-breaking waves for small freeboard $(0.3 \geq R > 0.0)$.

The analysis of these data leads to the following suggested design formulae for the case of small freeboard $\left(0.3 \geq R > 0.0\right)$:

- Breaking waves ($\xi_p < 2$): $Q = 0.053\exp\left(-2.05R\right)$	(6.2.1)
- Non-breaking waves ($\xi_p \geq 2$): $Q = 0.227\exp\left(-0.94R\right)$	(6.2.2)

R^2 (square of the Pearson product moment correlation coefficient) is an indicator that reveals how closely the estimated values for the formula trend line correspond to the actual input data. The formula trend line is most reliable when R^2 value is at or near 1. The R^2 values for Equations (6.2.1) and (6.2.2) are 0.92 and 0.94 respectively.

6.2.2 Wave overtopping at small positive freeboard under irregular wave attack for 1:4 sloped seawall

Table 6.2.2 shows wave characteristics, freeboard, surf similarity parameter and dimensionless freeboard used for 1:4 sloped seawall. Definition sketch of the computational domain and the free water surface after 15 second are shown in Figure 6.2.7 for case study No. (18), with H_s = 0.72, T_m = 4.7, T_p = 7.30 and water depth = 4.5m. The same concept of previous section is considered as these characteristics are chosen to cover wide range of significant wave heights, mean and peak wave periods and freeboard height in the breaking and non-breaking zone in small dimensionless freeboard $\left(0.3 \geq R > 0.0\right)$.

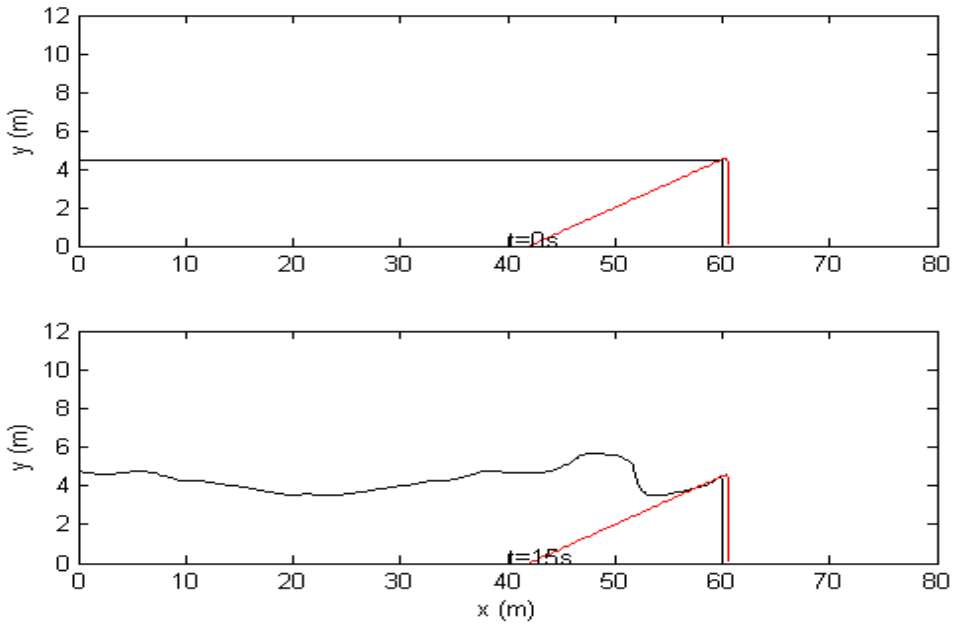

Figure 6.2.7: Definition sketch of the computational domain and free water surface used for the numerical simulation of wave overtopping at small freeboard $(0.3 \geq R > 0.0)$ [Run no. 18 (Table 6.2.2): H_s = 0.72m, T_m = 4.70s and T_p = 7.30s].

The JONSWAP spectrum is also chosen to simulate the nature of irregular wave with the same details as discussed in Section 6.2.1.

In total 400 cells were used in *x*-direction and 120 in *y*-direction. The cell size is 0.25m and 0.1m in x and y directions. The period of simulation was 90 second with initial time step 0.04 second.

Figure 6.2.8 shows the overtopping mass rate calculated by the numerical model. The irregular nature of the waves affects the rate of wave overtopping which is evident from the figure.

Run No.	H_s (m)	T_m (s)	T_p (s)	R_c (m)	ξ_p [-]	R [-]
1	1.22	3.8	5.00	0.1125	1.41	0.07
2	1.22	3.8	5.00	0.2250	1.41	0.13
3	1.22	3.8	5.00	0.3375	1.41	0.20
4	1.22	3.8	5.00	0.4500	1.41	0.26
5	1.39	4	5.00	0.1125	1.33	0.06
6	1.39	4	5.00	0.2250	1.33	0.12
7	1.39	4	5.00	0.3375	1.33	0.18
8	1.39	4	5.00	0.4500	1.33	0.24
9	1.48	4.6	6.02	0.1125	1.55	0.05
10	1.48	4.6	6.02	0.2250	1.55	0.10
11	1.48	4.6	6.02	0.3375	1.55	0.15
12	1.48	4.6	6.02	0.4500	1.55	0.20
13	1.48	4.6	6.02	0.5625	1.55	0.25
14	1.48	4.6	6.02	0.6750	1.55	0.29
15	0.81	4.1	5.73	0.1125	1.99	0.14
16	0.81	4.1	5.73	0.2250	1.99	0.28
17	0.72	4.7	7.30	0.0563	2.69	0.08
18	0.72	4.7	7.30	0.1125	2.69	0.16
19	0.72	4.7	7.30	0.1688	2.69	0.23
20	0.72	4.7	7.30	0.2250	2.69	0.31

Table 6.2.2: Irregular wave characteristics used in the case of small freeboard wave overtopping at 1:4 sloped seawall $\left(0.3 \geq R > 0.0\right)$.

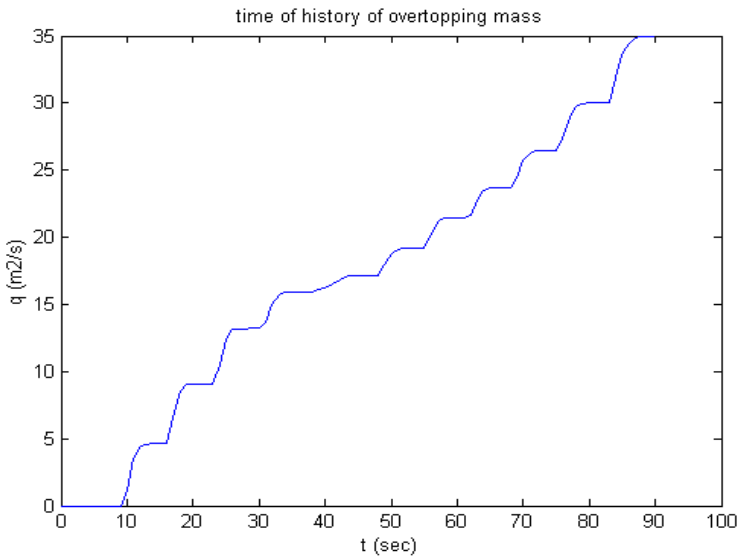

Figure 6.2.8: Time history of the cumulative wave overtopping volume for 1:4 sloped seawall for small positive freeboard $(0.3 \geq R > 0.0)$ [Run no. 18 (Table 6.2.2): H_s = 0.72m, T_m = 4.70s and T_p = 7.30s].

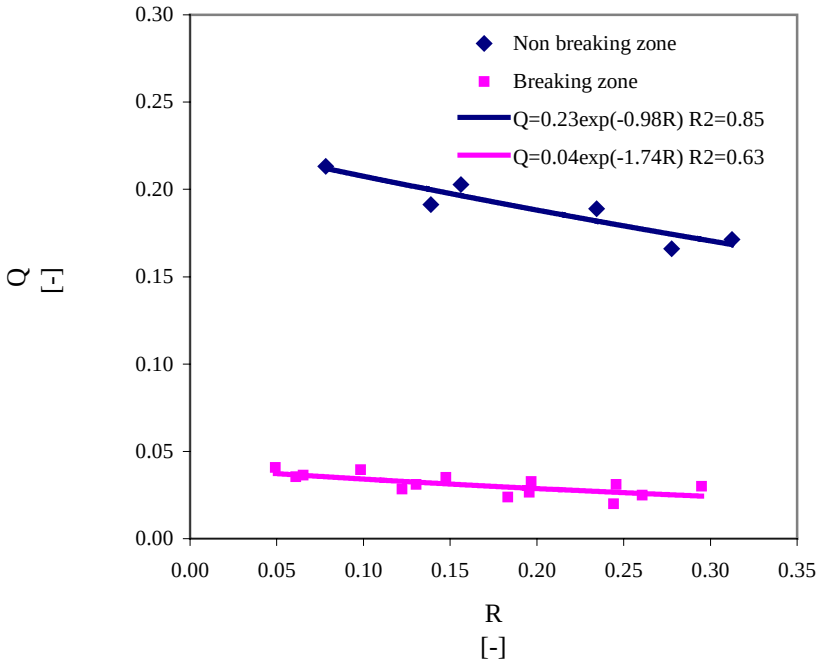

Figure 6.2.9: New design formulae for irregular wave overtopping over 1:4 sloped seawall for breaking and non-breaking waves for small freeboard $(0.3 \geq R > 0.0)$.

The analysis of the overtopping volume results calculated from the 2-D BWNM leads to the following formulae for breaking and non-breaking waves:

- Breaking waves ($\xi_p < 2$): $Q = 0.041\exp(-1.74R)$ (6.2.3)

- Non-breaking waves ($\xi_p \geq 2$): $Q = 0.229\exp(-0.98R)$ (6.2.4)

The R^2 values for Equations (6.2.3) and (6.2.4) are 0.85 and 0.63 as shown in Figure 6.2.9. The values of R^2 are less than calculated for slope 1:3 (Figure 6.2.6). The decreasing in R^2 values is due to the decreasing in surf similarity parameter values (ξ_p). As shown in Tables 6.2.1 and 6.2.2, the values of ξ_p ranges from 1.33 to 1.55 in slope 1:4 while in slope 1:3 ranges from 1.77 to 1.89. The decrease in surf similarity parameter (ξ_p) leads to more wave breaking which affect directly the amount of wave overtopping. These give more scatter to the dimensionless wave overtopping which reduced the values of R^2.

6.3 Wave overtopping at zero freeboard under irregular wave condition in breaking and non-breaking zone

The case of zero freeboard has not received much attention. Most of the existing formulae for wave overtopping do not account for the case of zero freeboard. Schüttrumpf (2001) conducted model tests with zero freeboard (R_c=0) and without overtopping (R_c>R_{max}) and derived the following formulae:

$$Q = \frac{q}{\sqrt{2gH_s^3}} = 0.038.\xi_m \exp\left(-b\frac{R_c}{R_{u,2\%}}\right) \qquad \xi_m < 2 \qquad (6.2.6)$$

$$Q = \frac{q}{\sqrt{2gH_s^3}} = (0.096 - \frac{0.160}{\xi_m^3})\exp\left(-b\frac{R_c}{R_{u,2\%}}\right) \qquad \xi_m \geq 2 \qquad (6.2.7)$$

with: $R_{u,2\%} = \xi_m \times H_s$ = run-up height exceeded by 2% of the incident waves.

More details about Schüttrumpf (2001)'s formulae and theirs goodness of fit were presented in Chapter 2 (Section 2.8). Schüttrumpf (2001)'s is used here to validate the 2-D BWNM results for the case of zero freeboard.

A series of cases has been performed using the 2-D BWNM for 1:3 and 1:4 sloped seawall, for both breaking and non-breaking irregular waves to obtain average overtopping rates for the case of zero freeboard. Details of the wave characteristics are shown in Table 6.3.3. JONSWAP spectrum is chosen also here to present the irregular wave. Figure 6.3.10 presents the computational domain of 1:3 sloped seawall and the free water surface at time = 5.0s. in the numerical simulation. The number of cells in *x*-direction is 320 cells with cell size = 0.25 m and 120 cells in *y*-direction with cell size = 0.1 m. with water depth = 4.5m. The duration of the simulation was 90 seconds with an initial time step of 0.04 seconds.

Run No.	H_s (m)	T_m (s)	T_p (s)
1	0.56	3.50	5.06
2	0.72	4.70	7.30
3	0.80	4.70	7.20
4	0.81	4.10	5.73
5	0.82	3.60	5.00
6	0.83	3.60	5.00
7	0.83	3.70	5.00
8	1.22	3.80	5.00
9	1.23	3.90	5.00
10	1.24	3.90	5.00
11	1.39	4.00	5.00
12	1.48	4.60	6.02

Table 6.3.3: Irregular wave characteristics used in case of zero freeboard.

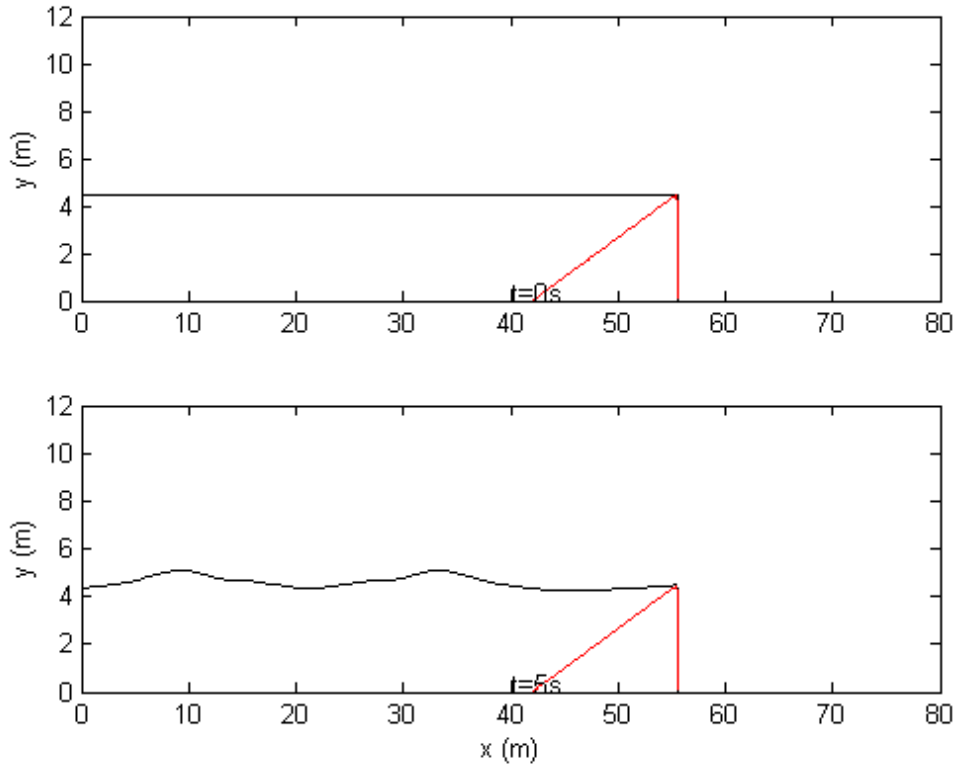

Figure 6.3.10: Definition sketch of the computational domain and free water surface used for the numerical simulation of wave overtopping at zero freeboard. [Run no. 6 (Table 6.3.3): H_s = 0.83m, T_m = 3.60s and T_p =5.00s].

The free surface profile over the time of calculation is shown in Figures 6.3.11 and 6.3.12. The surf similarity parameter (ξ_p) in this case is equal to 1.715. The plunging breaking is expected for this value. The numerical model produces the plunging wave well as presented in Figure 6.3.13. Details of the irregular waves propagation over sloped seawall at zero freeboard can be found in Appendix B.

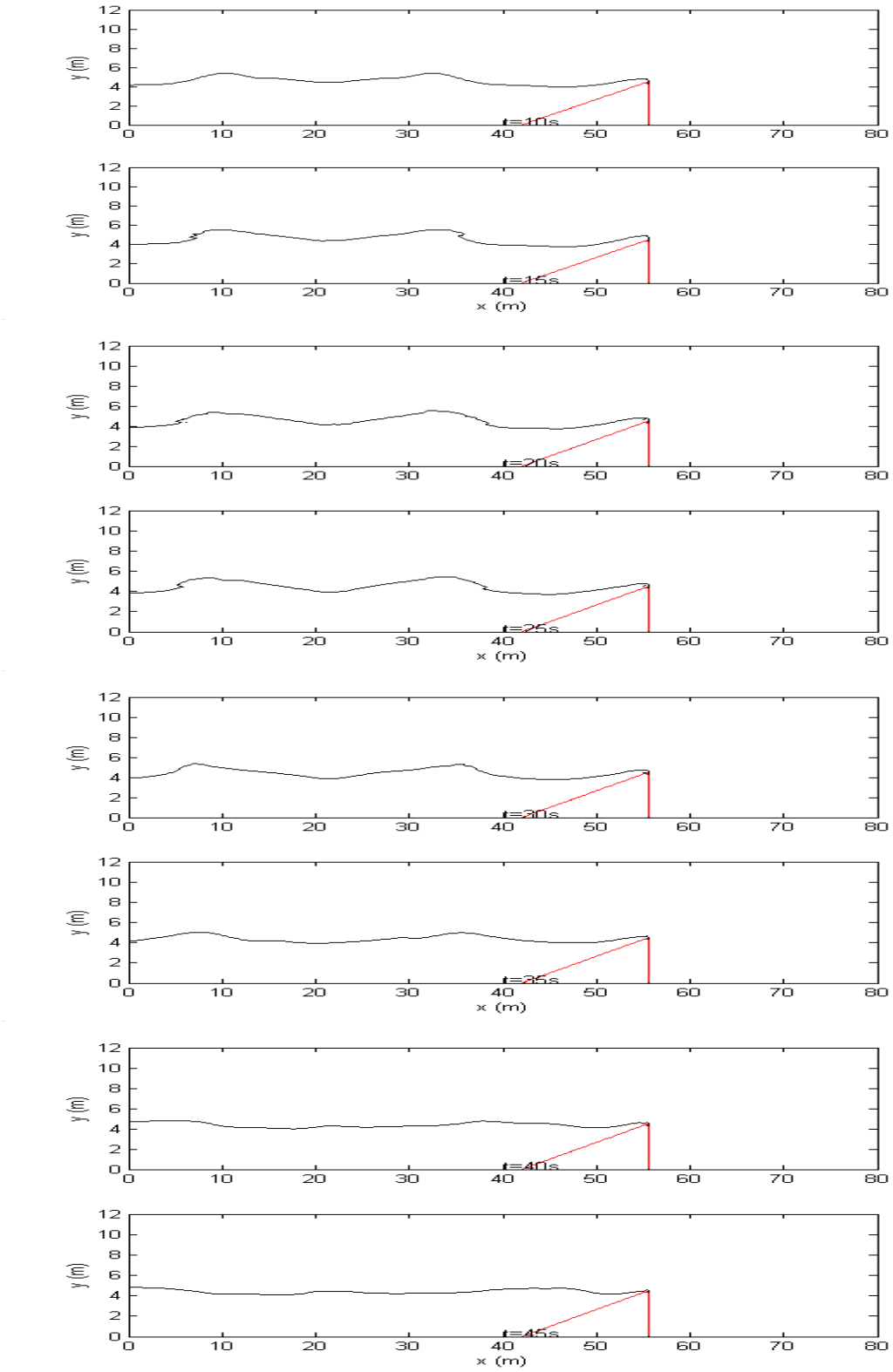

Figure 6.3.11: Irregular wave overtopping on a 1:3 sloping seawall from time 10 to 45s. [Run no. 6 (Table 6.3.3): H_s = 0.83m, T_m = 3.60s and T_p =5.00s].

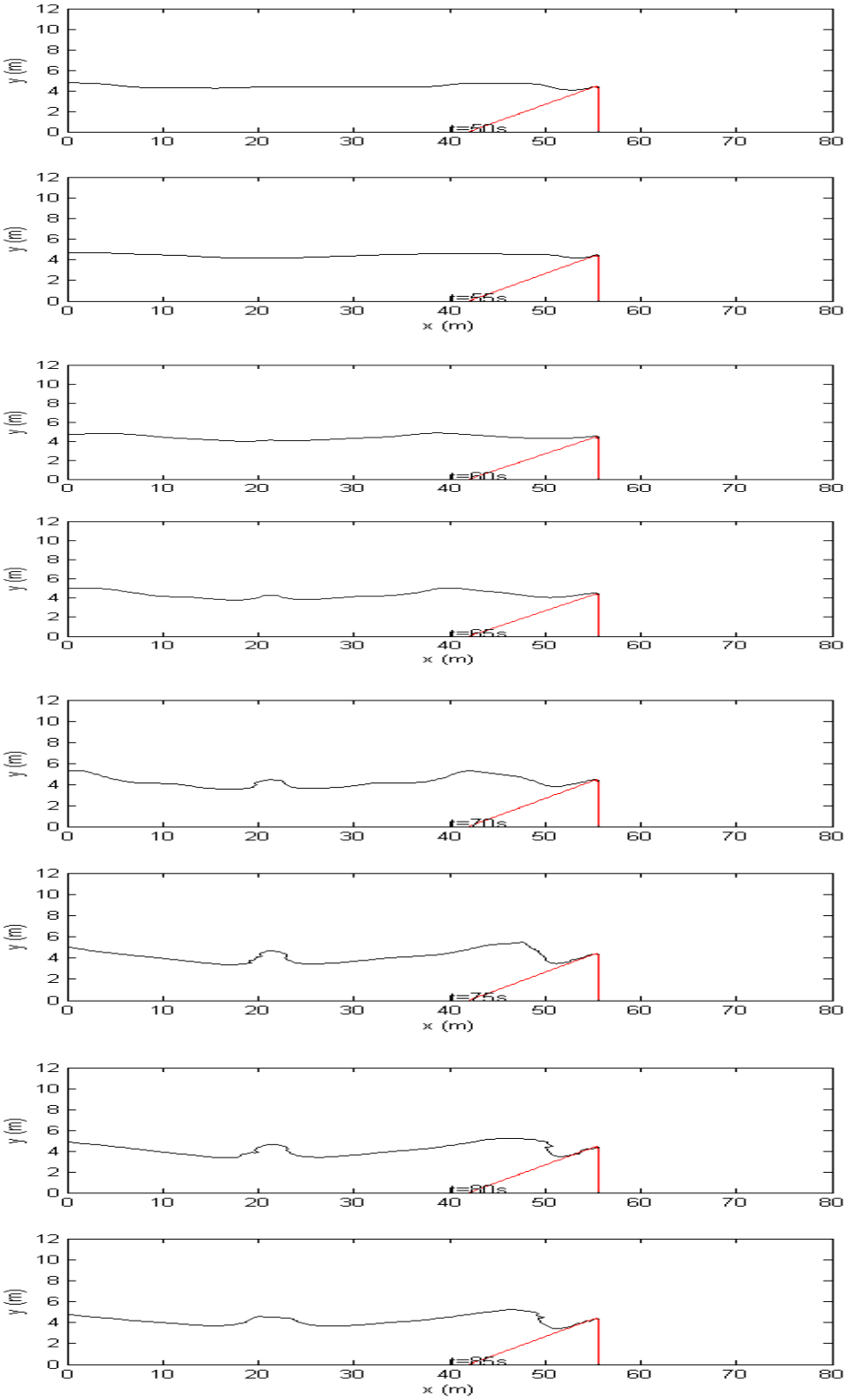

Figure 6.3.12: Irregular wave overtopping on a 1:3 sloping seawall from time 50 to 85s. [Run no. 6 (Table 6.3.3): H_s = 0.83m, T_m = 3.60s and T_p =5.00s].

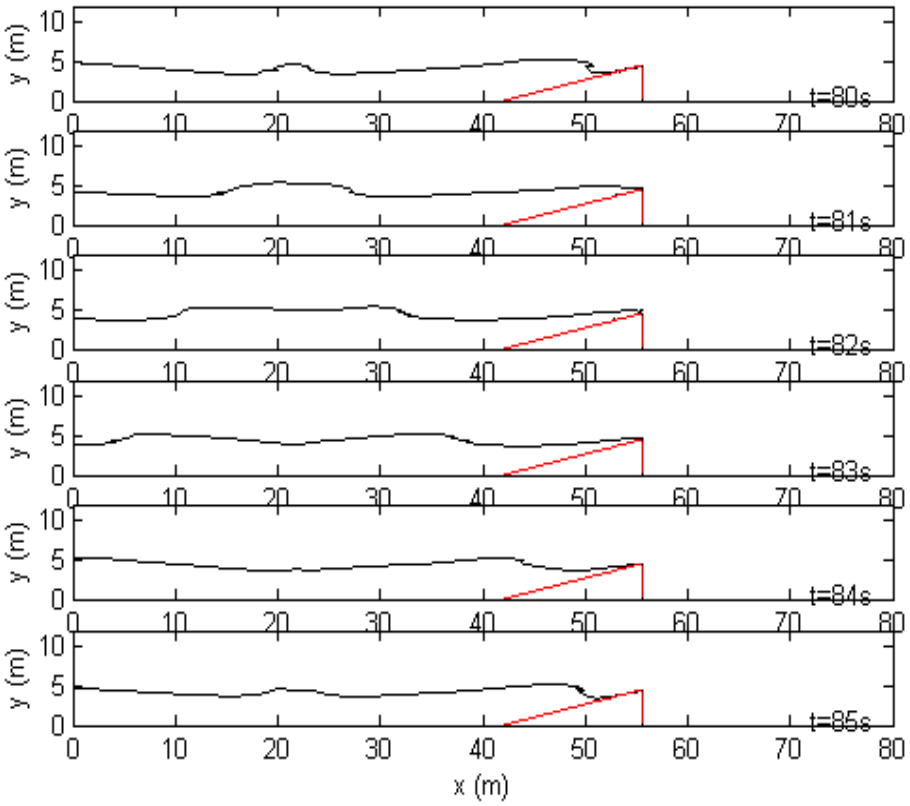

Figure 6.3.13: Details of breaking free surface profile [Run no. 6 (Table 6.3.3): H_s = 0.83m, T_m = 3.60s, T_p =5.00s, and ξ_p =1.89].

Figure 6.3.14 presents the overtopping rate which is considered an important parameter in wave overtopping phenomena. As before the unsteady volume of the overtopping is clear from this figure. The comparison between the 2-D BWNM dimensionless overtopping discharges with the formulae presented by Schüttrumpf (2001) formulae is shown in Figure 6.3.15. This shows a good agreement between the numerical model and Schuttrumpf's formulae in most cases. The average differences between numerical and laboratory results are 16%. However, Figure 6.3.15 could also be interpreted as showing the model consistently over predicts observations for larger overtopping. This could be due

to the measurement uncertainties in the volume of wave overtopping in the laboratory work.

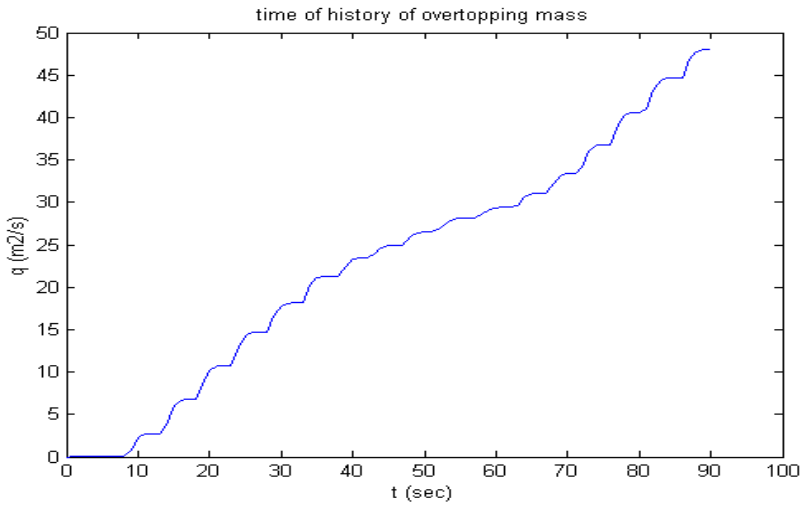

Figure 6.3.14: Time history of the wave cumulative overtopping volume for 1:3 sloped seawall for zero freeboard [Run no. 6 (Table 6.3.3): H_s = 0.83m, T_m = 3.60s and T_p =5.00s].

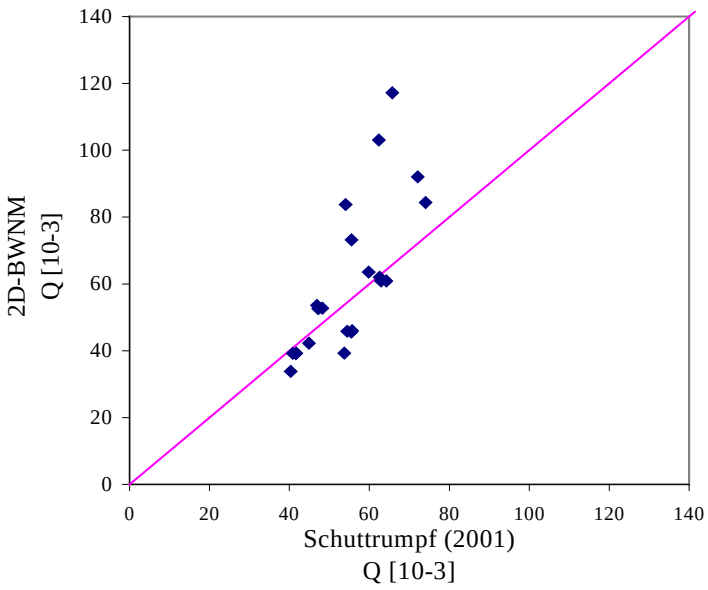

Figure 6.3.15: Comparison between 2-D BWNM and Schuttrumpf et al (2001) dimensionless overtopping discharge for breaking waves on a sloping seawall.

6.3.1 New design formulae for zero freeboard under irregular wave attack for sloped seawall in the breaking and non-breaking zone

The relation between the surf similarity parameter and the dimensionless wave overtopping is shown in Figure 6.3.16 in the breaking and non-breaking zone. It can be concluded from the Figure that there is a strong relation between the wave overtopping and the surf similarity parameter. The wave overtopping is increased with the increased surf similarity parameter in both breaking and non-breaking cases.

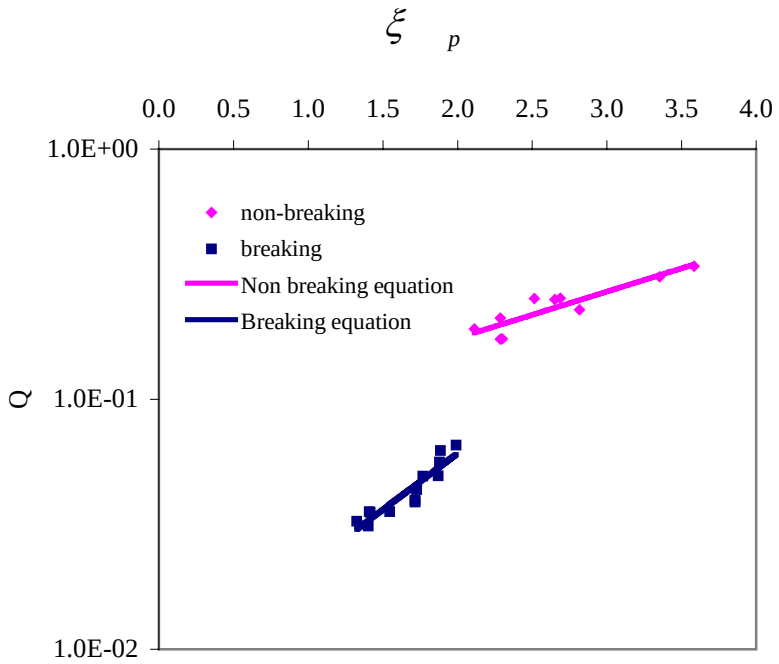

Figure 6.3.16: Relation between dimensionless wave overtopping and surf similarity parameter at zero freeboard at sloped seawall.

More analysis for the numerical results has been done and this analysis leads to a new suggested design formulae for wave overtopping at zero freeboard of 1:3 and 1:4 sloped smooth seawall under irregular wave attacks.

These equations are illustrated in Figures 6.3.17 and 6.3.18. These formulae give exponential relation between dimensionless wave overtopping and wave characteristics (H_s, T_p) and seawall slope ($\tan\alpha$) and are written as following:

- Breaking waves ($\xi_p < 2$): $Q = 0.20 \exp\left(-2.51 \frac{\sqrt{S_p}}{\tan\alpha} \right)$ (6.3.8)

- Non-breaking waves ($\xi_p \geq 2$): $Q = 0.83 \exp\left(-3.28 \frac{\sqrt{S_p}}{\tan\alpha} \right)$ (6.3.9)

R^2 (square of the Pearson product moment correlation coefficient) values for both equations are 0.83, indicating that Equations (6.3.8) and (6.3.9) are a good fit to the data.

Generally, there is shortage of laboratory data for the case of zero freeboard. The suggested formulae should be validated using laboratory, field or other numerical model data before being used for design purposes.

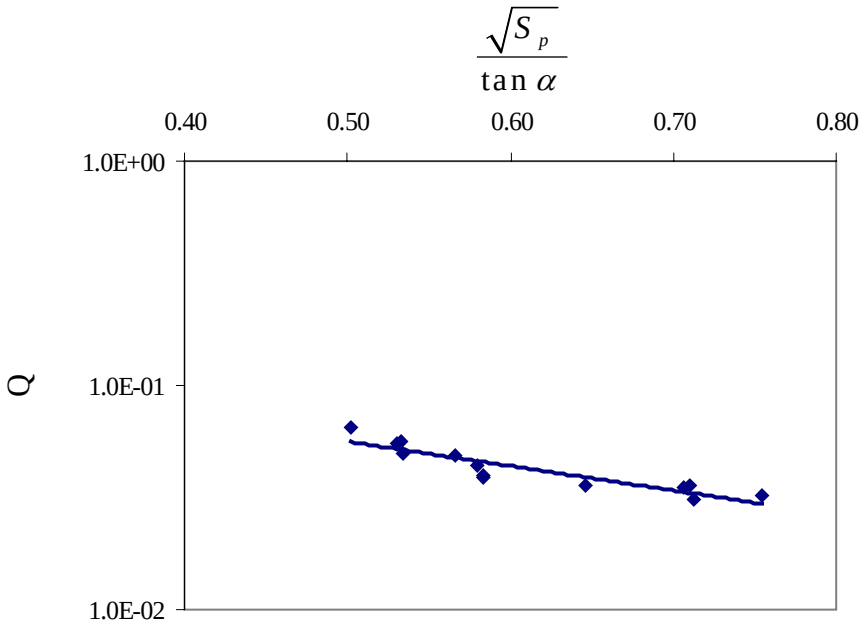

Figure 6.3.17: Wave overtopping at zero freeboard for breaking waves at 1:3 and 1:4 sloped seawall.

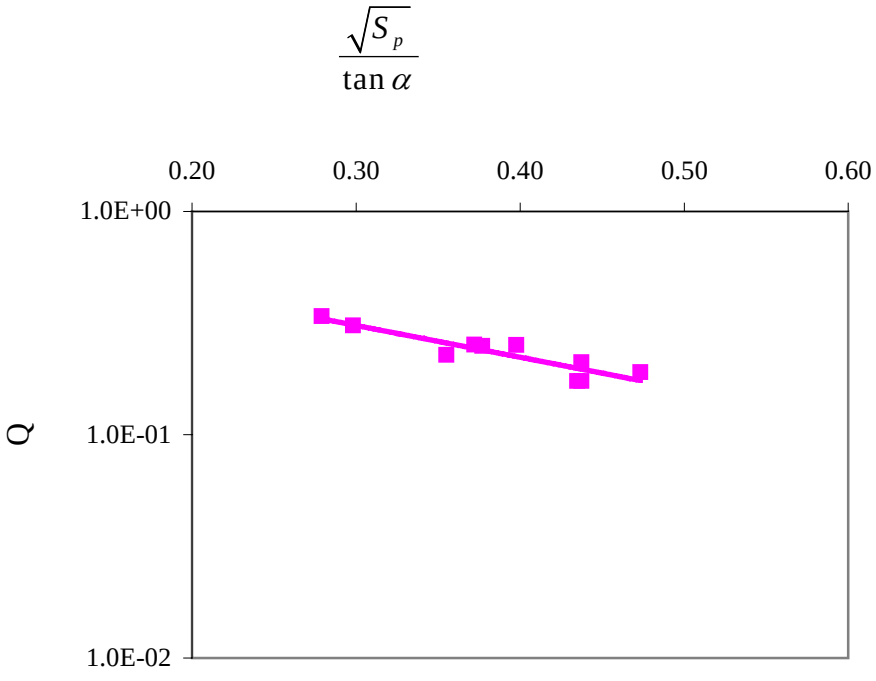

Figure 6.3.18: Wave overtopping at zero freeboard for non-breaking waves at 1:3 and 1:4 sloped seawall.

6.4 Summary

This chapter concentrated in two main parts which are not covered by any design formulae in recent times. The two parts are:

1- Small positive freeboard $\left(0.3 \geq R > 0.0\right)$.

2- Zero freeboard $\left(R = 0.0\right)$.

Using numerical simulation the cases of breaking and non-breaking wave attack on a smooth sloped seawall have been studied. The dimensionless freeboard and wave overtopping of Van der Meer and Janssen (1995) have been used to extend existing formulae. Also, the surf similarity parameter used by Van der Meer and Janssen (1995) has been used to define the breaking and non-breaking zone. The rationale behind Van der Meer's definitions can be found in the literature review, Chapter (2).

In the following chapter the case of overtopping and overflow for smooth sloped seawalls under irregular breaking and non-breaking wave attack is studied. The results are used to define new design formulae.

CHAPTER 7
Wave Overtopping and Overflow

7.1 Introduction

In some cases, especially during storms, water levels can rise above the crest level. In these cases, overflow may also occur in addition to wave overtopping. This phenomenon may cause great damage to the coastal structures. On the other hand, existing formulae for overflow (e.g. weir formulae) do not take into account the effect of waves. The case of wave overtopping and overflow for smooth sloped seawalls under irregular wave attack is presented in this chapter and the output results are used to define new design formulae.

7.2 Wave overtopping and overflow

During storm surges seawalls are exposed to waves. Depending on the crest level of the structure wave overtopping can occur. The amount of overtopping water increases when the water level rises. If the water level rises above the crest level of the structure, for example during extreme storm surges, flood water is not only caused by the wave overtopping action, but also by overflow.

On the other hand, global climate has been changed during the last years and the mean water levels have increased all over the world. For example tide-gauge records, in some cases covering the last 100 years, show a general increase in sea level of 2.4±0.9 mm per year (Hardy, 2003). Existing coastal structures that have not been designed to account for this will be more vulnerable to combined overflow and overtopping. It therefore important to be able to predict flood water volumes for these structures.

There is currently no guidance on estimating these volumes. Hence, the case of combined wave overtopping and overflow for different sloped seawalls has been studied using the two-dimensional breaking wave numerical model (2-D BWNM).

The structure of this chapter is as follows. First, overtopping and overflow due to irregular breaking waves on three different seawall slopes 1:3, 1:4 and 1:6 (Sections 7.2.1, 7.2.2 and 7.2.3 in sequence). Then, the case of overtopping and overflow due to irregular non-breaking waves on two different seawall slopes 1:3 and 1:4 is investigated (Sections 7.2.4 and 7.2.5 in sequence). Finally, a synthesis of results is presented in Section 7.3 accompanying with suggested design formulae.

7.2.1 Wave overtopping and overflow under irregular breaking wave attack for 1:3 sloped seawall

A series tests were performed for 1:3 sloped seawall using the two-dimensional breaking wave numerical model (2-D BWNM). Figure 7.2.1 presents the cross section and the water surface profile at 5s. The water depth ranges from 4.5m to 5.75m. The generated JONSWAP spectrum characteristics associated with the dimensional and dimensionless freeboard are shown in Table 7.2.1. The wave characteristics are chosen in the breaking zone area to achieve a surf similarity parameter of less than 2 ($\xi_p < 2$). In total, 320 cells were used in the x-direction with a cell size of 0.25m. In the y-direction 120 cells are used with a cell size of 0.1m. The initial time step is 0.04 second and the duration of calculation is 90 seconds.

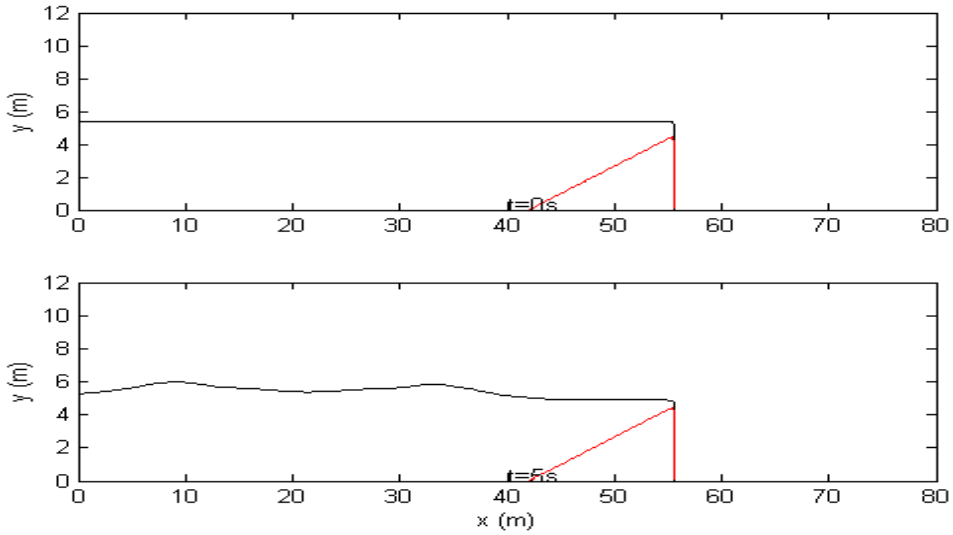

Figure 7.2.1: Cross section and free surface profile at t=5s for breaking waves overtopping and overflow over 1:3 sloped seawall. [Run no. 12 (Table 7.2.1): H_s = 1.24m, T_m = 3.90s and T_p = 5.00s].

Run No.	H_s (m)	T_m (s)	T_p (s)	R_c (m)	R [-]
1	1.22	3.80	5.00	-0.061	-0.027
2	1.22	3.80	5.00	-0.122	-0.053
3	1.22	3.80	5.00	-0.244	-0.106
4	1.39	4.00	5.00	-0.278	-0.113
5	1.22	3.80	5.00	-0.366	-0.159
6	1.22	3.80	5.00	-0.488	-0.212
7	1.39	4.00	5.00	-0.556	-0.226
8	1.22	3.80	5.00	-0.610	-0.265
9	1.24	3.90	5.00	-0.620	-0.267
10	1.22	3.80	5.00	-0.732	-0.318
11	1.22	3.80	5.00	-0.854	-0.371
12	1.24	3.90	5.00	-0.868	-0.374
13	1.22	3.80	5.00	-0.976	-0.424
14	1.22	3.80	5.00	-1.098	-0.477
15	1.22	3.80	5.00	-1.220	-0.530

Table 7.2.1: Irregular breaking wave characteristics and dimension and dimensionless freeboard for the case of wave overtopping and overflow over 1:3 sloped seawall.

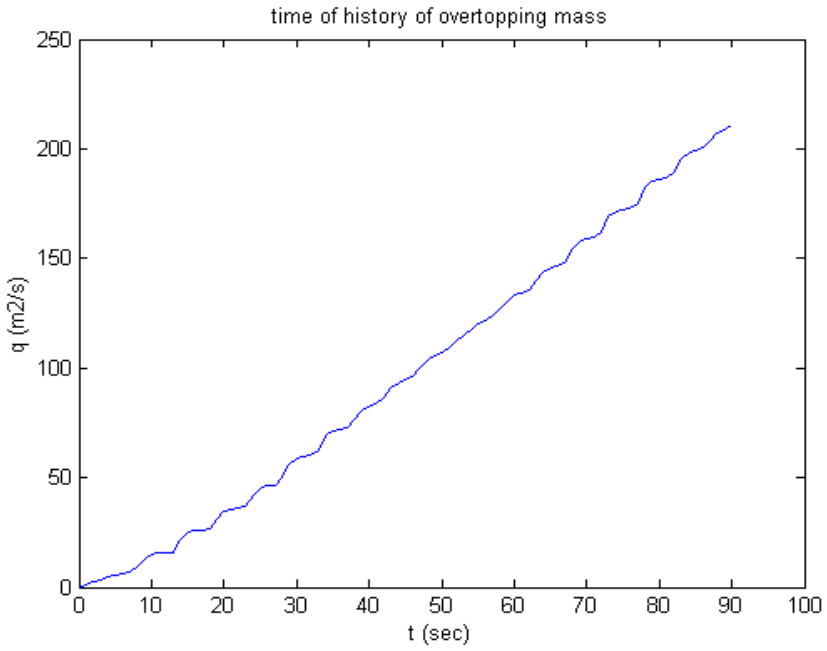

Figure 7.2.2: Time history of cumulative breaking waves overtopping and overflow volume for 1:3 sloped seawall [Run no. 12 (Table 7.2.1): H_s = 1.24m, T_m = 3.90s and T_p = 5.00s].

The time history of wave overtopping and overflow volume is shown in Figure 7.2.2. The flat spots in Figure 7.2.2 happen when no overtopping and overflow is occurring. This happens because of the passage of a wave trough takes the instantaneous water level at the structure below its crest. This is an important difference to the case of overflow only. The simulation of wave overtopping and overflow over the 1:3 sloped seawall is shown in Figures 7.2.3 and 7.2.4. These figures show how the wave propagates towards the seawall. The free surface profile during time of simulation is shown in these figures every 5 seconds.

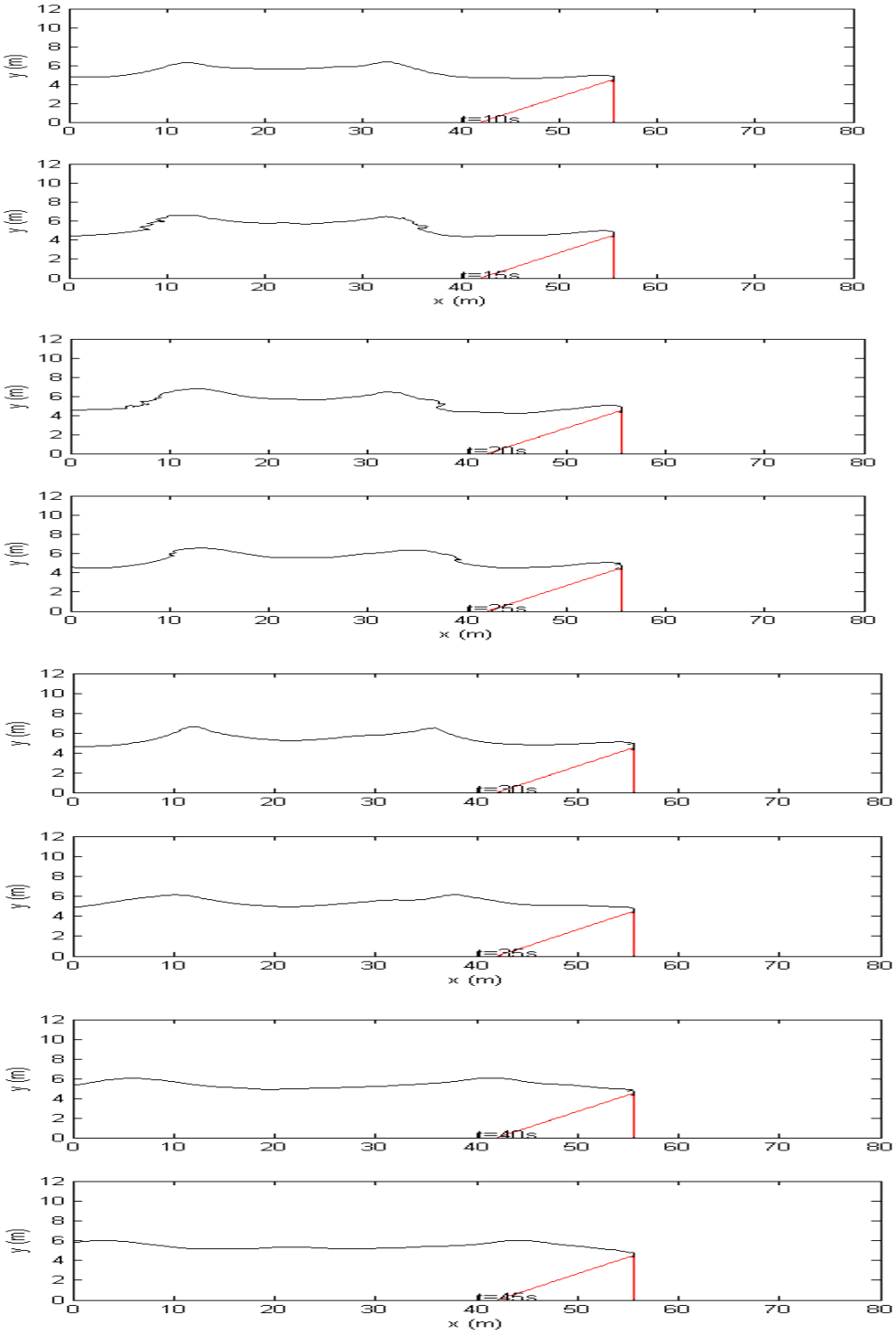

Figure 7.2.3: Breaking waves overtopping and overflow on 1:3 slope seawall from time 10.0 to 45.0s. [Run no. 12 (Table 7.2.1): H_s = 1.24m, T_m = 3.90s and T_p = 5.00s].

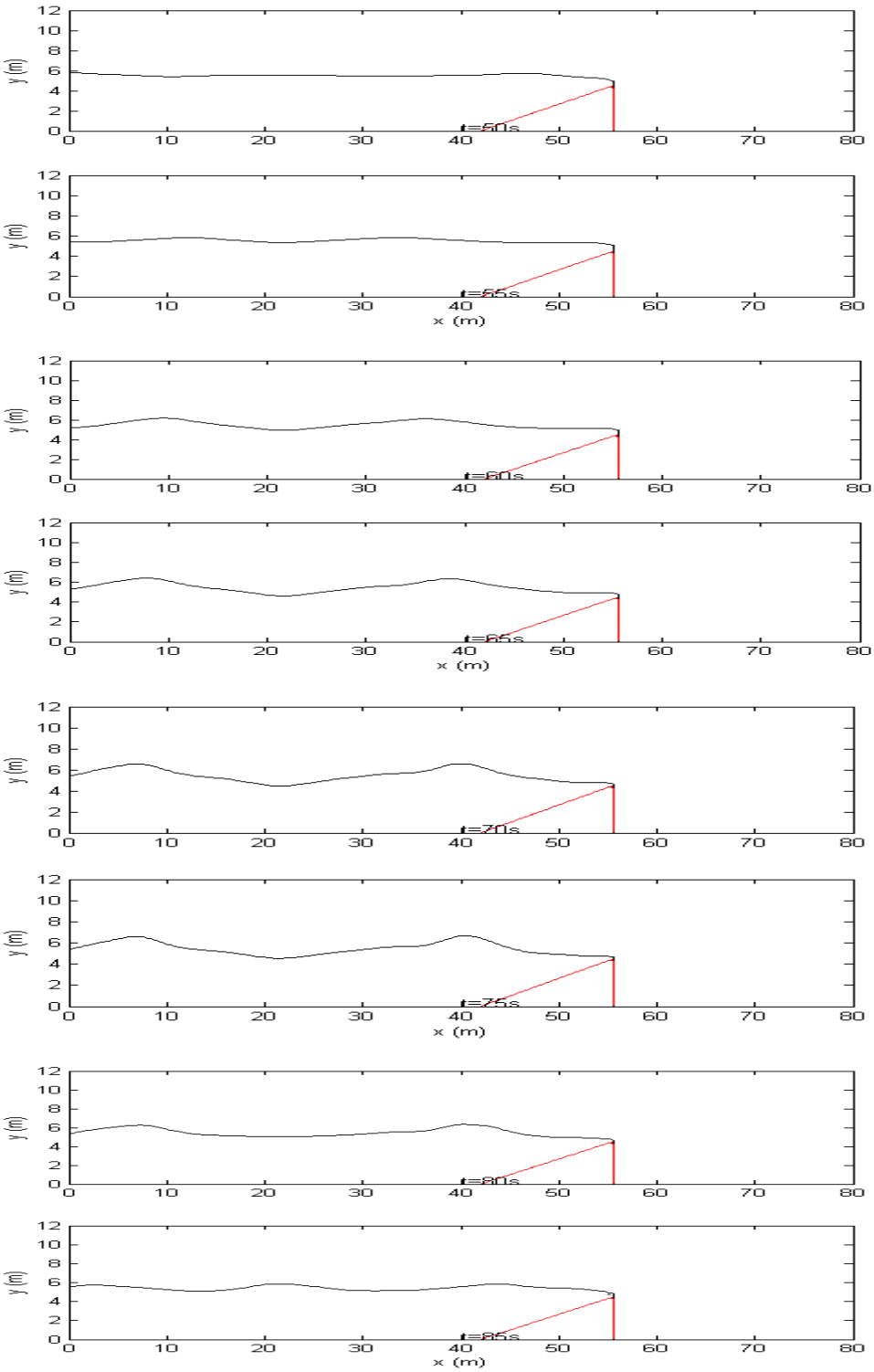

Figure 7.2.4: Breaking waves overtopping and overflow on 1:3 slope seawall from time 50.0 to 85.0s [Run no. 12 (Table 7.2.1): H_s = 1.24m, T_m = 3.90s and T_p = 5.00s].

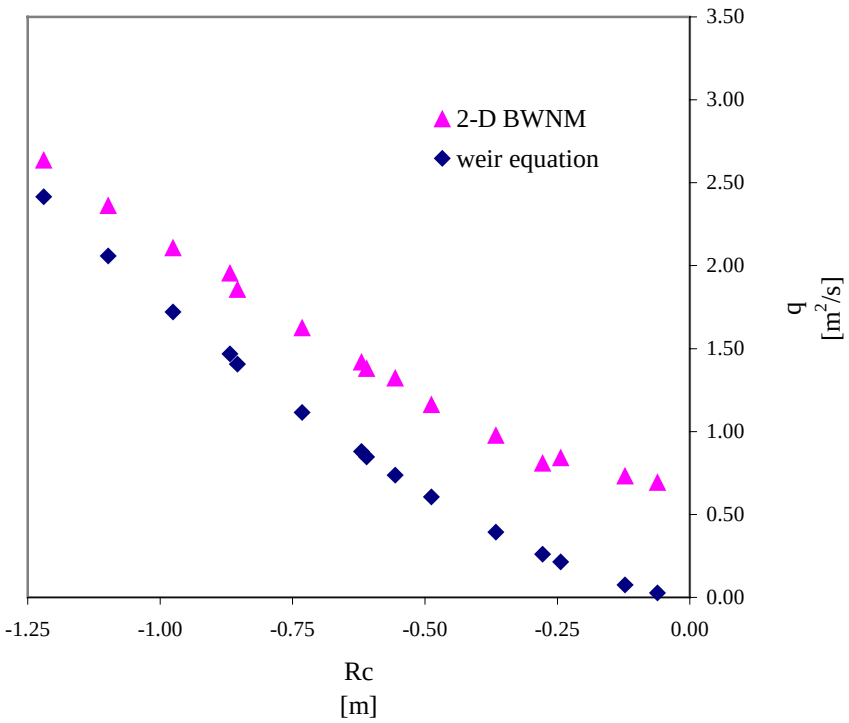

Figure 7.2.5: Comparison between weir equation and 2-D BWNM for irregular breaking waves on a 1:3 sloped seawall.

There is shortage of field, laboratory or numerical data for the case of small negative freeboard. So, 2-D BWNM results are compared with results obtained from the well-known weir equation as shown in Figure 7.2.5. Chadwick and Morfett (1998) presented formula that expresses the discharge over a sharp edged weir as follows:

$$q_{weir} = \frac{2}{3} C_d \sqrt{2g} \left| R_c \right|^{\frac{3}{2}} \qquad (7.2.1)$$

where, R_c is the overflow depth and C_d is the discharge coefficient.

The comparison shows some differences between the two results. The difference decreases as the magnitude of the freeboard, R_c, increases. The difference is expected, as the weir equation does not include the effect of waves. As the magnitude of the freeboard, R_c, increases, the effect of the waves reduces and the

results converge to those obtained from the weir equation. This was also indicated in Chapter 5 (Section 5.3) when the case of overflow without waves presented. In the case of overflow without waves the overflow volumes of 2-D BWNM were in very good agreement with the weir equation as shown in Figure 5.3.2.

7.2.2 Wave overtopping and overflow under irregular breaking wave attack for 1:4 sloped seawall

Figure 7.2.6 presents the cross section and the water surface profile at 10s. for 1:4 sloped seawall in the breaking zone. The water depth ranges from 4.5 to 5.6m. The generated JONSWAP spectrum characteristics associated with the dimension and dimensionless freeboard are shown in table 7.2.2. Number of cells in the x-direction increased to 400 with a cell size of 0.25m and the duration of calculation is increased 90 seconds. The rate of overtopping and overflow volume calculated by the numerical model is shown in Figure 7.2.7. The flat spots is noticed also in Figure 7.2.7 which are happened when no overtopping and overflow is occurring. This happens because of the passage of a wave trough takes the instantaneous water level at the structure below its crest.

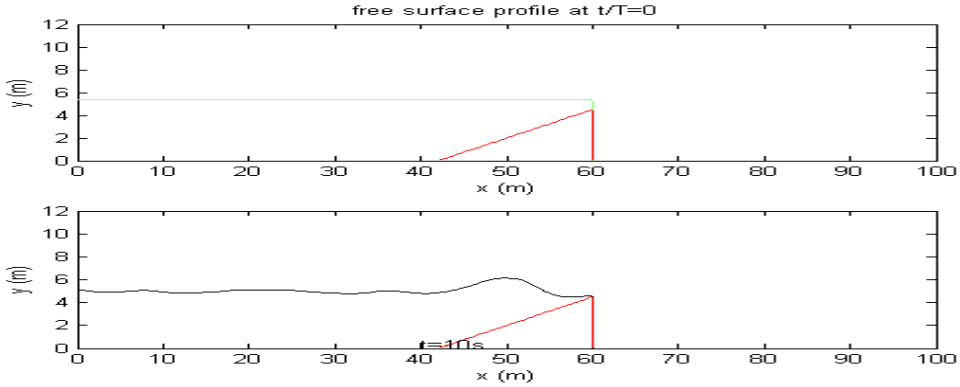

Figure 7.2.6: Cross section and free surface profile at t=10s for the breaking waves overtopping over 1:4 sloped seawall [Run no. 11 (Table 7.2.2): H_s = 1.22m, T_m = 3.80s and T_p = 5.00s].

Run No.	H_s (m)	T_m (s)	T_p (s)	R_c (m)	R [-]
1	1.22	3.80	5.00	-0.061	-0.035
2	1.22	3.80	5.00	-0.122	-0.071
3	1.48	4.60	6.02	-0.296	-0.129
4	1.22	3.80	5.00	-0.244	-0.141
5	0.83	3.70	5.00	-0.249	-0.175
6	1.22	3.80	5.00	-0.366	-0.212
7	1.22	3.80	5.00	-0.488	-0.283
8	1.22	3.80	5.00	-0.610	-0.353
9	1.48	4.60	6.02	-0.888	-0.388
10	1.22	3.80	5.00	-0.732	-0.424
11	1.22	3.80	5.00	-0.854	-0.495
12	0.83	3.70	5.00	-0.747	-0.525
13	1.22	3.80	5.00	-0.976	-0.566
14	1.22	3.80	5.00	-1.098	-0.636

Table 7.2.2: Irregular breaking wave characteristics and the dimension and dimensionless freeboard for the case of wave overtopping and overflow over 1:4 sloped seawall.

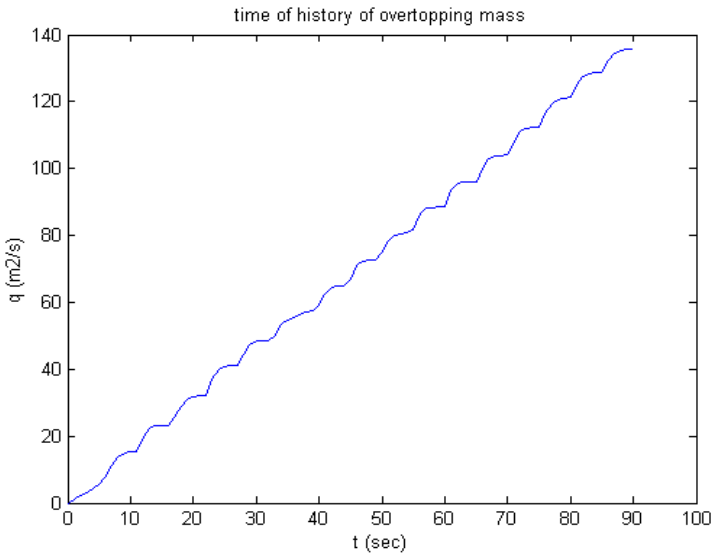

Figure 7.2.7: Time history of cumulative breaking waves overtopping volume for 1:4 sloped seawall [Run no. 11 (Table 7.2.2): H_s = 1.22m, T_m = 3.80s and T_p = 5.00s].

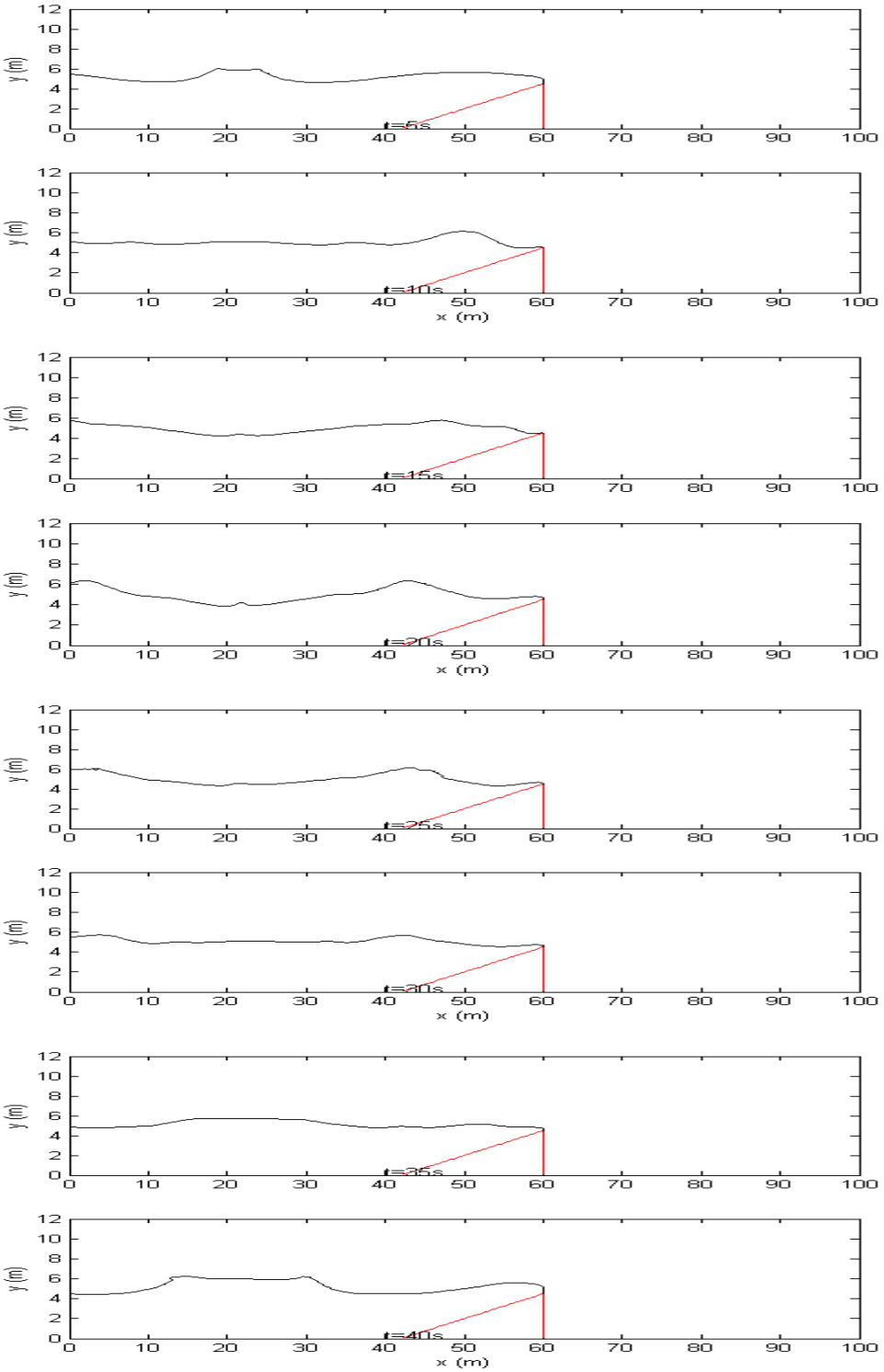

Figure 7.2.8: Breaking waves overtopping and overflow on 1:4 slope seawall from time 5.0 to 40.0s. [Run no. 11 (Table 7.2.2): H_s = 1.22m, T_m = 3.80s and T_p = 5.00s].

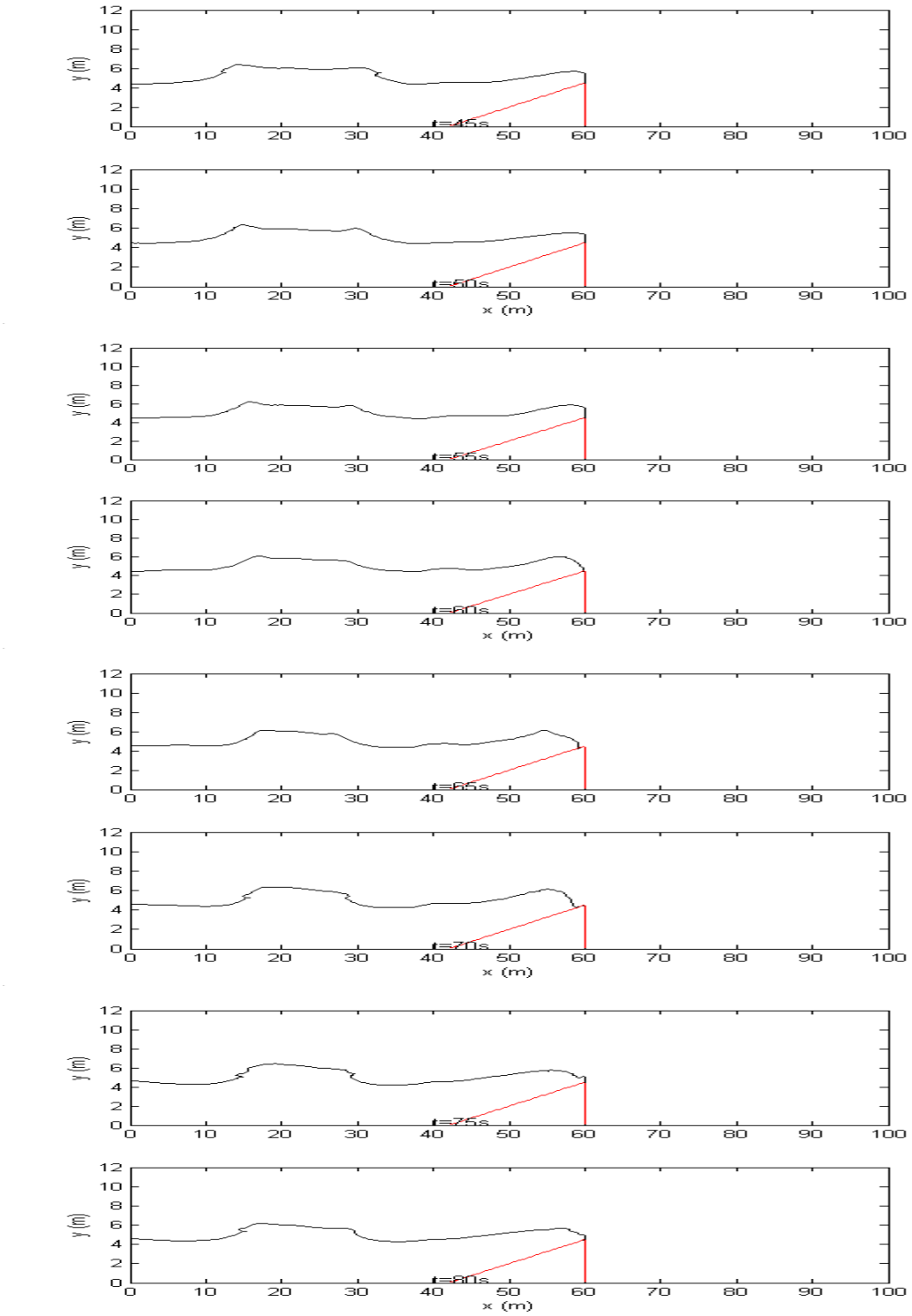

Figure 7.2.9: Breaking waves overtopping and overflow on 1:4 slope seawall from time 45.0 to 80.0s. [Run no. 11 (Table 7.2.2): H_s = 1.22m, T_m = 3.80s and T_p = 5.00s].

Figures 7.2.8 and 7.2.9 present the simulation of overtopping and overflow over 1:4 slope seawall. The free surface is presented during the numerical simulation time with time step 5.0 second. .

Figure 7.2.10 shows the analogous set of points to Figure 7.2.5. The difference between the numerical results and weir equation decreases as the magnitude of the freeboard, R_c increases.

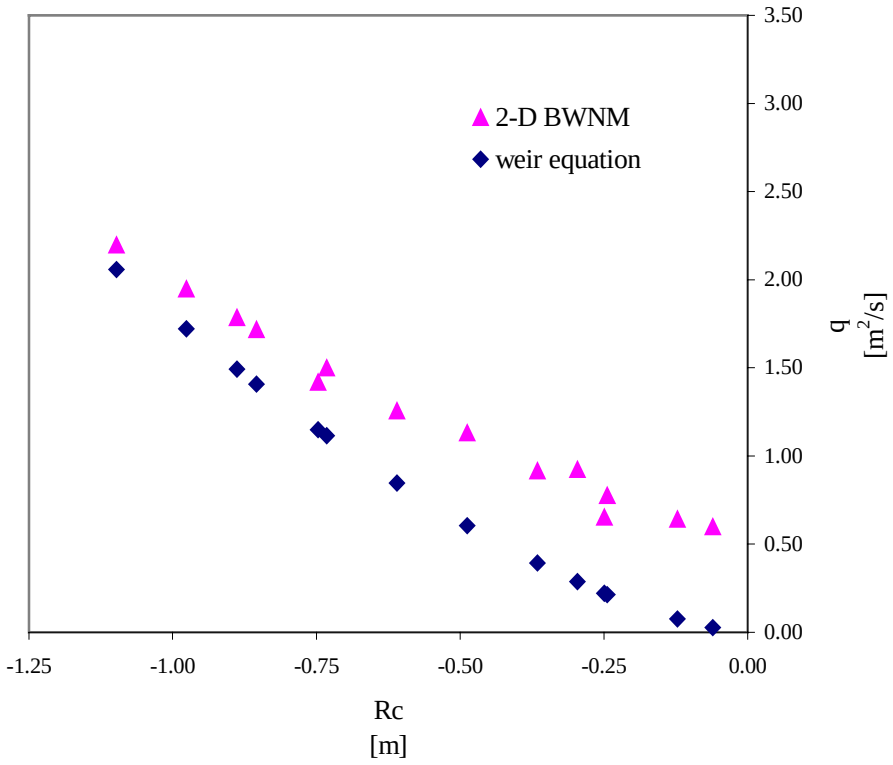

Figure 7.2.10: Comparison between weir equation and 2-D BWNM for irregular breaking waves on a 1:4 sloped seawall.

7.2.3 Wave overtopping and overflow under irregular breaking wave attack for 1:6 sloped seawall

Series tests are performed for 1:6 sloped seawall in the breaking zone using the two-dimensional breaking wave numerical model (2-D BWNM). Figure 7.2.11 presents the cross section and the water surface profile at 5s. The water depth ranges from 4.5 to 5.70m. The JONSWAP spectrum characteristics associated with the dimensional and dimensionless freeboard are shown in Table 7.2.3. The wave characteristics are chosen in the breaking zone area to achieve the surf similarity is less than 2 ($\xi_p < 2$). In total 480 cells used in the x-direction with a cell size of 0.25m and 120 cells in the y-direction with a cell size of 0.1m. The initial time step is 0.04 second and the duration of calculation is 90 seconds.

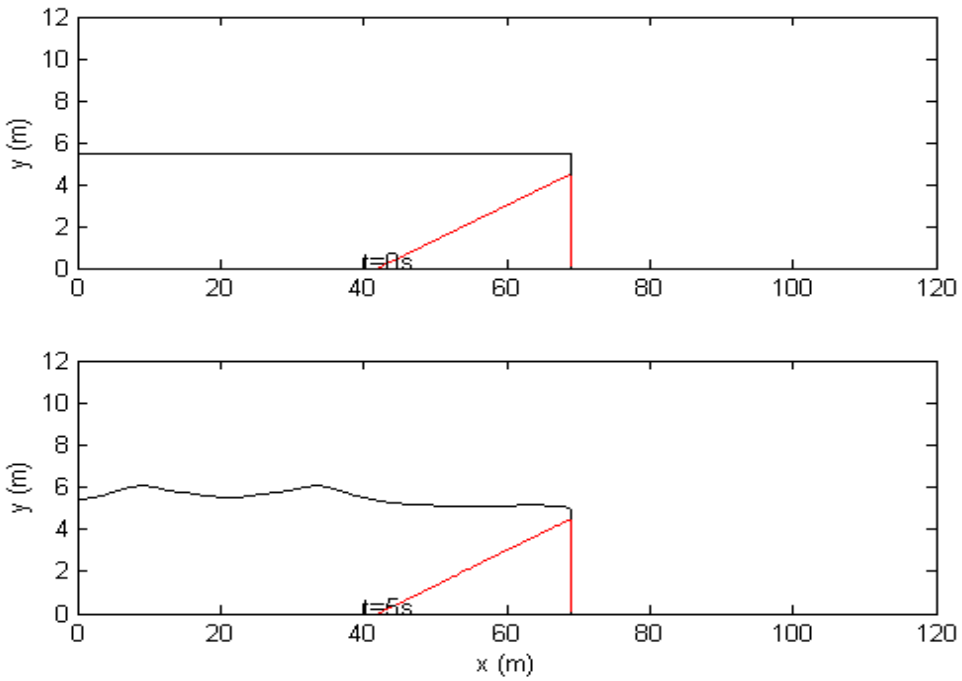

Figure 7.2.11: Cross section and free surface profile at t = 5.0s for breaking waves overtopping and overflow over 1:6 sloped seawall. [Run no. 12 (Table 7.2.3): H_s = 1.22m, T_m = 3.80s and T_p = 5.00s].

Run No.	H_s (m)	T_m (s)	T_p (s)	R_c (m)	R [-]
1	0.56	3.50	5.06	-0.056	-0.071
2	1.22	3.80	5.00	-0.061	-0.053
3	1.22	3.80	5.00	-0.122	-0.106
4	1.22	3.80	5.00	-0.244	-0.212
5	0.8	4.70	7.20	-0.320	-0.239
6	1.22	3.80	5.00	-0.366	-0.318
7	1.22	3.80	5.00	-0.488	-0.424
8	0.56	3.50	5.06	-0.560	-0.710
9	1.22	3.80	5.00	-0.610	-0.530
10	0.8	4.70	7.20	-0.640	-0.477
11	1.22	3.80	5.00	-0.732	-0.636
12	1.22	3.80	5.00	-0.854	-0.742

Table 7.2.3: Irregular breaking wave characteristics and the dimension and dimensionless freeboard for the case of wave overtopping and overflow over 1:6 sloped seawall.

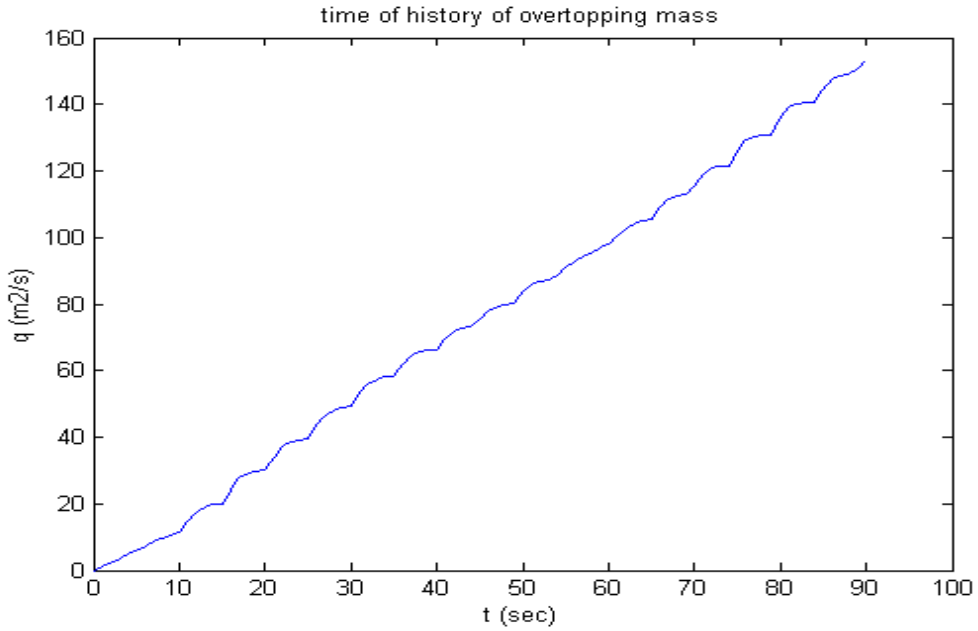

Figure 7.2.12: Time history of cumulative breaking waves overtopping and overflow volume for 1:6 sloped seawall [Run no. 12 (Table 7.2.3): H_s = 1.22m, T_m = 3.80s and T_p = 5.00s].

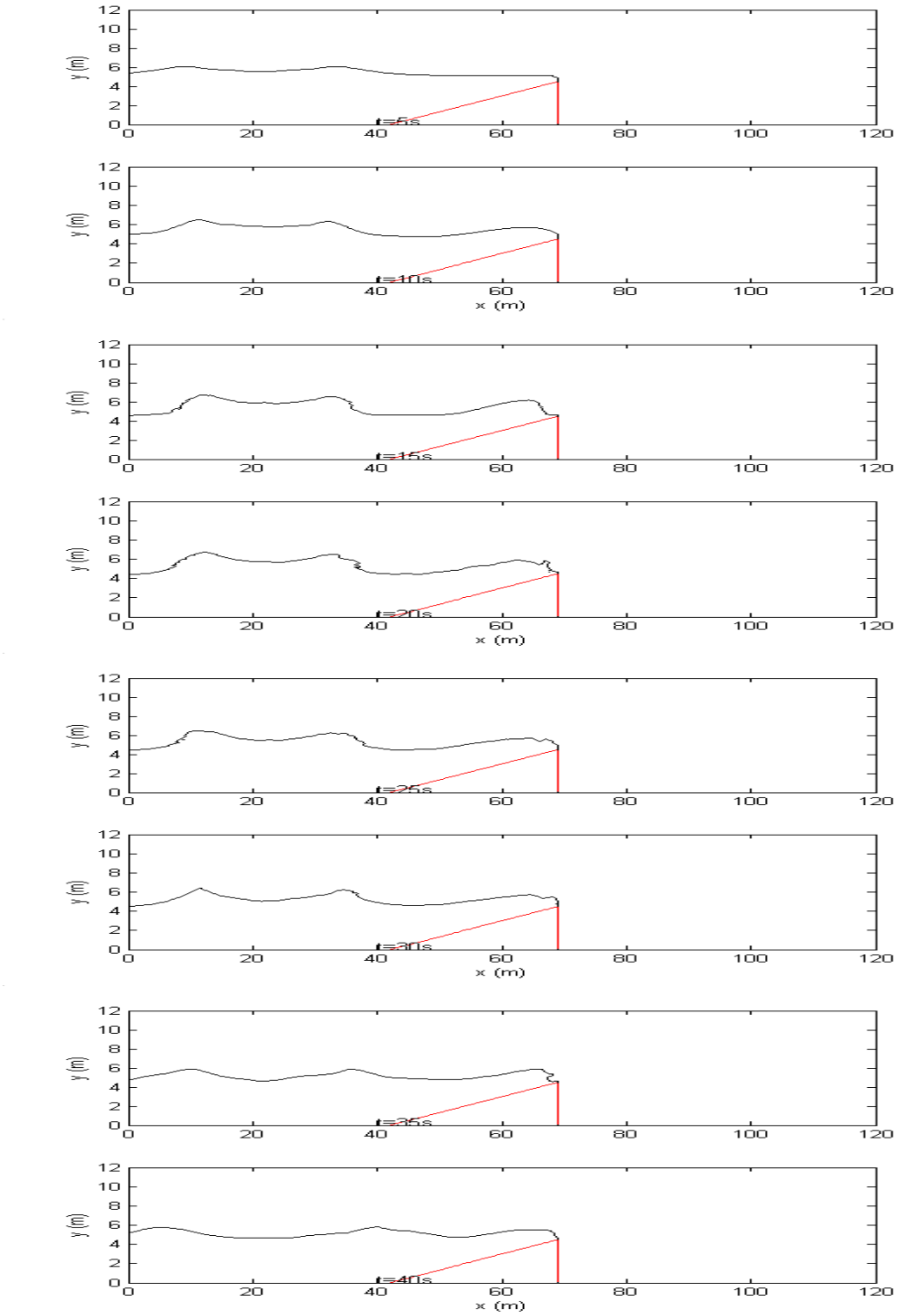

Figure 7.2.13: Breaking wave overtopping and overflow on 1:6 slope seawall from time 5.0 to 40.0s. [Run no. 12 (Table 7.2.3): H_s = 1.22m, T_m = 3.80s and T_p = 5.00s].

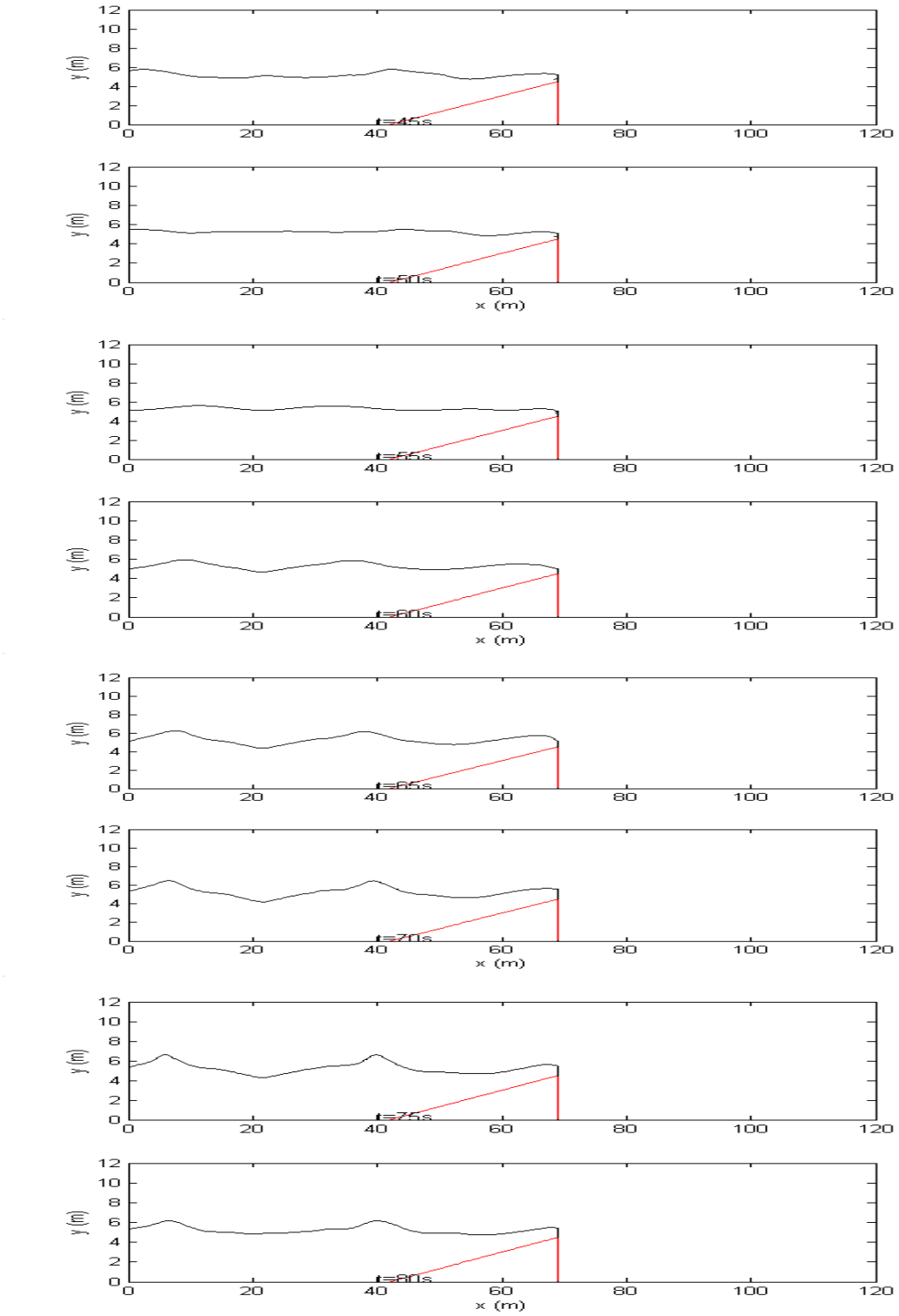

Figure 7.2.14: Breaking wave overtopping and overflow on 1:6 slope seawall from time 45.0 to 80.0s. [Run no. 12 (Table 7.2.3): H_s = 1.22m, T_m = 3.80s and T_p = 5.00s].

To demonstrate the accumulation of water volume, the rate of combined overtopping and overflow is calculated and presented in Figure 7.2.12. The flat spots in Figure 7.2.12 happen when no overtopping and overflow is occurring.

The snapshots from the simulation from Run no. 12 are shown in Figures 7.2.13 and 7.2.14.

Figure 7.2.15 shows the comparison between the 2-D BWNM results and weir equation and indicates similar trends to those found for seawalls slopes 1:3 and 1:4.

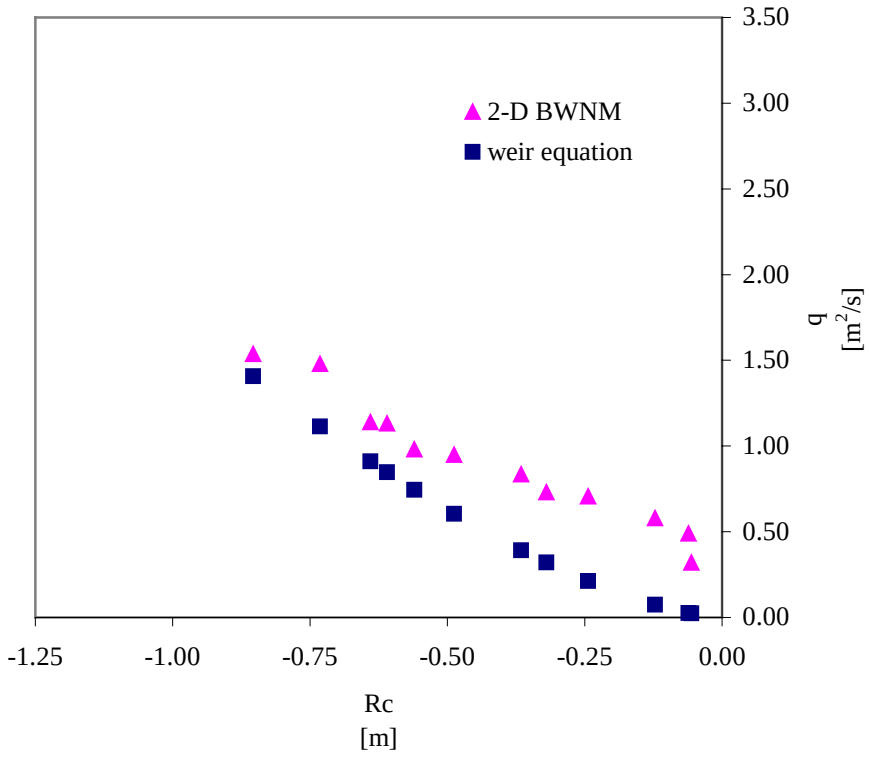

Figure 7.2.15: Comparison between weir equation and 2-D BWNM for irregular breaking waves on a 1:6 sloped seawall.

7.2.4 Wave overtopping and overflow under irregular non-breaking wave attack for 1:3 sloped seawall

A further series of tests were performed for 1:3 sloped seawall. The JONSWAP spectrum characteristics associated with the dimensional and dimensionless freeboard are shown in Table 7.2.4. Figure 7.2.16 presents the cross section and the water surface profile at 5s. The wave characteristics are chosen to achieve in the non-breaking waves by ensuring the surf similarity is more than 2 ($\xi_p > 2$). The mesh setup is the same as for case of seawall with slope 1:3 (Section 7.2.1). The initial time step is 0.04 second and the duration of the simulation is 90 seconds.

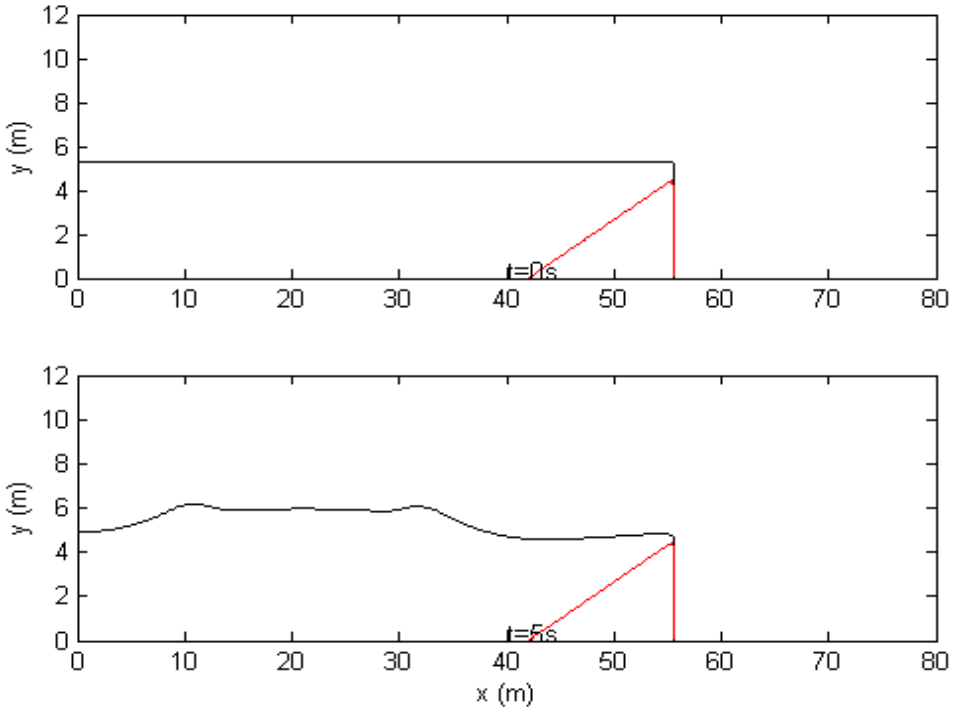

Figure 7.2.16: Cross section and free surface profile at t=5s for non-breaking wave overtopping and overflow over 1:3 sloped seawall. [Run no. 10 (Table 7.2.4): H_s = 0.80m, T_m = 7.20s and T_p = 4.70s].

Run No.	H_s (m)	T_m (s)	T_p (s)	R_c (m)	R [-]
1	1.48	4.60	6.02	-0.148	-0.1
2	0.80	4.70	7.20	-0.160	-0.2
3	0.80	4.70	7.20	-0.240	-0.3
4	0.80	4.70	7.20	-0.320	-0.4
5	0.56	3.50	5.06	-0.392	-0.7
6	0.80	4.70	7.20	-0.480	-0.6
7	0.56	3.50	5.06	-0.504	-0.9
8	0.80	4.70	7.20	-0.640	-0.8
9	1.48	4.60	6.02	-0.740	-0.5
10	0.80	4.70	7.20	-0.800	-1.0

Table 7.2.4: Irregular non-breaking wave characteristics, dimension and dimensionless freeboard for the case of wave overtopping and overflow over 1:3 sloped seawall.

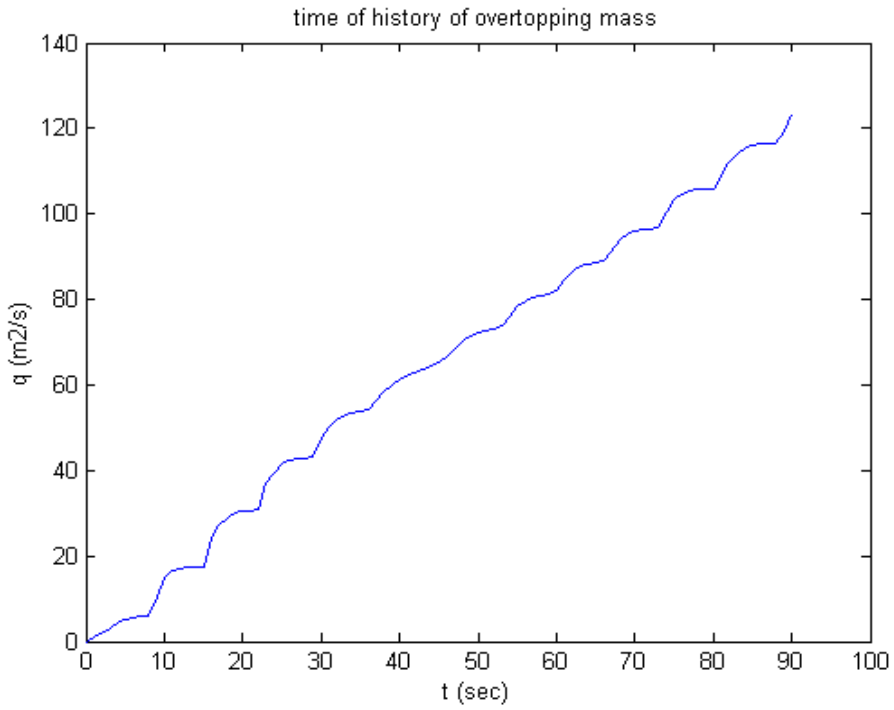

Figure 7.2.17: Time history of the cumulative non-breaking wave overtopping and overflow volume at a 1:3 sloped seawall. [Run no. 10 (Table 7.2.4): H_s = 0.80m, T_m = 7.20s and T_p = 4.70s].

Figure 7.2.17 represents the relation between cumulative overtopping volume and time of calculation. The non-linearity behaviour of irregular waves can be noticed. The flat spots in Figure 7.2.17 happen when no overtopping and overflow is occurring which is an important difference to the case of overflow only.

Figures 7.2.18 and 7.2.19 explain the propagation of non-breaking wave over the simulation period. The figures present free surface profile of irregular wave during time of simulation.

The overtopping and overflow rate of 2-D BWNM is compared with weir equation as shown in Figure 7.2.20. Figure 7.2.20 indicates similar trends to those shown in Figures 7.2.5, 7.2.10 and 7.2.15 for breaking waves on 1:3, 1:4 and 1:6 sloped seawalls respectively. There are significant differences between the two results. The difference decreases as the magnitude of the freeboard, R_c, increases. As explained before, this difference is expected, as the weir equation does not include the effect of waves.

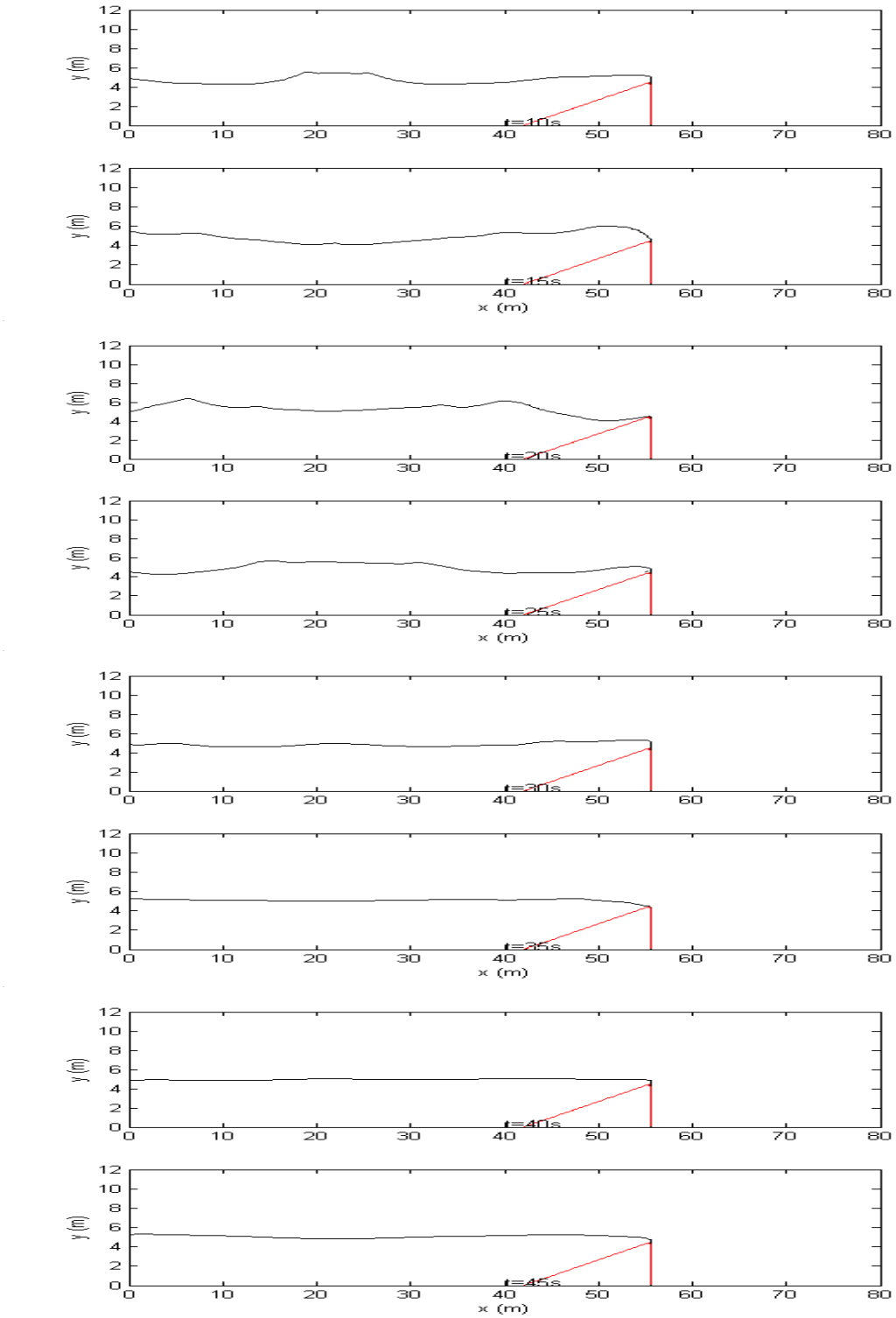

Figure 7.2.18: Wave overtopping and overflow on 1:3 slope seawall in non-breaking zone from time 10.0 to 45.0s. [Run no. 10 (Table 7.2.4): H_s = 0.80m, T_m = 7.20s and T_p = 4.70s].

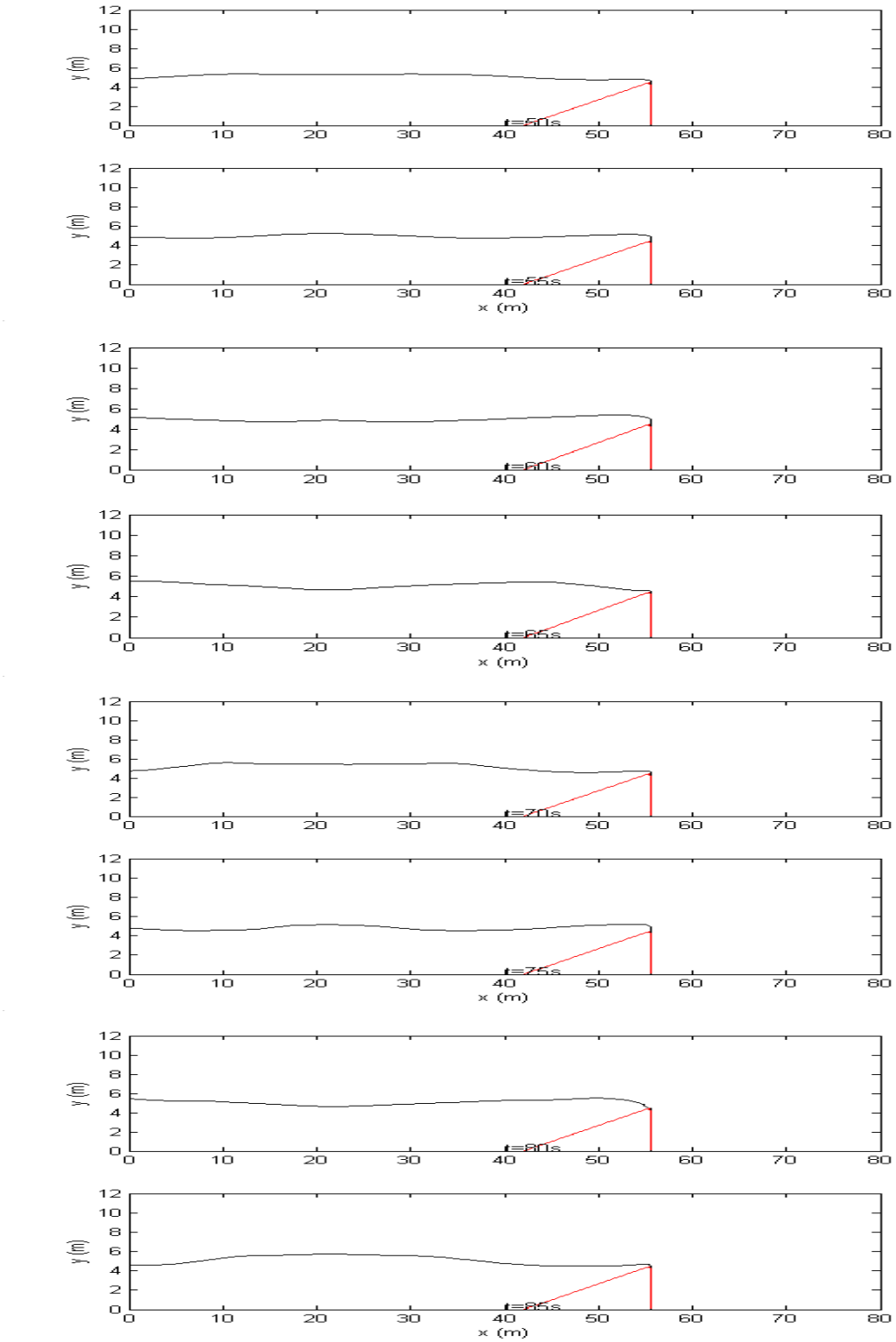

Figure 7.2.19: Wave overtopping and overflow on 1:3 slope seawall in non-breaking zone from time 50.0 to 85.0s. [Run no. 10 (Table 7.2.4): H_s = 0.80m, T_m = 7.20s and T_p = 4.70s].

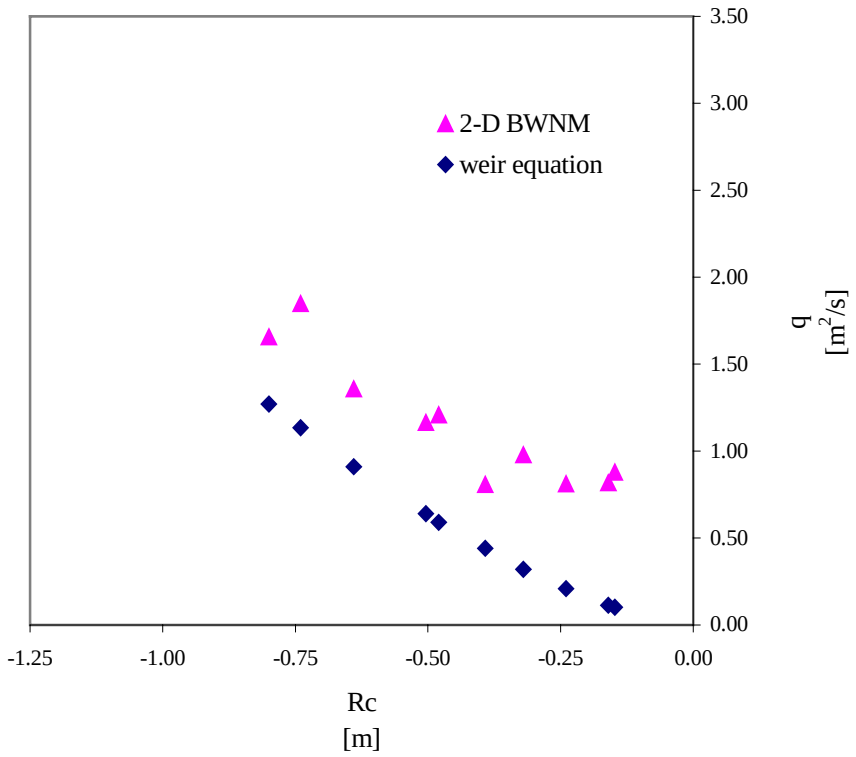

Figure 7.2.20: Comparison between weir equation and 2-D BWNM for irregular non-breaking waves on a 1:3 sloped seawall.

7.2.5 Wave overtopping and overflow under irregular non-breaking wave attack for 1:4 sloped seawall

Cross section and water surface profile of 1:4 sloped seawall attacks by irregular non-breaking waves are presented in Figure 7.2.21. The water depth ranges from 4.5 to 5.85m. The JONSWAP spectrum characteristics associated with the dimensional and dimensionless freeboard are shown in table 7.2.5. The mesh setup is the same as explained in Section 7.2.2.

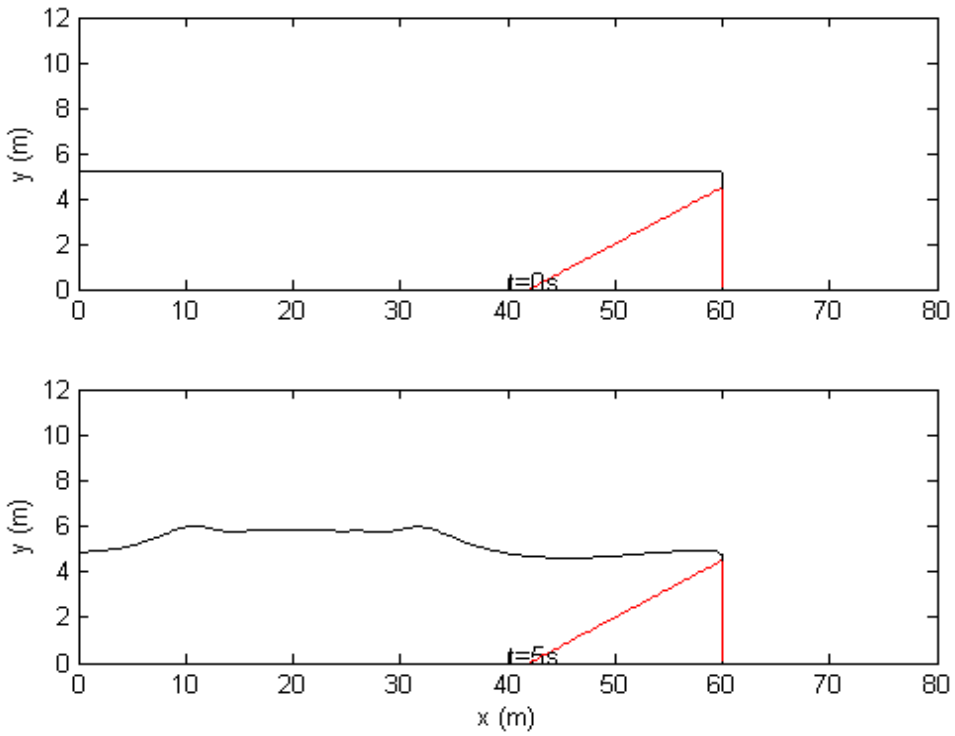

Figure 7.2.21: Cross section and free surface profile at t=5s for the non-breaking wave overtopping and overflow over 1:4 sloped seawall [Run no. 8 (Table 7.2.5): H_s = 0.72m, T_m = 7.30s and T_p = 4.70s].

Run No.	H_s (m)	T_m (s)	T_p (s)	R_c (m)	R [-]
1	0.80	4.70	7.2	-0.080	-0.1
2	0.56	3.50	5.06	-0.112	-0.2
3	0.80	4.70	7.2	-0.240	-0.3
4	0.80	4.70	7.2	-0.320	-0.4
5	0.56	3.50	5.06	-0.336	-0.6
6	0.80	4.70	7.2	-0.400	-0.5
7	0.80	4.70	7.2	-0.560	-0.7
8	0.72	4.70	7.3	-0.576	-0.8
9	0.80	4.70	7.2	-0.720	-0.9
10	0.72	4.70	7.3	-0.720	-1.0

Table 7.2.5: Irregular non-breaking wave characteristics, dimension and dimensionless freeboard for the case of wave overtopping and overflow over 1:4 sloped seawall.

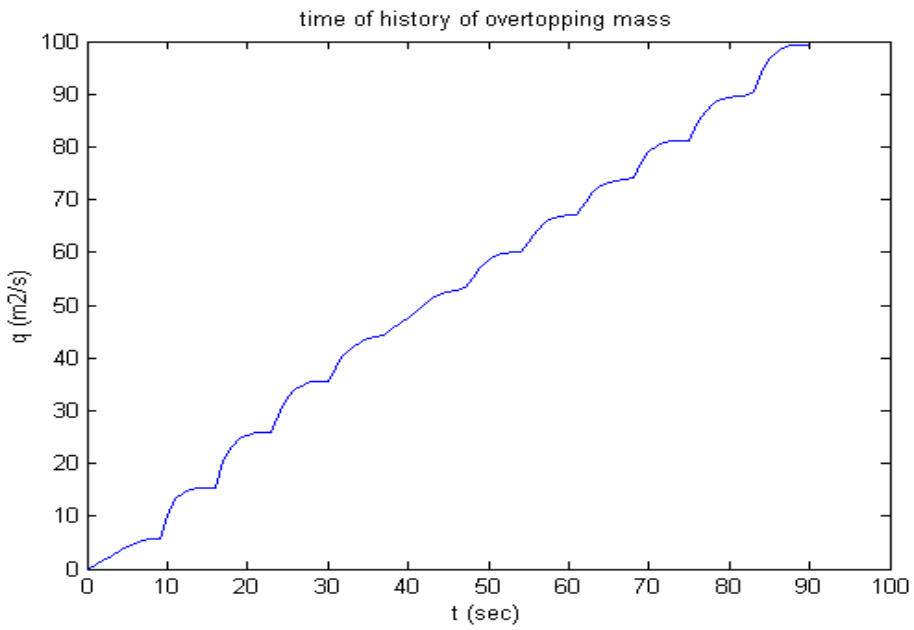

Figure 7.2.22: Time history of the cumulative non-breaking overtopping and overflow volume for 1:4 sloped seawall [Run no. 8 (Table 7.2.5): H_s = 0.72m, T_m = 7.30s and T_p = 4.70s].

The rate of overtopping and overflow volume for Run number 8 is shown in Figure 7.2.22. The figure gives the same trend of Figure 7.2.17 related to non-steady with overtopping/overflow volume increasing associated with the non-linearity of generated irregular waves.

Figures 7.2.23 and 7.2.24 present the simulation of non-breaking wave overtopping and overflow over 1:4 slope seawall. The free surface profiles of the generated wave over time of simulation are showed in these figures.

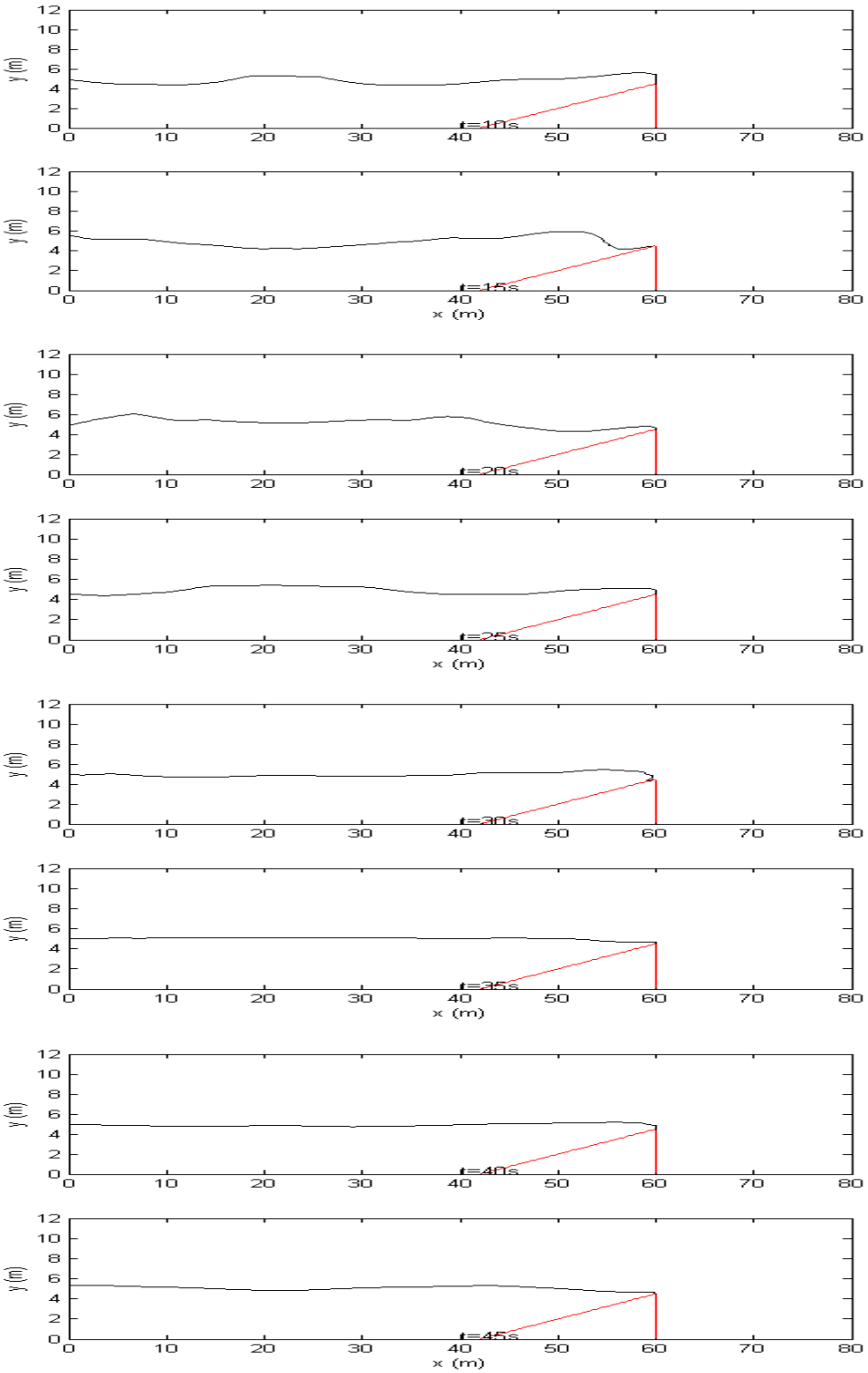

Figure 7.2.23: Wave overtopping and overflow on 1:4 slope seawall in the non-breaking zone from time 5.0 to 45.0s. [Run no. 8 (Table 7.2.5): Hs = 0.72m, Tm = 7.30s and Tp = 4.70s].

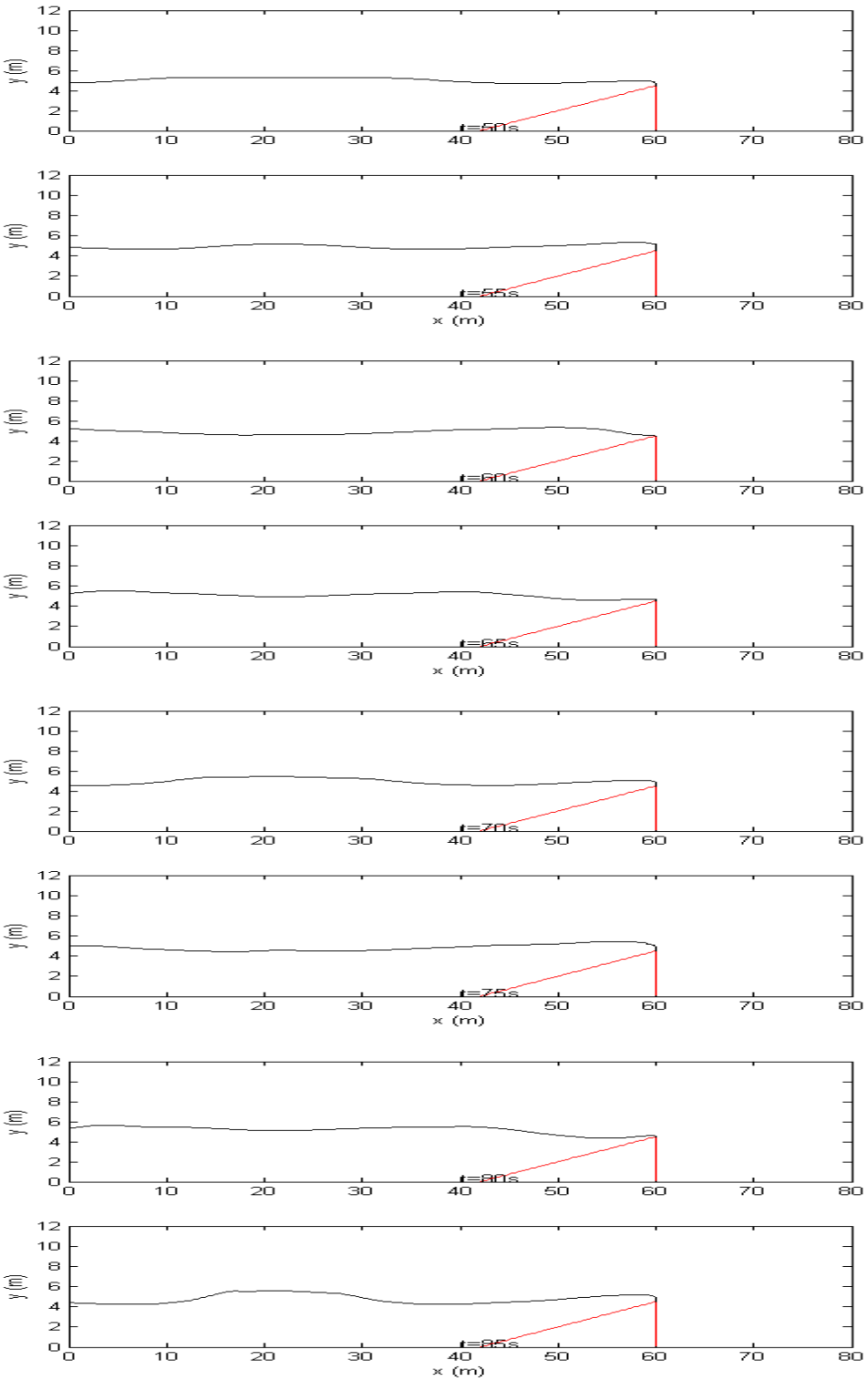

Figure 7.2.24: Wave overtopping and overflow on 1:4 slope seawall in the non-breaking zone from time 50.0 to 85.0s. [Run no. 8 (Table 7.2.5): Hs = 0.72m, Tm = 7.30s and Tp = 4.70s].

Figure 7.2.25 shows the comparison between the wave overtopping and overflow calculated from 2-D BWNM with weir equation. As explained before, the difference between the two results is due to weir equation did not include the effect of waves. Same conclusion arises before in Figures 7.2.5, 7.2.10, 7.2.15 and 7.2.20 is presented in Figure 7.2.25 also. The difference between 2-D BWNM and weir equation decreases as the magnitude of the freeboard, R_c, increases.

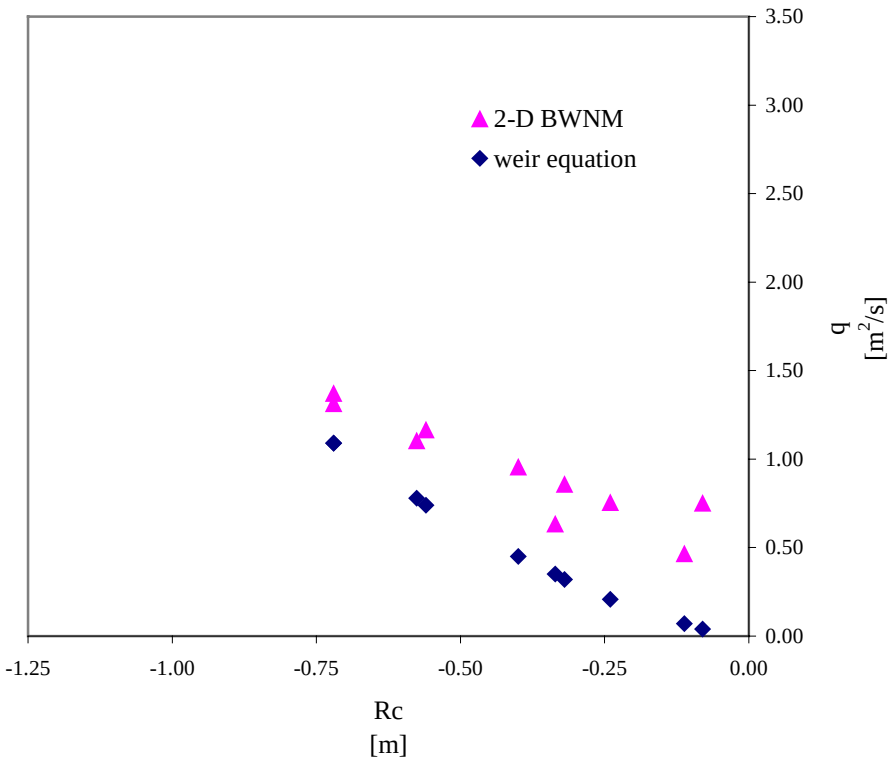

Figure 7.2.25: Comparison between weir equation and 2-D BWNM for irregular non-breaking waves at a 1:4 sloped seawall.

7.3 Synthesis of results

Results from numerical simulation of irregular breaking and non-breaking wave overtopping and overflow for different seawall slopes were presented in the previous sections (Sections 7.2.1, 7.2.2, 7.2.3, 7.2.4 and 7.2.5). Comparisons of numerical model results with the weir equation were shown in these previous sections.

In this section, relation the between the dimensionless wave overtopping and dimensionless freeboard for different sloped seawalls for small negative freeboard is presented (Soliman and Reeve, 2003). It is useful to mention here that the definition of the dimensionless parameters is due to Van der Meer and Janssen (1995). Reasons of that could be found in Chapter 2 (Section 2.2.1).

7.3.1 Breaking wave overtopping and overflow

The case of breaking wave overtopping and overflow $\left(\xi_p < 2\right)$ is studied first. Analysis of the numerical wave overtopping and overflow results for sloped seawalls (Section 7.2.1, 7.2.2 and 7.2.3) leads to the following suggested design formulae for small negative freeboard under breaking wave attack $\left(0.0 > R \geq -0.8\right)$:

Slope 1:3	$Q = 0.046\exp\left(-2.71R\right)$	(7.3.2)
Slope 1:4	$Q = 0.048\exp\left(-2.14R\right)$	(7.3.3)
Slope 1:6	$Q = 0.051\exp\left(-1.53R\right)$	(7.3.4)

Figure 7.3.26 presented the previous relation between the dimensionless wave overtopping and dimensionless freeboard. Values of R^2, which is an indicator of goodness of fit, reveals how closely the estimated values for the formula trend line correspond to the actual. For Equations (7.3.2), (7.3.3) and (7.3.4) the R^2 values are 0.98, 0.97 and 0.97 respectively. These values of R^2 are very near to one which indicates a very good level of fit.

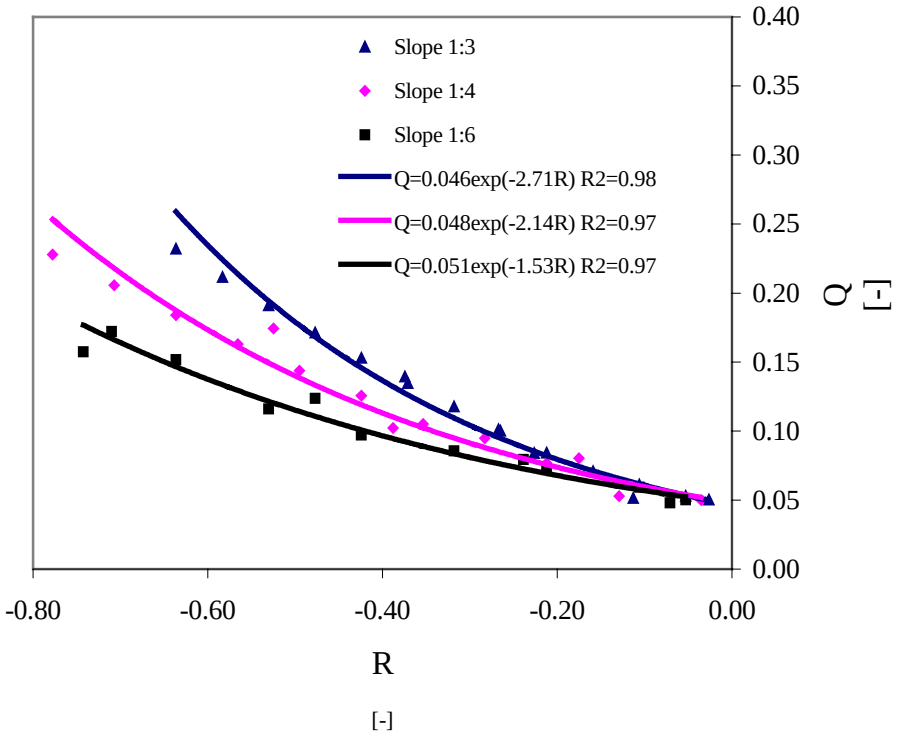

Figure 7.3.26: Breaking waves overtopping data as a basis for Equations 7.3.1, 7.3.2 and 7.3.3.

7.3.2 Non-breaking wave overtopping and overflow

Results for non-breaking waves (Sections 7.2.4 and 7.2.5) for sloped seawall are analysed also and are demonstrated in Figures 7.3.27 and 7.3.28. The concluded design formulae for small negative freeboard $\left(0.0 > R \geq -0.8\right)$ under irregular non-breaking wave attack are:

Slope 1:3	$Q = 0.198\exp\left(-1.62R\right)$	(7.3.5)
Slope 1:4	$Q = 0.288\exp\left(-0.83R\right)$	(7.3.6)

The R^2 values for Equations (7.3.5) and (7.3.6) are 0.84, 0.94 respectively.

R^2 for Equation (7.3.5) is less than Equations (7.3.2), (7.3.3) and (7.3.4) for breaking waves but still indicates a good level of fit.

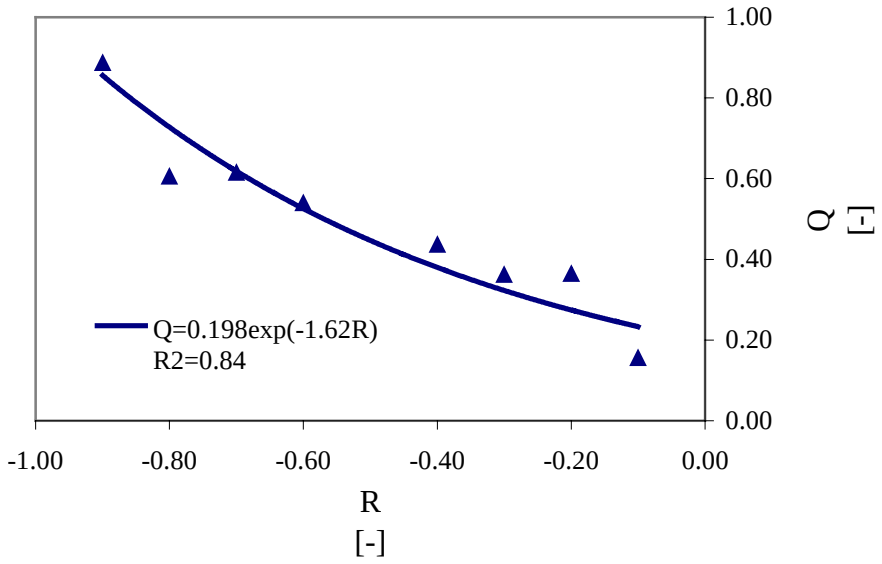

Figure 7.3.27:Non-breaking wave overtopping data as a basis for Equation 7.3.4.

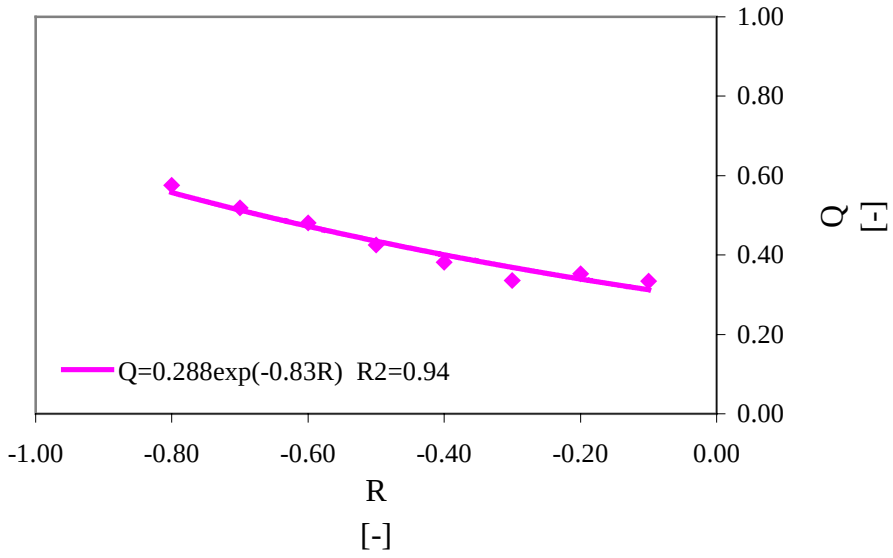

Figure 7.3.28: Non-breaking wave overtopping data as a basis for Equation 7.3.5.

7.4 Discussion

This chapter provided more information of irregular breaking and non-breaking wave overtopping and overflow. Using numerical simulation the cases of breaking and non-breaking wave attack on a smooth sloped seawall are studied.

To be consistent with the case of small positive freeboard which was presented in Chapter 6, the dimensionless freeboard and wave overtopping of Van der Meer and Janssen (1995) have been used here also. The surf similarity parameter used by Van der Meer and Janssen (1995), has been used to define the breaking and non-breaking zone. A multiplicity of formulae for different conditions is not helpful for the practitioner and from a theoretical viewpoint is not satisfying. Formulae covering the range of freeboards considered in the previous sections are derived in the next chapter.

CHAPTER 8

Design Formulae for Small Positive, Zero and Negative Freeboard

The two-dimensional breaking wave numerical model (2-D BWNM) has been applied to study wave overtopping for small positive, zero and negative freeboard under breaking and non-breaking waves attack. Results and suggested design formulae have been presented in details in previous two chapters.

A multiplicity of formulae for different conditions is not helpful for the practitioner and from a theoretical viewpoint is not satisfying. In this chapter, a simple and explicit mathematical solution is applied to merge small positive and negative formulae into a single composite equation.

In first section of this chapter (Section 8.1), the suggested design overtopping formulae in different cases is summarized and presented. Then definition of Logarithmic matching method and its wide applications is explained (Section 8.2). The logarithmic matching technique and its numerical models are illustrated in Section 8.3. In Section 8.4 the logarithmic matching method is applied to the overtopping formulae. One suggested design formulae cover range of small positive, zero and negative freeboards is conducted. Finally, Conclusion of this chapter and advantages of new suggested design overtopping formulae are presented in Section 8.5.

8.1 Synthesis of design formulae

Before using the mathematical solution, it useful first to summarize the suggested design formulae presented in the last chapter.

The set of suggested design formulae of wave overtopping under breaking and non-breaking waves attack for sloped seawall, which have been produced in the previous two chapters, are divided into four main categories as follows:

1- Breaking waves for 1:3 slope: $\left(\xi_p < 2\right)$

$$Q = 0.053\exp\left(-2.05R\right) \qquad \left(0.3 \geq R > 0.0\right) \qquad (8.1.1)$$

$$Q = 0.046\exp\left(-2.71R\right) \qquad \left(0.0 > R \geq -0.8\right) \qquad (8.1.2)$$

2- Non-breaking waves for 1:3 slope: $\left(\xi_p > 2\right)$

$$Q = 0.227\exp\left(-0.94R\right) \qquad \left(0.3 \geq R > 0.0\right) \qquad (8.1.3)$$

$$Q = 0.198\exp\left(-1.62R\right) \qquad \left(0.0 > R \geq -0.8\right) \qquad (8.1.4)$$

3- Breaking waves for 1:4 slope: $\left(\xi_p < 2\right)$

$$Q = 0.041\exp\left(-1.74R\right) \qquad \left(0.3 \geq R > 0.0\right) \qquad (8.1.5)$$

$$Q = 0.048\exp\left(-2.14R\right) \qquad \left(0.0 > R \geq -0.8\right) \qquad (8.1.6)$$

4- Non-breaking waves for 1:4 slope: $\left(\xi_p > 2\right)$

$$Q = 0.229\exp\left(-0.98R\right) \qquad \left(0.3 \geq R > 0.0\right) \qquad (8.1.7)$$

$$Q = 0.288\exp\left(-0.83R\right) \qquad \left(0.0 > R \geq -0.8\right) \qquad (8.1.8)$$

The logarithmic solution is applied to these four sections. One design formula for each case covers range of small positive, zero and negative freeboard is concluded.

8.2 Logarithmic matching method

Recently, Guo (2002b) proposed a logarithmic matching method. It states that for a complicated non-linear problem or an experimental curve, if one can find two asymptotes, in extreme cases, which can be expressed as logarithmic or power laws, then the logarithmic matching can combine the two asymptotes into a single composite solution. Guo (2002a) derived an explicit solution to the wave dispersion equation. The solution is very simple and reproduces the numerical result for any water depth. The maximum relative error of the proposed solution is about 0.75% which is sufficient for practical calculation.

The applications of the logarithmic matching have been successfully tried in several other cases in open channel flows, coastal hydrodynamics and sediment transport such as:

- Inverse problem of Manning equation in rectangular open-channels.
- Connection of different laws in computational hydraulics.
- Criterion of wave breaking.
- Wave current turbulence model.
- Sediment settling velocity.
- Velocity profiles of sediment-laden flows.
- Sediment transport capacity.

All these applications agree very well with numerical solutions or experimental data. More details of the previous application can be found in Guo (2002a).

8.3 Logarithmic matching technique

In this section, the logarithmic matching technique, which is applied to wave overtopping formulae, is illustrated.

Specifically, suppose one can find two asymptotic solutions for a non-linear problem, using an numerical or experimental method, the two asymptotes can be expressed by or transferred into the following form:

$$y = K_1 \ln x + C_1 \qquad \text{for } x < x_o, \tag{8.3.9}$$

and

$$y = K_2 \ln x + C_2 \qquad \text{for } x > x_o \tag{8.3.10}$$

In the two equations above, x is an independent variable, y is a dependent variable, K_1 and K_2 are two slopes based on logarithmic scale, C_1 and C_2 are two intercepts, and x_0 is the location of the cross point of the two asymptotes.

To merge the two asymptotes into a single composite equation, two logarithmic models are proposed, Guo (2002b), Model I is

$$y = K_1 \ln x + \frac{K_2 - K_1}{\beta} \ln\left[1 + \left(\frac{x}{x_o}\right)^{\beta}\right] + C_1 \tag{8.3.11}$$

and Model II is

$$y = K_2 \ln x + \frac{K_1 - K_2}{\beta} \ln\left\{1 - \exp\left[-\left(\frac{x}{x_o}\right)^{\beta}\right]\right\} + C_2 \tag{8.3.12}$$

In the two models, x_o is determined by

$$x_o = \exp\left(\frac{C_1 - C_2}{K_2 - K_1}\right) \tag{8.3.13}$$

and $\beta \neq 0$ is a transitional shape parameter that is determined by any of the following two methods:

- The collocation method: Using the measurement data at the cross point (x_o, y_o) to determine the value of β, i.e., solving β from the following equation.
  - $y(x_o, \beta) = y_o$ (8.3.14)

in which the function y is Equation (8.3.11) or Equation (8.3.12).

- The least squares method (Griffiths and Smith, 1991).

Model I and model II, Equations (8.3.11) and (8.3.12), can directly solve the problems with power laws or logarithmic laws. For two asymptotic exponential laws, the following transformation is helpful.

- Suppose that the two asymptotic exponential laws,
  - $Y = \lambda_1 e^{K_1 X}$ for $X \ll X_o$ (8.3.15)
  - $Y = \lambda_2 e^{K_2 X}$ for $X \gg X_o$ (8.3.16)
- Let
  - $\ln Y = y$ (8.3.17)
  - $X = \ln x$ (8.3.18)
  - $\ln \lambda_1 = C_1$ (8.3.19)
  - $\ln \lambda_2 = C_2$ (8.3.20)
- Equations (8.3.15) and (8.3.16) can be rewritten as:
  - $\ln Y = K_1 X + \ln \lambda_1$ for $X \ll X_o$ (8.3.21)
  - $\ln Y = K_2 X + \ln \lambda_2$ for $X \gg X_o$ (8.3.22)

- Substituting Equations (8.3.17), (8.3.18), (8.3.19) and (8.3.20) into Equations (8.3.21) and (8.3.22) leads to the following Equations:

  - $y = K_1 \ln x + C_1$ (8.3.23)

  - $y = K_2 \ln x + C_2$ (8.3.24)

- Equations (8.3.23), (8.3.24) are similar as Equations (8.3.9) and (8.3.10). Thus model I or model II can be applied to merge the two exponential laws. For example, substituting Equations (8.3.17), (8.3.18), (8.3.19) and (8.3.20) into Equation (8.3.11) gives:

  - $\ln Y = K_1 X + \ln \lambda_1 + \frac{K_2 - K_1}{\beta} \ln\left[1 + e^{\beta(X - X_o)}\right]$ (8.3.25)

  - $\ln Y = K_1 X + \ln\left\{\lambda_1 \left[1 + e^{\beta(X - X_o)}\right]^{(K2 - K1)/\beta}\right\}$ (8.3.26)

  or

  - $Y = \lambda_1 e^{K1X} \left[1 + e^{\beta(X - X_o)}\right]^{(K2 - K1)/\beta}$ (8.3.27)

  and Equation (8.3.13) becomes

  - $X_o = \frac{\ln(\lambda_1 / \lambda_2)}{K_2 - K_1}$ (8.3.28)

- Since value of dimensionless freeboard (R) is small, the exponential law then becomes

  - $Q = a \exp(-bR) \approx a(1 - bR)$ (8.3.29)

In this case Equation (8.3.23), (8.3.24), (8.3.25) and (8.3.28) can be simplified as

- $Y = K_1 X + C_1$ (8.3.30)

- $Y = K_2 X + C_2$ (8.3.31)

- $Y = K_1 X + C_1 + \frac{K_2 - K_1}{\beta} \ln\left[1 + e^{\beta(X - X_o)}\right]$ (8.3.32)

- $X_o = \frac{C_1 - C_2}{K_2 - K_1}$ (8.3.33)

8.4 New suggested design formulae for wave overtopping and overflow:

In this section Guo's logarithmic matching method, Equations (8.3.30), (8.3.31), (8.3.32) and (8.3.33), is applied to get one design formula for the cases of small positive, zero and negative $(0.3 \geq R \geq -0.8)$.

General procedures of applying the logarithmic matching is as follows:

- Using two equations of small positive and small negative freeboards which are summarized in Section 8.1.
- Since value of R is small, the exponential Equations (8.1.1) to (8.1.8) can be simplified using Equation 8.3.29.
- Determine the slopes K_1 and K_2 and the intercepts C_1 and C_2
- Calculate the cross point X_o from Equation (8.3.33).
- Construct a general approximate solution by Equation (8.3.32).
- Solve the parameter β by applying the collocation method, Equation (8.3.14).

The following cases will be studied:

- Breaking waves for 1:3 sloped seawall.
- Non-Breaking wave for 1:3 sloped seawall.
- Breaking wave for 1:4 sloped seawall.
- Non-breaking wave for 1:4 sloped seawall.

Applying the previous procedures in the previous four cases is presented in the following sections.

8.4.1 Combined formulae for wave overtopping and overflow for breaking wave of 1:3 smooth sloped seawall

By applying the logarithmic matching technique, which was described in previous section, to Equations (8.1.1) and (8.1.2) following equation has been conducted:

$$Q = 0.02\ln\left[1+\exp\left(15.04R+2.57\right)\right]-0.37R-0.005 \quad \left(0.3 \geq R > -0.8\right) \qquad (8.4.34)$$

Comparison of Equation (8.4.34) with numerical data is presented in Figure 8.4.1.

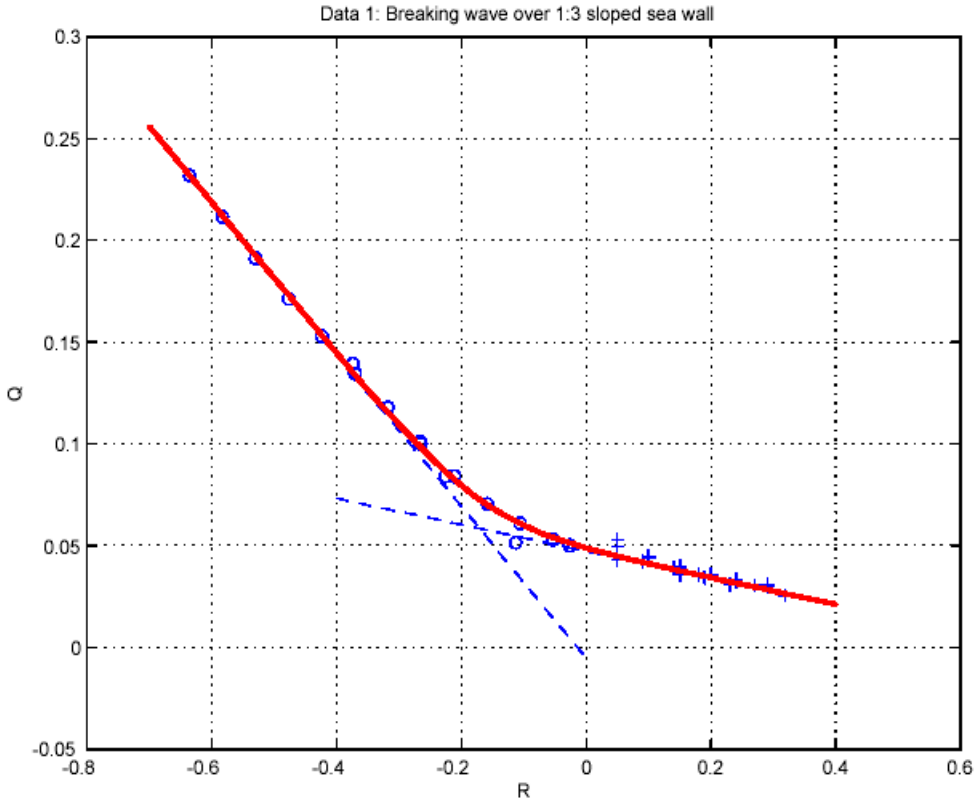

Figure 8.4.1: Comparison between the 2-D BWNM results and the logarithmic matching solution.

Relative error can be defined as:

$$Error = \frac{Q_{calculated} - Q_{numerical}}{Q_{numerical}} \times 100\% \qquad (8.4.35)$$

The average relative error over the freeboard range $(0.3 \geq R > -0.8)$ is 5.2 % that is sufficient in practice.

8.4.2 Combined formulae for wave overtopping and overflow for non-breaking wave of 1:3 smooth sloped seawall

The same logarithmic matching technique can be applied to Equations (8.1.3) and (8.1.4). Following equation could be derived:

$$Q = 0.029 \ln\left[1 + \exp\left(15R + 1.92\right)\right] - 0.63R + 0.173 \quad (0.3 \geq R > -0.8) \qquad (8.4.36)$$

Figure 8.4.2 shows a comparison of Equation (8.4.36) with 2-D BWNM results. An error analysis shows that Equation (8.4.36) has an accuracy of 7.9 % over $(0.3 \geq R > -0.8)$.

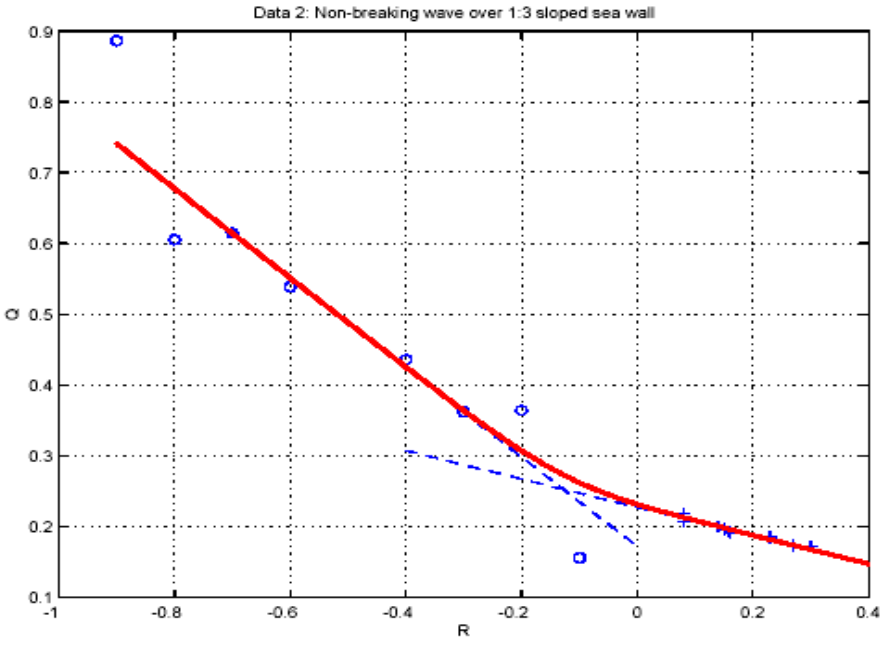

Figure 8.4.2: Comparison of Equation (8.4.36) with numerical data.

8.4.3 Combined formulae for wave overtopping and overflow for breaking wave of 1:4 sloped seawall

The logarithmic matching technique is applied to Equations (8.1.5) and (8.1.6).

Following equation has been conducted:

$$Q = 0.029\ln\left[1+\exp\left(7.94R+2.04\right)\right]-0.313R-0.016 \quad \left(0.3 \geq R > -0.8\right) \quad (8.4.37)$$

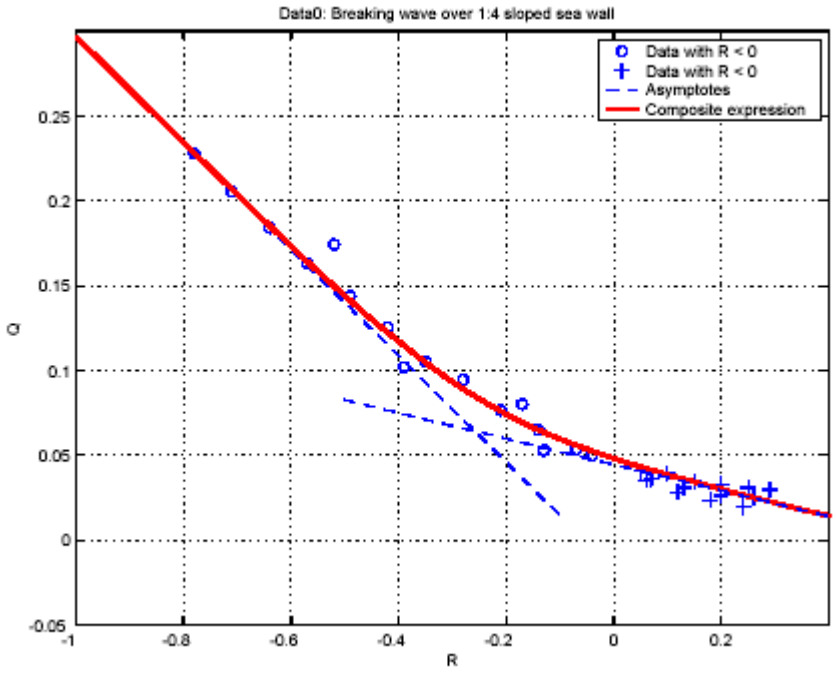

Figure 8.4.3: Comparison between the 2-D BWNM results and the logarithmic matching solution.

Comparison of Equation (8.4.37) with numerical data is presented in Figure 8.4.3.

Equation 8.4.37 has an accuracy of 8.9 % over the freeboard range.

8.4.4 Combined formulae for wave overtopping and overflow for non-breaking wave of 1:4 smooth sloped seawall

By applying the logarithmic matching technique to Equations (8.1.7) and (8.1.8) following equation has been conducted:

$$Q = 0.019\ln\left[1+\exp\left(15R+1.92\right)\right]-0.48R+0.192 \qquad \left(0.3 \geq R > -0.8\right) \qquad (8.4.38)$$

Figure 8.4.4 shows a good agreement between Equation (8.4.38) and a numerical data. Equation (8.4.38) has an accuracy of 4.4 % over the freeboard range.

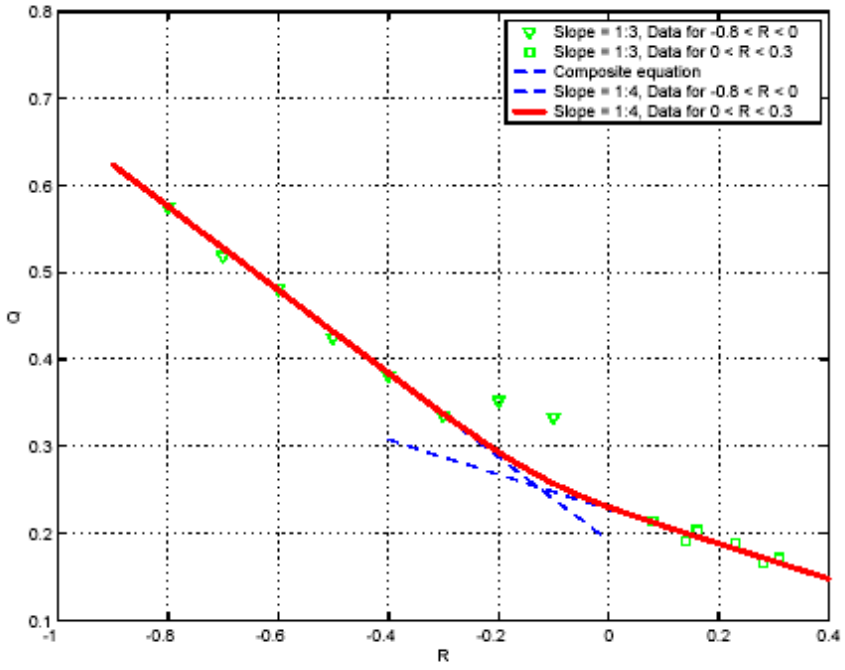

Figure 8.4.4: Comparison of Equation (8.4.38) with numerical data.

8.5 Synthesis of results

In this section, Summary of new suggested design formulae between the dimensionless wave overtopping and dimensionless freeboard for different sloped seawalls for small positive, zero and negative freeboard, $\left(0.3 \geq R > -0.8\right)$, are presented as follows:

<u>1- Breaking waves for 1:3 smooth slope:</u> $\left(\xi_p < 2\right)$

$$Q = 0.02\ln\left[1+\exp\left(15.04R+2.57\right)\right]-0.37R-0.005 \qquad (8.4.39)$$

2- Non-breaking waves for 1:3 smooth slope: $\left(\xi_p > 2\right)$

$$Q = 0.029\ln\left[1+\exp\left(15R+1.92\right)\right]-0.63R+0.173 \quad (8.4.40)$$

3- Breaking waves for 1:4 smooth slope: $\left(\xi_p < 2\right)$

$$Q = 0.029\ln\left[1+\exp\left(7.94R+2.04\right)\right]-0.313R-0.016 \quad (8.4.41)$$

4- Non-breaking waves for 1:4 smooth slope: $\left(\xi_p > 2\right)$

$$Q = 0.019\ln\left[1+\exp\left(15R+1.92\right)\right]-0.48R+0.192 \quad (8.4.42)$$

8.6 Summary

The logarithmic matching technique of Guo's (2002b) has been applied to merge small positive, zero and negative freeboard formulae into a single composite equation. New overtopping expressions for breaking and non-breaking waves on smooth impermeable slopes are presented. The new expressions for wave overtopping and overflow are simple and easy to applied by engineers.

The new expressions can be used to predict overtopping discharges of smooth seawalls in small positive, zero and negative freeboard.

CHAPTER 9

Conclusion

9.1 Summary

The concept of wave overtopping over smooth sloped seawalls has been described. Examples of empirical engineering design formulae widely used in design purposes have been presented. It was evident from the existing knowledge that additional investigations into overtopping of small positive, zero and negative freeboard were needed.

Numerical model tests have been conducted using varying slope geometries have been used during the tests. All tested setups have been subjected to a wide range of sea states. Simulation of irregular wave spectrum (JONSWAP) was developed in the two-dimensional breaking wave numerical model (2-D BWNM) using an internal designed mass source.

The results of the model tests have been compared with results from the literature. A new overtopping expression for breaking and non-breaking waves on smooth impermeable slopes is presented. This new expression is based on formulae proposed expression given by Van der Meer and Janssen (1995). The original formula has been modified to be valid for the following cases:

- Small positive freeboard $\left(0.3 \geq R > 0.0\right)$.
- Zero freeboard $\left(R = 0.0\right)$.
- Small negative freeboard $\left(0.0 > R \geq -0.8\right)$.

With the new expressions it is possible to predict overtopping discharges of smooth seawalls in small positive, zero and negative freeboard.

The newly developed numerical model (2-D BWNM) has been validated against the following:

- Analytical solution of the weir equation.
- Laboratory data with linear waves [Saville (1955)].
- Laboratory data for JONSWAP irregular wave [Van der Meer and Janssen (1995)].
- Numerical Model (AMAZON) for linear waves [Hu *et al.* (2000)].
- Empirical design formulae based on laboratory experiments [Owen (1980); Van der Meer *et al.* (1992); Hedges and Reis (1998); Schüttrumpf (2001)].

9.2 Wave overtopping at small positive freeboard

The two-dimensional breaking wave numerical model (2-D BWNM) that is based on the breaking wave model developed by Lin (1998) has been presented. Simulation of irregular wave attacks using an internal mass source has been added and tested. The model accuracy in simulating propagation of different kind of waves (linear wave and irregular wave) has been evaluated. The overall performance of the model is considered satisfactory.

New design formulae based on numerical results of two-dimensional breaking wave numerical model for breaking and non-breaking wave overtopping at small positive freeboard $\left(0.3 \geq R > 0.0\right)$ have been proposed. These formulae are an

extension of the existing overtopping expression for breaking and non-breaking waves presented by Van der Meer and Janssen (1995).

The proposed expression allows for the prediction of overtopping discharges for relative crest freeboards down to zero.

Furthermore, the new expression also includes the effect of breaking waves in the shallow water zone. Two different seawall slopes (1:3 and 1:4) have been tested with a wide range of irregular wave characteristics.

The numerical tests with different freeboards indicate that wave overtopping decreases as the seawall slope increases. The tests also indicate that breaking wave overtopping is less than non-breaking wave overtopping for different seawall slopes. These observations are in line with the existing design formulae [Owen (1980); Van der Meer *et al.* (1992); Hedges and Reis (1998); Schüttrumpf (2001)].

In the last years, the climate has been changing and global sea level are rising (Hardy, 2003). The new formulae will be useful to engineers in assessing existing coastal structures which were designed for conditions that may have been defined without the benefit of recent climate change research. The new expressions cover the range of small positive and zero freeboard which was not covered by design formulae until now.

9.3 Wave overtopping and overflow at small negative freeboard

If the water level rises above the crest level of the structure, for example during extreme storm surges, flooding is not only caused by wave overtopping action, but also by overflow. Existing coastal structures that have not been designed to

account for this will be more vulnerable to combined overflow and overtopping. There is currently no guidance on estimating these volumes.

The case of overtopping and overflow for smooth sloped seawalls under irregular wave attack has been studied using a two-dimensional breaking wave numerical model. A new expression covering freeboard range $\left(0.0 > R \geq -0.8\right)$ has been presented. Three different seawall slopes (1:3, 1:4 and 1:6) have been tested with wide range of irregular wave characteristics. The new expression covers cases of both breaking and non-breaking waves.

The issues that arise in small positive freeboard cases are also present in the case of negative freeboard. The numerical tests with different freeboards indicate that wave overtopping decreases as the seawall slope decreases and breaking wave overtopping is less than non-breaking wave overtopping for different seawall slopes.

9.4 Future research

The 2-D BWNM model can be used as a numerical flume for studying any practical problems in the future. Flexibility of the model and its time of calculation are considered two main important advantages. The model is very encouraging in this point, as one second simulation for irregular wave needs about ten minutes calculation using a personal computer with a typical configuration. As new generations of computers become available, processing time will reduce and more detailed numerical simulation will be possible.

The new model has been implemented to study cases of wave overtopping for the range of small positive, zero and small negative freeboard which are not covered by any current design formulae.

New expressions have been presented that cover cases of small positive, zero and small negative freeboard for smooth sloped seawalls. Using the equations described in Chapter 8, it is possible to develop preliminary designs, and to improve the performance of existing seawalls. The researcher recognises that the progression of research results into design practice can take some time. Nevertheless, the researcher hopes that the new formulae will be used by designers to investigate and improve the performance of seawalls.

Part of the results conducted from this research has been published in the following conferences:

- Soliman, A., M. S. Raslan and D. E. Reeve (2003). Numerical simulation of wave overtopping using two dimensional breaking wave model. Proceedings of Coastal Engineering VI: Computer modelling of seas and coastal regions, Cadiz, Spain, (Ed. C Brebia, D Almorza & F Lopez-Aguayo), pp. 439-447.

- Soliman, A. and D. E. Reeve (2003). Numerical study for small freeboard wave overtopping and overflow of sloping sea wall. To appear in Proceeding of Coastal Structures 2003, Portland, Oregon.

Other two journal papers are under preparation now and hopefully published in the next few months.

The investigation has dealt with a limited set of conditions. There are a number of ways in which the applicability of the approach has been adopted and could be extended. For example,

- More validation for the new wave overtopping expressions using full scale field data.
- Including more complicated seawall geometries, such as bermed slopes, slope with crown wall and recurved walls.
- The effects of surface roughness.
- Accounting for porosity in both the beach and defence structure.
- The infiltration and erosion on the landside of seawall. This study requires sediment transport calculations and morphological updating.

References

Ahrens, J. P. and M. S. Heimbaugh (1988). Seawall overtopping model**:** pp. 795-806.

Aminti, P. and L. Franco (1988). Wave overtopping on rubble mound breakwaters. Proc. 21st International Conference on Coastal Engineering, Malaga, Spain

Austin, D. I. and R. S. Schlueter (1982). A numerical model of wave breaking / breakwater interactions. In proceedings 18th International Conference on Coastal Engineering, Cape Town, Republic of South Africa **Vol. 3**: pp. 2079-2096.

Banyard, L. and D. M. Herbert (1995). The effect of wave angle on the overtopping of seawalls., HR Wallingford, SR396.

Barr, P. K. and W. T. Ashurst (1984). An interface scheme for turbulent flame propagation, Sandia National Laboratories, Report 82-8773.

Besley, P. (1999). Overtopping of seawalls: design and assessment manual, H R Wallingford, Report W178.

Besley, P., T. Stewart and N. W. H. Allsop (1998). Overtopping of vertical structures: new prediction methods to account for shallow water conditions. Proc. of the Conference on Coastlines, structures and breakwaters, ICE

Bleck, M., H. Oumeraci and H. Schuttrumpf (2000). Combined wave overtopping and overflow of dikes and seawalls. Proceeding of the 27th International Conference on Coastal Engineering - Poster session, Sydney, Australia

Bouws, F., H. Gunther, W. Rosenthal and C. L. Vincent (1985). "Similarity of the wind wave spectrum in finite depth water: 1. Spectral form." Jour. Geoph. Res. **C1-90**: pp. 975-986.

Bradbury, A. P. and W. Allsop (1988). Hydraulic effects of breakwater crown halls. In Proc. of Conf. on Design of Breakwaters, Institution of Civil Engineers, London, UK,: pp. 385-396.

Brorsen, M. and J. Larsen (1987). "Source generation of nonlinear gravity waves with boundary integral equation method." Coastal Engineering **Vol. 11**: pp. 93-113.

Burchartch, H. F. and S. A. Hughes (2003). Coastal Engineering Manual, Fundamentals of design. Chapter 5, Part VI, Design of coastal project elements, Coastal Engineering Research Centre, Waterways Experiment Station, US Army Corps of Engineering, Vicksburg, USA.

Carter, D. J. T. (1982). Estimation of wave spectra from wave height and period, Surrey, Institute of Oceanographic Science: pp. 1-19, MIAS Reference Publication No. 4.

Chadwick, A. and J. Morfett (1998). Hydraulics in civil and environmental engineering. London and New York, E & FN SPON.

Chan, K.-C. and R. L. Street (1970). "A computer study of finite amplitude water wave." J. Comp. Phys **Vol. 6**: pp. 68-94.

CIRIA / CUR (1991). Manual on the Use of Rock in Coastal and Shoreline Engineering, London, Constriction Industry Research and Information ass.,, Special pub. 83.

Dodd, N. (1998). "Numerical model of wave run-up, overtopping, and regeneration." Journal of Waterway, Port, Coastal and Ocean Engineering **Vol. 124**(2): pp. 73-81.

Douglass, S. L. (1986). Review and comparison of methods for estimating irregular wave overtopping rates, U. S. Army Corps of Engineers, Rep. CERC-86-12.

Floryan, J. M. and H. Rasmussen (1989). "Numerical methods for viscous flows with moving boundaries." Appl. Mech. Rev. **Vol. 42**(12): pp. 323-341.

Franco, C., L. Franco, C. Restano and J. W. Van der Meer (1995). The effect of obliquity and Short-Crestedness on the overtopping rate and volume distribution on caisson breakwaters, Final proceedings MCS project, Monolithic (vertical) breakwaters

Franco, L., M. de Gerloni and J. W. Van der Meer (1994). Wave overtopping on vertical and composite breakwaters. Proceedings of the 24th International Coastal Engineering Conference, American Society of Civil Engineers **Vol. 1**: pp. 1030-1045.

Goda, Y. (2000). Random seas and design of maritime structures. University of Tokyo Press, Tokyo, Japan.

Grantham, K. N. (1953). "Wave run-up on sloping structures." Transactions, American Geophysical Union **Vol. 34**(5): pp. 720 - 724.

Griffiths, D. V. and I. M. Smith (1991). Numerical methods for engineers. CRC Press, Boston, USA: pp. 246-266.

Grune, J. (1982). Wave run-up caused by nature storm surge. Proceeding of 18th coastal engineering conference, ASCE, New York **Vol. 1**: pp. 785-803.

Guo, J. (2002a). "Logarithmic matching and its applications in computational hydraulic and sediment transport." Journal of hydraulic Research, IAHR **Vol. 40**(5).

Guo, J. (2002b). "Simple and explicit solution of wave dispersion equation." Coastal Engineering **Vol. 45**: pp. 71-74.

Hardy, J. T. (2003). Climate change- causes, effects, and solutions. Sussex, England.

Harlow, F. H. and J. E. Welch (1965). "Numerical calculation of time-dependent viscous incompressible flow." Phys. fluids **Vol. 8**: pp. 2182-2189.

Hasselmann, K. (1973). Measurements of wind-waves and swell decay during the Joint North Sea Wave Project (JONSWAP), Hamburg, Deutsches Hydrographisches Institute: pp. 12-95

Hawkes, P. J. (1999). "Mean overtopping rate in swell and bimodal seas." Proceedings of the Institution of Civil Engineers - Water Maritime and Energy **Vol. 136**(4): pp. 235-238.

Hebsgaard, M., P. Sloth and J. Juhl (1998). Wave overtopping of rubble mound breakwaters. Proc. of the Coastal Engineering Conference 2: pp. 2235-2248.

Hedges, T. S. and M. T. Reis (1998). Random wave overtopping of simple sea walls: a new regression model. Proceedings ICE: Water, Maritime and Energy **Vol. 130 -1**: pp. 1-10.

Hedges, T. S. and M. T. Reis (1999). "Wave overtopping models and seawall freeboards." Coastal engineering and marina developments (C.A. Brebbia and P. Anagnostopoulos (Eds.), Computational Mechanics Publications: pp. 567-576.

Hiraishi, T. and H. Maruyama (1998). Directional wave overtopping estimation model and experimental verification. Proc. of the Coastal Engineering Conference: pp. 2249-2261.

Hiroyoshi, S. and T. Kono (1970). Analytical approach on wave overtopping on levees. 12 th Coastal Engineering Conference, Washington, D.C. **Vol. 1**: pp. 563-573.

Hirt, C. W. and R. P. Harper (1985). Sample Problem for an Oil/Water/Gas Separator, Flow Science Technical Note 1, (FSI-85-00-TN1).

Hirt, C. W. and B. D. Nichols (1981). "Volume of fluid (VOF) method for dynamics of free boundaries." Journal of Comp. Phys. **Vol. 39**: pp. 201-225.

Hirt, C. W., B. D. Nichols and N. C. Romero (1975). SOLA - A numerical solution algorithm for transient fluid flows, Los Alamos, CA, USA, Report LA-5852.

Hu, K., C. G. Mingham and D. M. Causon (2000). "Numerical simulation of wave overtopping of coastal structure using the non-linear shallow water equation." Coastal Engineering **Vol. 41**: pp. 433-465.

Isobe, M. (2001). A review of numerical models for wave trans-formation in shallow water. Proc. of International Work-shop on Advanced Design of maritime Structures in the 21st century, Port and Harbour research Institute: pp. 200-205.

Isobe, M., S. Takahashi, S. P. Yu, T. Sakakiyama, K. Fujima, K. Kawasaki, Q. Jiang, M. Akiyama and H. Oyama (1999). "Interim report on development of numerical wave flume for maritime structure design." Proceeding of Civil Engineering in the Ocean,J.S.C.E., **Vol. 15**: pp. 321-326.

Iwata, K., R. C. Kawasaki and D. Kim (1996). Breaking limit, breaking and post-breaking wave deformation due to submerged structures. In: Proceedings 25th Conference on Coastal Engineering, Orlando, USA **Vol. 3**: pp. 2338-2351.

Johnson, B. D., N. Kobayashi and C. D. T. (1996). Formulation and validation of vertically 2-D shallow-water model. Proc. 25th Intentional Conference in Coastal Engineering, ASCE: pp. 551-564.

Johnson, W. E. (1970). Development and application of computer programs related to hypervelocity Impact, system, Science and software report, Report 3SR - 353.

Juhl, J. and P. Sloth (1995). Wave Overtopping of Breakwaters under Oblique Waves. Proceedings of the Coastal Engineering Conference 1: pp. 1182-1196.

Karambas, T. V. and C. Koutitas (1992). "A breaking wave propagation model based on the Boussinesq equations." Coastal Engineering **Vol. 18**: pp. 1-19.

Kim, J., Moin P. and M. R. (1987). "Turbulence statistics in fully developed channel flow at low Reynolds number." Journal of Fluid Mechanics **Vol. 177**: pp. 133-166.

Kobayashi, N. and A. Wurjanto (1989). "Wave overtopping on coastal structures." Journal of Waterway, Port, Coastal and Ocean Engineering **Vol. 115**(2): pp. 235-251.

Koford, J. P. (2002). Wave overtopping of marine structures. Hydraulics & Coastal Engineering Laboratory. Aalborg, Denmark, Aalborg University**:** pp. 171.

Kothe, D. B., R. C. Ferrell, J. A. Turner and S. J. Mosso (1997). A high resolution finite volume method for efficient parallel simulation of casting processes on unstructured meshes, Los Alamos, NM, USA, Los Alamos National Laboratory. In: Proceeding 8th SIAM Conference on Parallel Processing for Scientific Community, Minneapolis, NM, USA, Report LA-UR-97-30.

Kothe, D. B., R. C. Mjolsness and M. D. Torrey (1991). RIPPLE: a computer program for incompressible flows with free surfaces, Los Alamos, NM, USA, Los Alamos Scientific Report, Report LA-12007-MS.

Larsen, J. and H. Dancy (1983). "Open boundaries in short wave simulations - a new approach." Coastal Engineering **Vol. 7**: pp. 285-297.

Launder, B. E., A. Morse, W. Rodi and D. B. Spalding (1972). Prediction of free shear flows: a comparison of the performance of six turbulence models. In Free Shear Flow, NASA Conference: pp. 361-426.

Launder, B. E., G. T. Reece and W. Rodi (1975). "Progress in development of a Reynolds stress turbulence closure." Journal of Fluid Mechanics **Vol. 68**: pp. 537-566.

Le Méhauté, B., R. C. Y. Koh and L. Hwang (1968). "A synthesis of wave run-up." Journal of the waterways and coastal engineering division, ASCE **Vol. 94**: No. WW1, proc. paper 5807 - pp. 77-92.

Lemos, C. M. (1992). Wave breaking, a numerical study, Lecture Notes in Engineering No. 71. Springer-Verlag, Berlin, Germany

Lin, P. (1998). Numerical modelling of breaking waves, Cornell University, U.S.A.

Lin, P. and P. L.-F. Liu (1998). "A numerical study of breaking waves in the surf zone." Journal of Fluid Mechanics **359**: pp. 239-264.

Lin, P. and P. L.-F. Liu (1999). "Internal wave-maker for Navier-Stokes equations models." Waterway, Port, Coastal, and Ocean Engineering **Vol. 125**(4): pp. 207-215.

Lin, P. and P. L.-F. Liu (2000). A user`s manual for a breaking wave model, Ithaca, New York 14853, School of civil and environmental engineering, Cornell University

Liu, P. L.-F. and P. Lin (1997). A numerical model for breaking waves: The volume of fluid method, Newark, Delaware, Centre for Applied Coastal Research, Ocean Engineering Laboratory, University of Delaware

Liu, P. L.-F., P. Lin and K. A. Chang (1999). "Numerical modeling of wave interaction with porous structures." Waterway, Port, Coastal, and Ocean Engineering **Vol. 125**(6): pp. 322-330.

McMaster, W. H. and E. Y. Gong (1979). PELE-IC User `s manual, Lawrence Livermore Laboratory, Report UCRL-52609.

McMaster, W. H., C. S. Quinones, D. M. Landram, D. M. Norris, E. Y. Gong, N. A. Machen and R. E. Nickell (1980). Applications of the coupled fluid-

structure code PELE-IC to pressure suppression analysis, Annual Report to NRC for 1979, NURER/CR-1179, Report UCRL-52733.

Napp, N., J. Pearson, S. Richardson, T. Bruce, W. Allsop and T. Pullen (2002). Overtopping of seawalls under oblique and 3-d wave conditions. Proceeding of the 28th International Conference, Coastal Engineering 2002, Cardiff, UK. **Vol. 2**: pp. 2178-2190.

Nichols, B. D. and C. W. Hirt (1971). "Improved free surface boundary conditions for numerical incompressible-flow calculations." J. Comp. Phys. **Vol. 8**: pp. 434-448.

Nichols, B. D. and C. W. Hirt (1975). Methods for calculating multi-dimensional, transient free surface flows past bodies. Proc. of 1st International Conference in Numerical Ship Hydrodynamics, Gaithersburg, Maryland

Nichols, B. D., C. W. Hirt and R. S. Hotchkiss (1980). SOLA-VOF: A solution algorithm for transient fluid flow with multiple free boundaries, Los Alamos, CA, USA, Los Alamos Scientific Report, Report LA-8355.

Ochi, M. K. (1979). A series of JONSWAP wave spectra for offshore structure design. 2nd International Conference on the Behaviour of offshore Structures (BOSS 79), London, U.K., BHRA Fluid Engineering, Cranfield, Bedford, U.K **Vol. 1**: pp. 301-328.

Oezhan, E. and A. C. Yalciner (1991). Overtopping of solitary waves at model sea dikes. Proceedings of the Coastal Engineering Conference 2: pp. 1487-1498.

Orszag, S. A. and G. S. Patterson (1972). "Numerical simulation of three-dimensional homogeneous isotropic turbulence." Phys. Rev. Lett., **Vol. 28**: pp. 76-69.

Oumeraci, H., H. Schüttrumpf, J. Moller and M. Kudella (2001). Loading of inner slope of sea dikes by wave overtopping - Results from large scale model tests-, LWI-Report No. 858

Oumeraci, H., H. Schüttrumpf, W. Sauer, J. Moller and T. Droste (1999). Physical model tests on wave overtopping with nature sea state - 2D model tests with single, double and multi-peaked wave energy spectra, LWI-Report No. 852

Owen, M. W. (1980). Design of seawalls allowing for wave overtopping, HR-Wallingford, UK., Technical Report EX-924.

Owen, M. W. (1982). The hydraulic design of seawall profiles. Proc. Conf. on Shoreline Protection, ICE, London, UK: pp. 185-192.

Pedersen, J. (1996). Experimental Study of Wave Forces and Wave Overtopping on Breakwater Crown Walls. Hydraulics & Coastal Engineering Laboratory, Department of Civil Engineering. Aalborg, Denmark, Aalborg University.

Pedersen, J. and H. F. Burchartch (1992). Wave Forces on Crown Walls. Proc. 23rd International Conference on Coastal Engineering, Venice, Italy

Peregrine, D. H. (1967). "Long waves on a beach." J. Fluid Mech. **Vol. 27**(4): pp. 815-827.

Pope, S. B. (1975). "A more general effective-viscosity hypothesis." Journal of Fluid Mechanics **Vol. 72**: pp. 331-340.

Rodi, W. (1980). Turbulence Models and Their Application in Hydraulics - A state of the Art Review, I.A.H.R. publication.

Rogallo, R. S. (1981). Numerical Experiments in Homogeneous Turbulence, NASA, Technical Rep. TM81315.

Sakakiyama, T. and R. Kajima (1997). Wave overtopping and stability of armor units under multidirectional waves. Proceedings of the Coastal Engineering Conference 2: pp. 1862-1875.

Saville, T. (1955). Laboratory data on wave run up and overtopping on shore structures, Dayton, Ohio, U.S. Army, Beach Erosion Board, Document Service Centre, No. 64.

Schaffer, H. A., P. A. Madsen and R. Deigaard (1993). "A Boussinesq model for waves breaking in shallow water." Coastal Engineering **Vol. 20**: pp. 185-202.

Schüttrumpf, H. (2001). Wellenüberlaufströmung an Seedeichen Experimentelle und theoretische untersuchungen, Dissertation. Leichtweiss-Institut, TU Braunschweig.

Schuttrumpf, H., Kortenhaus, A. and Oumeraci, H. (1998). Application of overtopping models to vertical walls against storm surges. Proceeding of the 26th International Conference on Coastal Engineering, Copenhagen.

Schuttrumpf, H., J. Moller, H. Oumeraci, J. Grune and R. Weissmann (2001). Effects of natural sea states on wave overtopping of sea dikes. Proceeding of international symposium on Ocean wave measurements and analysis (Waves 2001), San Francisco.

Schüttrumpf, H. and H. Oumeraci (2000). EAK-Empfehlungen a2 - wellenauflauf und wellenuberlauf (kurzfassung) hansa - schiffahrt - schiffbau - hafen., (in German).

Shih, T.-H., J. Zhu and J. L. Lumley (1996). "Calculation of wall-bounded complex flows and free shear flows." International Journal. for Numerical Methods in Fluids **Vol. 23**: pp. 1133-1144.

Soliman, A., M. S. Raslan and D. E. Reeve (2003). Numerical simulation of wave overtopping using two dimensional breaking wave model. Coastal Engineering VI, Cadiz, Spain: pp. 439-447.

Soliman, A. and D. E. Reeve (2003). Numerical study for small freeboard wave overtopping and overflow of sloping sea wall. Coastal Structures 2003 Conference, Portland, Oregon.

TACPAI (1974). Wave run-up and overtopping, Technical Advisory Committee on Protection Against Inundation Government Publishing Office, The Hague.

Takahashi, S., Y. Kotako, R. Fujiwara and M. Isobe (2002). Performance evaluation of perforated-wall caissons by VOF numerical simulations. Proceeding of the 28th International Conference, Coastal Engineering 2002, Cardiff, UK.: pp. 1365-1376.

Ting, F. C. K. and J. T. Kirby (1995). "Dynamics of surf-zone turbulence in a strong plunging breaker." Coastal Engineering **Vol. 24**: pp. 177-204.

Ting, F. C. K. and J. T. Kirby (1996). "Dynamics of surf-zone turbulence in a strong spilling breaker." Coastal Engineering **Vol. 27**: pp. 131-160.

Torrey, M. D., L. D. Cloutman, R. C. Mjolsness and C. W. Hirt (1985). NASA-VOF2D: a computer program for incompressible flows with free surfaces, Los Alamos, NM, USA, Los Alamos Scientific Report, Report LA-10612-MS.

Troch, P. (1997). VOFbreak^2, a numerical model for simulation of wave interaction with rubble mound breakwaters. Proceedings 27th IAHR Congress, San Francisco, USA: pp. 1366-371.

Troch, P. and J. De Rouck (1998). Development of two-dimensional numerical wave flume for wave interaction with rubble mound breakwater. Proc. of the Coastal Engineering Conference: pp. 1639-1649.

Troch, P. and J. De Rouck (1999). "An active wave generation-absorbing boundary condition for VOF type numerical model." Coastal engineering **Vol. 38**: pp. 223-247.

Umeyama, M. (1993). "Wave overtopping on vertical boundary and water surface displacement." Journal of Waterway, Port, Coastal and Ocean Engineering **Vol. 119**(3): pp. 243-260.

Van de Walle, B., J. De Rouck and P. Frigaard (2002). Full scale measurements of wave run-up on a rubble mound breakwater. Proceeding of 28th International conference on coastal engineering, Cardiff, Wales.

Van der Meer, J. W. and J. P. F. M. Janssen (1995). Wave run-up and wave overtopping at dikes. Wave forces on inclined and vertical structures**:** pp. 1-27.

Van der Meer, J. W., H. A. H. Petit, P. Van den Bosch, G. Klopman and R. D. Broekens (1992). Numerical simulation of wave motion on and in coastal structures. In Proceeding 23 rd International Conference on Coastal Engineering, Venice, Italy **Vol. 2**: pp. 1172-1784.

Van Gent, M. R. A. (1999). Physical model investigations on coastal structures with shallow foreshores. 2D model tests with single and double peak wave energy spectra, Delft Hydraulics, Report H3608.

Versteeg, H. K. and W. Malalasekera (1995). An introduction to computational fluid dynamics - The finite volume method, Addison Wesley Longman Limited: pp. 257.

Welch, J. E., F. H. Harlow, J. P. Shannon and B. J. Daly (1966). The MAC method: A computing technique for solving viscous incompressible, transient fluid flow problems involving free surfaces, Los Alamos, NM, USA, Los Alamos Scientific Laboratory, Report LA-3425.

Wu, N. (1994). Numerischen simulation der druckschlagbelastung durch brechende wellen auf senkrechte bauwerke. Ph.D thesis Franziüs - Institut für Wasserbau und Küsteningenieurwesen - Universität Hannover. Hannover, Germany.

Zelt, J. A. (1991). "The run-up of non-breaking and breaking solitary waves." Coastal Engineering **Vol. 15**: pp. 205-246.

Appendix A

Irregular wave propagation on 1:3 sloping sea wall at small positive freeboard

[Hs = 0.83 m, T_m = 3.60s and T_p = 5.00 sec.]

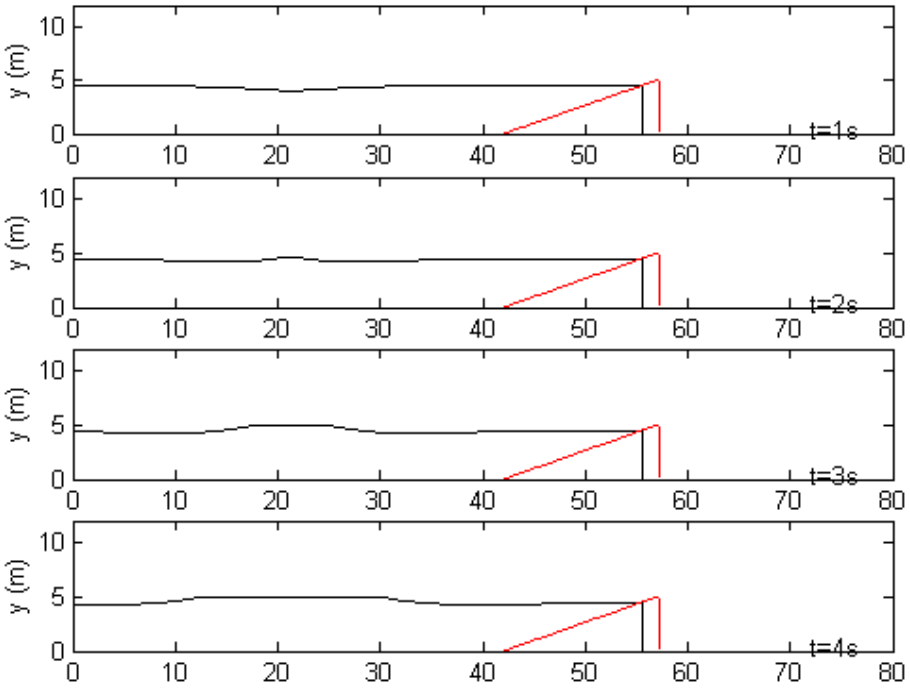
y (m)
t=1s
t=2s
t=3s
t=4s

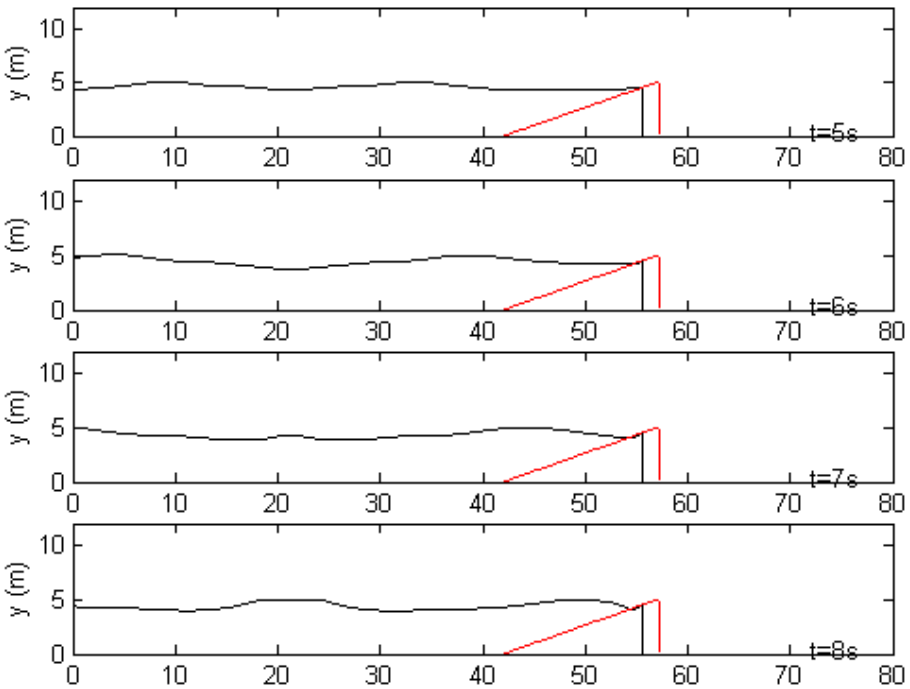
y (m)
t=5s
t=6s
t=7s
t=8s

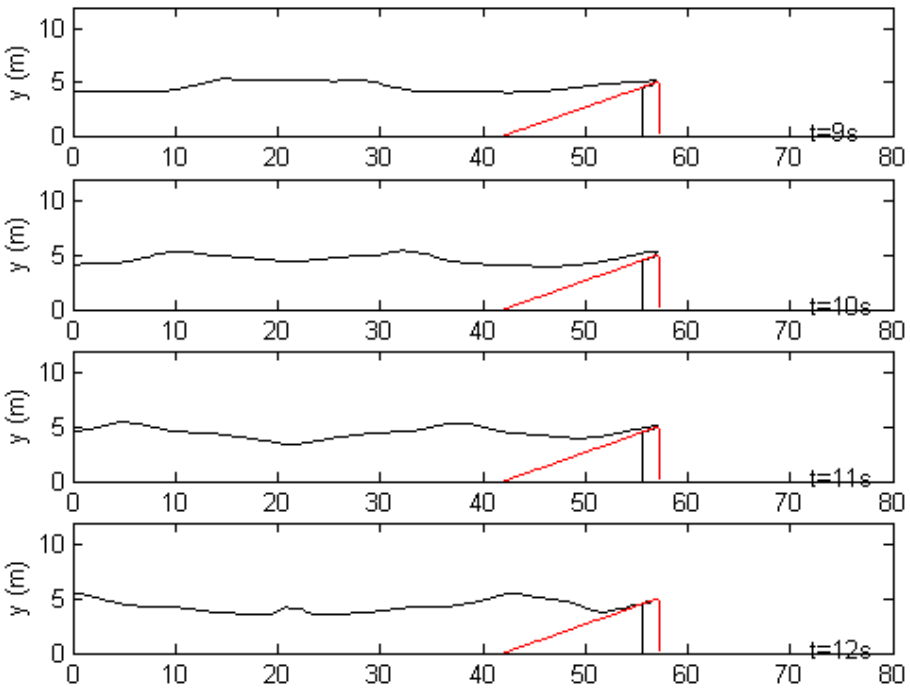
y (m)
t=9s
t=10s
t=11s
t=12s

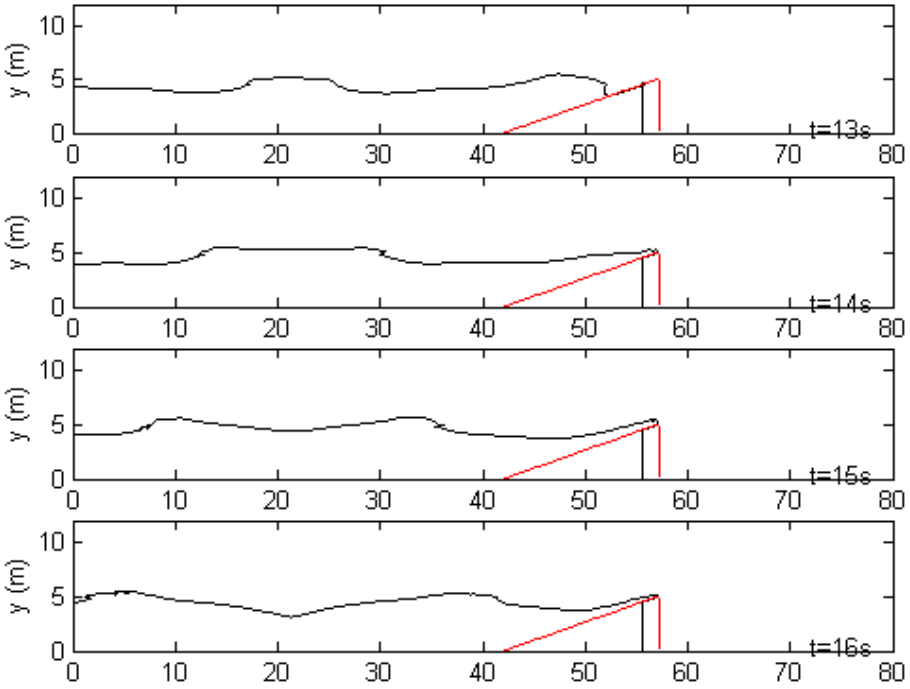
y (m)
t=13s
t=14s
t=15s
t=16s

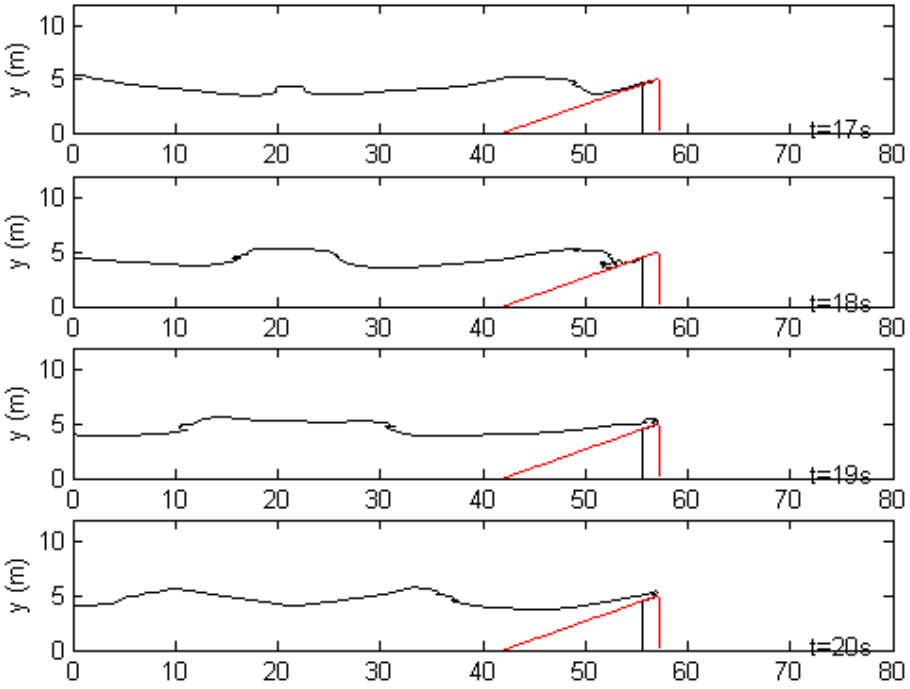
y (m)
t=17s
t=18s
t=19s
t=20s

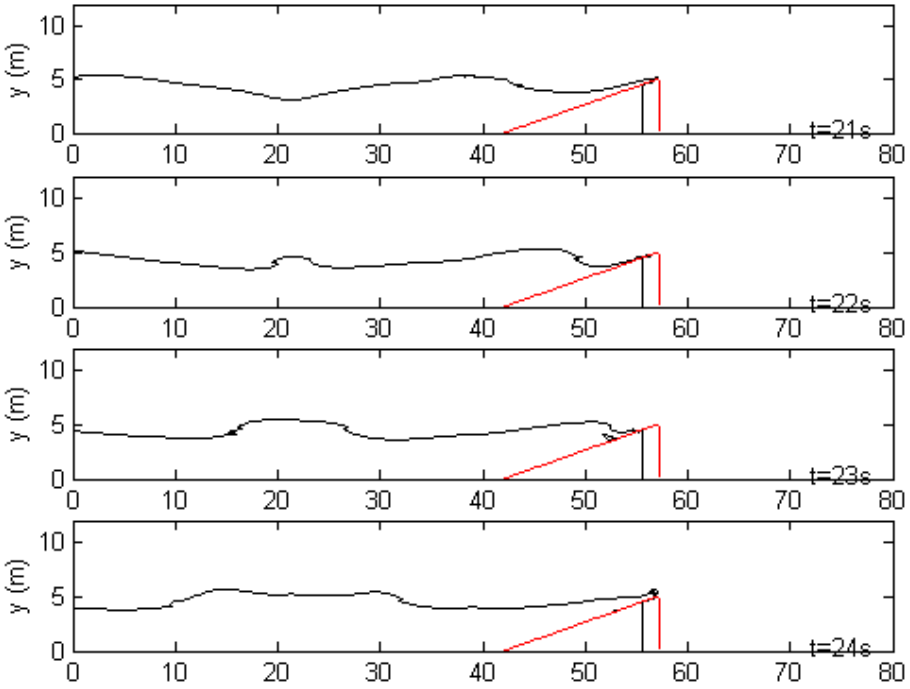
y (m)
t=21s
t=22s
t=23s
t=24s

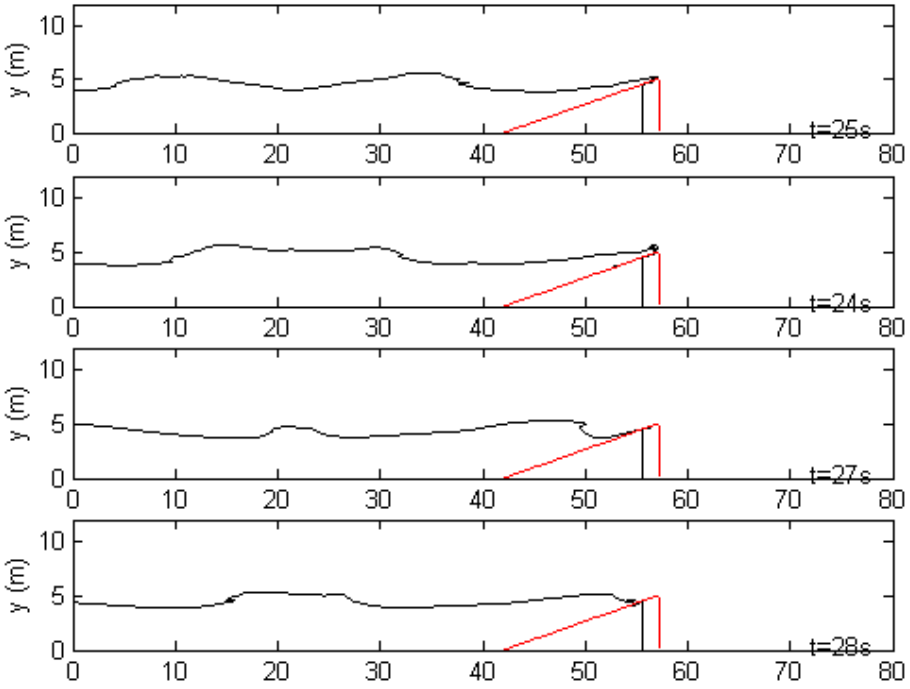
y (m)
t=25s
t=24s
t=27s
t=28s

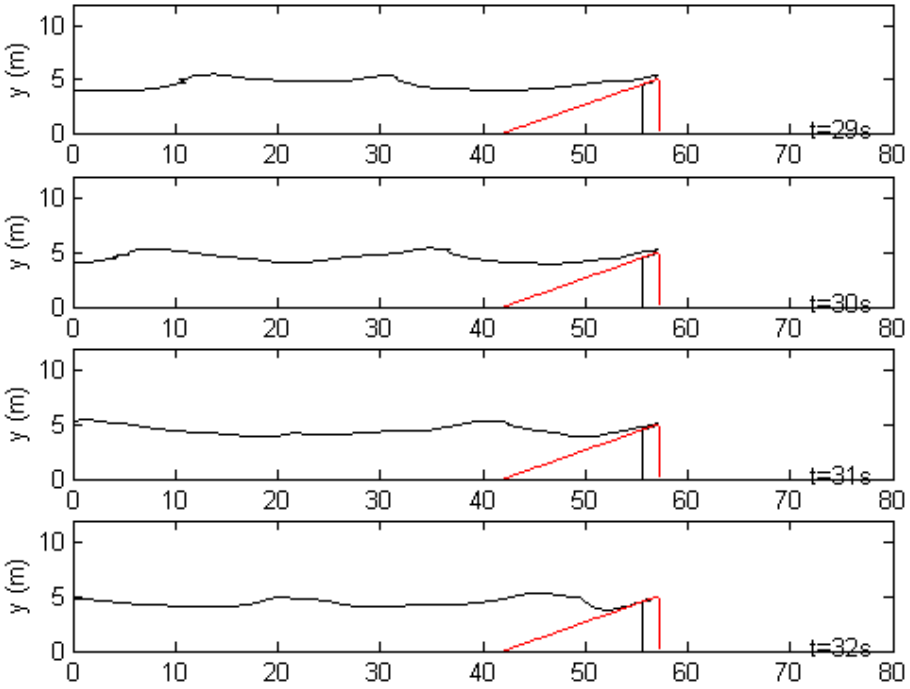
y (m)
t=29s
t=30s
t=31s
t=32s

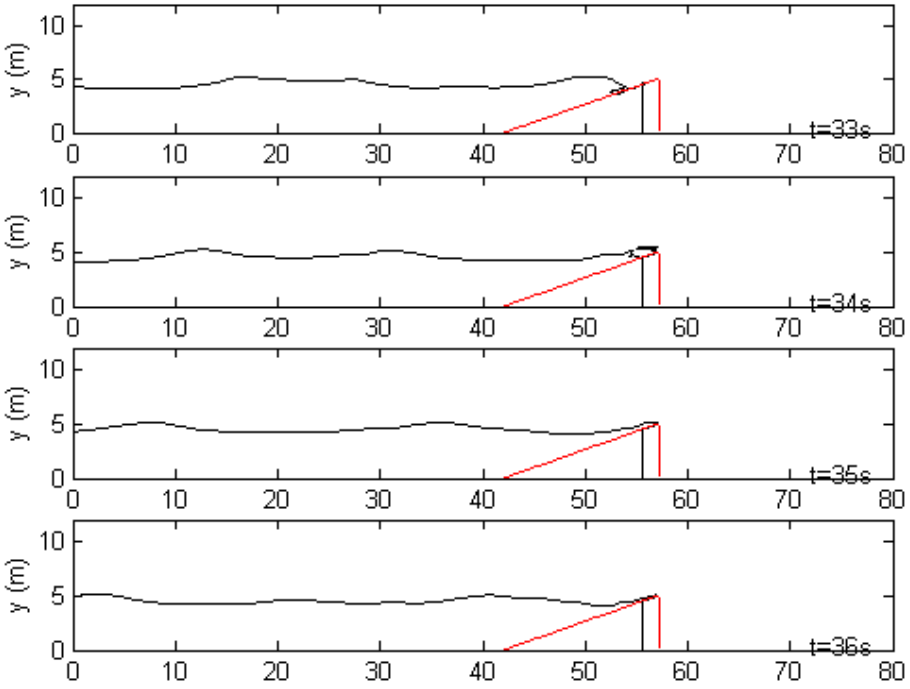
y (m)
t=33s
t=34s
t=35s
t=36s

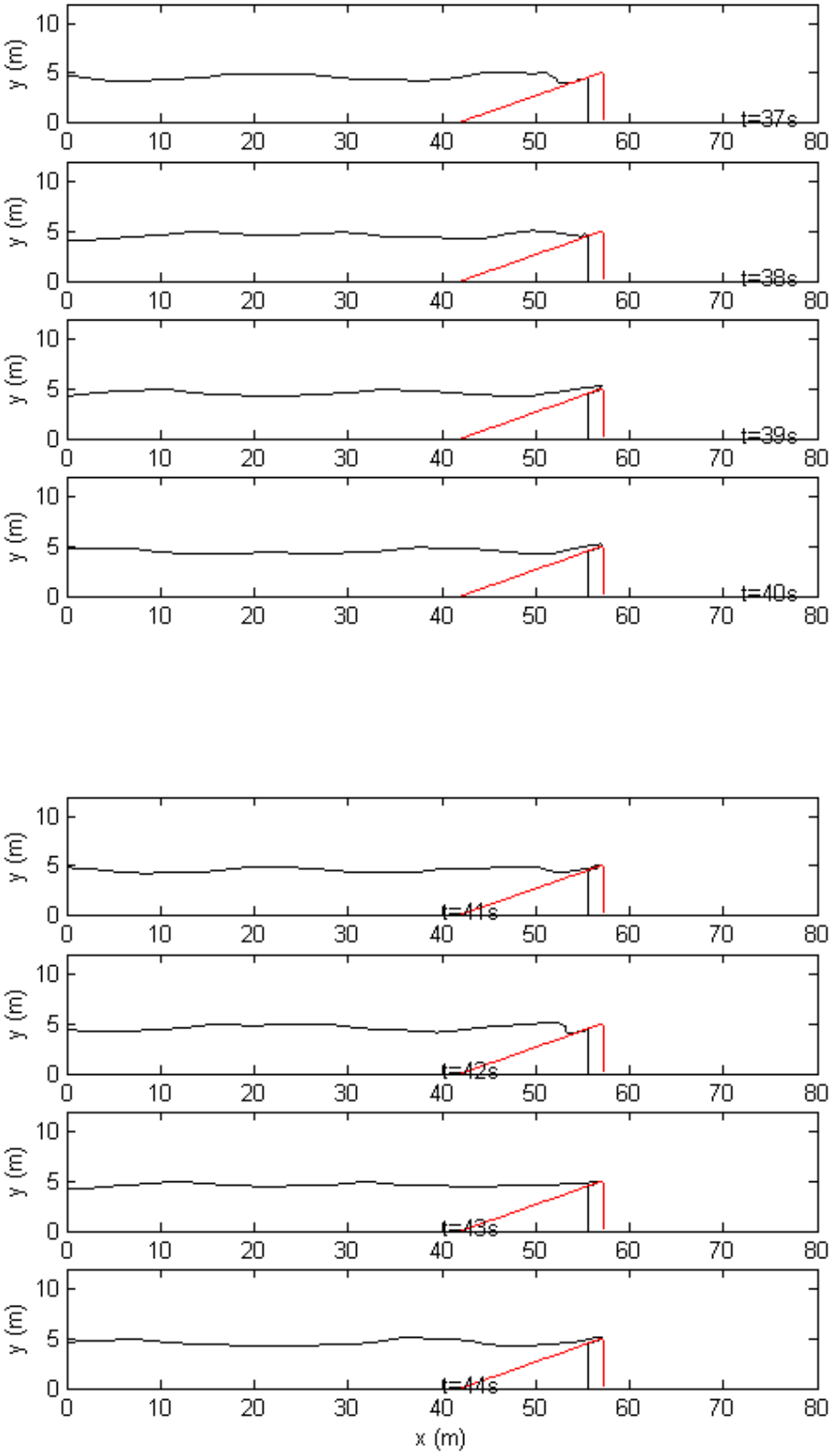
y (m)
x (m)
t=37s
t=38s
t=39s
t=40s
t=41s
t=42s
t=43s
t=44s

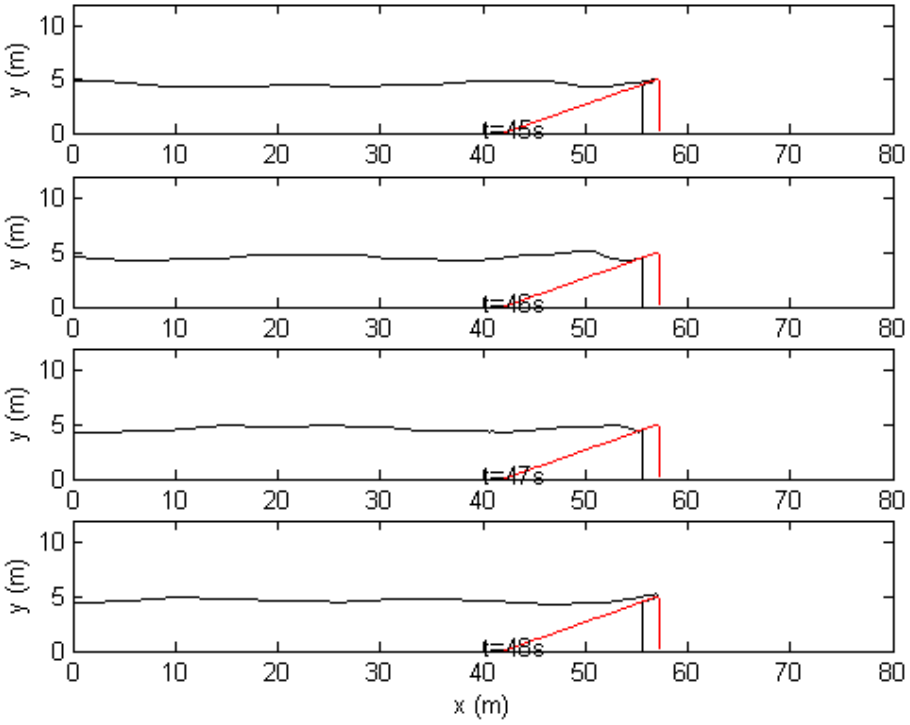
y (m)
t=45s
t=46s
t=47s
t=48s
x (m)

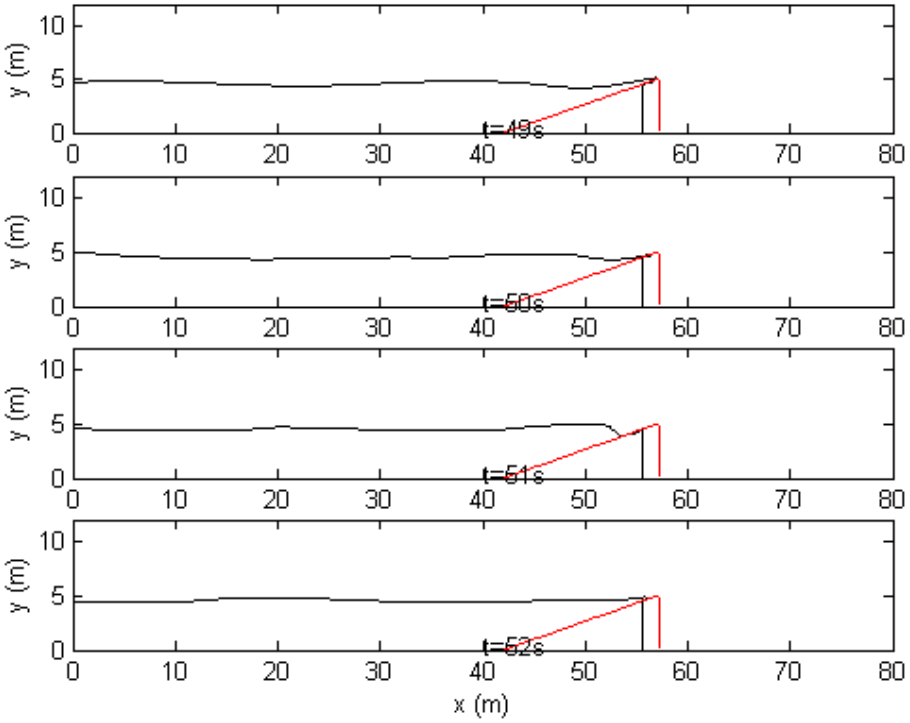
y (m)
t=49s
t=50s
t=51s
t=52s
x (m)

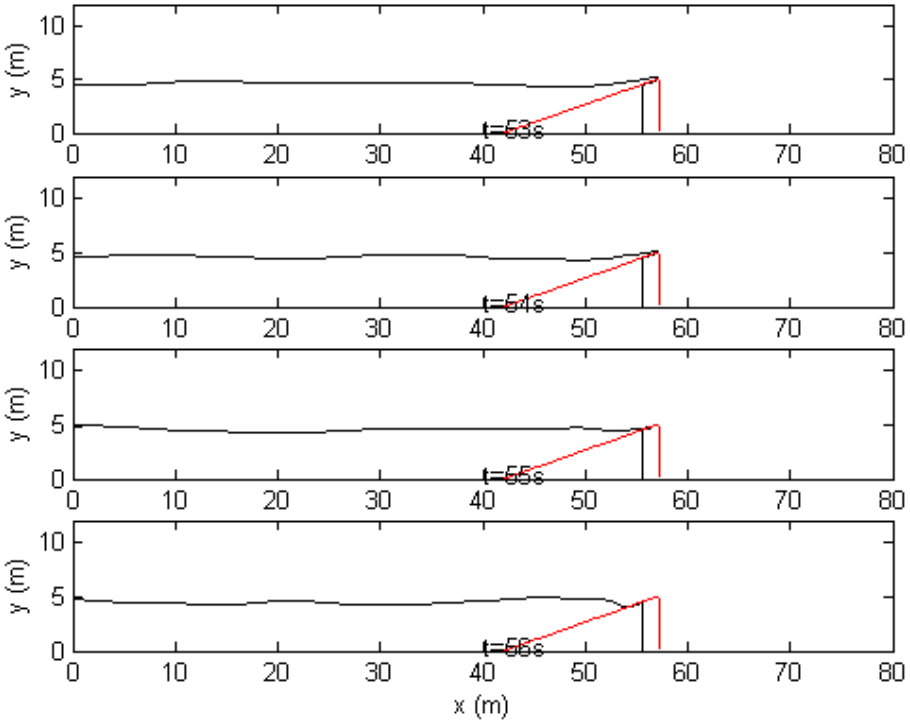
y (m)
t=63s
t=64s
t=65s
t=66s
x (m)

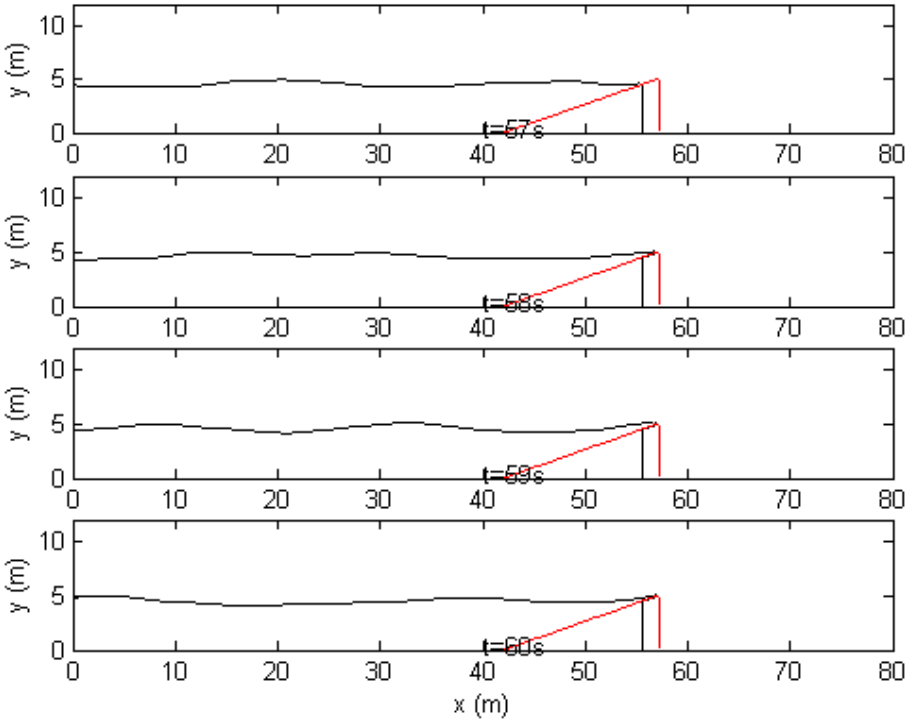
y (m)
t=67s
t=68s
t=69s
t=60s
x (m)

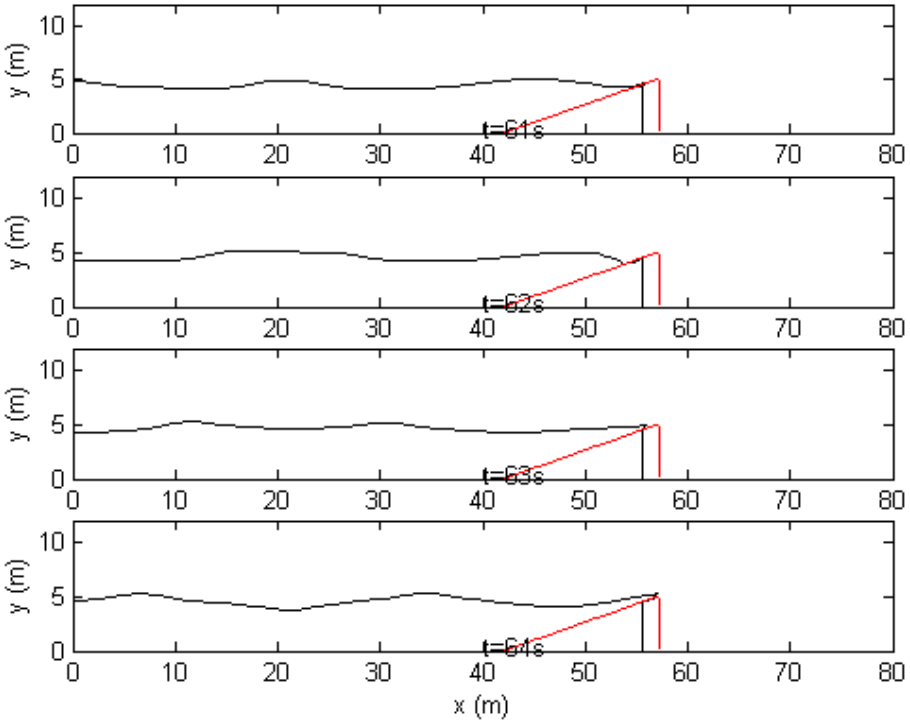
y (m)
t=61s
t=62s
t=63s
t=64s
x (m)

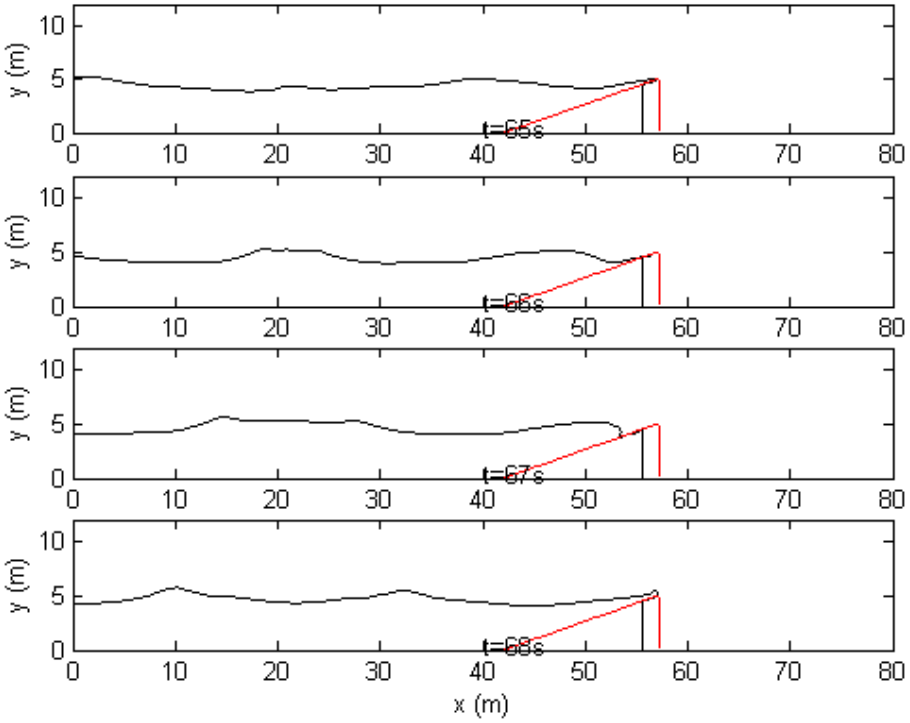
y (m)
t=65s
t=66s
t=67s
t=68s
x (m)

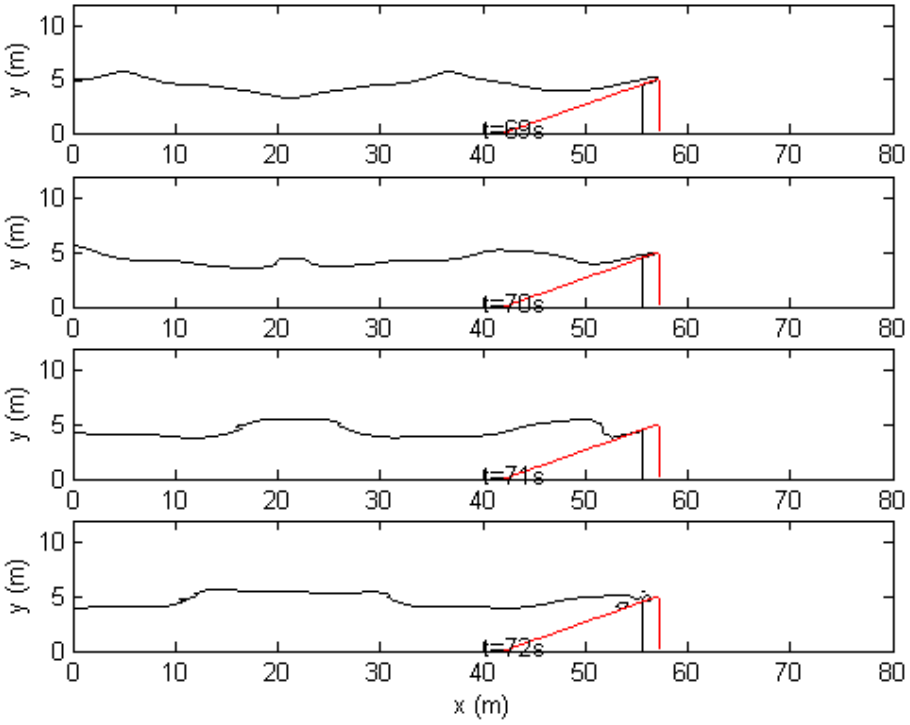
y (m)
t=69s
t=70s
t=71s
t=72s
x (m)

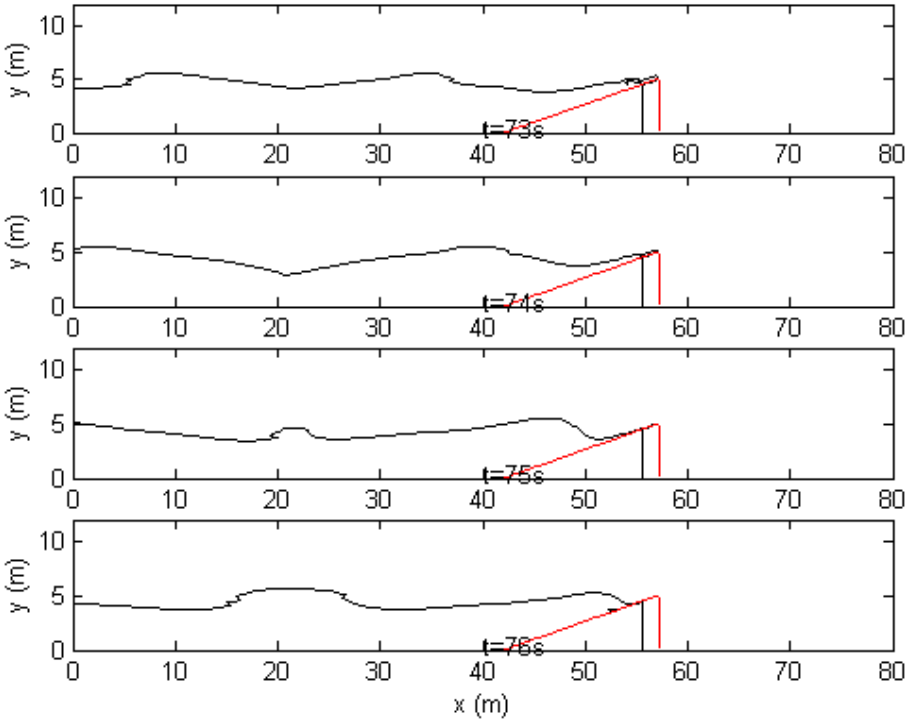
y (m)
t=73s
t=74s
t=75s
t=76s
x (m)

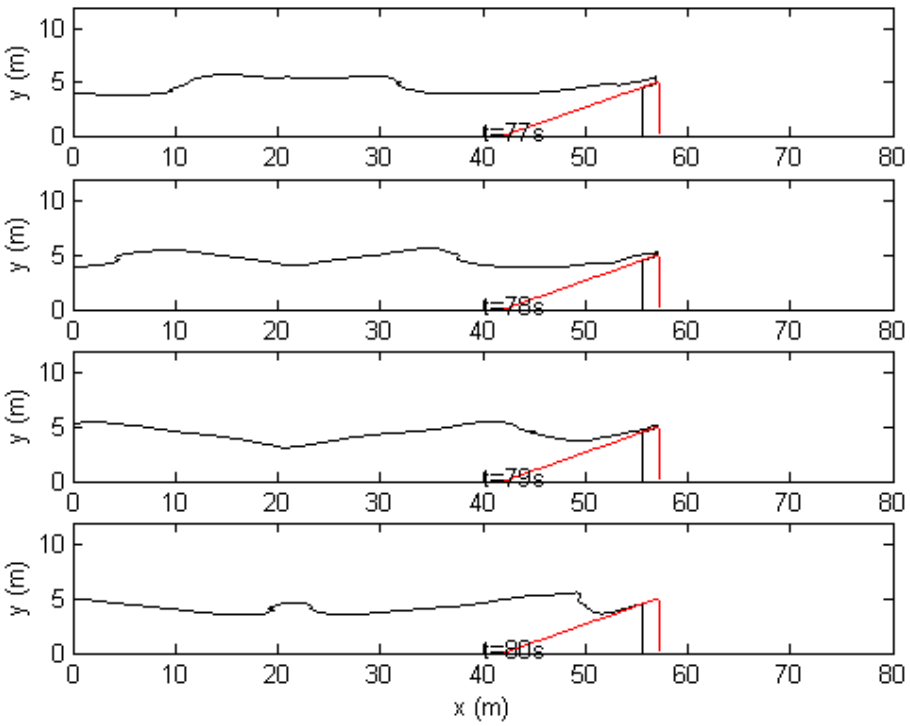
y (m)
t=77s
t=78s
t=79s
t=80s
x (m)

Appendix B

Irregular wave propagation on 1:3 sloping sea wall at zero freeboard

[Hs = 0.83 m, T_m = 3.60s and T_p = 5.00 sec.]

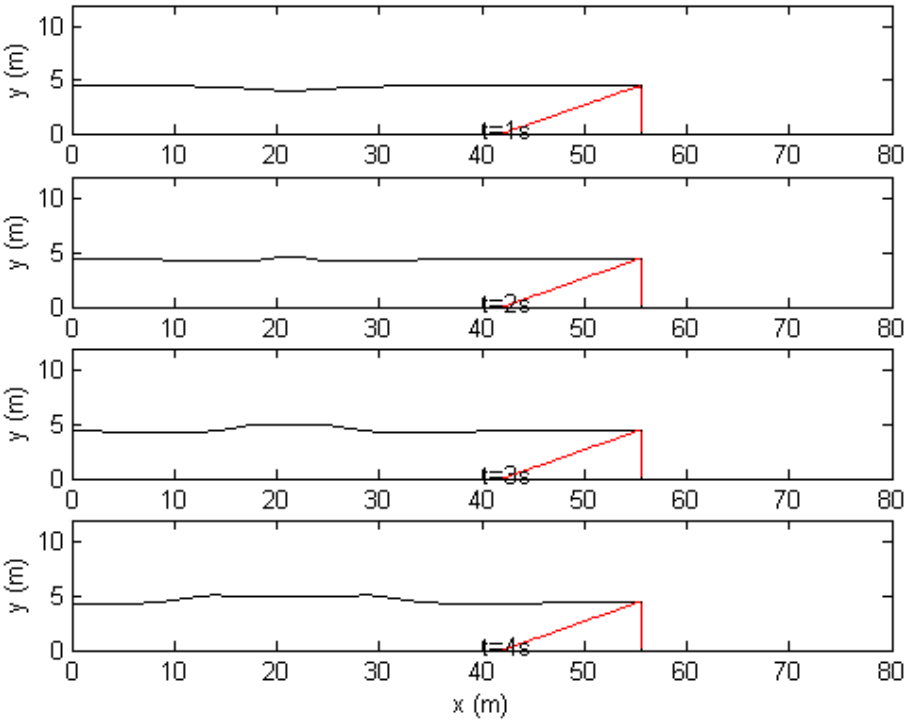
y (m)
t=1s
t=2s
t=3s
t=4s
x (m)

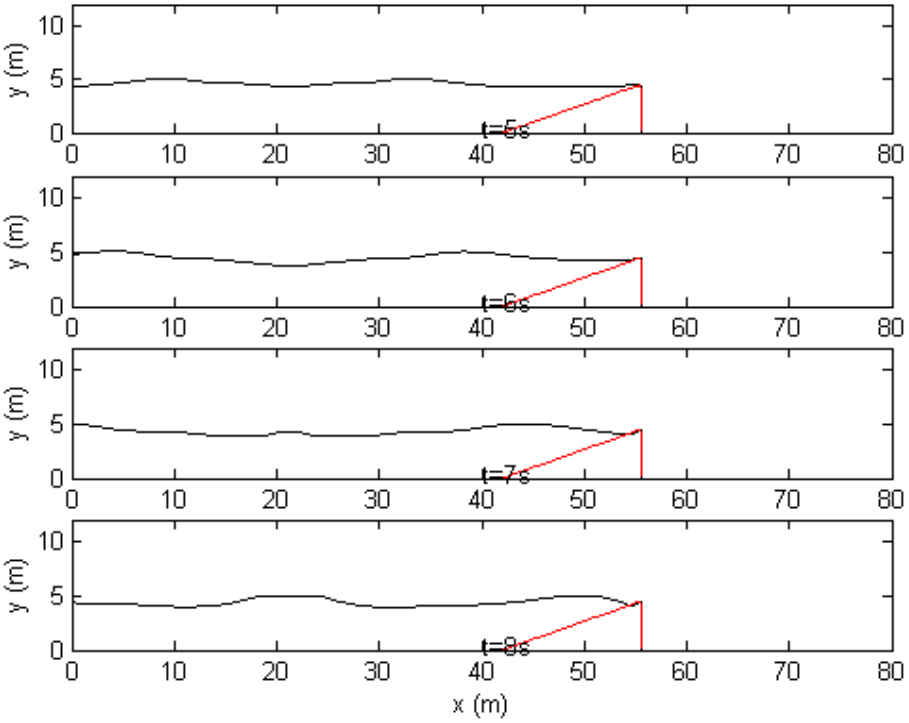
y (m)
t=5s
t=6s
t=7s
t=8s
x (m)

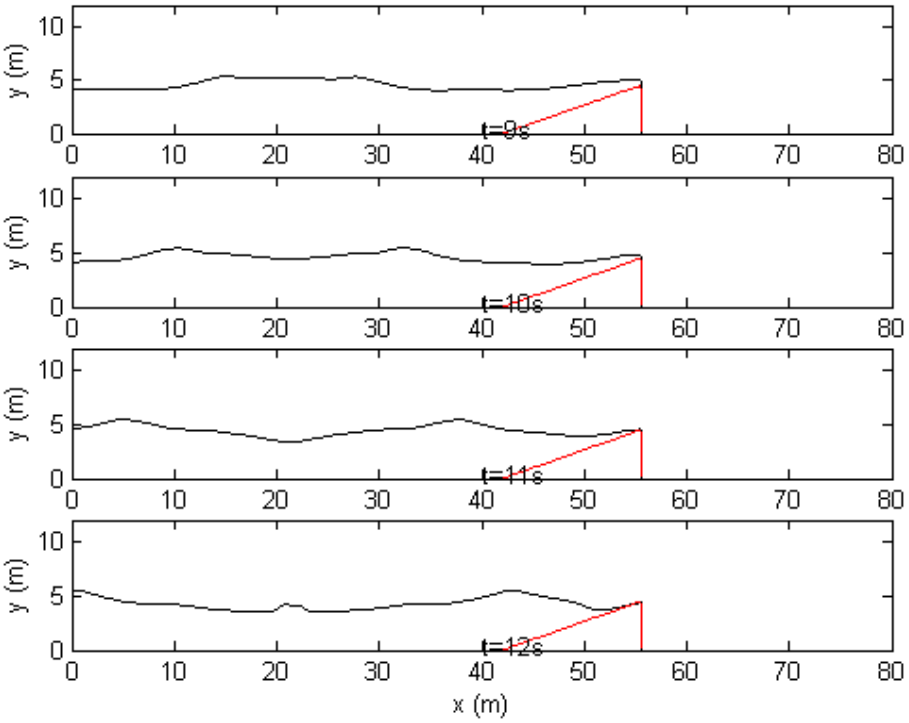
y (m)
t=9s
t=10s
t=11s
t=12s
x (m)

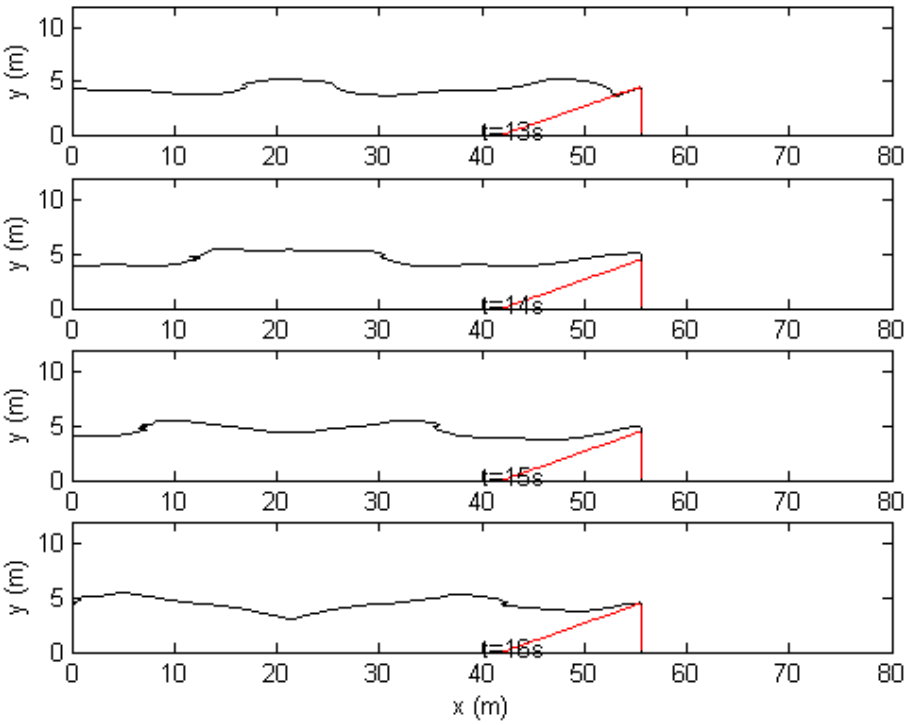
y (m)
t=13s
t=14s
t=15s
t=16s
x (m)

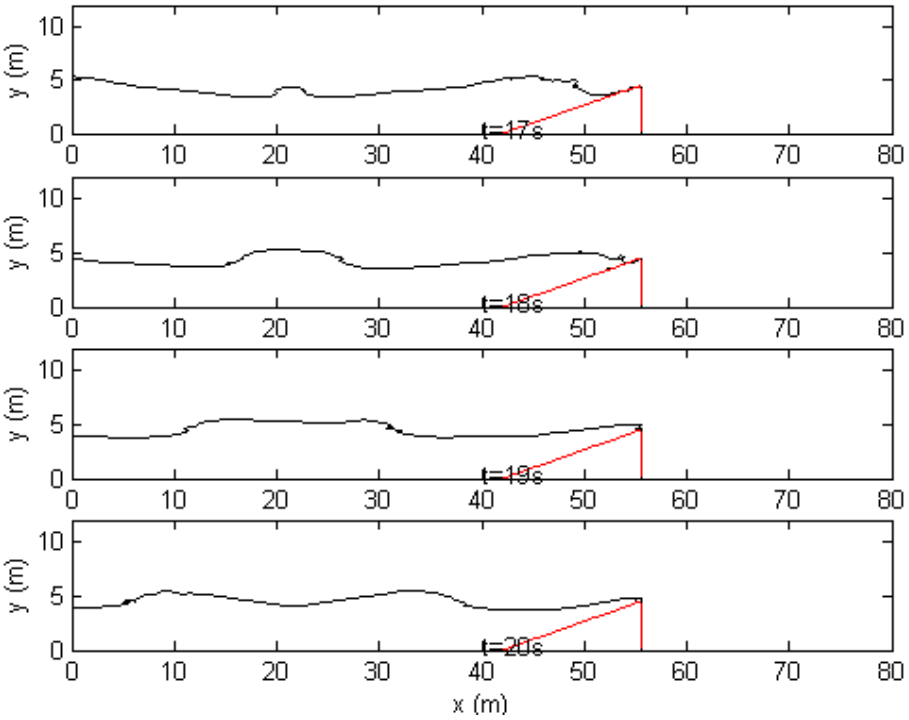
y (m)
t=17s
t=18s
t=19s
t=20s
x (m)

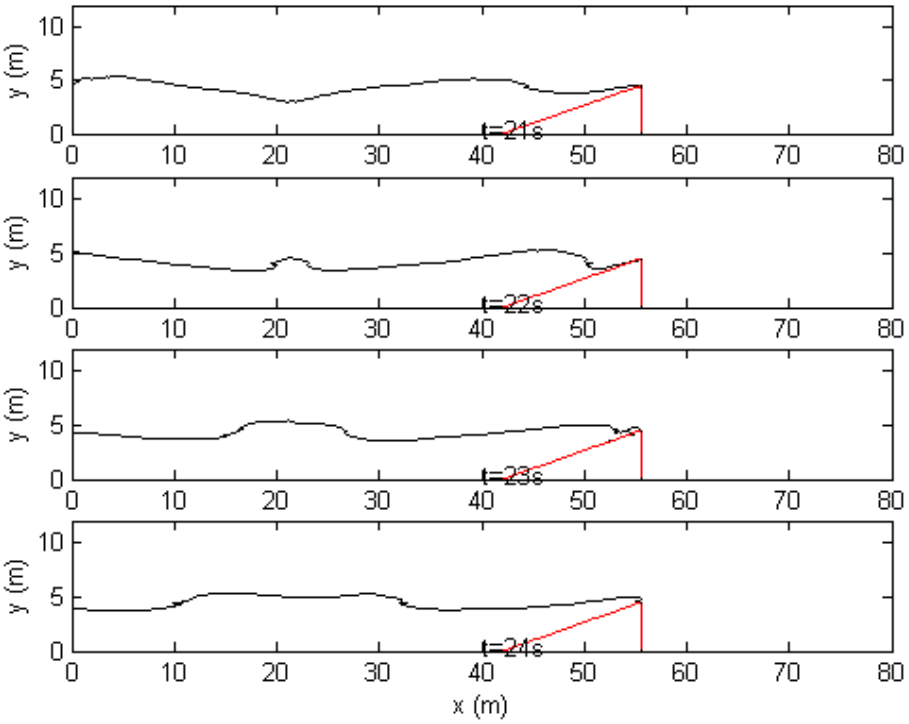
y (m)
t=21s
t=22s
t=23s
t=24s
x (m)

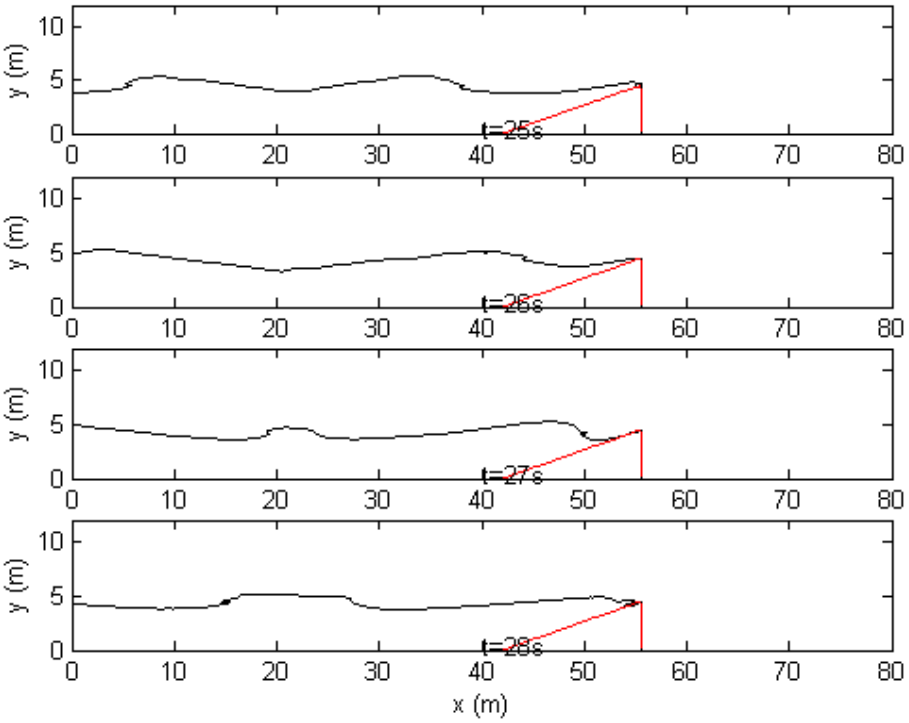
y (m)
t=25s
t=26s
t=27s
t=28s
x (m)

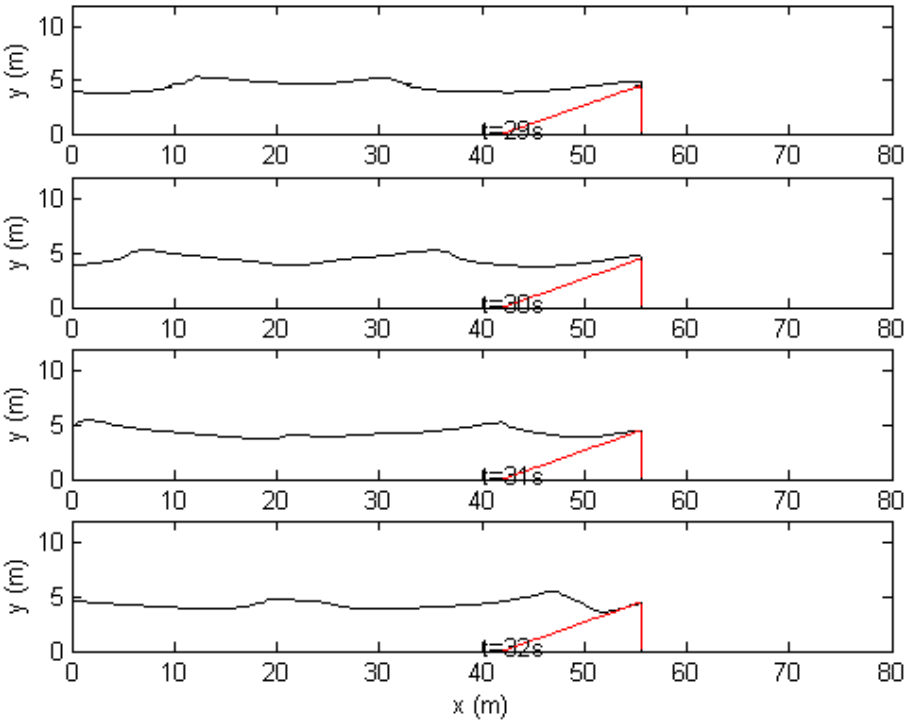
y (m)
t=29s
t=30s
t=31s
t=32s
x (m)

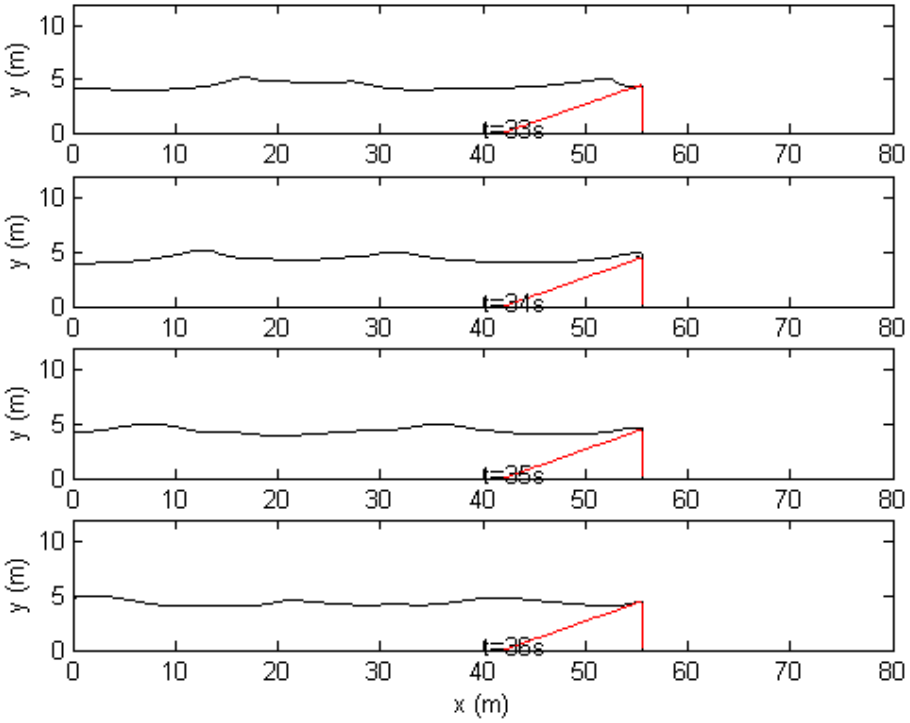
y (m)
t=33s
t=34s
t=35s
t=36s
x (m)

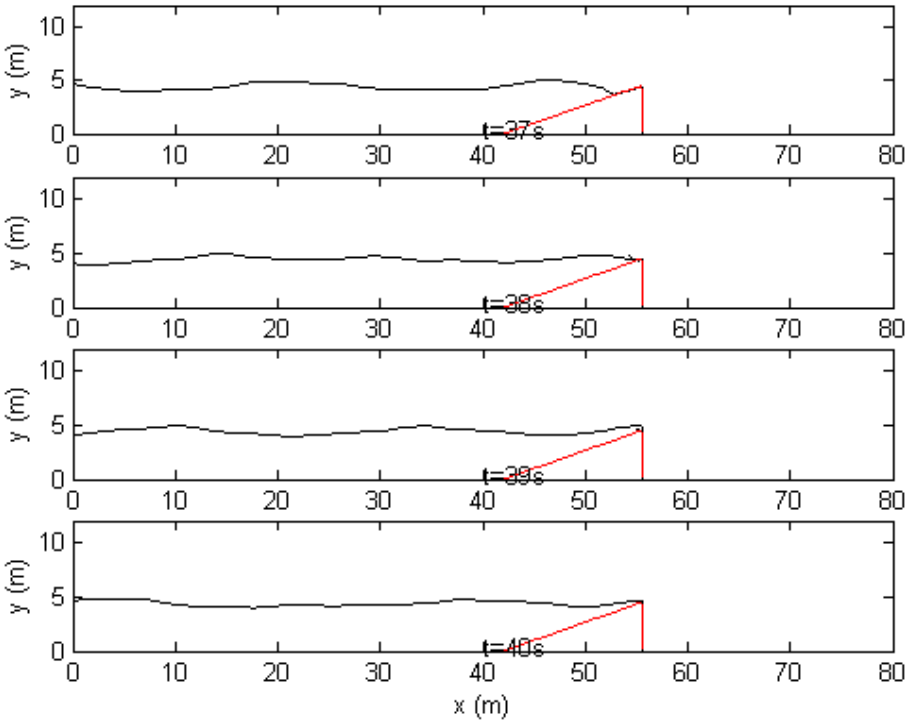
y (m)
t=37s
t=38s
t=39s
t=40s
x (m)

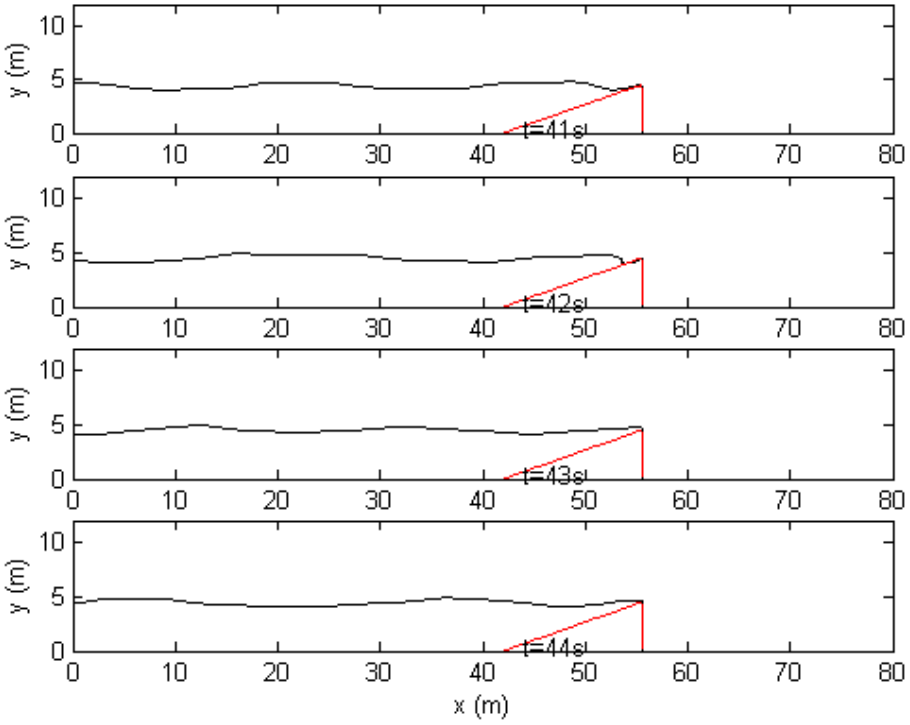
y (m)
t=41s
t=42s
t=43s
t=44s
x (m)

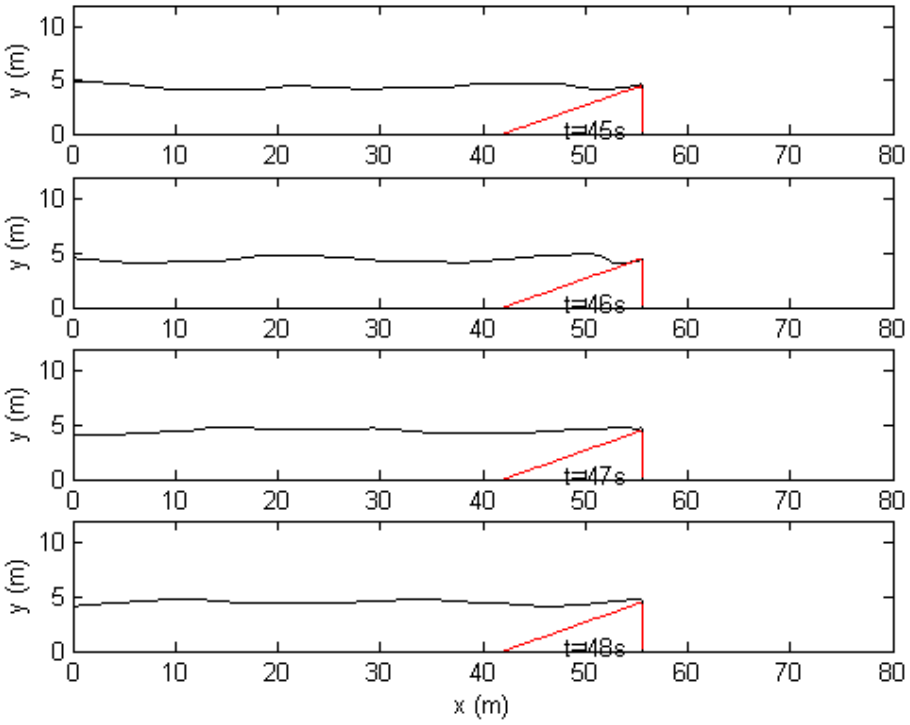
y (m)
t=45s
t=46s
t=47s
t=48s
x (m)

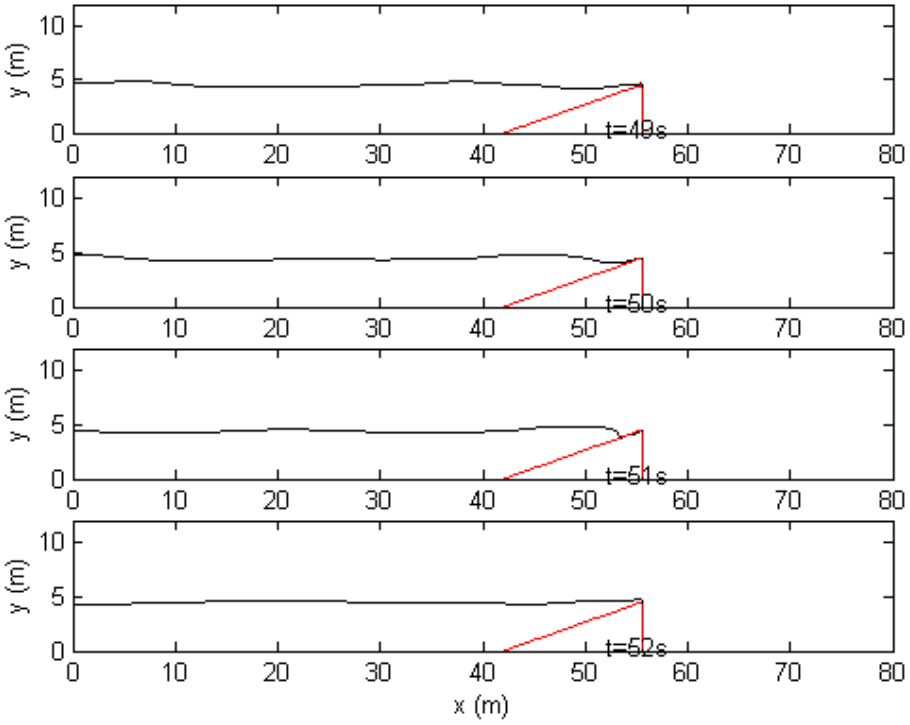
y (m)
t=49s
t=50s
t=51s
t=52s
x (m)

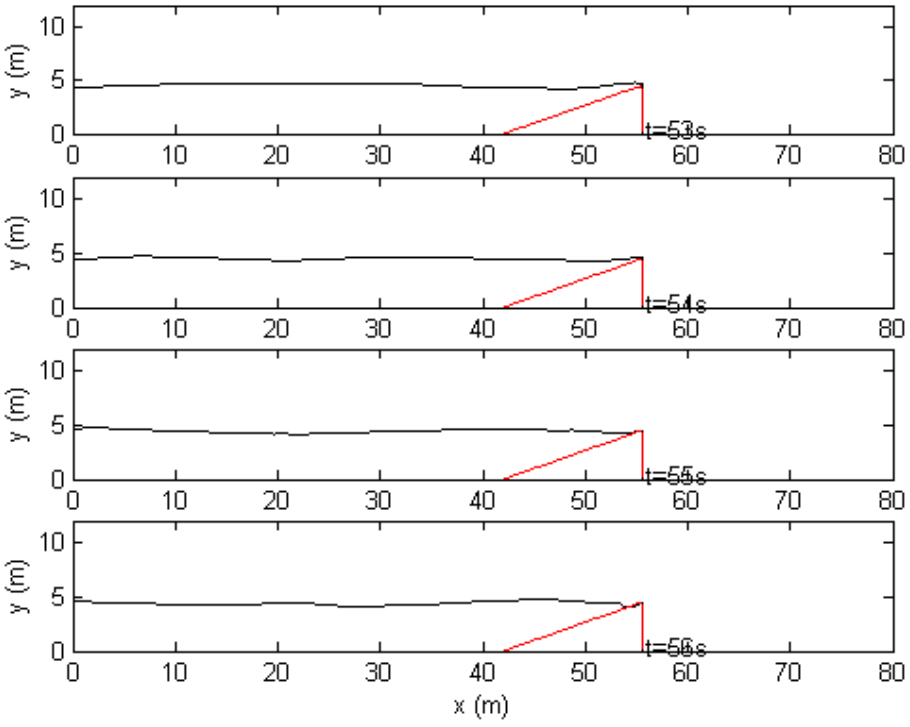
y (m)
t=53s
t=54s
t=55s
t=56s
x (m)

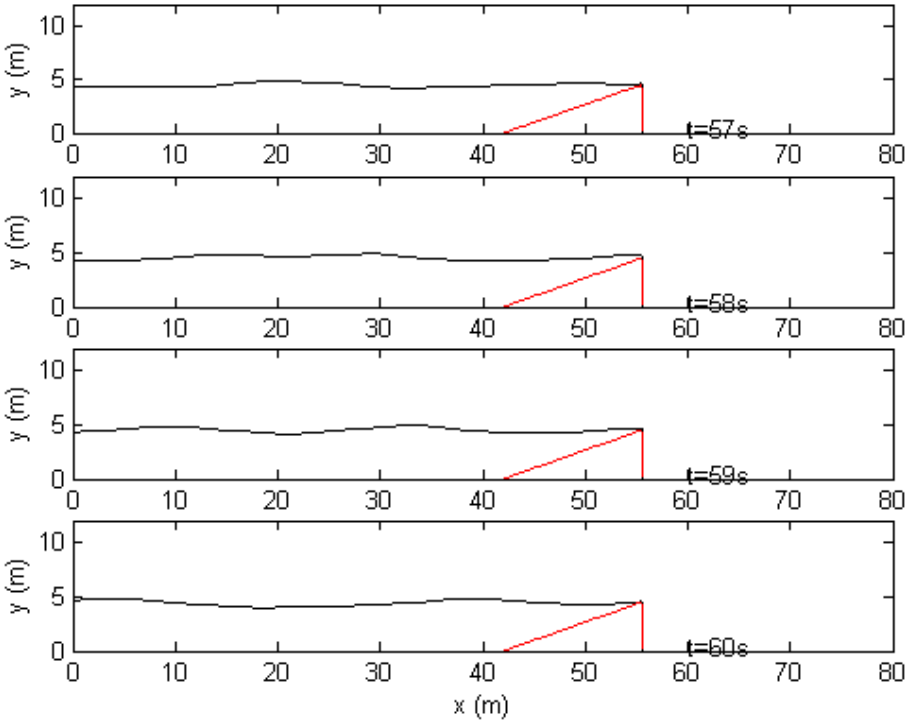
y (m)
t=57s
t=58s
t=59s
t=60s
x (m)

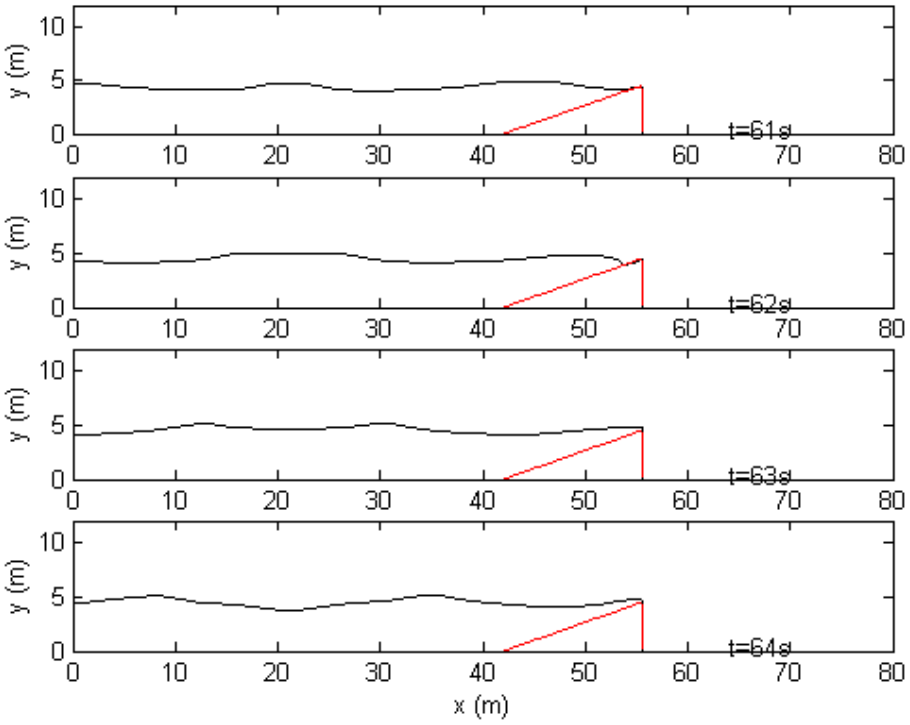
y (m)
t=61s
t=62s
t=63s
t=64s
x (m)

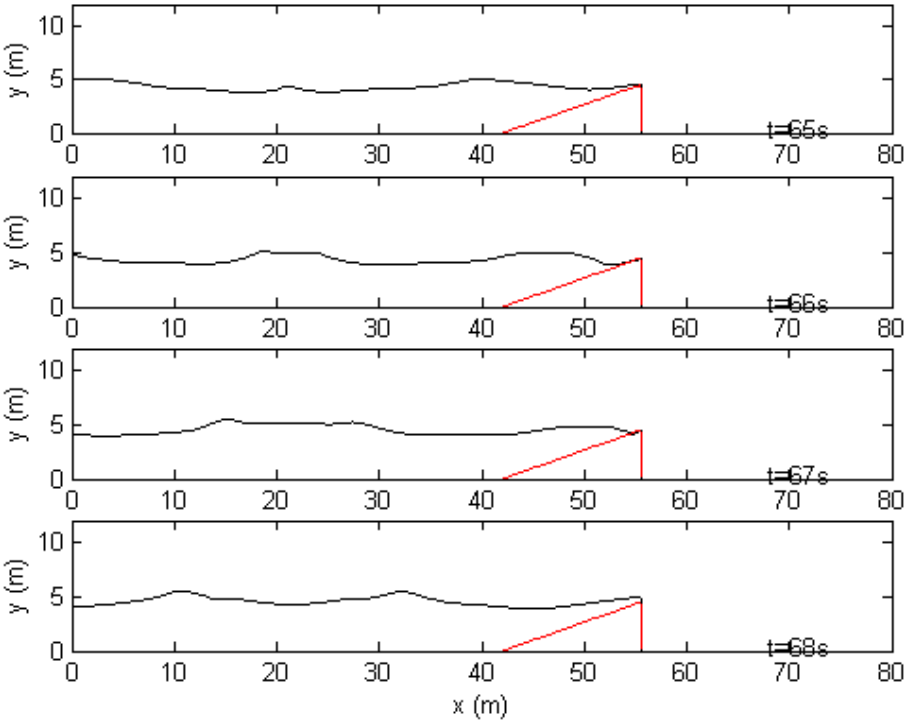
y (m)
x (m)
t=65s
t=66s
t=67s
t=68s

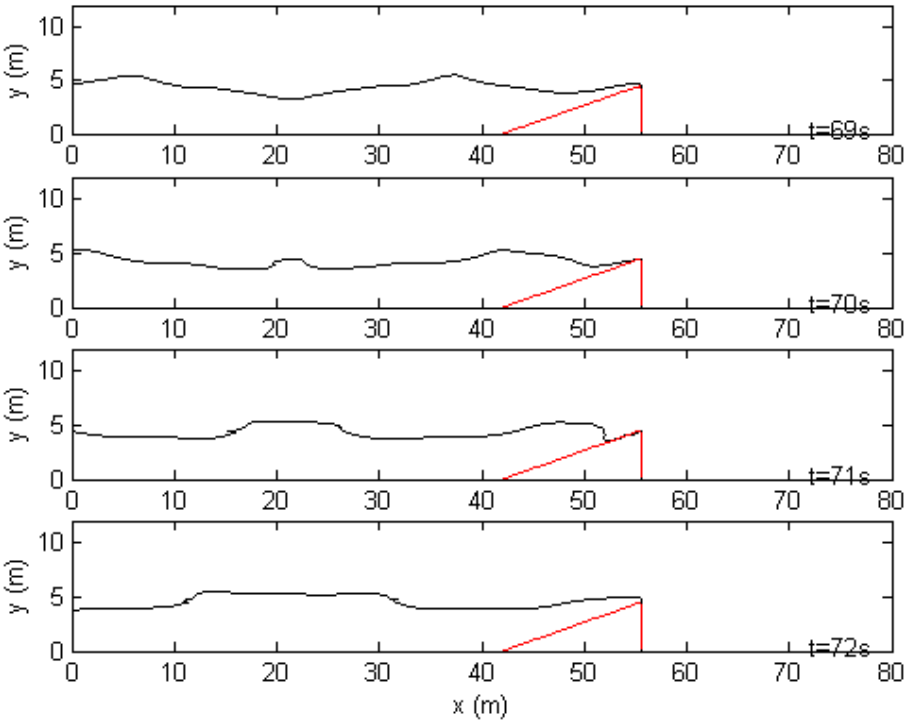
y (m)
x (m)
t=69s
t=70s
t=71s
t=72s

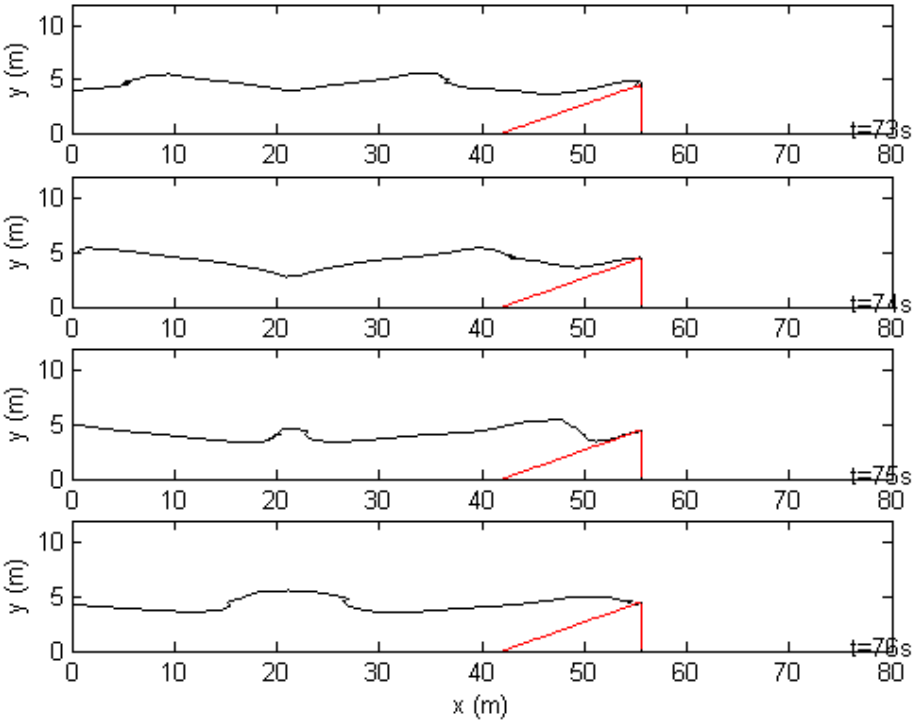
y (m)
x (m)
t=73s
t=74s
t=75s
t=76s

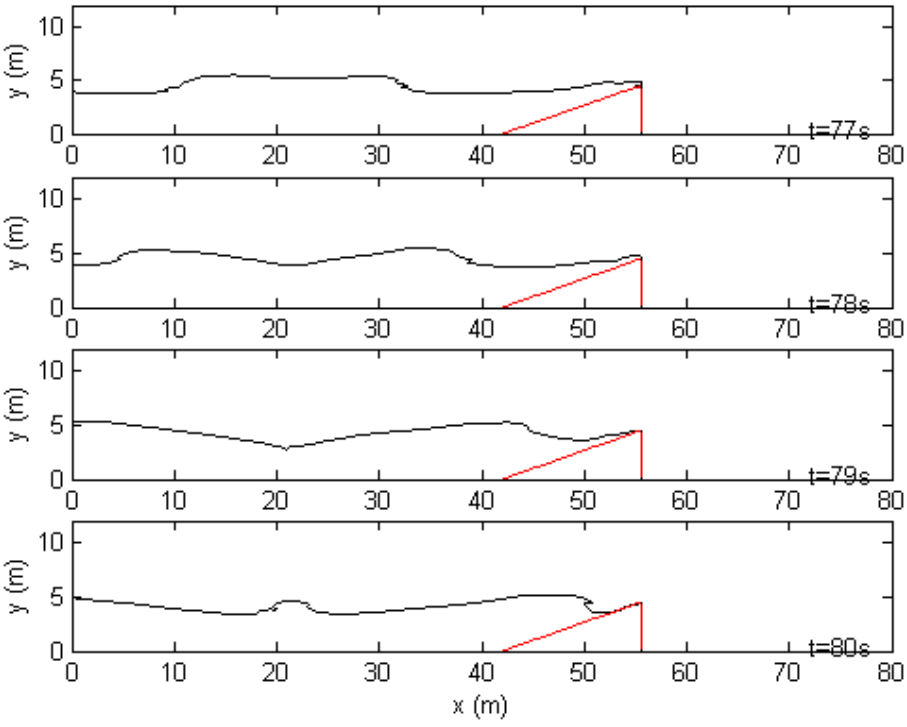
y (m)
x (m)
t=77s
t=78s
t=79s
t=80s

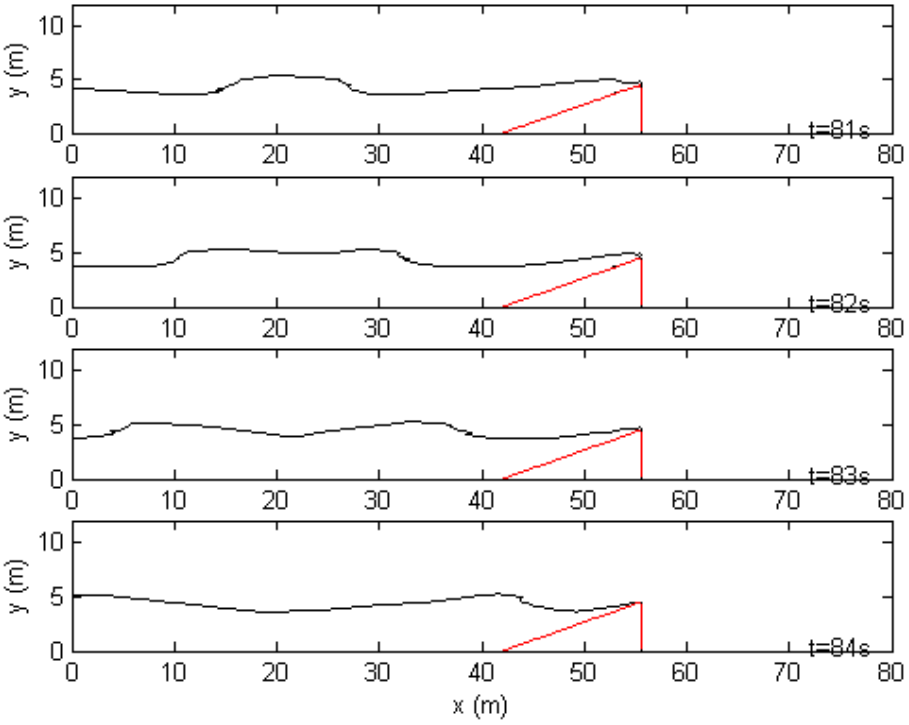
y (m)
x (m)
t=81s
t=82s
t=83s
t=84s

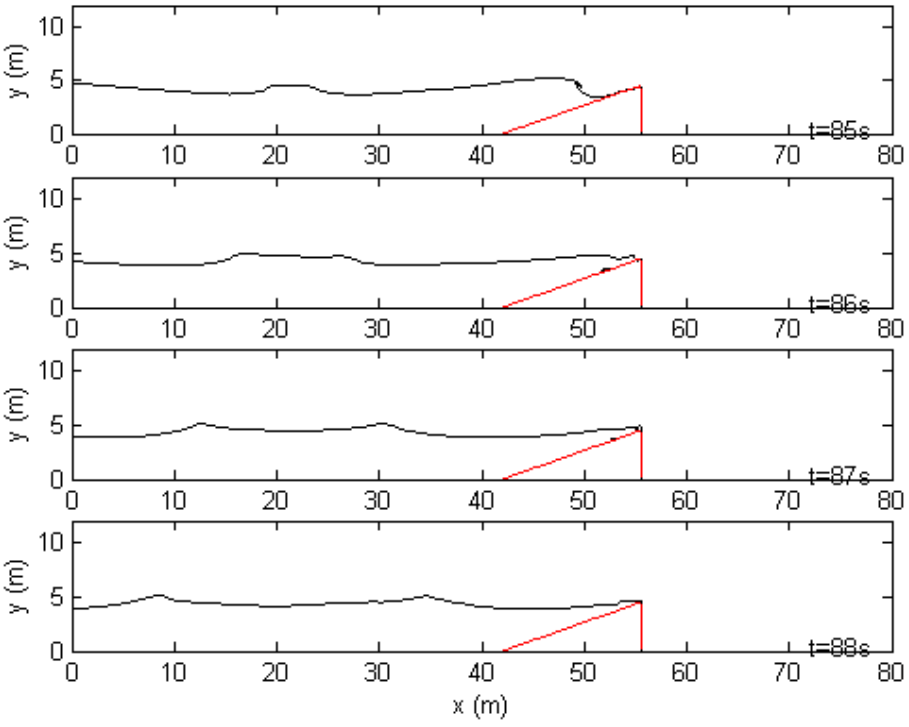
y (m)
x (m)
t=85s
t=86s
t=87s
t=88s